Design and Synthesis of *β*-Pyrrole Functionalized Push-Pull Porphyrins

Ph.D. Thesis

By

BIJESH S

DISCIPLINE OF CHEMISTRY

INDIAN INSTITUTE OF TECHNOLOGY INDORE

September 2021

Design and Synthesis of *β*-Pyrrole Functionalized Push-Pull Porphyrins

A THESIS

Submitted in partial fulfillment of the
requirements for the award of the degree
of
DOCTOR OF PHILOSOPHY

by
BIJESH S

DISCIPLINE OF CHEMISTRY
INDIAN INSTITUTE OF TECHNOLOGY INDORE
September 2021
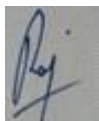
INDIAN INSTITUTE OF TECHNOLOGY INDORE

CANDIDATE'S DECLARATION

I hereby certify that the work which is being presented in the thesis entitled **"Design and Synthesis of β-Pyrrole Functionalized Push-Pull Porphyrins"** in the partial fulfillment of the requirements for the award of the degree of **DOCTOR OF PHILOSOPHY** and submitted in the **DISCIPLINE OF CHEMISTRY, Indian Institute of Technology Indore**, is an authentic record of my own work carried out during the time period from **December 2015** to **September 2021** under the supervision of **Dr. Rajneesh Misra, Professor, Discipline of Chemistry, IIT Indore**.

The matter presented in this thesis has not been submitted by me for the award of any other degree of this or any other institute.

22/04/2022
signature of the student with date
(BIJESH S)

This is to certify that the above statement made by the candidate is correct to the best of my/our knowledge.
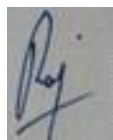
22/04/2022

Signature of Thesis Supervisor #1 with date

(Dr. RAJNEESH MISRA)

Signature of Thesis Supervisor #2 with date

(NAME OF THESIS SUPERVISOR)

BIJESH S has successfully given his Ph.D. Oral Examination held on **…………22/04/2022………………**

22/04/2022

Signature of Thesis Supervisor #1 with date

(Dr. RAJNEESH MISRA)

Signature of Thesis Supervisor #2 with date

(NAME OF THESIS SUPERVISOR)

ACKNOWLEDGEMENT

DEDICATED TO

MY TEACHERS, FAMILY AND

FRIENDS

- BIJESH S

SYNOPSIS

Porphyrins are aromatic tetrapyrrolic macrocycle, composed of four pyrrole rings and four bridging methine carbon atoms, exhibits a planar conformation (Figure 1). Porphyrin macrocycle undergoes peripheral functionalization at the four *meso* positions of the methine bridges and eight *β*-positions on the pyrrolic rings. Porphyrin exhibits two characteristic absorption band, Soret band and the Q-band around 400–700 nm in the visible region. The photonic and electronic properties of the porphyrin macrocycle can be tuned by peripheral functionalization. Porphyrin derivatives have been used in various applications such as, photosynthesis, organic photovoltaic, P450-related biocatalysts, bioimaging probes, photodynamic therapeutic agents, chemosensors, information storage, light emitting materials, conductive organic materials, near-infrared dyes, molecular wires, nonlinear optical materials, supramolecules, metal ligands and many more.
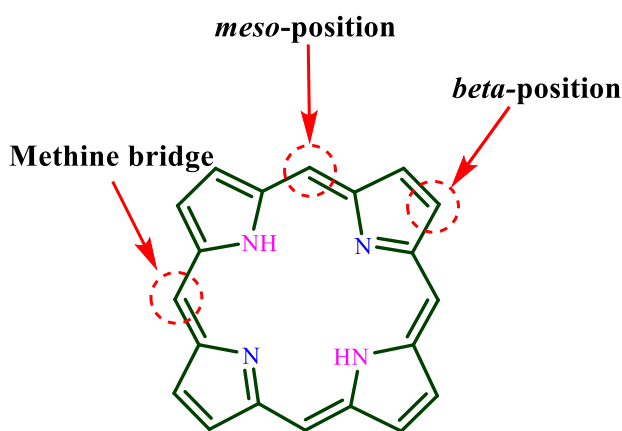
Figure 1. The structure of the porphyrin molecule.

The photonic and electronic properties of the porphyrin macrocycle can be tuned by introducing the donor and acceptor units at the *β*-pyrrolic positions. A wide variety of donor (triphenylamine, phenothiazine, ferrocene, *N*, *N*-dimethylaniline, 1,1,2,2-tetraphenylethene and carbazole) and acceptor (tetracyanoethylene, naphthalimide, benzothiazole and quinoxaline) functionalized porphyrin based donor–acceptor systems were explored. The Frontier

molecular orbital energy levels of these porphyrin based donor–acceptor molecular systems was stabilized to attain low HOMO–LUMO gap. The photophysical, electrochemical and computational studies of these porphyrin π-systems were investigated, which reveals its application in optoelectronics.
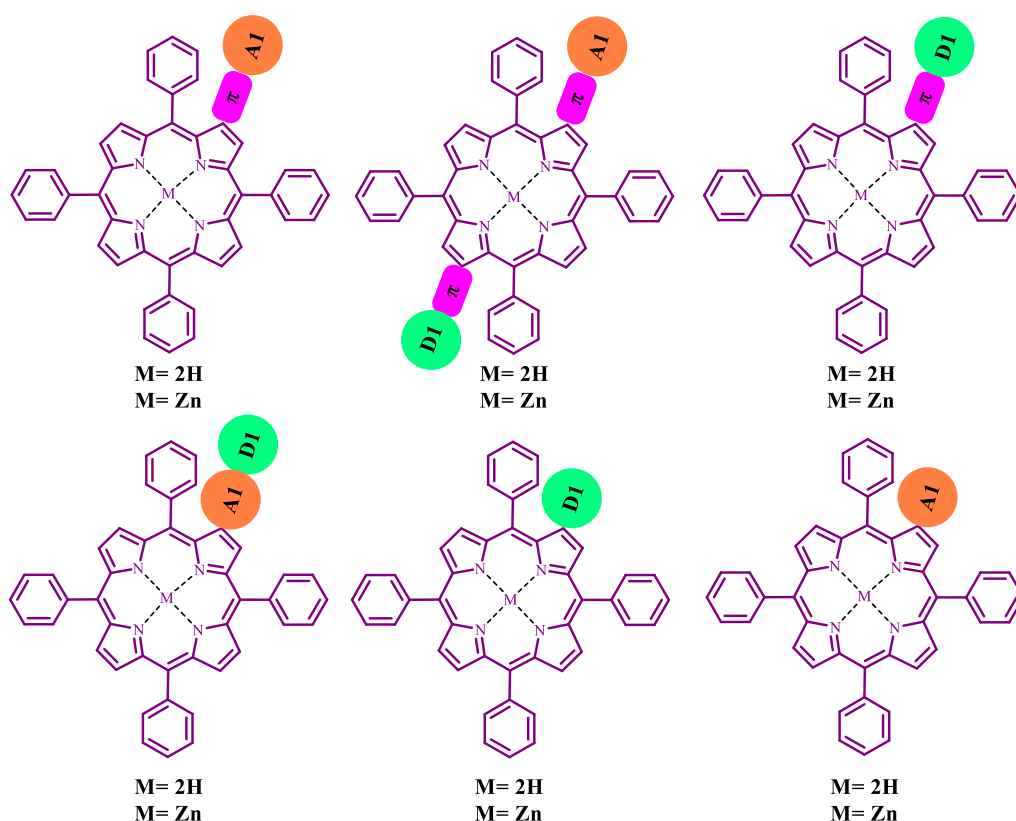
Figure 2. General representation of donor-acceptor functionalized porphyrins in this work.

The main objectives of present study are:

- ✓ To synthesize donor and acceptor substituted *β*, *β′*-push–pull porphyrins and to investigate the effect of donor and acceptor units on the photophysical and computational studies.

- ✓ To understand the effect of TCBD functionalization on *β*-substituted porphyrins and its photophysical and computational studies were investigated.

- ✓ To fine-tune the photophysical and electrochemical properties of the porphyrin macrocycle by incorporating the donor substituents at the β-pyrrolic position of the porphyrin π-system.
- ✓ To explore the influence of acceptor units on the photophysical and computational studies of the porphyrin π-system.
- ✓ To investigate the effect of 2,3,3-triphenylacrylonitrile, 1,1,2,2-tetraphenylethene and 9-propyl-9H-carbazole units on the photophysical and electrochemical properties of the porphyrin π-systems.

Chapter 1: Introduction

This chapter describes the synthesis and functionalization at the β-pyrrolic position of the porphyrin macrocycle *via* bromo, formyl, vinyl, ethynyl, nitro and amino groups for the construction of more elaborate push-pull architectures and their applications in diverse fields.

Chapter 2: Materials and experimental techniques

This chapter summarizes the general experimental methods, characterization techniques and details of instruments used for characterization.

Chapter 3: Unsymmetrical β-substituted push–pull tetraarylporphyrins

In chapter 3, β-pyrrole functionalized unsymmetrical push−pull porphyrins **1**–**6** were designed and synthesized *via* β-mono and dibrominated TPP **10** and **11**, using Sonogashira cross-coupling reaction and zinc metallation reaction. The photophysical and computational studies of porphyrin **1**–**6** were investigated. The absorption spectra of the porphyrin **5** and **6** with triphenylamine donor and the naphthalimide acceptor units at the opposite β, β'-positions exhibit a red shifted absorption in the Soret band and the Q-band region compared to porphyrin **1**, **2**, **3** and **4**. The Steady state fluorescence spectra show considerable red shift in fluorescence maxima of porphyrin **5** and **6** compared to porphyrin **1**, **2**, **3** and **4** due to the strong

electronic communication between the electron donor and the acceptor units. The computational study of porphyrin **5** and **6** reveals that the HOMOs are concentrated on triphenylamine donor unit and the LUMO are populated over the porphyrin macrocycle and the naphthalimide acceptor units.

1, M = 2H
2, M = Zn

3, M = 2H
4, M = Zn

5, M = 2H
6, M = Zn
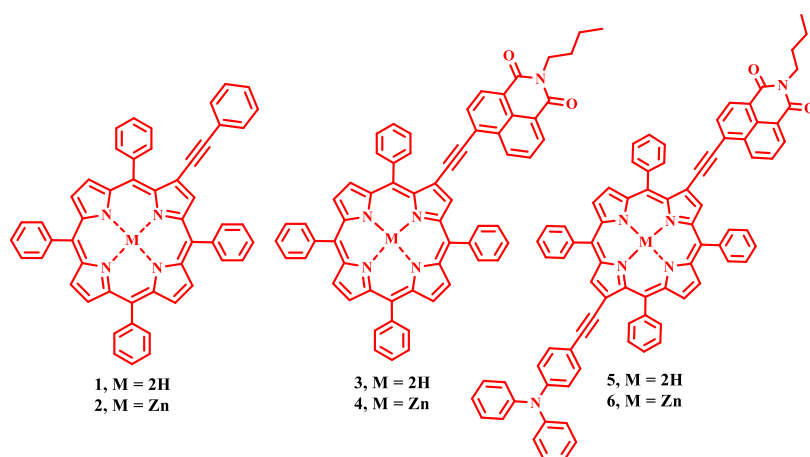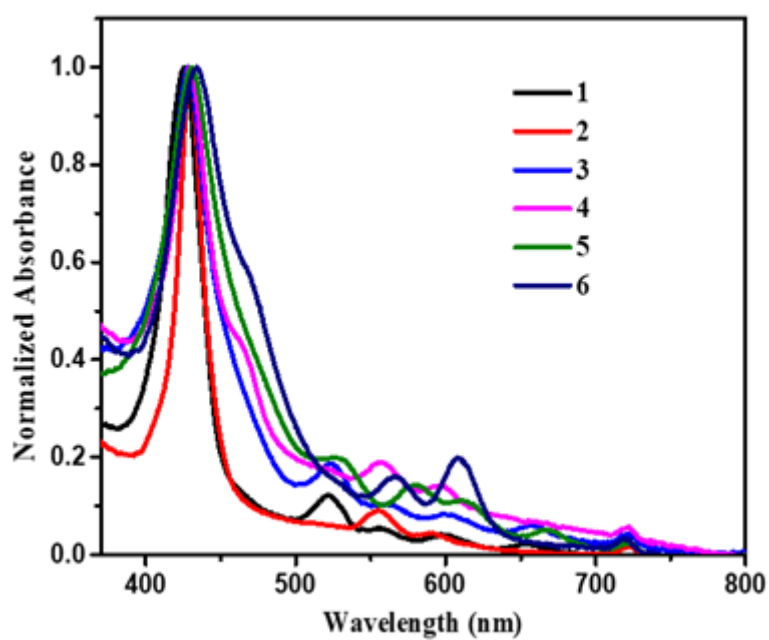
Chapter 4: *β*-Substituted TCBD Functionalized Push–Pull Porphyrins

In Chapter 4, the free base and Zn(II) metallated, *β*-donor (phenothiazine and *N, N*-dimethylaniline) substituted porphyrins **1**, **2**, **5** and **6** were designed and synthesized *via* Pd-catalyzed Sonogashira cross-coupling reaction. Their TCBD analogues **3**, **4**, **7** and **8** were synthesized by the [2+2] cycloaddition–retro electrocyclization (CA-RE) reaction. The photophysical and computational studies of porphyrin **1**–**8** were investigated. The UV-visible absorption spectra of TCBD functionalized porphyrin **3**, **4**, **7** and **8**, exhibits a red shift in Soret band and Q band region compared to their corresponding donor substituted porphyrins **1**, **2**, **5** and **6**. The red shifted electronic absorption spectra of

1, M= H
2, M= Zn

3, M= H
4, M= Zn

5, M= H
6, M= Zn

7, M= H
8, M= Zn
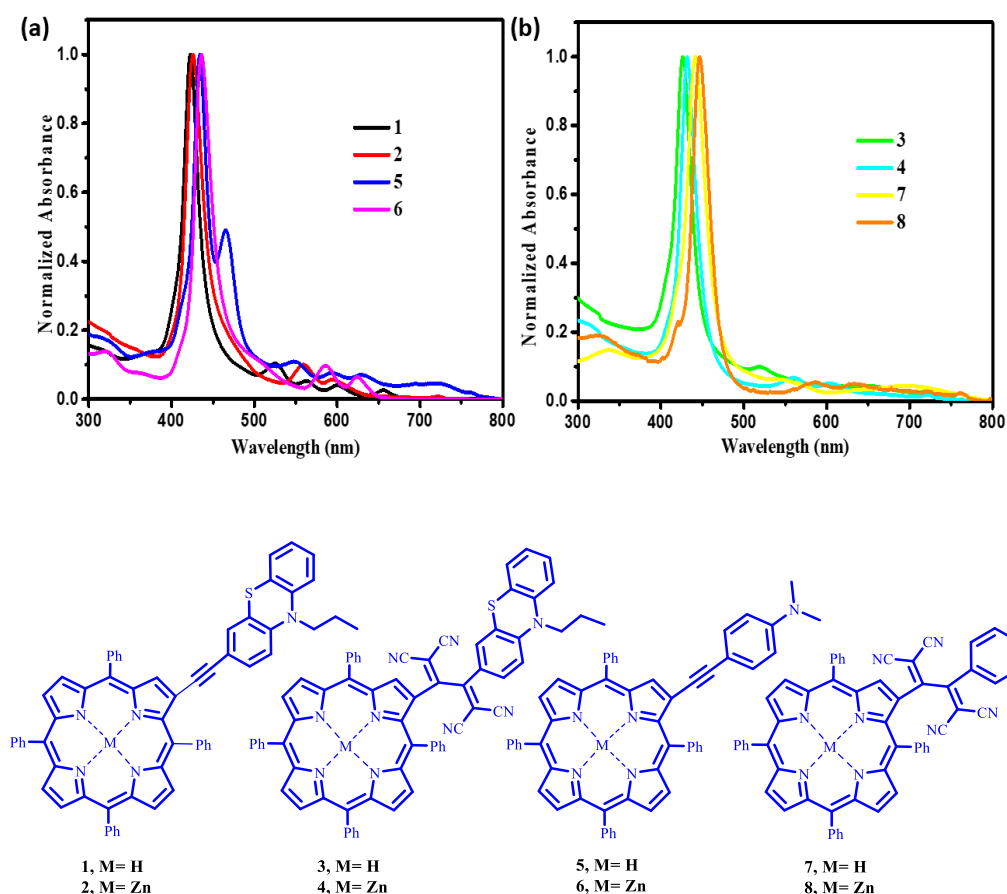
TCBD functionalized porphyrin **3**, **4**, **7** and **8** are attributed to the incorporation of electron accepting TCBD unit with strong intramolecular charge-transfer (CT). The blue shifted emission spectra of TCBD functionalized porphyrins **3**, **4** and **8** are due to the twisted nonplanar conformation between the porphyrin and TCBD units. The frontier molecular orbitals of the push–pull porphyrin **3**, **4**, **7** and **8** shows the electronic delocalization of HOMO are concentrated on the porphyrin unit whereas the LUMO are localized on the TCBD unit.

Chapter 5: Donor Substituted Unsymmetrical *β*-Pyrrole Porphyrins

In chapter 5, the donor substituted unsymmetrical free base *β*-pyrrole porphyrins **1**, **3**, **5** and **7** were designed and synthesized by the Suzuki cross-coupling reaction and their metallation was carried out using $Zn(OAc)_2$, which resulted in zinc complexes of porphyrin **2**, **4**, **6** and **8**. The UV-visible absorption spectra of the zinc complexes of porphyrin **2**, **4**, **6** and **8** exhibits a slight red shift in the Soret band compared to its free base analogues **1**, **3**, **5** and **7**. The porphyrin **1** and **2** exhibits a red shifted absorption in the soret band compared to other donor substituted porphyrins **3**−**8**. The TPA substituted porphyrin **3** exhibits slight red shift in the fluorescence maxima compared to the free base porphyrin **1**, **5** and **7**. The Zn(II) porphyrin **4** and **6** exhibits a red shifted emission compared to **2** and **8**. The porphyrin **5** and **7** exhibits low electrochemical band gap of 0.71 and 0.70 V compared to rest of the porphyrins. The computational studies on porphyrin **3**−**8** show, the HOMO is spread on the donor unit whereas the LUMO is localized on the porphyrin macrocycle, whereas in **1** and **2** the HOMO and LUMO are populated on porphyrin macrocycle.

a) and b) UV-visible absorption spectra

1, M= H
2, M= Zn

3, M= H
4, M= Zn

5, M= H
6, M= Zn

7, M= H
8, M= Zn
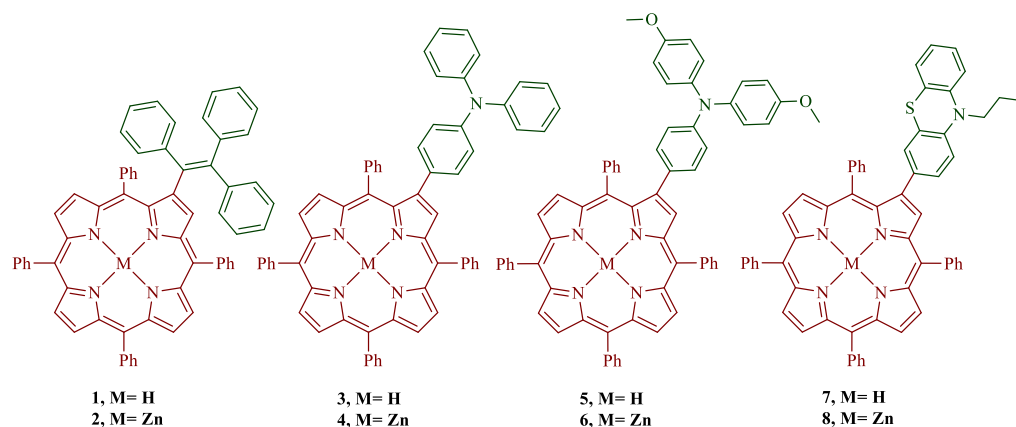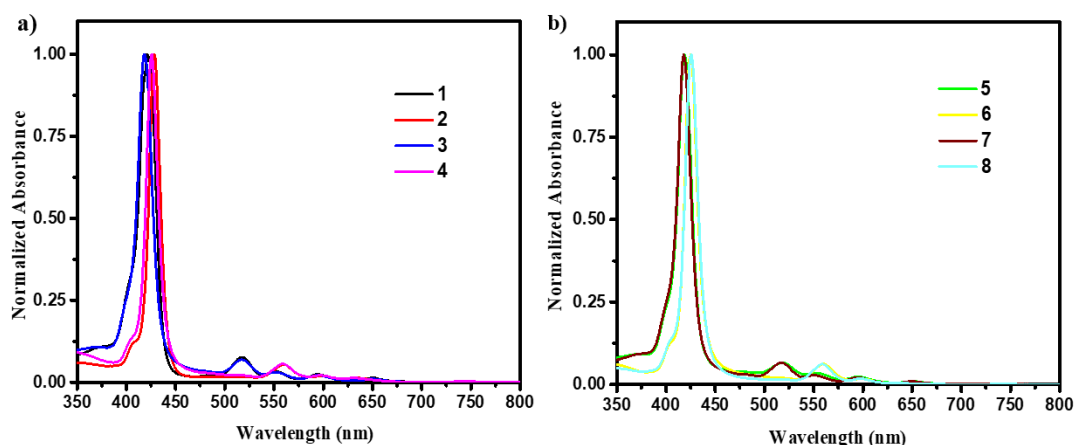
Chapter 6: Acceptor Functionalized Unsymmetrical *β*-Porphyrins

In chapter 6, a series of acceptor functionalized unsymmetrical *β*-porphyrin **1a**–**8d** were designed and synthesized by reacting *β*-monobrominated tetraphenyl porphyrin **9** with the corresponding boronate ester of acceptors *via* Pd-catalyzed Suzuki cross-coupling reaction, followed by the Zn(II) metallation with $Zn(OAc)_2.2H_2O$. The photophysical and computational studies of porphyrins **1a**–**8d** were investigated. The UV-visible absorption spectra of zinc complexes **2a**, **4b**, **6c** and **8d** exhibited a red shifted absorption around 6−8 nm in the high energy region compared to its corresponding free bases **1a**, **3b**, **5c**, and **7d**. The porphyrins **3b**, **4b**, **5c** and **6c** with *p*- and *m*-substituted benzothiazoles at the *β*-pyrrolic position of the porphyrin macrocycle

exhibits a similar absorption spectrum in the Soret and the Q–band region. The emission spectra of electron-deficient naphthalimide substituted Zn(II) porphyrin **2a** exhibits a red shifted emission of about 2–5 nm in the longer wavelength region, compared to benzothiazole and quinoxaline substituted porphyrins **4b**, **6c** and **8d**. The computational study of porphyrin **1a**–**8d** reveals that the porphyrin **1a** and **7d** exhibits a low HOMO–LUMO band gap compared to other free base and Zn(II) porphyrins.

1a, M= H
2a, M= Zn

3b, M= H
4b, M= Zn

5c, M= H
6c, M= Zn

7d, M= H
8d, M= Zn
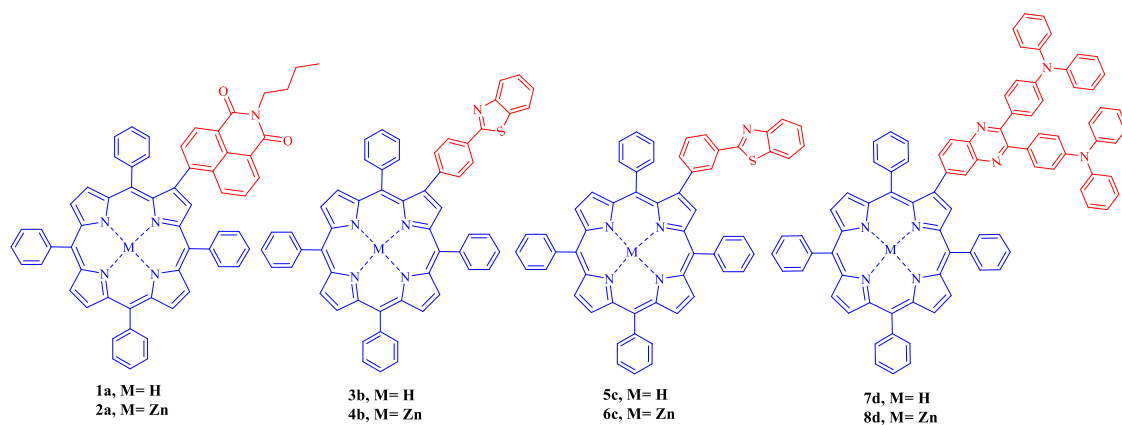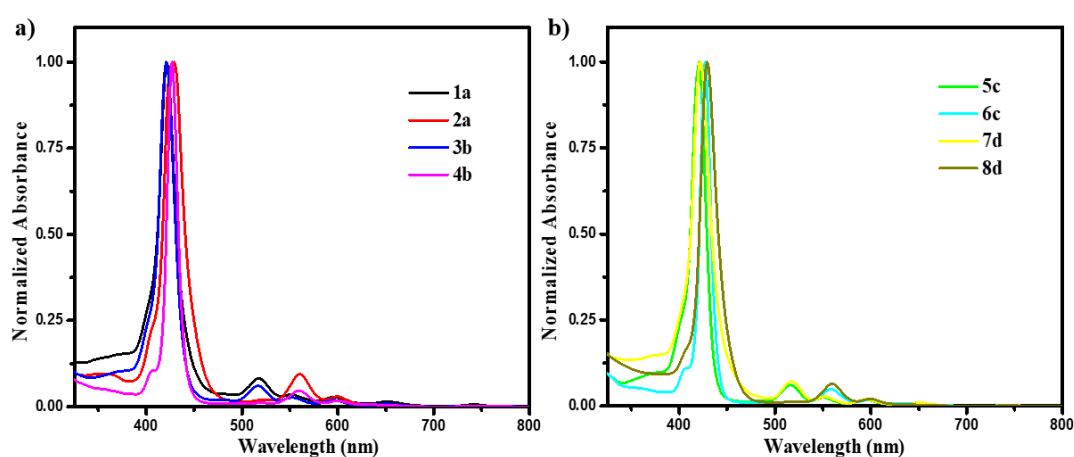
Chapter 7: Triphenylacrylonitrile (TPAN), 1,1,2,2-tetraphenylethene (TPE) and Carbazole Functionalized *β*-Porphyrins

In chapter 7, TPAN, TPE and carbazole substituted unsymmetrical *β*-porphyrins **11**–**18** were synthesized *via* Pd-catalyzed Suzuki cross-coupling reaction and zinc metallation reaction. The photophysical, electrochemical and computational studies of these unsymmetrical porphyrins **11**–**18** were investigated. The UV-Visible absorption spectra of zinc complexes **12**, **14**, **16**, and **18** exhibit red shifted absorption of around 7−9 nm in the soret band region compared to its corresponding free base analogues **11**, **13**, **15** and **17**. The absorption spectra of 2,3,3-triphenylacrylonitrile substituted porphyrin **11**–**14** exhibit similar absorption band in the Soret band and Q-band region. The emission spectra of 2,3,3-triphenylacrylonitrile and 1,1,2,2-tetraphenylethene substituted unsymmetrical porphyrin **11**–**16** exhibits a red shift in the emission maxima of around 4–5 nm, compared to the carbazole substituted porphyrin **17** and **18**. The electrochemical properties of 2,3,3-triphenylacrylonitrile substituted porphyrin **13** exhibits a stabilized HOMO energy levels with low electrochemical band gap of about 1.70 V. The computational studies of porphyrin **11**–**18** shows that the electron density is localized on the porphyrin macrocycle in HOMO whereas in LUMO it is mainly populated on the porphyrin macrocycle with parts dispersed over the phenyl ring of the 2,3,3-triphenylacrylonitrile, 1,1,2,2-tetraphenylethene and carbazole entity.

| 11, M= H | 13, M= H | 15, M= H | 17, M= H |
| 12, M= Zn | 14, M= Zn | 16, M= Zn | 18, M= Zn |
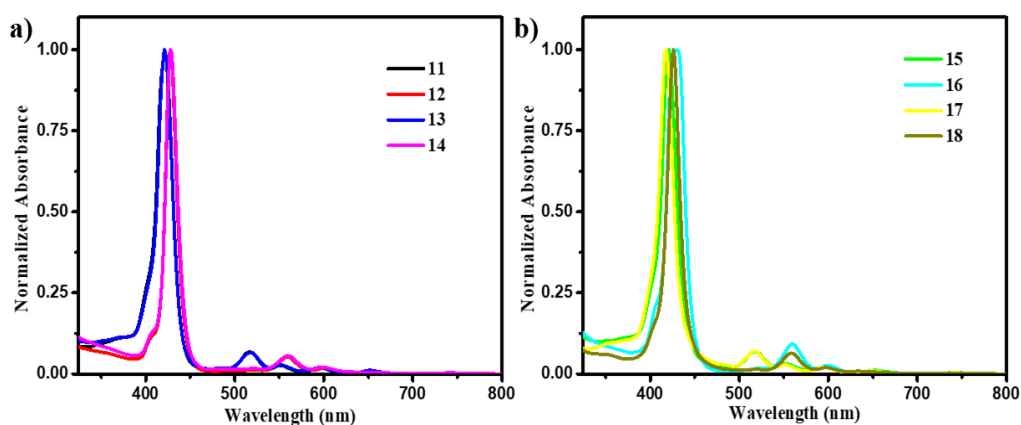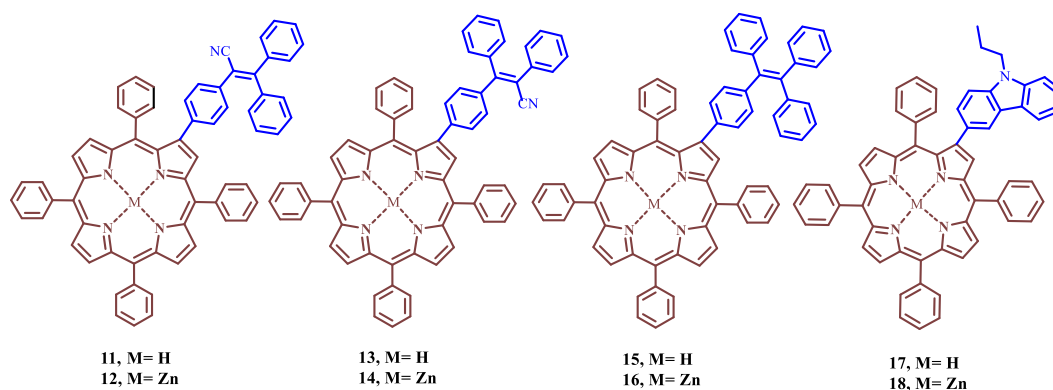
Chapter 8: Conclusions and future scope

This chapter summarizes the salient features of the work and future prospective to develop new materials for optoelectronic applications.

List of Publications

[1] **Bijesh, S.**, Misra, R. (2018). Triphenylamine Functionalized Unsymmetrical Quinoxalines. *Asian J. Org. Chem.*, 7(9), 1882-1892. (DOI: 10.1002/ajoc.201800384).

[2] **Sekaran, B.**, Jang, Y., Misra, R., D'Souza, F. (2019). Push–Pull Porphyrins via β-Pyrrole Functionalization: Evidence of Excited State Events Leading to High-Potential Charge-Separated States. *Chem. Eur. J.*, 25(56), 12991-13001. (DOI: 10.1002/chem.201902286). †

[3] **Sekaran, B.**, Dawson, A., Jang, Y., MohanSingh, K. V., Misra, R., D'Souza, F, (2021) Charge-Transfer in Panchromatic Porphyrin-Tetracyanobuta-1,3-diene-Donor Conjugates: Switching the Role of Porphyrin in the Charge Separation Process. *Chem. Eur. J. Accepted Author Manuscript.* (DOI: 10.1002/chem.202102865) †

[4] Maragani, R., **Bijesh, S.**, Sharma, R., Misra, R. (2017). Cs-Symmetric Donor-Acceptor Bisthiazoles: Synthesis, Photophysical, Electrochemical and Computational Studies. *Asian J. Org. Chem.*, 6(10), 1408-1414 (DOI: 10.1002/ajoc.201700274).

†Papers pertaining to the thesis.

TABLE OF CONTENTS

LIST OF FIGURES

LIST OF SCHEMES

LIST OF TABLES

LIST OF CHARTS

ACRONYMS

D–A	Donor–acceptor
NMR	Nuclear Magnetic Resonance
PPh$_3$	Triphenylphosphine
DMF	Dimethylformamide
DCM	Dichloromethane
Ph	phenyl
IR	Infrared
UV-Vis	UV-Visible Spectroscopy
Calcd.	Calculated
CDCl$_3$	Chloroform-d
ESI-MS	Electrospray Ionization- Mass Spectrometry
EtOH	Ethanol
MeOH	Methanol
THF	Tetrahydrofuran
TLC	Thin Layer Chromatography
TEA	Triethylamine
TPA	Triphenylamine
TCBD	Tetracyanobutadiene
HOMO	Highest Occupied Molecular Orbital
LUMO	Lowest Unoccupied Molecular Orbital
TPP	Tetraphenyl Porphyrin
DSSC	Dye Sensitized Solar Cells
NLO	Nonlinear Optics
PDT	Photodynamic Therapy
CT	Charge-Transfer
TPE	Tetraphenylethene
CHCl$_3$	Chloroform
TPAN	Triphenylacrylonitrile

NOMENCLATURE

λ	Wavelength
ε	Extinction coefficient
α	Alfa
β	Beta
γ	Gamma
π	Pi
ϕ	Fluorescence quantum yield
σ	Sigma
Å	Angstrom
nm	Nanometer
cm	Centimeter
°	Degree
°C	Degree Centigrade
mmol	Millimol
mL	Milliliter
μL	Microliter
a. u.	Arbitrary Unit

Chapter 1

Introduction

1.1. Porphyrin

Porphyrins are a class of tetrapyrrole compounds and are found in nature such as chlorin in chlorophyll, corrin in vitamin B_{12} and as heme in hemoglobin and myoglobin. The porphyrins are promising scaffolds which are intensively investigated in many biological processes such as photosynthesis, electron transfer, detoxification, oxygen storage and transport.[1–8] The porphyrin macrocycle are composed of four pyrrole rings connected by a methine bridge, which consists of four *meso-*positions and eight *beta*-positions as shown in Figure 1.1. The aromatic character of the porphyrin macrocycle, which consists of 18-π electron is evident by its strong diatropic ring current.[9–12] The natural photosynthetic process is carried out by the light harvesting pigments containing porphyrin derivatives such as chlorophylls and bacteriochlorophylls, which convert light energy into chemical energy. The artificial photosynthetic process are used to mimic the natural system by employing the porphyrin chromophores as light harvesting antennae and are used in energy-transfer and electron-transfer processes such as storage and transport of respiratory gases and photosynthesis.[13–16]

The electronic absorption spectra of the porphyrin macrocycles are in the UV-Visible region around 400–600 nm with a characteristic absorption, the Soret and the Q-bands. The different relative intensities of the Q-bands depends on the substitutions at the β-pyrrolic positions of the porphyrin macrocycles.[17–19] The nature of the substituents at the β- pyrrolic positions of the porphyrin are of interest, as it perturbs the photonic and electrochemical redox properties of the porphyrin macrocycle by inducing varying degree of distortion on the planarity of molecules.[20,21] Upon light irradiation, the porphyrin chromophores are excited to a singlet state *via* energy transfer process to produce a triplet excited state by undergoing intersystem crossing (ISC). The long triplet

state lifetime and their high quantum yield for intersystem crossing for porphyrin chromophore, employs them as a robust electron transporter.[22–24] Due to the ability of porphyrin macrocycles to transfer energy and electron in their excited state, these chromophores are employed in photosensitization and photoredox catalysis.[23,25–27] The porphyrin macrocycle have been used as a building block in the design and synthesis of donor–acceptor (D–A) molecular systems and shows a wide range of applications in areas such as catalysis, sensing, dye-sensitized solar cells (DSSCs), photodynamic therapy (PDT) and nonlinear optics (NLO).[28–34]

The peripheral substitution of donor and acceptor units on the porphyrin macrocycle perturbs its photonic and electronic properties.[35–37] The porphyrin based D–A systems are employed in organic solar cells (OSC) due to its light harvesting ability, efficient electron transfer capability and tunable optical and electronic properties.[38–43] The porphyrin-based D–A systems are extensively used in dye sensitized solar cell (DSSCs) applications.[44,45] This chapter focus on the synthetic aspects of the β-substituted porphyrins and their optical and electrochemical properties for better understanding about their application in organic photovoltaics, non-linear optics, photodynamic therapy and its supramolecular chemistry as chemosensors.
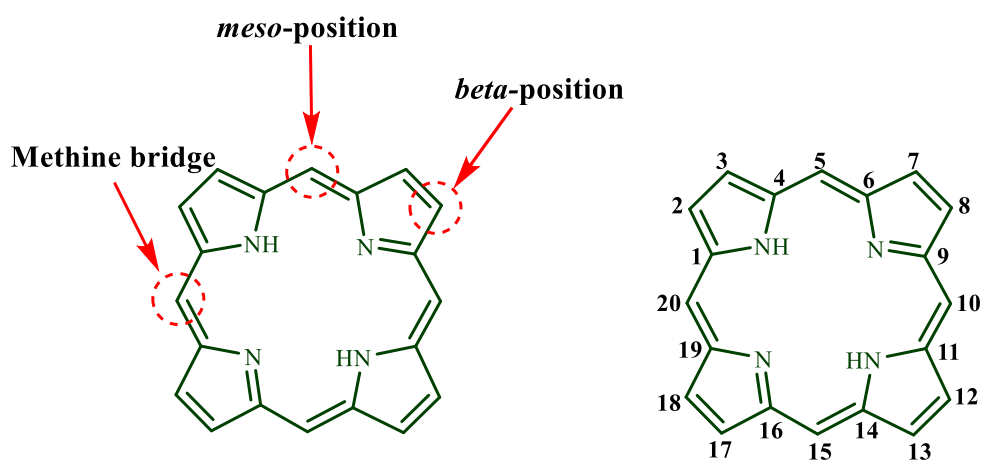
Figure 1.1. The structure and numbering of porphyrin molecule.

1.2. Synthesis

Porphyrins are highly versatile, due to the ability to fine-tune its photophysical and electrochemical properties of the macrocycle by *meso* and *β*-substitutions. The modification of the *β*-substituents on the porphyrin ring can results in a highly unsymmetrical porphyrinic architecture. [20, 21] The synthetic approach of the *β*-functionalized porphyrins are tedious and remains much unexplored till date due its difficulties in separation. In this section, we discuss the functionalization at the *β*-pyrrolic positions *via* bromo, formyl, vinyl, ethynyl, nitro and amino groups for the construction of more elaborate push-pull architectures.

1.2.1. General Synthesis of *meso*-Tetraphenylporphyrins (1)

5,10,15,20-tetraphenylporphyrin (H$_2$TPP) **1** and its analogues are of interest for researcher due to its ease of preparation, diverse metal coordination and facile functionalization at the *meso* and *β*-positions. The symmetrical free base porphyrin was synthesized in low yield by Rothemund *et al*. in 1935 by treating aldehyde and pyrrole in pyridine and methanol at 220 °C for 48 hours. [46–48] Later Alder *et al*. improved this method to attain higher yield, by using propionic or acetic acid at 141 °C for 30 min (Scheme 1.1).[49] The 2-step 1-flask synthetic procedure of 5,10,15,20-tetraarylporphyrins **1** was reported by Lindsey *et al*. with first step involving the condensation of aldehyde and pyrrole using trifluoroacetic acid (TFA) or boron trifluoride (BF$_3$)–etherate as catalyst in CH$_2$Cl$_2$ around 1 h, which resulted in porphyrinogen. The second step involves the conversion of porphyrinogen to porphyrin with the addition of an oxidant, DDQ or p-chloranil to attain 30–40% yields (Scheme 1.1). [50–52] The porphyrins are aromatic in nature and can be functionalized at its *β*-pyrrolic positions. Porphyrins undergo a series of reactions at the *β*-pyrrolic positions such as aromatic electrophilic substitution, oxidation, reduction and pericyclic reactions.

i.) Rothemund: Pyridine, CH$_3$OH, 220 °C
ii.) Alder: CH$_3$CH$_2$COOH/CH$_3$COOH reflux, 30 min.
iii.) Lindsey: a.) TFA (or) BF$_3$-etherate, CH$_2$Cl$_2$,
b.) DDQ
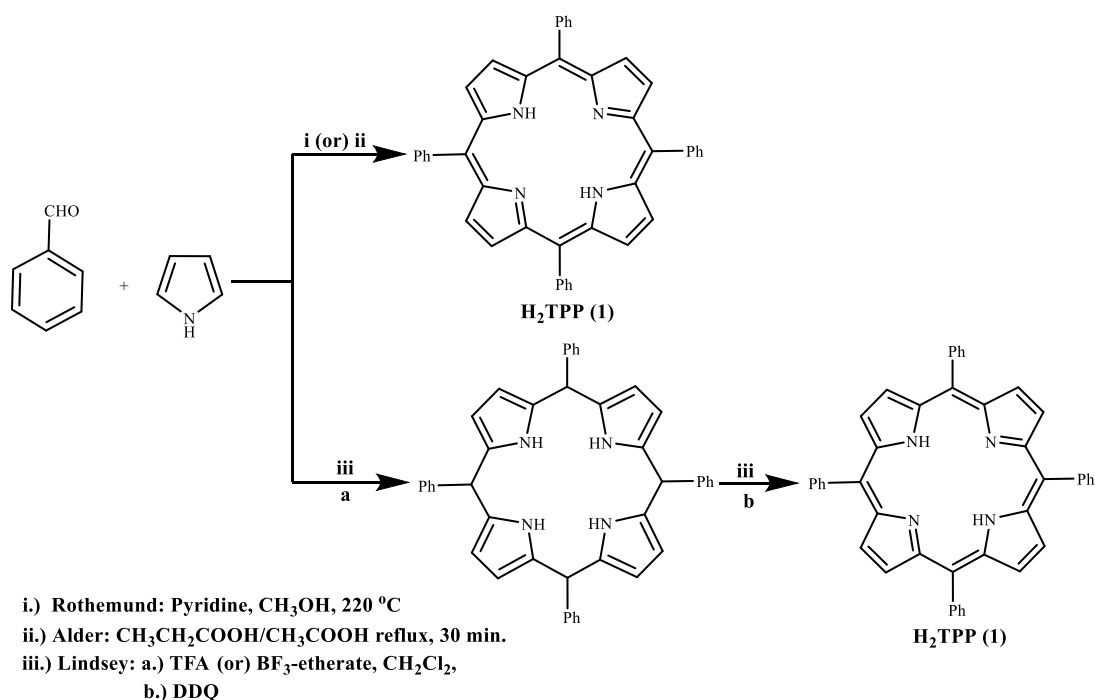
Scheme 1.1. Synthetic scheme of *meso*-tetraphenylporphyrins **1**.

1.2.2. Synthesis of *β*-bromo substituted tetraphenyl porphyrin (H$_2$TPPBr$_n$) (2)

The *β*-pyrrole halogenated porphyrins are of interest owing to their use as precursors for synthetic modification and further functionalization. The bromo substituents at the *β*-pyrrolic positions influence the π-electron system of the porphyrin macrocycles, which can further alter their optical and electrochemical properties. The *β*-bromo substituted tetraphenylporphyrin **2a**, **2b**, **2c** and **2d** were first reported by Callot *et al.* in 1973 by treating tetraphenylporphyrin **1** with N-bromosuccinimide (NBS) in chloroform, which resulted in a complex mixture of mono and poly *β*-bromo substituted tetraphenylporphyrins (H$_2$TPPBr$_n$) (n=1–8) **2** (Scheme 1.2). [53a,54] Bhyrappa *et al.* reported the synthesis of *β*-dibrominated TPP, by treating tetraphenylporphyrin **1** with 2.8 equiv. of N-bromosuccinimide (NBS) in chloroform at room temperature for 24 hours, which resulted in H$_2$TPPBr **2a** and H$_2$TPPBr$_2$ **2b** as a isomeric mixture of the products. The *β*-dibromoporphyrin H$_2$TPPBr$_2$ **2b** consists of mixture of isomers with (2,12) or (2,13) as major product and (2,3) as minor dibrominated product. [53a, 53b] Crossley *et al.* reported

4

7,8,17,18-tetrabromo-5,10,15,20-tetraphenylporphyrin by treating tetraphenylporphyrin **1** with 4.3 equiv. of N-bromosuccinimide (NBS) in chloroform, which resulted in H_2TPPBr_4, **2c** in 80% yield. [53a, 53c] Krishnan *et* *al*. synthesized the free-base octabromotetraphenylporphyrin (H_2TPPBr_8) using the bromination reaction on (*meso*-tetraphenylporphyrinato) copper(II), (CuTPP) followed by an acid demetallation reaction. The CuTPP was dissolved in $CHCl_3/CCl_4$ (1:l v/v) was treated with excess amount of liquid bromine in $CHCl_3/CCl_4$ solvent mixture and stirred for a period of 4 hours at room temperature and then pyridine in solvent mixture was added dropwise and the solution was stirred for another 12 h, which resulted in H_2TPPBr_8 **2d**. [53a, 53d] The steric crowding in the porphyrin ring results in a non-planar conformation of **2d** due to the increased number of substituents at the β-pyrrolic positions.
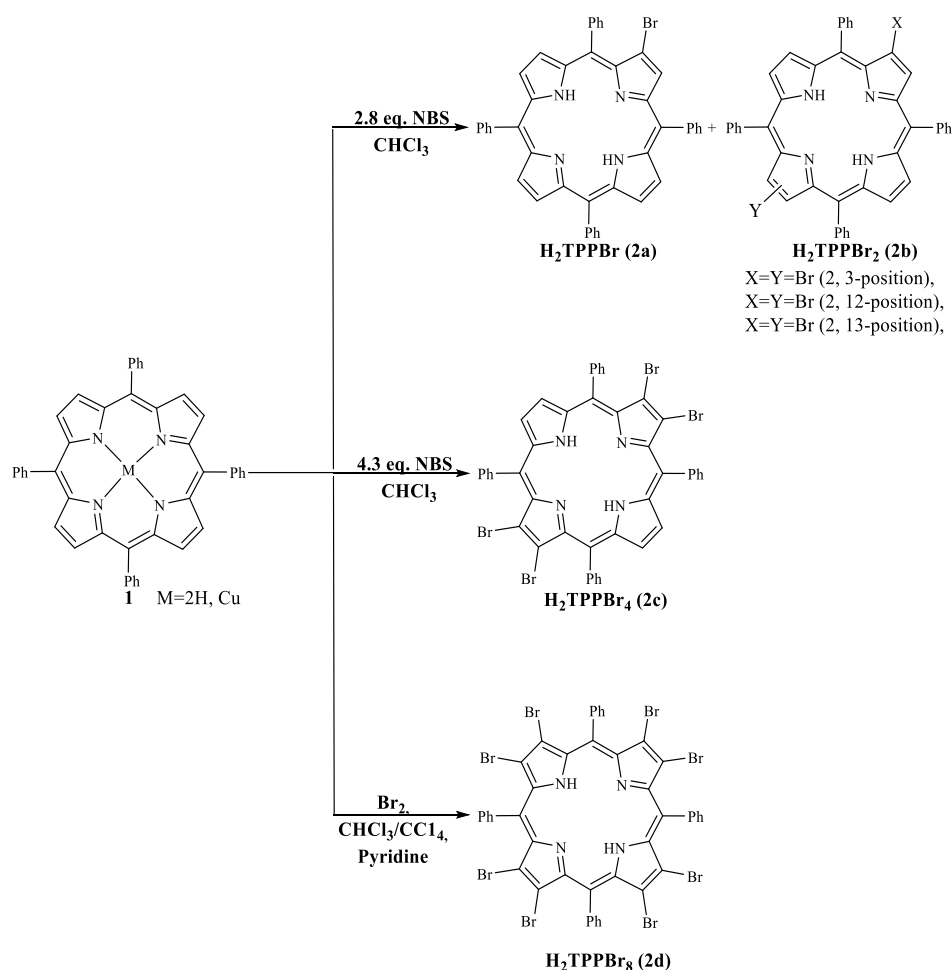
Scheme 1.2. Synthesis of β-bromo substituted tetraphenyl porphyrin (H_2TPPBr_n) (n=1–8) **2**.

1.2.3. Synthesis of *β*-formyl-*meso*-tetraphenylporphyrin (3)

In 1966, Inhoffen and Johnson reported the use of Vilsmeier-Haack reaction to introduce the formyl group at the *β*-pyrrolic position of the porphyrins.[55–57] The Vilsmeier–Haack formylation at the *β*-pyrrolic position of *meso*-tetraarylporphyrin **1** was carried out by Ni (II) or Cu(II) complexes due to their acid lability (Scheme 1.3). The formylation of *meso*-tetraarylporphyrins **1** using Zn(II) and Mg(II) complexes resulted in low reactivity, due to the demetallation of porphyrin macrocycles.[58–62] Later, Crossley *et al.* reported the *β*-formyl-*meso*-tetraphenylporphyrin (*β*-H$_2$TPPCHO) **3** in 95% yield by the demetallation of the iminium salts using concentrated H$_2$SO$_4$ and basic hydrolysis (Scheme 1.3).[63]
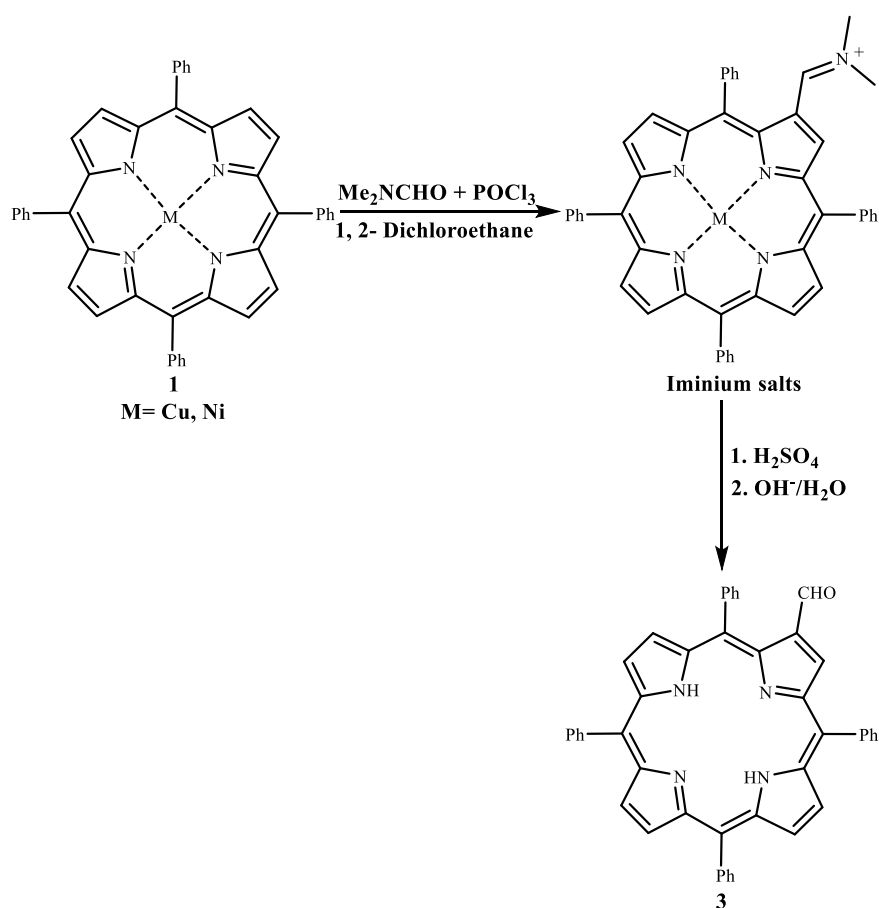
Scheme 1.3. Synthesis of *β*-formyl-*meso*-tetraphenylporphyrin **3**.

1.2.4. Synthesis of *β*-vinyl-*meso*-tetraarylporphyrins (4)

The *β*-vinyl-*meso*-tetraarylporphyrins **4** was reported by callot *et al.* in 1973 using wittig reaction, by treating Ni(II) complex of *β*-formyl-*meso*-tetraphenylporphyrin **3** with methyltriphenylphosphonium bromide in the presence of n-butyllithium in THF at room temperature which resulted *β*-vinylTPP **4** in 52% yield (Scheme 1.4).[58] This synthetic protocol results in good yield with free-base, zinc and copper complexes. Later, Officer and co-worker prepared *β*-vinylTPP **4** in free-base and Zn metallated form with quantitative yields using wittig reactions performed under mild conditions. The Wittig reaction was performed by treating porphyrin aldehyde with three equivalent of phosphonium salt dissolved in toluene with DBU in excess under reflux condition which results in *β*-vinyl-*meso*-tetraarylporphyrins **4**. The *β*-vinyl-*meso*-tetraarylporphyrin **4** is used as 4π and 2π dienes and dienophiles in Diels–Alder Cycloaddition reaction.[64–67]
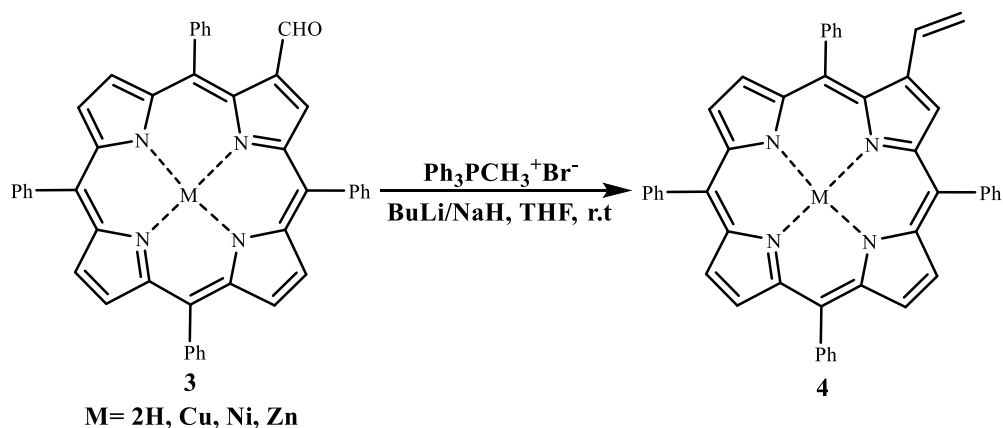
Scheme 1.4. Synthesis of *β*-vinyl-*meso*-tetraarylporphyrins **4**.

1.2.5. Synthesis of *β*-ethynyl-*meso*-tetraarylporphyrins (5)

In 1994, Lier *et al.* reported the synthesis of *β*-ethynyl porphyrin **5** by the Pd-catalysed Sonogashira cross-coupling reaction. The Ni(II) or Cu(II) *β*-halogenated porphyrins was treated with TMS-acetylene in the presence of bis(triphenylphosphine)palladium(II) chloride and CuI, dissolved in a mixture of triethylamine and DMF solvent at 85 °C for 48 h resulted in *β*-ethynyl porphyrin **5** in 60–80% yields (Scheme 1.5).[68] Later in 2006, Schuster and co-worker reported *β*-ethynyl tetraarylporphyrin **5** *via* *β*-(Trimethylsilyl)ethynyl porphyrin intermediate **2a** using sonogashira cross-coupling reaction and further deprotection of **2a** was carried out using tetrabutylammonium fluoride (TBAF) in THF at room temperature.[69] Recently in 2016, Zhao *et al.* reported the synthesis of Zn(II) *β*-ethynyl-*meso*-tetraarylporphyrin **5** by treating Zn(II) *β*-bromo tetraarylporphyrin with triisopropylacetylene in the presence of Pd(PPh$_3$)$_2$Cl$_2$ in triethylamine and THF solvent, resulted in 82% yields.[70]
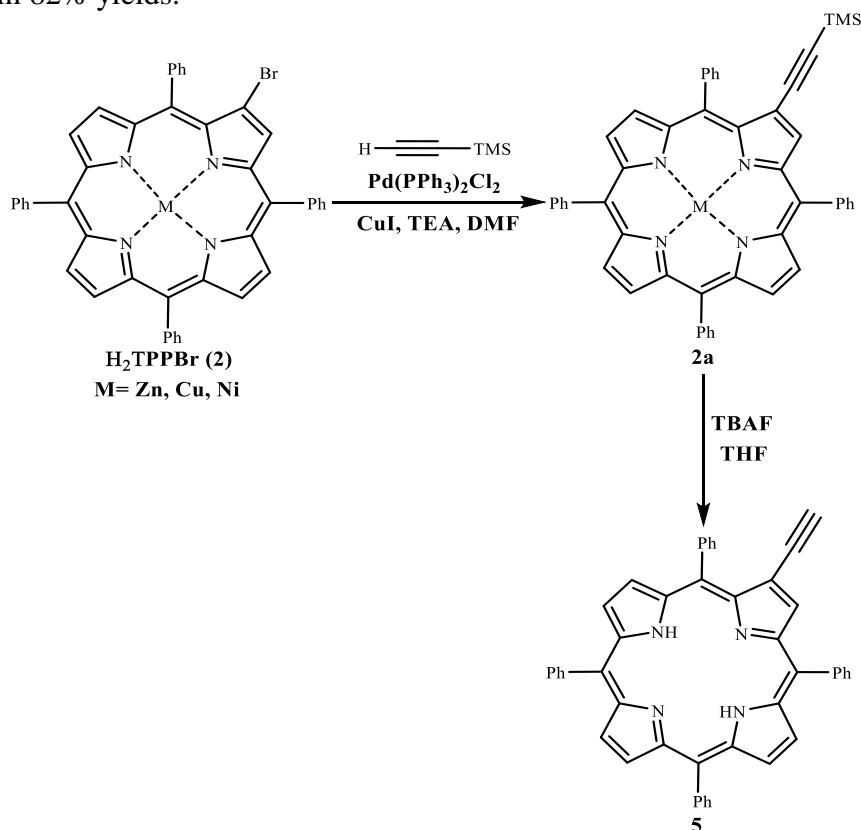
Scheme 1.5. Synthesis of *β*-ethynyl-*meso*-tetraarylporphyrins **5**.

1.2.6. Synthesis of *β*-nitro-*meso*-tetraarylporphyrins (6)

In 1977, Callot and Jordan synthesized Cu(II) complex of *β*-nitro tetraphenylporphyrin **6** by reacting Cu(II) complex of tetraphenylporphyrin Cu(II)TPP with $Cu(NO_3)_2.6H_2O$ in acetic anhydride dissolved in a mixture of chloroform and acetic acid for 1 h at 30–35 °C (Scheme 1.6).[71] The *β*-nitro tetraphenylporphyrin **6** was synthesized from the demetallation of $Cu(II)TPPNO_2$ by treating with concentrated sulfuric acid and aqueous ammonia and then recrystallization from DCM : MeOH solvent mixture. In 1982, Baldwin *et al.* synthesized Zn(II) complex of *β*-nitro tetraphenylporphyrin **6** using Zn(II) complex of tetraphenylporphyrin (Zn(II)TPP) with silver nitrite dissolved in acetonitrile followed by iodine in dichloromethane solvent (Scheme 1.6).[72] Later in 1986, Jackson and coworkers reported the nitration of TPP using nitronium tetrafluoroborate in pyridine : chloroform mixture at 140 °C, resulted in *β*-nitro tetraphenylporphyrin **6** (Scheme 1.6).[73] Smith *et al.* in 1998, reported an alternate method for nitration of Cu(II)TPP using dinitrogen tetraoxide (N_2O_4), followed by demetallation in H_2SO_4.[74]

i.) $Cu(NO_3)_2.6H_2O/N_2O_4$, AC_2O, CH_3COOH, $CHCl_3$
ii.) $AgNO_2$, CH_3CN, I_2, CH_2Cl_2
iii.) NO_2BF_4, Pyridine, $CHCl_3$,
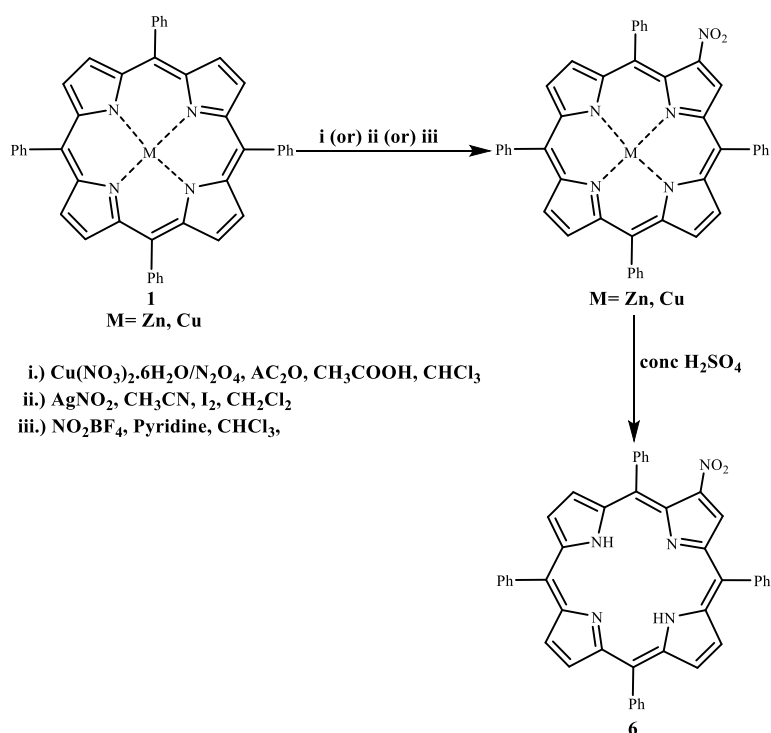
Scheme 1.6. Synthesis of *β*-nitro *meso*-tetraarylporphyrins **6**.

1.2.7. Synthesis of *β*-amino-*meso*-tetraarylporphyrins (7)

The most common protocol for the synthesis of *β*-amino-tetraarylporphyrins **7** is the reduction of *β*-nitro tetraphenylporphyrin **6** using SnCl$_2$/HCl, Sn/HCl, HCOONH$_4$/Zn, HCOONH$_4$/Pd/C, NaBH$_4$/Pd/C and H$_2$/Pd/C.[75–79] In 1982, Baldwin *et al.* synthesized *β*-aminoporphyrin **7** in quantitative yield, by hydrogenating *β*-nitroporphyrin **6** using sodium borohydride in presence of palladium on carbon catalyst in a mixture of DCM : methanol solvent (Scheme 1.7).[72] The alternate method for the reduction of *β*-nitroporphyrin **6** was carried out using Sn(II)chloride with hydrochloric acid which resulted in *β*-aminoporphyrins **7** (Scheme 1.7).

i.) SnCl$_2$/HCl
ii.) NaBH$_4$-Pd/C
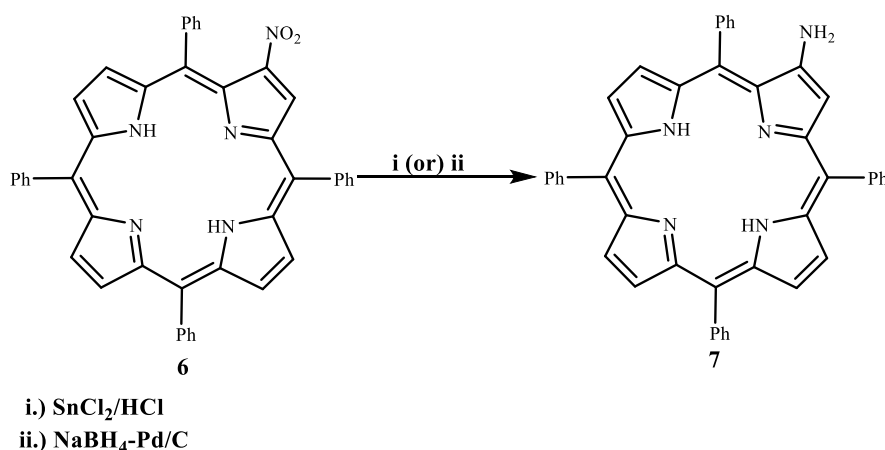
Scheme 1.7. Synthesis of *β*-amino-*meso*-tetraarylporphyrins **7**.

The porphyrin macrocycle having bromo, formyl, vinyl, ethynyl, nitro and amino substituents at the *β*-pyrrolic position act as a versatile building block for the design and synthesis of diverse porphyrin analogues. The porphyrin π-system conjugated with the *β*-substituents significantly modulate the electronic absorption, electrochemical redox potential, HOMO–LUMO gap and the planarity of the macrocycle. The degree of nonplanarity on the porphyrin macrocycle depends on the steric hindrance caused by the donor or acceptor substituents at the *β*-pyrrolic position, which in turn induce large dipole moment in the molecule.

1.3. Electronic properties

The porphyrin macrocycle exhibits a characteristic absorption profile in the UV−visible region, which includes a high energy Soret band with high intensity and a low energy Q band with low intensity. Tuning of the optical and electronic properties of the porphyrin macrocycle have been investigated over years to improve the efficacy of a wide range of applications including organic light emitting diodes, photodynamic therapy, nonlinear optics, dye sensitized solar cells, single molecule switches and many more. [28–34] The photophysical properties of the porphyrins can be tuned by altering the electron donor or acceptor substituents at the *meso* or *β*-position of the macrocycle. Porphyrin analogues are used in the investigation of the intramolecular excitation energy transfer to mimic the natural photosynthetic systems.

Gupta *et al.* investigated the energy transfer of *β*-donor substituted porphyrin dyads **8−13** with *N*-butylcarbazole and triphenylamine as donor units (Chart 1.1).[80] The dyads show an efficient energy transfer up to 93% from the *β*-donors to the porphyrin macrocycle. The efficiency of energy transfer in the *β*-pyrrolic position of porphyrins showed better result compared to those of the *meso*-substituted porphyrins. The optical, electrochemical and DFT studies of porphyrin dyads **8−13** were investigated. The UV-visible absorption spectra of *β*-donor substituted porphyrin dyads **8−13** exhibits a red shifted absorption in the Soret bands region compared to unsubstituted porphyrins H_2TPP, ZnTPP and PdTPP. The fluorescence spectra of dyads **8−11** exhibits red shifted emission in the visible region compared to the unsubstituted porphyrins due to the effect of donor substitutents at the *β*-pyrrolic positions. The reduced emission quantum yields of the dyads **8−11** may be attributed to the increased non-radiative decay processes in the systems. The electrochemical band gap of dyads **8** and **9** were similar to that of H_2TPP, whereas in dyads **10** and **11** there was a slight difference from that of ZnTPP. The computational study reveals that the transitions involved in dyads **8** and dyads **10−13** belongs to π–π* transitions,

whereas intramolecular charge transfer (ICT) was observed in the dyad **9**.

8, M= 2H
10, M= Zn
12, M= Pd

9, M= 2H
11, M= Zn
13, M= Pd
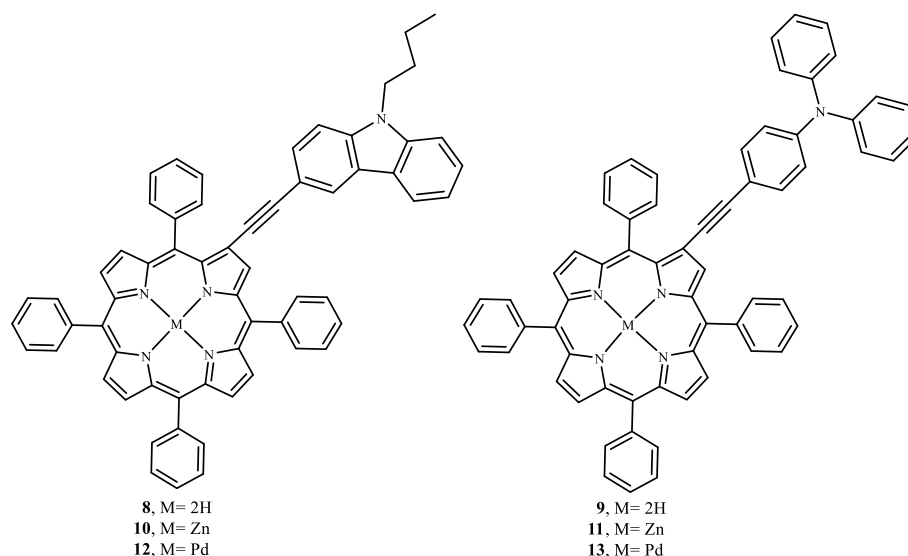
Chart 1.1. Porphyrin based chromophore **8−13**.

Kadish *et al.* investigated the electrochemistry of two series of ethyl acetoacetate (EAA), acetylacetone (acac) and ethyl acetate (EA) appended β-substituted tetraphenylporphyrins MTPP(EAA)X_2 **14**, MTPP(acac)X_2 **15** and MTPP(EA)X_2 **16** with two antipodal positions occupied by H, Br or Ph groups. The porphyrin **14**, **15** and **16** was investigated in dichloromethane containing 0.1 M tetrabutylammonium perchlorate both in neutral and basic conditions (Chart 1.2).[81] The trisubstituted porphyrins **14**, **15** and **16** can be switched into their enolate form which is highly electroactive and can be obtained by the chemical deprotonation processes and the electrochemical reduction method. The singly reduced porphyrins are highly stable on the cyclic voltammetry timescale whereas the doubly reduced porphyrins are highly reactive leading to a deprotonated substituent. The doubly reduced EAA and acac porphyrin derivatives **14** and **15** are highly reactive leading to a deprotonated EAA$^-$ or acac$^-$ (enolate) substituents. Compared to neutral porphyrins, the mono-anionic porphyrins are harder to reduce by 110–160 mV due to their interaction between the porphyrin π-ring system and deprotonated EAA$^-$ or acac$^-$ (enolate) substituents.
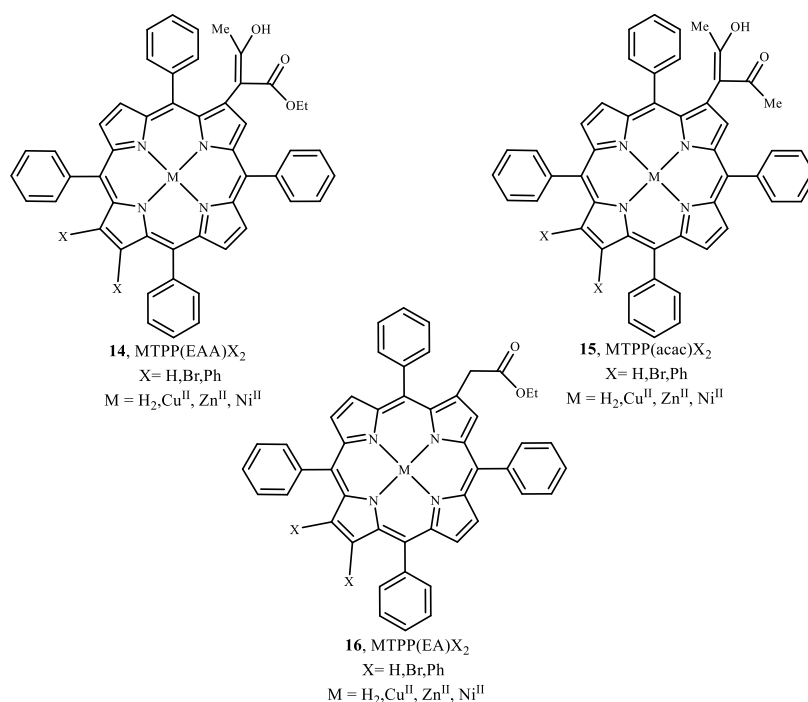
Chart 1.2. Porphyrin based chromophore **14−16**.

Gordon *et al.* reported a series of ethenyl ferrocene substituted *β*-pyrrolic Zn(II) porphyrin, ZnTPP-Fc-R, **17−20** with various electron-accepting groups attached to the other cyclopentadiene unit of the ferrocene (Chart 1.3). The computational study and electronic properties of ethenyl ferrocene substituted *β*-pyrrolic Zn(II) porphyrin **17−20** were studied.[82] The transient absorption spectra of these molecules were recorded in dichloromethane and their singlet and triplet-state lifetimes were investigated. The ethenyl ferrocene substituted *β*-porphyrin **17** shows decreased lifetime (18.1 μs) in triplet excited states compared to that of ZnTPP (22 μs). The substituted ethenyl ferrocene porphyrins **18−20** does not show any influence in singlet state but shows further decrease in the triplet-state lifetime by 10.4−10.6 μs, compared to the unsubstituted ferrocene porphyrin **17** with an increase in the nonradiative decay pathways which confirms that the ferrocene units are deactivating the triplet state.
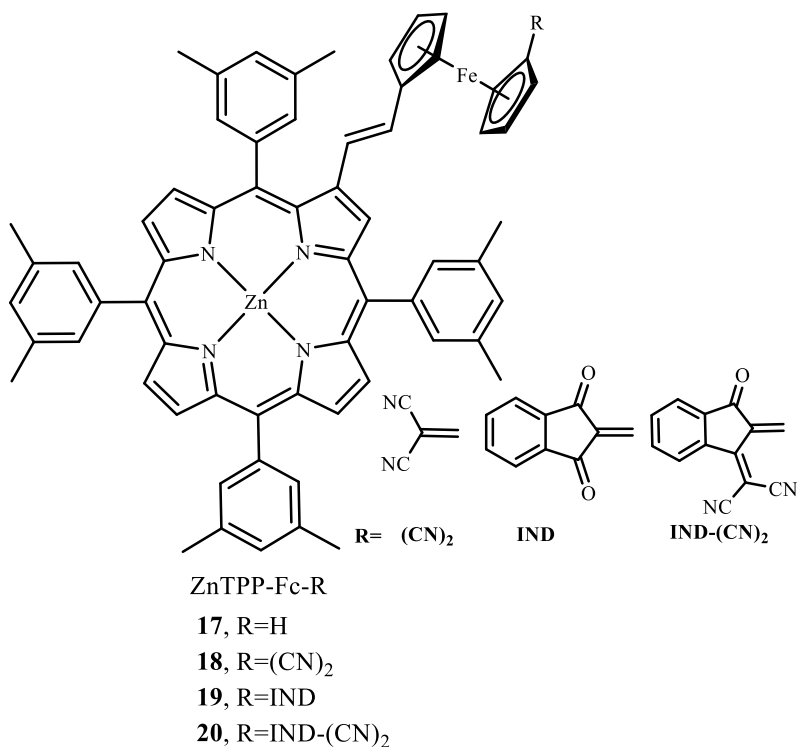
Chart 1.3. Porphyrin based chromophore **17−20**.

Sankar *et al.* synthesized fused nickel (II) porphyrin Ni(II)(NH)TPP **21**, Ni(II)(NH)(CHO)TPP **22** and Ni(II)(N−CH₃)(CHO)TPP **23** with electron donating methyl group in it (Chart 1.4.). The influence of electron donating methyl group on optical and electrochemical redox properties were investigated.[83] The *N*-methylated fused nickel(II) porphyrin **23** showed a red-shifted absorption spectrum compared to their precursors Ni(II)-fused porphyrin **21** and *β*-formyl Ni(II)-fused porphyrin **22** which might be due to the presence of electron donating methyl group. The electrochemical properties of Ni(II)(N-CH₃)(CHO)TPP **23** exhibits a anodic shift in the first oxidation and the reduction wave compared to Ni(II)(NH)TPP **21**. The Ni(II)(N-

CH$_3$)(CHO)TPP **23** exhibits the third oxidation wave related to the oxidation of Ni(II) to Ni(III) ions.

21, Ni(II)(NH)TPP   **22**, Ni(II)(NH)(CHO)TPP

23, Ni(II)(N-CH$_3$)(CHO)TPP
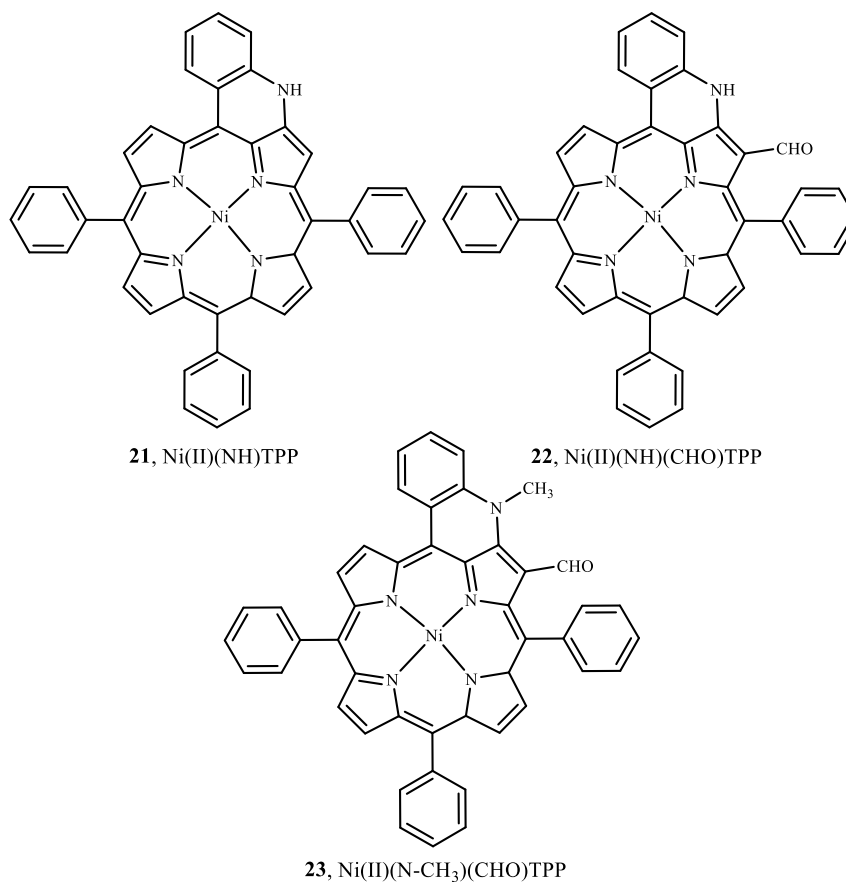
Chart 1.4. Porphyrin based chromophore **21−23**.

Sankar and co-worker synthesized and characterized two series of β-substituted push-pull porphyrin (M= H$_2$, Co, Ni, Cu, or Zn and R= Br/Ph), MTPP(R$_2$)acac **24** and MTPP(R$_2$)EA **25** with acetylacetone (acac) or ethyl acetate (EA) acceptor units and the Br/Ph group at the opposite antipodal β,β'-positions of the porphyrin macrocycle (Chart 1.5).[84] The nickel porphyrin with acetylacetone (NiTPP(Br)$_2$acac) **24** exhibits a nonplanar conformation whereas the free base H$_2$TPP(Br)$_2$EA **25** and zinc porphyrin ZnTPP(Ph)$_2$EA **25** shows quasi-planar conformation, which was evidenced from the single crystal X-ray diffraction analysis. The acetylacetone appended dibromo substituted porphyrins MTPP(Br)$_2$acac **24** shows hydrogen bonded dimers which may be due to the formation of keto-enol tautomerism. The frontier molecular orbitals of H$_2$TPP(Ph)$_2$acac **24** shows that the HOMO and

LUMO had a contribution from the porphyrin macrocycle as expected for electron deficient porphyrins, whereas the LUMO+2 shows the contribution from both, the meso-phenyl units and the porphyrin ring.
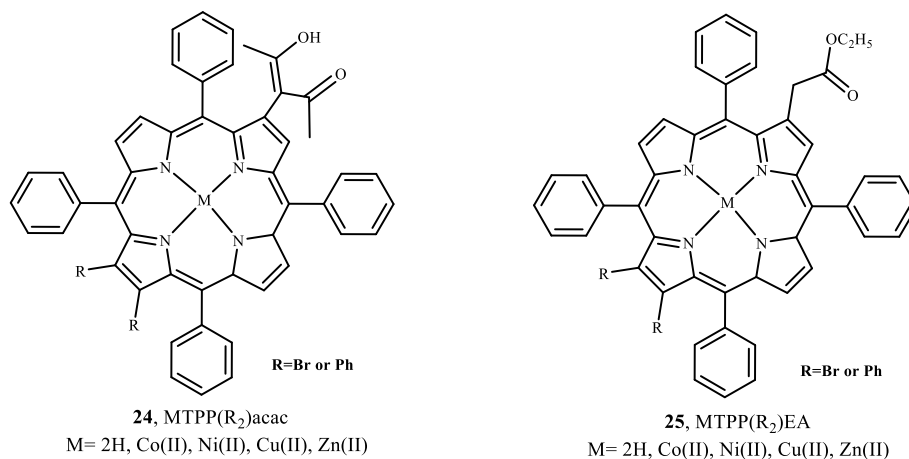
Chart 1.5. Porphyrin based chromophore **24** and **25**.

Maurya and co-worker reported β-substituted tetrabromo vanandyl porphyrin **26** and investigated their optical, electrochemical, computational and catalytic applications in the epoxidation of alkenes (Chart 1.6).[85] The optical spectrum of porphyrin **26** show one Soret and two Q-band in which the soret band exhibits similar absorption maxima whereas first Q-band shows redshift and the second Q-band exhibits blue shift compared to H_2TPPBr_4. The electrochemical studies show two oxidation and two reduction potential for porphyrin **26**. The β-substituted tetrabromo vanandyl porphyrin **26** was used as the catalyst in the epoxidation of alkenes which shows good conversion efficiency and TOF of 7600–9800 h^{-1} with low reaction time of 0.5 h.

. X= Br
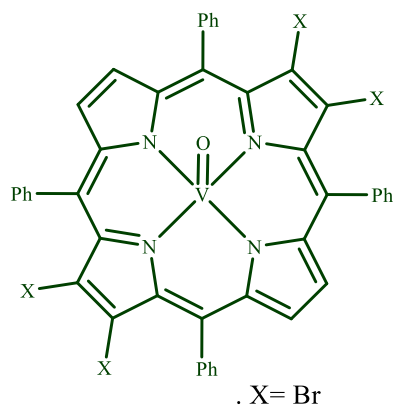
26

Chart 1.6. Porphyrin based chromophore **26**.

1.4. Applications of *β*-functionalized porphyrins

The porphyrin based *β*-substituted D–A systems have been explored for various applications. Some of the important applications are discussed here.

1.4.1. Sensors

Chemosensors based on porphyrins are well known for anion sensing, such as CN^-, F^- and ^-OAc ions. The complexation of anionic species by an appropriate binding sites using *β*-substituted porphyrin systems are gaining much attention in supramolecular chemistry. The molecular sensing can be detected using spectrophotometric and spectrofluorimetric measurements with the changes observed in the absorption and emission spectra. The porphyrin sensors are mostly based on *meso*-substituted porphyrin macrocyles whereas the *β*-substituted porphyrins are not much explored.[86] In this section, we have explored the ion-sensing properties of *β*-substituted porphyrin and their analogues which are employed as chemosensors in the detection of anions and metal ions. Here we have discussed the excellent available examples of *β*-porphyrin analogues with ion-sensing properties.

Sankar *et al.* reported *β*-substituted octa-phenylethynyl porphyrin, ZnTPP(PE)$_8$ **27** and their Co(II), Ni(II), Cu(II) and Zn(II) metal complexes (Chart 1.7).[87] The photophysical and solvatochromic studies on porphyrin **27** were carried out. In *β*-substituted octa-phenylethynyl porphyrins and their metal complexes, only ZnTPP(PE)$_8$ **27** was utilized as chemosensors for the naked-eye detection of Cl$^-$, Br$^-$, CN$^-$, F$^-$, CH$_3$COO$^-$ and H$_2$PO$_4^-$ ions. The Zn(II) metal centre shows high binding constants of 10^{12} to 10^7 M^{-2} through axial coordination of anions, which was explained by axial ligation studies with anions in toluene.

27
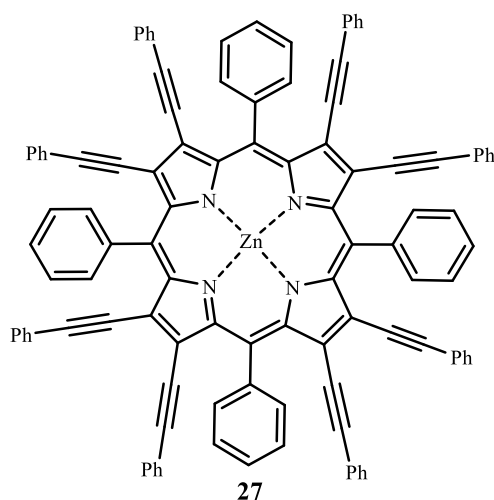
Chart 1.7. Porphyrin based chromophore **27**.

The *β*-substituted dicyanovinyl porphyrin and its nickel complexes **28−31** were synthesized by Sankar *et al.* and were employed as chemodosimeters for the detection of cyanide ions (Chart 1.8).[88] The electronic absorption spectra, electrochemical redox properties and single crystal X- ray of these porphyrins **28−31** were explored. The *β*-substituted dicyanovinyl porphyrin exhibits excellent sensing ability after the addition of CN$^-$ ions with the unperturbed blue shifted absorption spectrum and the lowest detection limit (LOD) of 0.023-0.082 ppm. The sensing ability of chemodosimeter was confirmed by the formation of cyanide addition adduct which was confirmed by the ^{1}H-NMR titrations and ESI-mass spectrometry.
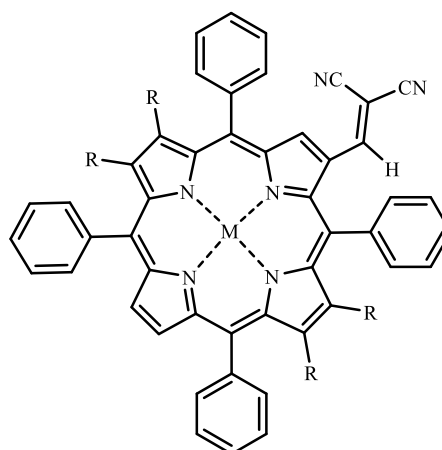
28, R=H; M= Ni
29, R=H; M= 2H
30, R=Ph; M= Ni
31, R=Ph; M= 2H

Chart 1.8. Porphyrin based chromophore **28−31**.

The efficient synthetic protocol for porphyrin–pyrazole conjugates **32a–d** were reported by Lodeiro *et al.* by treating phenylhydrazine with *β*-porphyrin–chalcone derivatives in acetic acid (Chart 1.9).[89] The metal binding ability of porphyrin–pyrazole analogues with Cu^{2+}, Zn^{2+}, Cd^{2+}, and Hg^{2+} were investigated. The porphyrin–pyrazole conjugates shows significant changes in the ground state and excited state of the absorption spectra. The sensing ability of porphyrin–pyrazole conjugates with Zn^{2+} ion and selective detection of Cu^{2+} and Ag^+ in gas phase shows considerable changes in the emission spectra, which was analysed by spectrophotometric and spectrofluorimetric titrations.
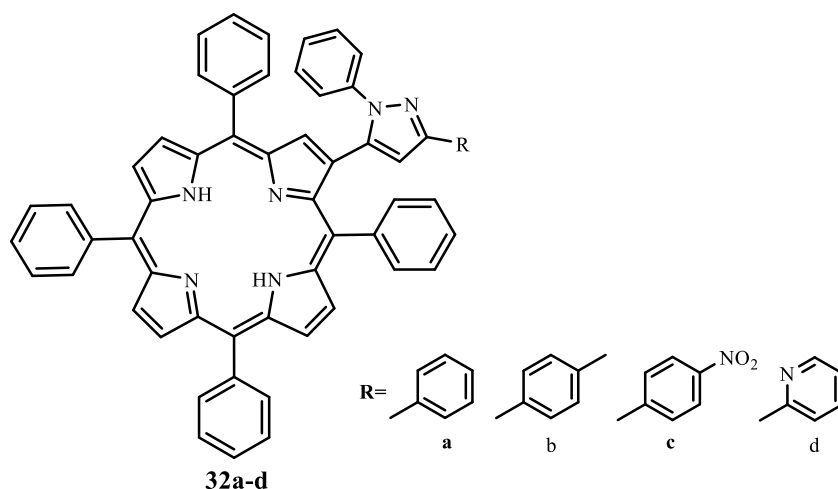
Chart 1.9. Porphyrin based chromophore **32a–d**.

1.4.2. Dye-sensitized solar cells (DSSCs)

In recent years, the global energy consumption has increased drastically due to the population growth in developing countries. The fossil fuels such as coal, crude oil and natural gas are the major energy resources which contributes around 80% of the global energy consumtion. The environmental pollution and the depletion of the fossil fuels are the major concern to approach for the alternate source of energy. The solar energy remains as an alternate for fossil fuels, which are highly desirable due to its artificial photosynthetic technology. After Grätzel *et al.* reported their revolutionary work on Dye Sensitized Solar Cells (DSSCs) in 1991, it has emerged as a cutting-edge technology in the field of photovoltaics (PV) due to the low-cost production and high-power conversion efficiency.[90]

Segawa *et al.* synthesized a series of mono/di acetylene-bridged push-pull porphyrin, **33–37** with phenylcarboxyl, thienylcyanoacryl, pyridinyl and fluorophenylcarboxyl group at the *β*-pyrrolic position (Chart 2.0).[91] The absorption spectra of porphyrin **37** exhibits a red shifted absorption band compared to porphyrin **33–36**, which may be due the extension of π-conjugated system. The photovoltaic performance of these dyes were investigated, in which porphyrin dye **37** shows maximum PCE of 5.7% and an IPCE of up to 92% compared to other porphyrins which shows IPCE between 76–80%.

R₁= ―〈〉―COOH

R₂= (pentafluorophenyl)―COOH

R₃= (thiophene)―C(NC)=CH―COOH

R₄= ―〈N〉

X= 1, 2, 3, 4

33, R₁= P-PhCOOH
34, R₂= P-FPhCOOH
35, R₃= P-ThCNCOOH
36, R₄= P-Py

37
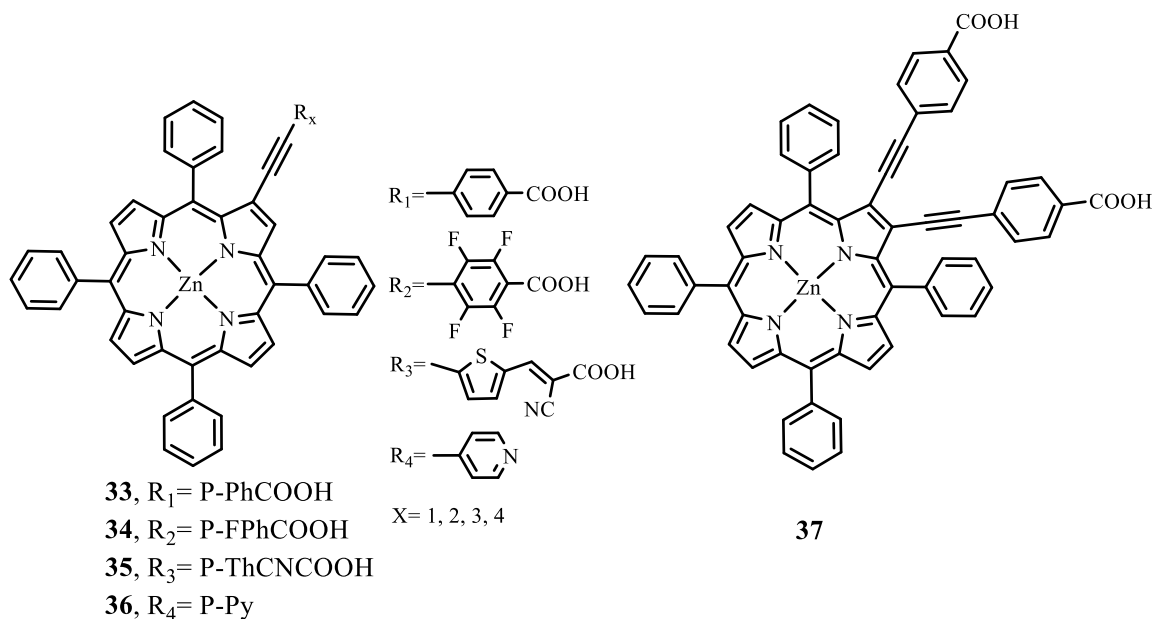
Chart 2.0. Porphyrin based chromophore **33–37**.

Imahori *et al.* reported quinoxaline-fused porphyrin dyes **38** and **39**. In porphyrin **39** one of the pyrrole unit of tetraarylporphyrins was fused with electron-withdrawing carboxy quinoxalino anchoring group. In porphyrin **38**, two pyrrole unit of the tetraarylporphyrin were fused with imidazole group and carboxyquinoxalino anchoring group at the *β, β'*-edge (Chart 2.1).[92] Recently quinoxaline-fused porphyrins are utilized as sensitizers due to its strong light-harvesting properties. The porphyrin **38** shows broader soret band with a red shifted absorption towards the longer wavelength region compared to porphyrin **39**. The performance of porphyrins **38** and **39** with chenodeoxycholic acid (CDCA) as co-adsorbent exhibits a highest PCE of 6.8% and 6.3% with high J_{sc} value of 13.9 mAcm^{-2} and 13.2 mAcm^{-2}.
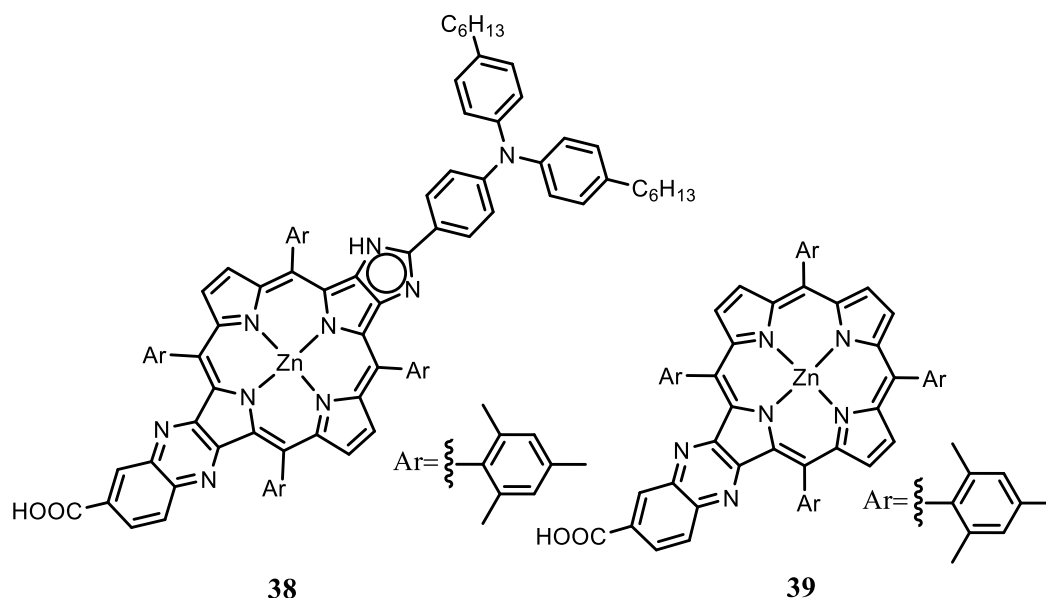
Chart 2.1. Porphyrin based chromophore **38** and **39**.

Kim and co-worker synthesized zinc porphyrin dyes **40**, **41** and **42** of donor–π–acceptor architecture in which the meso-position was appended by electron-donating bis(4-tert-butylphenyl) amino group and the opposite β-pyrrolic position was substituted by 2-propenoic acid or 2,4-pentadienoic acid moiety (Chart 2.2).[93] The acid moiety substituted at the *β*-position serve as a anchoring groups for interacting with the TiO$_2$ surface. The electron-donating group on the porphyrin architecture provides a considerable electronic coupling which results in low HOMO–LUMO energy gap with a broad red shift in the absorption spectra (Figure 21). The DSSC device were composed of TiO$_2$ spheres with a diameter of 600–800 nm prepared from P-25 and anatase TiO$_2$ nanoparticles functioning as photoelectrodes. The porphyrin dyes **42** were sensitized with anatase TiO$_2$ nanoparticles and P-25 TiO$_2$ spheres, in which the anatase TiO$_2$-based DSSC showed enhanced power conversion efficiencies (η) of 7.47% with high J$_{sc}$ value of 18.4 mAcm^{-2}.
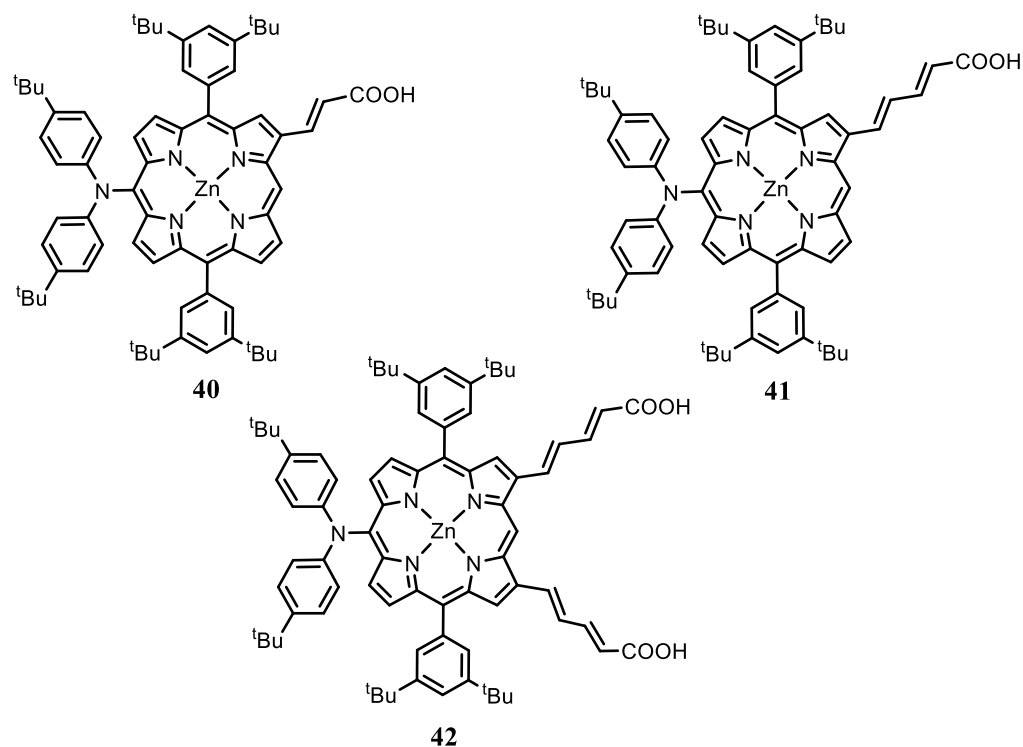
Chart 2.2. Porphyrin based chromophore **40–42**.

Kim *et al.* studied the performances of push–pull porphyrin dyes, **43–46** for DSSC application in which the porphyrins was substituted with diarylamine group at the *meso*-position and the *β*-position were functionalized with benzoic acid for porphyrin **43** and **44** and vinylbenzoic acid for porphyrin **45** and **46** (Chart 2.3).[94] The photophysical study reveals a red shifted absorption spectra for vinylbenzoic acid substituted porphyrin **45** and **46** relative to the benzoic acid substituted porphyrin **43** and **44**. The DFT study shows intrinsic intramolecular charge-transfer character of push–pull dyes and the extent of charge-transfer depends on the *β*-conjugated linkage. The photovoltaic performances of push–pull porphyrin sensitizers **43–46**, the vinylbenzoic acid substituted porphyrin **45** and **46** shows higher power conversion efficiency due to the vinyl linkage compared to the benzoic acid substituted porphyrin **43** and **44**. The DSSC performance of cells were made to improve by more than 1% by employing cobalt (II/III)-based electrolyte instead of I^-/I^{3-} reference electrolytes. The highest PCE were shown by **45** and **46** were about 6.6% and 5.3%.
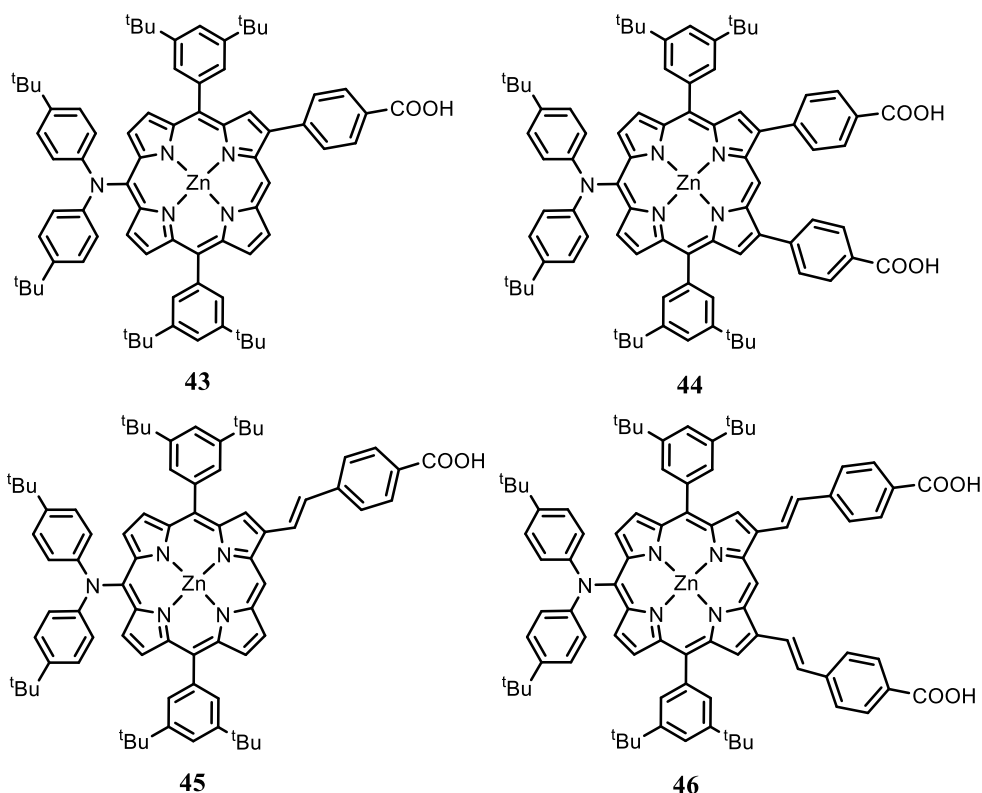
Chart 2.3. Porphyrin based chromophore **43**–**46**.

Imahori *et al.* reported quinoxaline-fused porphyrins **47**–**49**, with carboxylic-acid anchoring group, and investigated the effects of π-conjugation due to the fused quinoxaline moiety on photophysical, electrochemical, and photovoltaic properties (Chart 2.4).[95] The porphyrins **48** and **49** showed a red-shifted abosorption compared to porphyrin **108**. The photovoltaic properties were compared in a sealed device structure under the optimized conditions, using TiO$_2$ double layers, treated with TiCl$_4$. The porphyrins **47** and **48** exhibited a relatively high-power conversion efficiency (η) of 6.3% and 5.1% with high J$_{sc}$ value of 13.2 mAcm^{-2} and 11.1 mAcm^{-2}, while the **49** showed a low PCE (η) value of 0.80%.
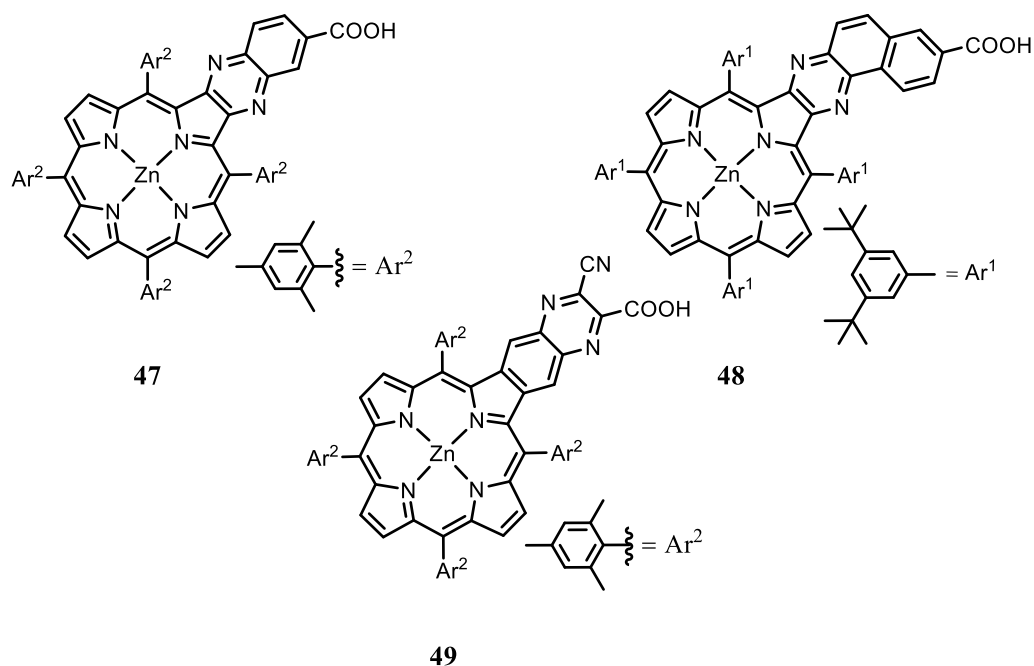
Chart 2.4. Porphyrin based chromophore **47**–**49**.

Zhao and co-worker synthesized *β*-functionalized porphyrin with diphenylquinoxaline unit in **51** and benzothiadiazole unit in **52** (Chart 2.5). The influence of electron-withdrawing moiety such as quinoxaline and benzothiadiazole unit on the photovoltaic performance in DSSC were investigated relative to the porphyrin dye **50**.[96] On addition of the acceptor unit at the *β*-position of the porphyrin macrocyle, **51** and **52**, results in decreased LUMO energy levels with broader absorption spectra and higher short-circuit current density (J$_{sc}$) compared to **50** reference dye. These results provide an insight, to manipulate the LUMO energy levels of the porphyrin sensitizers *via* the modification of *β*-linker for the photovoltaic applications. The PCE were recorded for porphyrin dye **52** of 6.14% with high J$_{sc}$ value of 11.47 mAcm^{-2}.
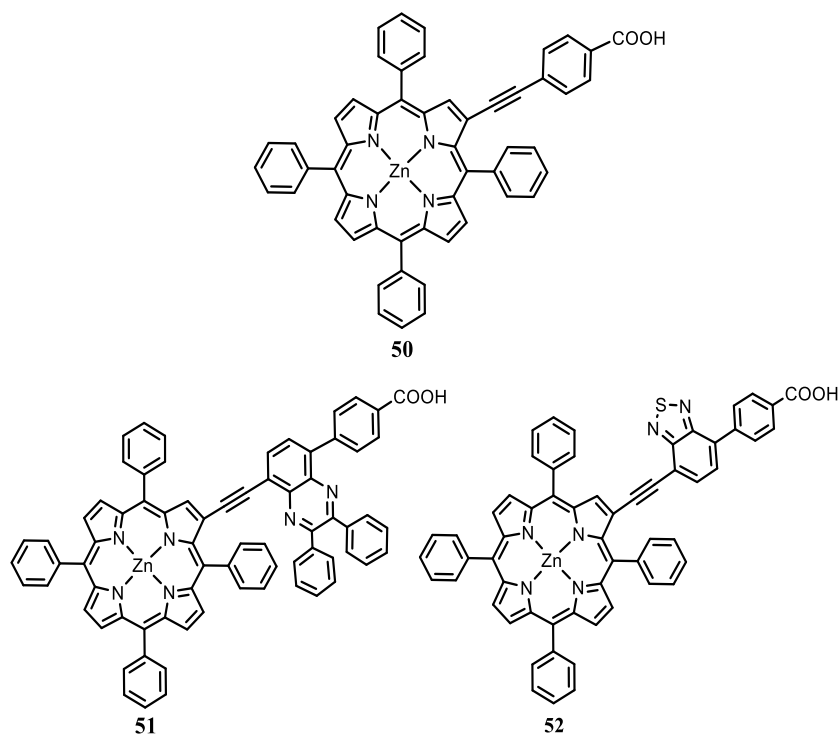
Chart 2.5. Porphyrin based chromophore **50–52**.

1.4.3. Nonlinear optics

Sankar *et al.* synthesized two series of triphenylamine (TPA) substituted β-porphyrins **53**, MTPP(TPA)$_2$X, (where M = 2H, Co(II), Ni(II), Cu(II), Zn(II) and X = NO$_2$/CHO) and investigated their photophysical, electrochemical, computational and nonlinear optical (NLO) properties (Chart 2.6).[97] The UV-Visible spectra of MTPP(TPA)$_2$X shows red shifted absorption in the soret and Q band region compared to their MTPPs due to the inductive and resonance effect caused by the triphenylamine donor unit appended at the β-pyrrolic position of the porphyrin π-systems. The fluorescence lifetime and quantum yields of MTPP(TPA)$_2$X are very low for nitro appended porphyrins compared to the formyl substituted porphyrins. The CuTPP(TPA)$_2$ with NO$_2$ and CHO group shows a anodic shift compared to CuTPP due to the electron withdrawing nature of NO$_2$ and CHO groups. The DFT studies on porphyrin MTPP(TPA)$_2$X reveals a nonplanar saddle shape conformation of the porphyrin ring due to the presence of TPA and NO$_2$/CHO units.

26

53, MTPP(TPA)$_2$X
X=NO$_2$, CHO
M = 2H, Co^{II}, Ni^{II}, Cu^{II}, Zn^{II}
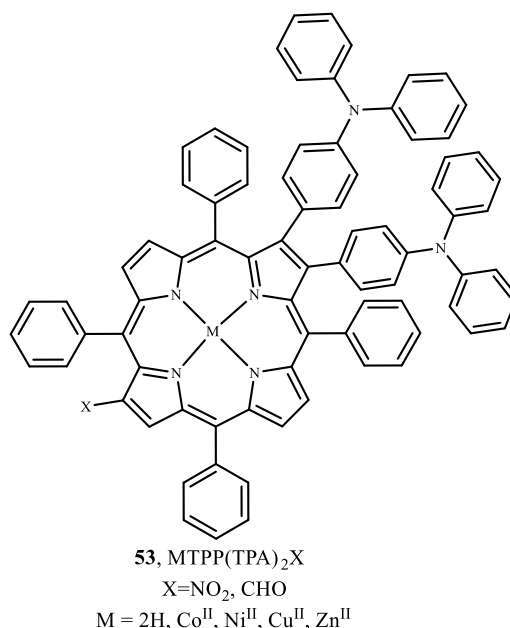
Chart 2.6. Porphyrin based chromophore **53**.

1.4.4. Bulk heterojunction (BHJ) solar cells

The bulk heterojunction solar cell is a promising approach for increased efficiency and light harvesting properties of organic photovoltaic cells (OPV). The bulk heterojunction solar cells have been utilized because of their mechanical flexibility and low processing costs compared to other conventional solar cells. The solution-processed bulk heterojunction (BHJ) solar cells have reduced the manufacturing costs through spray deposition at low temperatures. The conjugated organic molecules as donors and electron withdrawing fullerene derivatives as acceptors are commonly used in bulk heterojunction solar cells. Marks *et a1*. reported the solution-processed bulk-heterojunction (BHJ) solar cell in 1994, followed by Yu *et al.* in 1995. [98, 99] Currently, the binary and ternary BHJs, have reported the best PCEs of about 14% using non-fullerene and fullerene acceptors along with conjugated polymer donors.
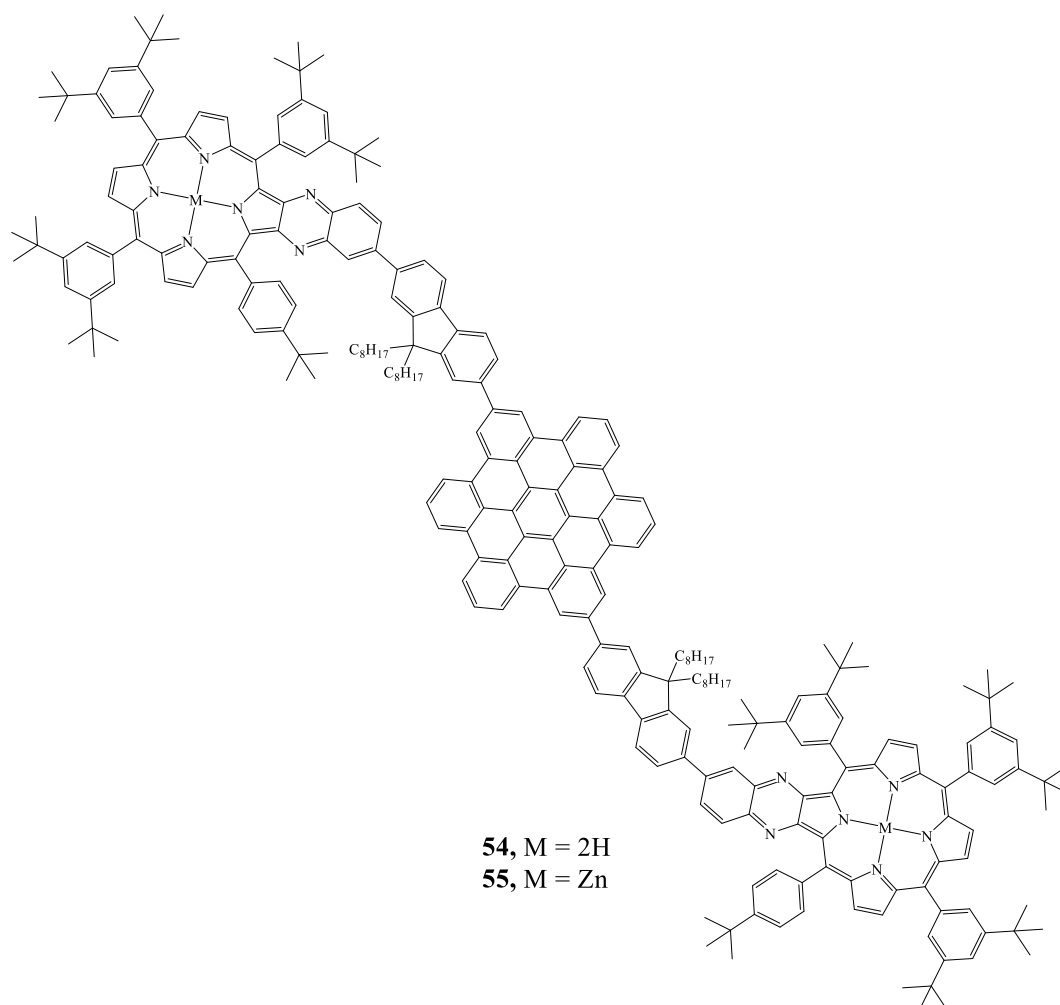
Chart 2.7. Porphyrin based chromophore **54** and **55**.

In bulk heterojunction solar cells, organic molecules with low HOMO-LUMO gap and good charge transport properties are used as donors. Wong *et al*. reported the synthesis of FHBC-quinoxalinoporphyrin hybrid using bromo-quinoxalinoporphyrin and 9,9-dioctylfluorenyl hexa-peri-hexabenzocoronene (FHBC) boronate ester.[100] The photoluminescence studies suggests that the emission from the higher energy hexa-peri-hexabenzocoronene (HBC) unit was completely quenched by the porphyrin macrocycle indicating efficient energy transfer. The FHBC-quinoxalinoporphyrin hybrid were investigated for bulk heterojunction photovoltaic devices and Porphyrin **54** showed a PCE of around 1.2%.

1.4.5. Photodynamic therapy (PDT)

Photodynamic therapy (PDT) consists of a photosensitizing chemical substance to treat a wide range of medical conditions, involving wet age-related macular degeneration, acne, atherosclerosis, psoriasis and malignant cancers. The development of PDT is related with the involvement of non-toxic photosensitizers capable of providing the maximum therapeutic effect without affecting the non-malignant tissues. The β-substituted tetraphenyl porphyrin **56** and **57** was used to determine the ability of the porphyrin photosensitizers to accumulate in cancer cells by measuring the fluorescence intensity after incubation for 2 and 24 h. [101] The estimated binding constant between the bovine serum albumin and porphyrin suggest that the length and the position of functional group influences the binding affinity of porphyrin photosensitizers in cancer cells.

56, n=0
57, n=14
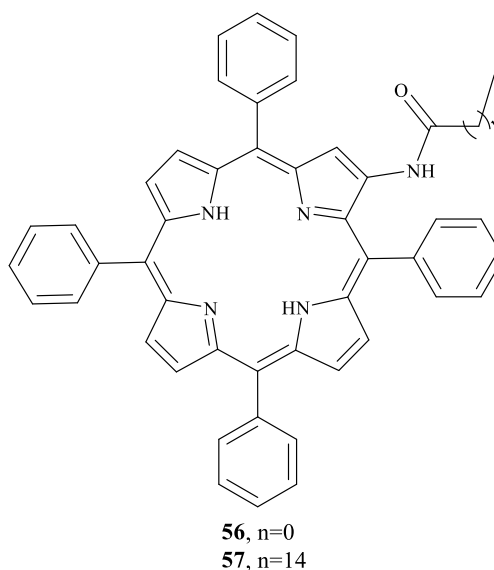
Chart 2.8. Porphyrin based chromophore **56** and **57**.

The main objectives of present study are:

  ✓ To synthesize donor and acceptor substituted β, β'-push–pull porphyrin *via* β-mono and dibrominated tetraphenylporphyrin by the Sonogashira cross-coupling reaction and zinc metallation reaction

29

- ✓ To understand the effect of TCBD functionalization on β-substituted porphyrins and their photophysical and computational studies were investigated
- ✓ To fine-tune the photophysical and electrochemical properties of the porphyrin macrocycle by incorporating the donor substituents at the β-pyrrolic position of the porphyrin π-system.
- ✓ To explore the influence of acceptor units on the electronic properties of the porphyrin π-system.
- ✓ To investigate the effect of 2,3,3-triphenylacrylonitrile, 1,1,2,2-tetraphenylethene and 9-propyl-9H-carbazole units on the photonic and electronic properties of the porphyrin π-systems.

Figure 1.2. General representation of donor-acceptor functionalized porphyrins in this work.

1.5. Organization of thesis

Chapter 1: This chapter gives an outline of various design and synthetic strategies of porphyrin chromophores at the β-pyrrolic positions and their applications in diverse fields.

Chapter 2: This chapter summarizes the instrumentation and general methods used for the present study.

Chapter 3: In this chapter, we discuss the design and synthesis of donor and acceptor substituted push–pull porphyrins and their photophysical and computational studies were investigated in order to understand the effect of donor and acceptor on the porphyrin π-systems.

Chapter 4: In this chapter, we discuss the design and synthesis of β-donor, acceptor functionalized porphyrins and their photophysical and computational studies were explored to understand the effect of TCBD functionalization on β-substituted porphyrins.

Chapter 5: In this chapter, we discuss the synthesis of donor substituted unsymmetrical free base β-pyrrole porphyrins and investigated their electronic properties of the porphyrin π-system by incorporating the donor substituents at the β-pyrrolic position.

Chapter 6: In this chapter, we discuss the synthesis of acceptor functionalized unsymmetrical β-porphyrin and investigated the influence of acceptor units on the electronic properties of the porphyrin π-system.

Chapter 7: In this chapter, we discuss the synthesis of TPAN, TPE and carbazole substituted unsymmetrical β-porphyrins and their photophysical, electrochemical and computational studies were explored. The effect of TPAN, TPE and carbazole entity on the photonic and electronic properties of the porphyrin π-systems were investigated.

1.6. References

[1] Kadish, K. M., Smith, K. M., Guilard, R. (2010). The porphyrin handbook. *World scientific*, 2011, 1-20.

[2] Chatterjee, T., Shetti, V. S., Sharma, R., Ravikanth, M. (2017). Heteroatom-containing porphyrin analogues. *Chem. Rev.* 117(4), 3254-3328. (DOI: 10.1021/acs.chemrev.6b00496).

[3] Singhal, A. (2017). Meso-linked multiporphyrins as model for light harvesting systems: Review. *Nat Prod Chem Res*, 5, 259. (DOI: 10.4172/2329-6836.1000259).

[4] Tutel, Y., Sevinç, G., Küçüköz, B., Akhuseyin Yildiz, E., Karatay, A., Dumanoğulları, F. M., Yılmaz, H., Hayvali, M., Elmali, A. (2021). Ultrafast Electron/Energy Transfer and Intersystem Crossing Mechanisms in BODIPY-Porphyrin Compounds. *Processes*, 9(2), 312. (DOI: 10.3390/pr9020312).

[5] Mirkovic, T., Ostroumov, E. E., Anna, J. M., Van Grondelle, R., Scholes, G. D. (2017). Light absorption and energy transfer in the antenna complexes of photosynthetic organisms. *Chem. Rev.* 117(2), 249-293. (DOI: 10.1021/acs.chemrev.6b00002).

[6] Zhou, W.-L.; Zhao, X.; Chen, Y.; Liu, Y. (2019) Construction and Heterogeneous Photooxidization Reactivity of a Cyclodextrin/Porphyrin Polyrotaxane Network. *Org. Chem. Front.*, 6 (1), 10–14. (DOI: 10.1039/C8QO00790J).

[7] Vonesch, M.; Wytko, J. A.; Kitagishi, H.; Kano, K.; Weiss, J. (2019) Modelling Haemoproteins: Porphyrins and Cyclodextrins as Sources of Inspiration. Chem. Commun., 55 (97), 14558–14565. (DOI: 10.1039/C9CC07545C).

[8] Sagrillo, F. S.; Dias, C.; Gomes, A. T. P. C.; Faustino, M. A. F.; Almeida, A.; Gonçalves de Souza, A.; Costa, A. R. P.; Boechat, F. da C. S.; Bastos Vieira de Souza, M. C.; Neves, M. G. P. M. S.; Cavaleiro, J. A. S. (2019) Synthesis and Photodynamic Effects of New Porphyrin/4-Oxoquinoline Derivatives in the Inactivation of S. Aureus. Photochem. Photobiol. Sci., 18 (8), 1910–1922. (DOI: 10.1039/C9PP00102F).

[9] Supriya, S., Shetti, V. S., Hegde, G. (2020) *Review of Conjugated Porphyrin Systems*. (DOI: 10.31219/osf.io/xs3gf).

[10] Hiroto, S., Miyake, Y., Shinokubo, H. (2017). Synthesis and functionalization of porphyrins through organometallic methodologies. *Chem. Rev.*, 117(4), 2910-3043. (DOI: 10.1021/acs.chemrev.6b00427).

[11] Peeks, M. D., Claridge, T. D., Anderson, H. L. (2017). Aromatic and antiaromatic ring currents in a molecular nanoring. *Nature*, 541(7636), 200-203. (DOI: 10.1038/nature20798).

[12] Osuka, A., Saito, S. (2011). Expanded porphyrins and aromaticity. *Chem. Commun.* 47(15), 4330-4339. (DOI: 10.1039/c1cc10534e).

[13] Ethirajan, M., Chen, Y., Joshi, P., Pandey, R. K. (2011). The role of porphyrin chemistry in tumor imaging and photodynamic therapy. *Chem. Soc. Rev.*, 40(1), 340-362. (DOI: 10.1039/B915149B).

[14] Imahori, H., Mori, Y., Matano, Y. (2003). Nanostructured artificial photosynthesis. *J. Photochem. Photobiol. C: Photochem. Rev.*, 4(1), 51-83. (DOI: 10.1016/S1389-5567(03)00004-2).

[15] Li, L. L., Diau, E. W. G. (2013). Porphyrin-sensitized solar cells. *Chem. Soc. Rev.* 42(1), 291-304. (DOI: 10.1039/C2CS35257E).

[16] Mauzerall, D. (1977). Porphyrins, chlorophyll, and photosynthesis. In Photosynthesis I (pp. 117-124). *Springer*, Berlin, Heidelberg. (DOI: 10.1007/978-3-642-66505-9_5).

[17] Rio, Y., Rodriguez-Morgade, M. S., Torres, T. (2008). Modulating the electronic properties of porphyrinoids: a voyage from the violet to the infrared regions of the electromagnetic spectrum. *Org. Biomol. Chem.*, 6(11), 1877-1894. (DOI: 10.1039/b800617b).

[18] Bromby, A. D., Jansonius, R. P., Sutherland, T. C. (2013). Synthesis and optical and electronic properties of core-modified 21, 23-dithiaporphyrins. *J. Org. Chem.* 78(4), 1612-1620. (DOI: 10.1021/jo302707f).

[19] Ragoussi, M. E., de la Torre, G., Torres, T. (2013). Tuning the Electronic Properties of Porphyrin Dyes: Effects of meso Substitution on Their Optical and Electrochemical Behaviour. *Eur. J. Org. Chem.* 2013(14), 2832-2840. (DOI: 10.1002/ejoc.201300124).

[20] Bhyrappa, P., Sankar, M., Varghese, B. (2006). Mixed substituted porphyrins: structural and electrochemical redox properties. *Inorg. Chem.*, 45(10), 4136-4149. (DOI: 10.1021/ic052035b).

[21] Li, C.; Zhang, J.; Song, J.; Xie, Y.; Jiang, J. (2018). Synthetic Porphyrin Chemistry in China. *Sci. China Chem.*, 61 (5), 511–514. (DOI: 10.1007/s11426-018-9245-6).

[22] Fukuzumi, S., Honda, T., Kojima, T. (2012). Structures and photoinduced electron transfer of protonated complexes of porphyrins and metallophthalocyanines. *Coord. Chem. Rev.*, 256(21-22), 2488-2502. (DOI: 10.1016/j.ccr.2012.01.011).

[23] Whitten, D. G. (1978). Photochemistry of porphyrins and their metal complexes in solution and organized media. *Rev. Chem. Intermed.,* 2(2), 107-138. (DOI: 10.1007/BF03155997).

[24] Wang, K.; Liu, P.; Zhang, F.; Xu, L.; Zhou, M.; Nakai, A.; Kato, K.; Furukawa, K.; Tanaka, T.; Osuka, A.; Song, J. (2021). A Robust Porphyrin-Stabilized Triplet Carbon Diradical. *Angew. Chem.*, 133 (13), 7078–7082. (DOI: 10.1002/ange.202015356).

[25] Miyagawa, K.; Hisaki, I.; Fukui, N.; Shinokubo, H. (2021). Redox-Induced Reversible [2 + 2] Cycloaddition of an Etheno-Fused Diporphyrin. *Chem. Sci.*, 12 (14), 5224–5229. (DOI: 10.1039/D1SC00438G).

[26] Parker, J. E.; Thomas, R. J.; Morisson, D.; Brancaleon, L. (2012), Combination of Resonance Raman Spectroscopy and Docking Simulations to Study the Nonspecific Binding of a Free-Base Porphyrin to a Globular Protein. *J. Phys. Chem. B*, 116 (36), 11032–11040. (DOI: 10.1021/jp304310z).

[27] Rao, Y.; Kim, J. O.; Kim, W.; Zhong, G.; Yin, B.; Zhou, M.; Shinokubo, H.; Aratani, N.; Tanaka, T.; Liu, S.; Osuka, A.; Kim, D.; Song, J. (2016). β-to-β 2,5-Pyrrolylene-Linked Cyclic Porphyrin Oligomers. *Chem. Eur. J.*, 22 (26), 8801–8804. (DOI: 10.1002/chem.201601306).

[28] Song, H. E., Kirmaier, C., Schwartz, J. K., Hindin, E., Yu, L., Bocian, D. F., Lindsey, J., Holten, D. (2006). Effects of multiple

pathways on excited-state energy flow in self-assembled wheel-and-spoke light-harvesting architectures. *J. Phys. Chem. B*, 110(39), 19131-19139. (DOI: 10.1021/jp064001a).

[29] Yella, A., Lee, H. W., Tsao, H. N., Yi, C., Chandiran, A. K., Nazeeruddin, M. K., Diau, E. W.-G., Yeh, C.-Y., Zakeeruddin, S. M., Grätzel, M. (2011). Porphyrin-sensitized solar cells with cobalt (II/III)–based redox electrolyte exceed 12 percent efficiency. *science*, 334(6056), 629-634. (DOI: 10.1126/science.1209688).

[30] Yang, W., Zhang, B. (2019). Porphyrin-based nanocomposites for tumor photodynamic therapy. *MRS Bull.*, 44(3), 189-194. (DOI: 10.1557/mrs.2019.42).

[31] Maeda, C., Ogawa, K., Sadanaga, K., Takaishi, K., Ema, T. (2019). Chiroptical and catalytic properties of doubly binaphthyl-strapped chiral porphyrins. *Chem. Commun.*, 55(8), 1064-1067. (DOI: 10.1039/C8CC09114E).

[32] Kumar, R., Chaudhary, N., Sankar, M., Maurya, M. R. (2015). Electron deficient nonplanar β-octachlorovanadylporphyrin as a highly efficient and selective epoxidation catalyst for olefins. *Dalton Trans.*, 44(40), 17720-17729. (DOI: 10.1039/C5DT02349A).

[33] Wu, Z.-Y.; Xue, H.; Wang, T.; Guo, Y.; Meng, Y.-S.; Li, X.; Zheng, J.; Brückner, C.; Rao, G.; Britt, R. D.; Zhang, J.-L. (2020). Mimicking of Tunichlorin: Deciphering the Importance of a β-Hydroxyl Substituent on Boosting the Hydrogen Evolution Reaction. *ACS Catal.*, 10 (3), 2177–2188. (DOI: 10.1021/acscatal.9b03985).

[34] Shing, K.-P.; Cao, B.; Liu, Y.; Lee, H. K.; Li, M.-D.; Phillips, D. L.; Chang, X.-Y.; Che, C.-M. (2018). Arylruthenium(III) Porphyrin-Catalyzed C–H Oxidation and Epoxidation at Room Temperature and [Ru V (Por)(O)(Ph)] Intermediate by Spectroscopic Analysis and Density Functional Theory Calculations. *J. Am. Chem. Soc.*, 140 (22), 7032–7042. (DOI: 10.1021/jacs.8b04470).

[35] Higashino, T., Imahori, H. (2015). Porphyrins as excellent dyes for dye-sensitized solar cells: recent developments and insights. *Dalton Trans*, 44(2), 448-463. (DOI: 10.1039/C4DT02756F).

[36] Blank, A., Galili, T., Levanon, H. (2001). Triplet porphyrins as donors in intramolecular electron transfer and their intermolecular interaction with free radicals. *J. Porphyrins Phthalocyanines*, 5(01), 58-66. (DOI: 10.1002/1099-1409(200101)5:1<58::AID-JPP297>3.0.CO;2-B).

[37] Reekie, T. A., Sekita, M., Urner, L. M., Bauroth, S., Ruhlmann, L., Gisselbrecht, J. P., Boudon, C., Trapp, N., Clark, T., Guldi, D. M., Diederich, F. (2017). Porphyrin Donor and Tunable Push–Pull Acceptor Conjugates—Experimental Investigation of Marcus Theory. *Chem. Eur. J.*, 23(26), 6357-6369. (DOI: 10.1002/chem.201700043).

[38] Sun, B., Ou, Z., Meng, D., Fang, Y., Song, Y., Zhu, W., Solntsev, P. V., Nemykin, V. N., Kadish, K. M. (2014). Electrochemistry and catalytic properties for dioxygen reduction using ferrocene-substituted cobalt porphyrins. *Inorg. Chem*, 53(16), 8600-8609. (DOI: 10.1021/ic501210t).

[39] Buczek, K., Deryło, K., Kutyła, M., Rybicka-Jasińska, K., Gryko, D., Borsuk, G., Rodzik, B., Trytek, M. (2020). Impact of Protoporphyrin Lysine Derivatives on the Ability of Nosema ceranae Spores to Infect Honeybees. *Insects*, 11(8), 504. (DOI: 10.3390/insects11080504).

[40] Lewtak, J. P., Koszarna, B., Charyton, M. K., Gryko, D. T. (2020). Extending a porphyrin chromophore via fusion with naphthalene. *J. Porphyrins Phthalocyanines*, 24(01n03), 448-455. (DOI: 10.1142/S1088424619501530).

[41] Possanza, F., Limosani, F., Tagliatesta, P., Zanoni, R., Scarselli, M., Ciotta, E., Pizzoferrato, R. (2018). Functionalization of carbon spheres with a porphyrin–ferrocene dyad. *ChemPhysChem*, 19(17), 2243-2249. (DOI: 10.1002/cphc.201800277).

[42] Vecchi, A., Sabin, J. R., Sabuzi, F., Conte, V., Cicero, D. O., Floris, B., Galloni, P., Nemykin, V. N. (2021). Similar, Yet Different: Long-Range Metal–Metal Coupling and Electron-Transfer Processes in Metal-Free 5, 10, 15, 20-Tetra (ruthenocenyl) porphyrin. *Inorg. Chem.* 60(11), 8227–8241 (DOI: 10.1021/acs.inorgchem.1c00908).

[43] Kaur, R.; Possanza, F.; Limosani, F.; Bauroth, S.; Zanoni, R.; Clark, T.; Arrigoni, G.; Tagliatesta, P.; Guldi, D. M. (2020). Understanding and Controlling Short- and Long-Range Electron/Charge-Transfer Processes in Electron Donor–Acceptor Conjugates. *J. Am. Chem. Soc.*, 142 (17), 7898–7911. (DOI: 10.1021/jacs.0c01452).

[44] Di Carlo, G., Orbelli Biroli, A., Pizzotti, M., Tessore, F. (2019). Efficient sunlight harvesting by A4 *β*-pyrrolic substituted ZnII porphyrins: a mini-review. *Front. Chem.*, 7, 177. (DOI: 10.3389/fchem.2019.00177).

[45] Di Carlo, G., Biroli, A. O., Tessore, F., Caramori, S., Pizzotti, M. (2018). β-Substituted Zn^{II} porphyrins as dyes for DSSC: A possible approach to photovoltaic windows. *Coord. Chem. Rev.*, 358, 153-177. (DOI: 10.1016/j.ccr.2017.12.012).

[46] Rothemund, P. (1935). Formation of porphyrins from pyrrole and aldehydes. *J. Am. Chem. Soc.*, 57(10), 2010-2011. (DOI: 10.1021/ja01313a510).

[47] Rothemund, P. (1936). A new porphyrin synthesis. The synthesis of porphin1. *J. Am. Chem. Soc.*, 58(4), 625-627. (DOI: 10.1021/ja01295a027).

[48] Rothemund, P. (1939). Porphyrin studies. III. The structure of the porphine ring system. *J. Am. Chem. Soc.,* 61, 2912–2915. (DOI: 10.1021/ja01265a096).

[49] Adler, A.D., Longo, F.R., Finarelli, J.D., Goldmacher, J., Assour, J., Korsakoff, L. (1967). A simplified synthesis for meso-tetraphenylporphin. *J. Org. Chem.,* 32, 476. (DOI: 10.1021/jo01288a053).

[50] Lindsey, J.S., Hsu, H.C., Schreiman, I.C. (1986). Synthesis of tetraphenylporphyrins under very mild conditions. *Tetrahedron Lett.,* 27, 4969–4970. (DOI: 10.1016/S0040-4039(00)85109-6).

[51] Lindsey, J.S., Schreiman, I.C., Hsu, H.C., Kearney, P.C., Marguerettaz, A.M. (1987). Rothemund and Adler–Longo reactions revisited: Synthesis of tetraphenylporphyrins under equilibrium conditions. *J. Org. Chem.,* 52, 827–836. (DOI: 10.1021/jo00381a022).

[52] Lindsey, J.S. Synthesis of meso-substituted porphyrins. In The Porphyrin Handbook; Kadish, K.M., Smith, K.M., Guilard, R., Eds.; Academic Press: Boston, MA, USA, 2000; Volume 1, pp. 45–118.

[53] [a]. H. J. Callot, (1974). BROMATION DE LA M-TETRAPHENYLPORPHINE. PREPARATION D'ALKYL- ET DE POLYCYANOPORPHINES(1). *Bull. Soc. Chim. Fr.*, 1492-1496. (DOI: PASCAL7517004840). [b]. Bhyrappa, P.; Velkannan, V. (2010). Synthesis of β-Di and Tribromoporphyrins and the Crystal Structures of Antipodal Tri-Substituted Zn(II)-Porphyrins. *Tetrahedron Letters*, 51 (1), 40–42. (DOI: 10.1016/j.tetlet.2009.10.039). [c]. Crossley, M. J.; Burn, P. L.; Chew, S. S.; Cuttance, F. B.; Newsom, I. A. (1991). Regiospecific Introduction of Four Substituents to Porphyrin Systems at Antipodal Pyrroienic Positions. *J . CHEM. SOC.*, 3. (DOI: 10.1039/C39910001564). [d]. Bhyrappa, P.; Krishnan, V. (1991). Octabromotetraphenylporphyrin and Its Metal Derivatives: Electronic Structure and Electrochemical Properties. *Inorg. Chem.*, 30 (2), 239–245. (DOI: 10.1021/ic00002a018).

[54] Callot, H. J. (1973). Bromuration de la meso-tetraphenylporphine.: Structure et reactivite des produits. *Tetrahedron Lett.,* 14(50), 4987-4990. (DOI: 10.1016/S0040-4039(01)87629-2).

[55] Inhoffen, H.H., Fuhrhop, J.-H., Voigt, H.; Brockmann, H., Jr. (1966). Zur weiteren Kenntnis des Chlorophylls und des

Hämins, VI. Formylierung der meso-kohlenstoffatome von alkyl-substituierten porphyrinen. *Justus Liebigs Ann. Chem.*, 695, 133–143. (DOI: 10.1002/jlac.19666950114).

[56] Inhoffen, H.H., Buchler, J.W., Thomas, R. (1969). Zur weiteren kenntnis des chlorophylls und des hamins, XXV. 3, 4,7,8-Tetrahydro-octaäthylporphin ("Bacterio-octaäthylchlorin"). *Tetrahedron. Lett.,* 10, 1141–1144. (DOI: 10.1016/S0040-4039(01)97760-3).

[57] Johnson, A.W., Oldfield, D. (1966). Meso-Substitution products of ætioporphyrin I. *J. Chem. Soc. C*, 0, 794–798. (DOI: 10.1039/J39660000794).

[58] Callot, H.J. (1973). Nouvelles voies d'accès aux vinylporphyrines. *Tetrahedron*, 29, 899–901. (DOI: 10.1016/0040-4020(73)80035-3).

[59] Callot, H.J. (1973). Wittig reaction on some formylporphyrins-example of extremely facile deformylation. *Bull. Soc. Chim. Fr.,* 12, 3413–3416.

[60] Callot, H.J., Castro, B., Selve, C. (1978). Porphyrines synthetic ues porteuses de chaines laterales peptidiques. Atropoisomérie d'amides cis(méso-tétraphénylporphyrinyl)-3-propénoïques. *Tetrahedron. Lett.,* 32, 2877–2880. (DOI: 10.1016/S0040-4039(01)94887-7).

[61] Momenteau, M., Loock, B., Bisagni, E., Rougee, M. (1979). Five-coordinate iron(II) porphyrins derived from Meso-tetraphenylporphin: Synthesis, characterization, and coordinating properties. *Can. J. Chem.,* 57, 1804–1813. (DOI: 10.1139/v79-288).

[62] Balakumar, A., Mutukumaran, K., Lindsey, J.S. (2004). A New route to meso-formyl porphyrins. *J. Org. Chem.,* 69, 5112–5115. (DOI: 10.1021/jo049819b).

[63] Bonfantini, E.E., Burrell, A.K., Campbell, W.M., Crossley, M.J., Gosper, J.J., Harding, M.M., Officer, D.L., Reid, D.C.W. (2002). Efficient synthesis of free-base 2-formyl-5,10,15,20-tetraarylporphyrins, their reduction and conversion to

[(porphyrin-2-yl)methyl]phosphonium salts. *J. Porphyrins. Phthalocyanines*, 6, 708–719. (DOI: 10.1142/S108842460200083X).

[64] Burrel, A.K., Officer, D.L., Reid, D.C.W., Wild, K.Y. (1998). Controlling the structure of supramolecular porphyrin arrays. *Angew. Chem. Int. Ed. Engl.*, 37, 114–117. (DOI: 10.1002/(SICI)1521-3773(19980202)37:1/2<114::AID-ANIE114>3.0.CO;2-G).

[65] Burrel, A.K., Officer, D.L. (1998). Functionalizing porphyrins via Wittig reactions: A building block approach. *Synlett*, 1998(12), 1297–1307. (DOI: 10.1055/s-1998-1938).

[66] Bonfantini, E.E., Officer, D.L. (1993). The synthesis of butadiene-bridged porphyrin dimers and styryl porphyrins using a porphyrin-derivedWittig reagent. *Tetrahedron Lett.,* 34(52), 8531–8534. (DOI: 10.1016/S0040-4039(00)61377-1).

[67] Burrell, A.K., Officer, D.L., Plieger, P.G., Reid, D.C.W. (2001). Synthetic routes to multiporphyrin arrays. *Chem. Rev.*, 101, 2751–2796. (DOI: 10.1021/cr0000426).

[68] Ali, H., van Lier, J. E. (1994). Synthesis of β-substituted porphyrins using palladium catalysed reactions. *Tetrahedron*, 50(41), 11933-11944. (DOI: 10.1016/S0040-4020(01)89306-6).

[69] Vail, S. A., Schuster, D. I., Guldi, D. M., Isosomppi, M., Tkachenko, N., Lemmetyinen, H., Palkar, A., Echegoyen, L., Chen, X., Zhang, J. Z. (2006). Energy and electron transfer in β-alkynyl-linked porphyrin−[60] fullerene dyads. *J. Phys. Chem. B*, 110(29), 14155-14166. (DOI: 10.1021/jp061844t).

[70] Lu, F., Feng, Y., Wang, X., Zhao, Y., Yang, G., Zhang, J., Zhang, B., Zhao, Z. (2017). Influence of the additional electron-withdrawing unit in β-functionalized porphyrin sensitizers on the photovoltaic performance of dye-sensitized solar cells. *Dyes Pigm.*, 139, 255-263. (DOI: 10.1016/j.dyepig.2016.12.027).

[71] Giraudeau, A., Callot, H. J., Jordan, J., Ezhar, I., Gross, M. (1979). Substituent effects in the electroreduction of porphyrins

and metalloporphyrins. *J. Am. Chem. Soc.*, 101(14), 3857-3862. (DOI: 10.1021/ja00508a024).

[72] Baldwin, J. E., Crossley, M. J., DeBernardis, J. (1982). Efficient peripheral functionalization of porphyrins. *Tetrahedron*, 38(5), 685-692. (DOI: 10.1016/0040-4020(82)80211-1).

[73] Cavaleiro, J. A., Neves, M. G., Hewlins, M. J., Jackson, A. H. (1986). Reactions of porphyrins with nitronium tetrafluoroborate in pyridine. *J. Chem. Soc., Perkin Trans. 1*, 575-579. (DOI: 10.1039/p19860000575).

[74] Shea, K. M., Jaquinod, L., Smith, K. M. (1998). Dihydroporphyrin synthesis: new methodology. *J. Org. Chem.*, 63(20), 7013-7021. (DOI: 10.1021/jo980965p).

[75] Crossley, M. J., King, L. G., Newsom, I. A., Sheehan, C. S. (1996). Investigation of a 'reverse'approach to extended porphyrin systems. Synthesis of a 2, 3-diaminoporphyrin and its reactions with α-diones. *J. Chem. Soc., Perkin Trans. 1*, (22), 2675-2684. (DOI: 10.1039/P19960002675).

[76] Kruper Jr, W. J., Chamberlin, T. A., Kochanny, M. (1989). Regiospecific aryl nitration of meso-substituted tetraarylporphyrins: a simple route to bifunctional porphyrins. *J. Org. Chem.*, 54(11), 2753-2756 (DOI: 10.1021/jo00272a057).

[77] Śniechowska, J., Paluch, P., Pawlak, T., Bujacz, G. D., Danikiewicz, W., Potrzebowski, M. J. (2018). New synthetic pathway leading to oxospirochlorins. *RSC Adv.*, 8(38), 21354-21362. (DOI: 10.1039/C8RA02445F).

[78] Blom, M., Norrehed, S., Andersson, C. H., Huang, H., Light, M. E., Bergquist, J., Grennberg, H., Gogoll, A. (2016). Synthesis and properties of bis-porphyrin molecular tweezers: effects of spacer flexibility on binding and supramolecular chirogenesis. *Molecules*, 21(1), 16. (DOI: 10.3390/molecules21010016).

[79] Tojo, T., Nishida, K., Kondo, T., Yuasa, M. (2020). Correlations between functional porphyrin positions and accumulation in cancer cells. *Bioorganic Med. Chem. Lett.*, 30(19), 127437. (DOI: 10.1016/j.bmcl.2020.127437).

[80] Kesavan, P. E., Pandey, V., Ishida, M., Furuta, H., Mori, S., Gupta, I. (2020). Synthesis, Photophysical Properties and Computational Studies of beta-Substituted Porphyrin Dyads. *Chem. Asian J.*, 15(13), 2015-2028. (DOI: 10.1002/asia.202000463).

[81] Fang, Y., Yadav, I., Osterloh, W. R., Chaudhri, N., Sankar, M., Kadish, K. M. (2020). Electrochemistry of Tri-substituted Porphyrins with *β*-Appended Ethyl Acetoacetate and Acetylacetone in Neutral and Basic Nonaqueous Solvents. *ChemElectroChem*, 7(7), 1723-1732. (DOI: 10.1002/celc.202000191).

[82] Mapley, J. I., Hayes, P., Officer, D. L., Wagner, P., Gordon, K. C. (2020). Investigation of Ferrocene Linkers in *β*-Substituted Porphyrins. *J. Phys. Chem. A*, 124(27), 5513-5522. (DOI: 10.1021/acs.jpca.0c00786).

[83] Ahmad Dar, T., Mandeep, Sankar, M. (2018). Synthesis, spectral and electrochemical redox properties of N-methyl fused nickel (II) porphyrin. *J. Porphyrins Phthalocyanines*, 22(12), 1106-1110. (DOI: 10.1142/S1088424618501109).

[84] Chaudhri, N., Cong, L., Grover, N., Shan, W., Anshul, K., Sankar, M., Kadish, K. M. (2018). Synthesis and electrochemical characterization of acetylacetone (acac) and ethyl acetate (EA) appended *β*-trisubstituted push–pull porphyrins: Formation of electronically communicating porphyrin dimers. *Inorg. Chem.*, 57(21), 13213-13224. (DOI: 10.1021/acs.inorgchem.8b01690).

[85] Dar, T. A., Tomar, R., Mian, R. M., Sankar, M., Maurya, M. R. (2019). Vanadyl β-tetrabromoporphyrin: synthesis, crystal structure and its use as an efficient and selective catalyst for olefin epoxidation in aqueous medium. *RSC Adv*, 9(18), 10405-10413. (DOI: 10.1039/C8RA09825E).

[86] Swamy, P. C. A., Mukherjee, S., Thilagar, P. (2014). Dual binding site assisted chromogenic and fluorogenic recognition and discrimination of fluoride and cyanide by a peripherally

borylated metalloporphyrin: overcoming anion interference in organoboron based sensors. *Anal. Chem*, 86(7), 3616-3624. (DOI: 10.1021/ac500230p).

[87] Kumar, R., Yadav, P., Rathi, P., Sankar, M. (2015). Synthesis, spectroscopic, electrochemical redox, solvatochromism and anion binding properties of β-tetra-and-octaphenylethynyl substituted meso-tetraphenylporphyrins. *RSC Adv.*, 5(100), 82237-82246. (DOI: 10.1039/C5RA15211A).

[88] Chahal, M. K., Sankar, M. (2015). Porphyrin chemodosimeters: synthesis, electrochemical redox properties and selective 'naked-eye'detection of cyanide ions. *RSC Adv*, 5(120), 99028-99036. (DOI: 10.1039/C5RA19847J).

[89] Moura, N. M., Núñez, C., Santos, S. M., Faustino, M. A. F., Cavaleiro, J. A., Neves, M. G. P. M. S., Capelo, J. L., Lodeiro, C. (2014). Synthesis, spectroscopy studies, and theoretical calculations of new fluorescent probes based on pyrazole containing porphyrins for Zn (II), Cd (II), and Hg (II) optical detection. *Inorg. Chem*, 53(12), 6149-6158. (DOI: 10.1021/ic500634y).

[90] O'regan, B., Grätzel, M. (1991). A low-cost, high-efficiency solar cell based on dye-sensitized colloidal TiO 2 films. *nature*, 353(6346), 737-740. (DOI: 10.1038/353737a0).

[91] Sakurada, T., Arai, Y., Segawa, H. (2014). Porphyrins with β-acetylene-bridged functional groups for efficient dye-sensitized solar cells. *RSC Adv*, 4(26), 13201-13204. (DOI: 10.1039/c3ra41317a).

[92] Hayashi, H., Touchy, A. S., Kinjo, Y., Kurotobi, K., Toude, Y., Ito, S., Saarenpää, H., Tkachenko, N. V., Lemmetyinen, H., Imahori, H. (2013). Triarylamine-Substituted Imidazole-and Quinoxaline-Fused Push–Pull Porphyrins for Dye-Sensitized Solar Cells. *ChemSusChem*, 6(3), 508-517. (DOI: 10.1002/cssc.201200869).

[93] Ishida, M., Park, S. W., Hwang, D., Koo, Y. B., Sessler, J. L., Kim, D. Y., Kim, D. (2011). Donor-substituted β-functionalized

porphyrin dyes on hierarchically structured mesoporous TiO2 spheres. Highly efficient dye-sensitized solar cells. *J. Phys. Chem. C*, *115*(39), 19343-19354. (DOI: 10.1021/jp202307b).

[94] Ishida, M., Hwang, D., Zhang, Z., Choi, Y. J., Oh, J., Lynch, V. M., Kim, D. Y., Sessler, J. L., Kim, D. (2015). *β*-Functionalized Push–Pull Porphyrin Sensitizers in Dye-Sensitized Solar Cells: Effect of π-Conjugated Spacers. *ChemSusChem*, 8(17), 2967-2977. (DOI: 10.1002/cssc.201500085).

[95] Kira, A., Matsubara, Y., Iijima, H., Umeyama, T., Matano, Y., Ito, S., Niemi, M., Tkachenko, N. V., Lemmetyinen, H., Imahori, H. (2010). Effects of π-elongation and the fused position of quinoxaline-fused porphyrins as sensitizers in dye-sensitized solar cells on optical, electrochemical, and photovoltaic properties. *J. Phys. Chem. C*, *114*(25), 11293-11304. (DOI: 10.1021/jp1004049).

[96] Lu, F., Feng, Y., Wang, X., Zhao, Y., Yang, G., Zhang, J., Zhang, B., Zhao, Z. (2017). Influence of the additional electron-withdrawing unit in *β*-functionalized porphyrin sensitizers on the photovoltaic performance of dye-sensitized solar cells. *Dyes Pigm.*, 139, 255-263. (DOI: 10.1016/j.dyepig.2016.12.027).

[97] Rathi, P., Kumar, S., Banerjee, D., Soma, V. R., Sankar, M. (2020). Unsymmetrical β-functionalized 'push–pull' porphyrins: synthesis and photophysical, electrochemical and nonlinear optical properties. *Dalton Trans.*, 49(10), 3198-3208. (DOI: 10.1039/C9DT04252K).

[98] Marks R. N., Halls, J. J. M., Bradley D. D. C., Friend R. H., Holmes A. B. (1994), The photovoltaic response in poly(p-phenylene vinylene) thin-film devices, R. N. Marks, *J. Phys.: Condens. Matter* 6, 1379, (DOI: 10.1088/0953-8984/6/7/009).

[99] Yu G., Gao J., Hummelen J. C., Wudl F., Heeger A. J. (1995), Polymer Photovoltaic Cells: Enhanced efficiencies via a network of internal donoracceptor heterojunctions, *Science*, 270, 1789-1791 (DOI: 10.1126/science.270.5243.1789).

[100] Wong, W. W., Khoury, T., Vak, D., Yan, C., Jones, D. J., Crossley, M. J., Holmes, A. B. (2010). A porphyrin-hexa-peri-hexabenzocoronene-porphyrin triad: synthesis, photophysical properties and performance in a photovoltaic device. *J. Mater. Chem*, 20(33), 7005-7014. (DOI: 10.1039/c0jm00311e).

[101] Tojo, T., Nishida, K., Kondo, T., Yuasa, M. (2020). Correlations between functional porphyrin positions and accumulation in cancer cells. *Bioorganic Med. Chem. Lett.*, 30(19), 127437. (DOI: 10.1016/j.bmcl.2020.127437).

Chapter 2

Materials and Experimental Techniques

2.1. Introduction

This chapter discusses about the materials used, spectroscopic techniques, the computational calculations and the instrumentation employed in the characterization of synthesized molecules.

2.2. Chemicals for synthesis

Common solvents used for syntheses were purified according to known procedures.[1] Benzaldehyde, pyrrole, propionic acid, N-bromosuccinimide, HCl, NaOH, bispinacolato diboron, 4-bromo-1,8-naphthalic anhydride, triphenylamine, phenothiazine, N, N-dimethylaniline and carbazole were obtained from S. D. Fine chem. Ltd. Triethylamine, was obtained from Spectrochem, $PdCl_2(PPh_3)_2$, $Pd(dppf)Cl_2 \cdot CH_2Cl_2$, $Pd(PPh_3)_4$, tetrabutylammonium hexafluorophosphate ($TBAPF_6$), ferrocene, were procured from Aldrich chemicals USA. Silica gel (100–200 mesh and 230–400 mesh) were purchased from Rankem chemicals, India. TLC pre-coated silica gel plates (Kieselgel 60F254, Merck) were obtained from Merck, India. Dry solvents chloroform, dichloromethane, N,N-dimethylformamide (DMF), tetrahydrofuran (THF), 1,2-dichloroethane, acetone, toluene and methanol were obtained from S. D. Fine chem. Ltd and Spectrochem India. All moisture sensitive reactions were performed under nitrogen/argon atmosphere using standard schlenk method. The N-Bromosuccinmide was recrystallized from hot water before use. The solvents and reagents were used as received unless otherwise indicated. Photophysical and electrochemical studies were performed using spectroscopic grade solvents.

2.3. Spectroscopic Measurements

2.3.1. NMR Spectroscopy

^{1}H NMR (400 MHz and 500 MHz), and ^{13}C NMR (101 MHz and 126 MHz) spectra were recorded on the Bruker Avance (III) 400 MHz and Model AVNACE NEO500 Ascend Bruker 500 MHz, using $CDCl_3$ as solvent. Chemical shifts in ^{1}H, and ^{13}C NMR spectra were reported in parts per million (ppm). In ^{1}H NMR chemical shifts are reported relative to the residual solvent peak ($CDCl_3$, 7.26 ppm). Multiplicities are given as: s (singlet), d (doublet), t (triplet), q (quartet), m (multiplet). ^{13}C NMR chemical shifts are reported relative to the solvent residual peak ($CDCl_3$, 77.02 ppm).

2.3.2. Mass Spectrometry

High resolution mass spectra (HRMS) were recorded on Brucker-Daltonics, micrOTOF-Q II mass spectrometer using positive and negative mode electrospray ionizations.

2.3.3. UV-Vis Spectroscopy

UV-Vis absorption spectra were recorded using a Varian Cary100 Bio UV-Vis and PerkinElmer LAMBDA 35 UV/Vis spectrophotometer.

2.3.4. Fluorescence Spectroscopy

Fluorescence emission spectra were recorded upon specific excitation wavelength on a Horiba Scientific Fluoromax-4 spectrophotometer. The slit width for the excitation and emission was set at 2 nm.

The fluorescence quantum yields (ϕ_F)

The fluorescence quantum yields (ϕ_F) of compounds were calculated by the steady-state comparative method using following equation,

$$\phi_F = \phi_{st} \times S_u/S_{st} \times A_{st} / A_u \times n_2D_u/n_2 D_{st} \quad \ldots\ldots\ldots\ldots\ldots\ldots \text{(Eq. 1)}$$

Where ϕ_F is the emission quantum yield of the sample, ϕ_{st} is the emission quantum yield of the standard, A_{st} and Au represent the absorbance of the standard and sample at the excitation wavelength, respectively,

while S_{st} and S_u are the integrated emission band areas of the standard and sample, respectively, and nD_{st} and nD_u the solvent refractive index of the standard and sample, u and st refer to the unknown and standard, respectively.

2.4. Electrochemical Studies

Cyclic voltammograms (CVs) were recorded on CHI620D electrochemical analyzer using Glassy carbon as working electrode and Pt wire as the counter electrode, Ag/Ag^+ as the reference electrode. The scan rate was 100 mVs^{-1}. A solution of tetrabutylammonium hexafluorophosphate (TBAPF$_6$) in CH_2Cl_2 (0.1 M) was employed as the supporting electrolyte.

2.5. Computational Calculations

The density functional theory (DFT) calculation were carried out at the B3LYP/6-31G level for C, N, O, H, Zn, S in the Gaussian 09 program.[2]

2.6. References

[1] (a) Vogel A. I., Tatchell A. R., Furnis B. S., Hannaford A. J., Smith, P. W. G. (1996), Vogel's Textbook of Practical Organic Chemistry (5th Edition) (5th ed.). (b) Wei Ssberger A. Proskraner E. S. Riddick J. A., Toppos Jr. E. F. (1970). Organic Solvents in Techniques of Organic Chemistry, Vol. IV, 3rd Edition, Inc. New York.

[2] (a) Frisch, M. J.; Trucks, G. W.; Schlegel, H. B.; Scuseria, G. E.; Robb, M. A.; Cheeseman, J. R.; Scalmani, G.; Barone, V.; Mennucci, B.; Petersson, G. A.; Nakatsuji, H.; Caricato, M.; Li, X.; Hratchian, H. P.; Izmaylov, A. F.; Bloino, J.; Zheng, G.; Sonnenberg, J. L.; Hada, M.; Ehara, M.; Toyota, K.; Fukuda, R.; Hasegawa, J.; Ishida, M.; Nakajima, T.; Honda, Y.; Kitao, O.; Nakai, H.; Vreven, T.; Montgomery, J. A. Jr.; Peralta, J. E.; Ogliaro, F.; Bearpark, M.; Heyd, J. J.; Brothers, E.; Kudin, K. N.; Staroverov, V. N.; Kobayashi, R.; Normand, J.; Raghavachari, K.; Rendell, A.; Burant, J. C.; Iyengar, S. S.; Tomasi, J.; Cossi, M.; Rega, N.; Millam, N. J.; Klene, M.; Knox, J. E.; Cross, J. B.; Bakken, V.; Adamo, C.; Jaramillo, J.; Gomperts, R.; Stratmann, R. E.; Yazyev,

O.; Austin, A. J.; Cammi, R.; Pomelli, C.; Ochterski, J. W.; Martin, R. L.; Morokuma, K.; Zakrzewski, V. G.; Voth, G. A.; Salvador, P.; Dannenberg, J. J.; Dapprich, S.; Daniels, A. D.; Farkas, O.; Foresman, J. B.; Ortiz, J. V.; Cioslowski, J.; Fox, D. J. (2009). Gaussian 09, revision A.02; *Gaussian, Inc*.: Wallingford, CT. (b) Lee, C., Yang, W., & Parr, R. G. (1988). Development of the Colle-Salvetti correlation-energy formula into a functional of the electron density. *Physical Review B*, 37(2), 785–789. (DOI: 10.1103/PhysRevB.37.785) (c) Becke, A. D. (1993). A new mixing of Hartree-Fock and local density-functional theories. *J. Chem. Phys*. 98, 1372–377. (DOI: 10.1063/1.464304).

Chapter 3

Unsymmetrical *β*-substituted push–pull tetraarylporphyrins

3.1. Introduction

Porphyrin molecules are often reported as a promising candidate for the generation of artificial photosynthetic system to mimic the natural photosynthetic process.[1] The energy-transfer and electron-transfer processes in the light-harvesting capability of porphyrin chromophores have been well studied for organic photovoltaics and photodynamic therapy. [2−7] Porphyrin chromophores have potential applications in biomimetic catalysis, molecular electronics and Supramolecular chemistry. [8−10] Push-pull chromophores with electron donors (D) and acceptors (A) have been a topic of interest due to its widespread applications.[11,12] Triphenylamine (TPA) unit have been used as an electron-donor and hole-transporting material for photovoltaic applications, whereas 1,8-naphthalimide chromophores act as a strong acceptor unit and possess high charge carrier mobility.[13−16] Over the years, porphyrin dyes have been used in the push−pull systems due to its potential light absorption ability.[17] The porphyrin macrocycle can be functionalized at the *meso* as well as at the *β*-positions. The substitution at the *β*-position have greater steric repulsion which leads to the distorted structures in the porphyrin molecules. The introduction of *β*-substituents has a substantial effect on the electronic properties of these molecules. The introduction of mono- and disubstituent at the *β*-pyrrole positions of the porphyrin ring are synthetically more attractive due to its synthetic challenges.[18, 19] The synthesis of di and trisubstitution on the *β*-pyrrole ring was reported by H. J. Callot in 1974.[20]

The synthesis and regiochemistry of *β*-disubstituted porphyrins and metalloporphyrins are largely unexamined due to the formation of

mixture products. Bhyrappa *et al.* have reported the preparation of partial β-pyrrole brominated TPP with isomers and the crystal structures of the complexes were explored.[21] Recently Pizzotti *et al.* synthesized β-disubstituted push–pull tetraaryl Zn[II] porphyrinates and were used for DSSC applications.[22] Sankar *et al.* have reported the synthesis of mixed antipodal β-substituted porphyrins and its electronic and the redox properties were explored.[23] Tagliatesta *et al.* have synthesized 2,12 positions of β-substituted porphyrin and its electron-transfer processes were investigated.[24]

In this chapter, we wish to report the design and synthesis of push–pull porphyrins **1**–**6** via β-pyrrole functionalization, wherein the push group, triphenylamine (TPA) and the pull group, naphthalimide (NI) units have been incorporated in the porphyrin π-system (Figure 3.1). Therefore, we have comparatively investigated the photophysical and computational studies of porphyrins **1**–**6**, in order to understand the effect of donor and acceptor on the push−pull porphyrin derivatives.

1, M = 2H	**3, M = 2H**	**5, M = 2H**
2, M = Zn	**4, M = Zn**	**6, M = Zn**
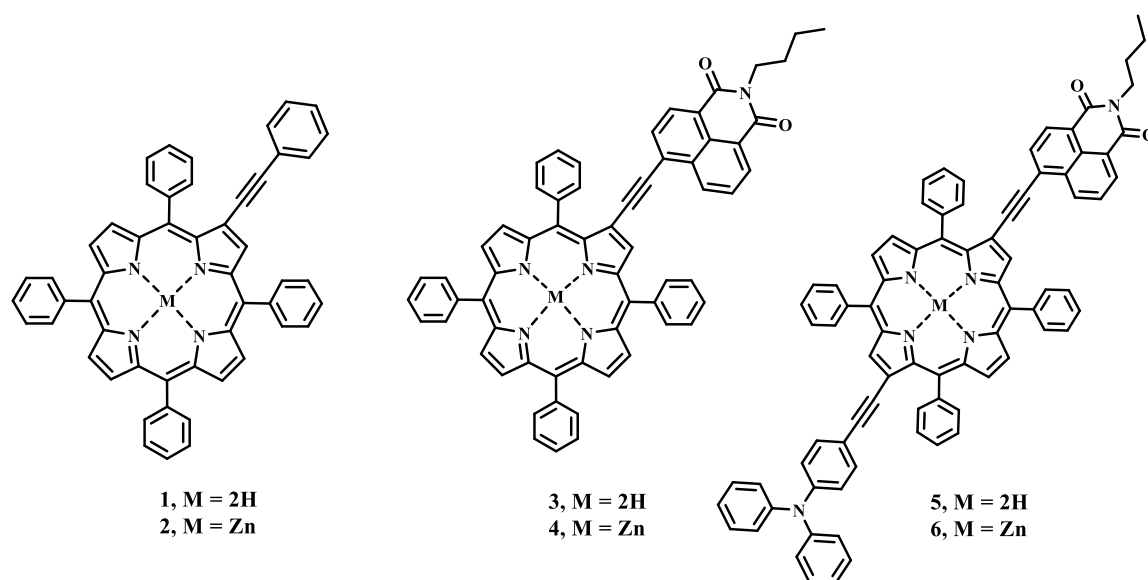
Figure 3.1. Structure of the push-pull porphyrins, **1-6**, used in the present study.

Scheme 3.1. Synthesis of porphyrins **1**−**6**.

3.2. Results and Discussion

Synthesis

The synthesis of push–pull porphyrin and its zinc derivatives **1**–**6** are shown in Scheme 3.1. The tetraphenylporphyrin (TPP) and monobrominated TPPBr, **10** were synthesized as per the reported procedures.[25] The synthesis of β-dibrominated TPP **11** was carried out using controlled amount of N-bromosuccinimide (NBS) (1.8 equiv) in $CHCl_3$ at room temperature for 24 hours, which resulted in H_2TPPBr_2 (**11**) as mixture of products (Scheme 3.1).[21] The Pd-catalyzed Sonogashira cross-coupling reaction using phenylacetylene **7** with TPPBr in the presence of $Pd(PPh_3)_4$ at 70 °C in THF solvent resulted in porphyrin **1** with 53% yield (Scheme 3.1). The Sonogashira cross-coupling reaction of β-monobrominated TPPBr with 1 equivalents of 2-butyl-6-ethynyl-1H-benzo[de]isoquinoline-1,3(2H)-dione **8** resulted in porphyrin **3** with 78% yield. The H_2TPPBr_2 **11** mixture was subjected to Sonogashira cross-coupling reaction with 4-ethynyl-N,N-diphenyl aniline **9** resulted in porphyrin **12** (expected **12a**/**12b**) isomers in 79% yield. The separation of the porphyrin **12a** was evidenced from ^{1}H NMR characterization. However, it may be mentioned here that we were unable to discriminate the positions of bromination, whether it was at the 2,12- or 2,13-positions, although there is clear ^{1}H NMR evidence that only one dibrominated product was isolated.[22] The Sonogashira crosscoupling reaction was further carried out on porphyrin **12** with 1 equivalent of 2-butyl-6-ethynyl-1H-benzo[de]isoquinoline-1,3(2H)-dione **8** resulted in porphyrin **5** with 47% yield. The zinc insertion on porphyrins **1**, **3** and **5** were carried out with $Zn(OAc)_2$ in $MeOH/CHCl_3$ (3:1) mixture, which resulted in zinc porphyrin **2**, **4** and **6** with 87, 86 and 81% yields, respectively. The porphyrin and its zinc derivatives **1**–**6** were purified and well characterized by ^{1}H and ^{13}C NMR, HRMS and MALDI-TOF mass spectra.

3.3. Photophysical Properties

The absorption and emission spectra of β-mono and disubstituted porphyrin and their zinc complexes **1**–**6** were recorded in dichloromethane (Figure 3.2), and the corresponding data are compiled in Table 3.1. The absorption spectrum of porphyrins **1**–**6** show the typical absorption spectra with intense Soret bands in the range of 426−436 nm and the Q-bands between 522–667 nm. The incorporation of electron withdrawing naphthalimide unit **8** on the β-position of the porphyrin **3** and **4** results in a slight red shift of the Soret band and the Q-bands compared to the porphyrin **1** and **2**. The Soret and Q band of push–pull porphyrin **5** and **6** containing triphenyl amine and naphthalimide unit at the opposite β, β'-positions of the porphyrin exhibits red shifted absorption in the soret and the Q band region. The Soret and Q band of the porphyrin **5** and **6** resulted in red shift by 4–6 nm in the Soret band region compared to porphyrin **1** and **2** respectively. The porphyrin **5** and **6** shows a redshifted absorption of about 2–7 nm in the soret band region compared to porphyrin **3** and **4** respectively. The observed red shift in the Soret and the Q-bands of porphyrin **5** and **6** resulted from the enhanced π-conjugation due to a stronger push−pull effect of the electron donor and the acceptor units at the opposite β, β'-positions.

The Steady state fluorescence spectra of the β-porphyrin and their zinc complexes was measured in dichloromethane (Figure 3.2) and the data are tabulated in Table 3.1. The porphyrin **1**–**6** shows emission band around 607–748 nm in the visible region. The free base porphyrin **1**, **3** and **5** shows a redshifted emission band compared to their zinc complexes **2**, **4** and **6**. The porphyrin **3** and **4** with naphthalimide unit at the β-pyrrolic position exhibits red shifted emission band
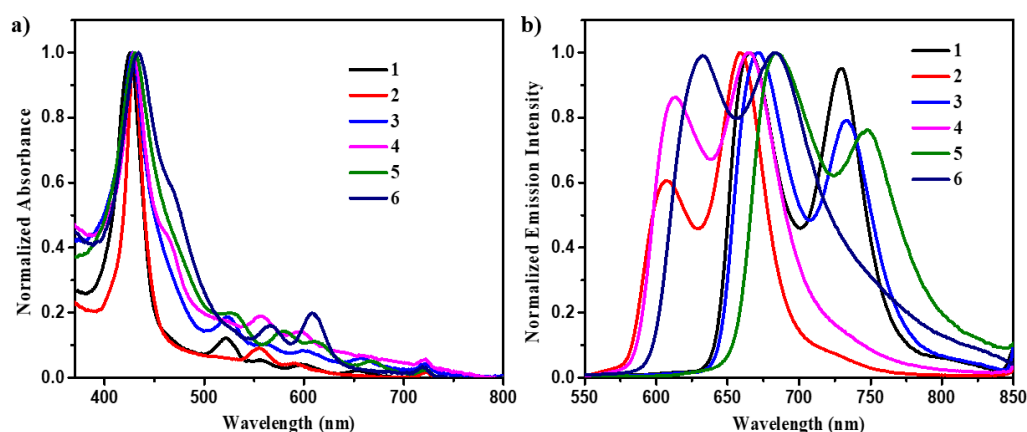
Figure 3.2. Normalized electronic absorption of porphyrin (a) **1**–**6** and emission spectra of porphyrin (b) **1**–**6** measured in dichloromethane at 1.0 × 10⁻⁵ M concentration.

Table 3.1. Photophysical and theoretical data of porphyrin **1**–**6**.

Compound	λ_{abs} (nm) [a]			λ_{em} (nm)	Φ_f [b]	H–L gap(eV) [c]
	Soret band	ε (M^{-1} cm^{-1})	Q-bands			
1	426	10810	522, 558, 599, 655	666, 729	0.08	2.50
2	430	12240	556, 590	659, 607	0.03	2.64
3	428	95410	524, 563, 602, 657	671, 733	0.07	2.38
4	429	10460	558, 597	664, 613	0.03	2.38
5	430	12170	529, 580, 612, 667	684, 748	0.05	2.06
6	436	08690	568, 610	683, 632	0.09	2.17

[a] Absorbance measured in dichloromethane at 1×10⁻⁵ M concentration; λ_{abs}: absorption wavelength; λ_{em}: emission wavelength; ε: extinction coefficient. [b] The fluorescence quantum yields were recorded using H₂TPP as a standard (Φ_{st} = 0.11). [c] Calculated from computational study.

compared to porphyrin **1** and **2**. The emission spectra show considerable red shift in the fluorescence maxima of push–pull porphyrin **5** and **6**

compared to porphyrin **1**, **2**, **3** and **4** respectively. The red shifted emission in porphyrin **5** and **6** confirms the strong electronic communication between the electron donor and the acceptor units. The fluorescence quantum yields (Φ) were recorded in dichloromethane using H_2TPP (Φ_{st} = 0.11) as a standard. The quantum yields (Φ) for porphyrin **1**–**6** were seen around 0.03–0.09. The highest quantum yield value of 0.09 were observed for porphyrin **6**.

3.4. Computational studies

To gain further insight into the electronic distribution of the push–pull porphyrin **1**–**6**, the density functional theory (DFT) calculations were performed at B3LYP/6-31G level using the Gaussian 09 W program.[26] The energy level diagram and the frontier orbitals of porphyrin **1**–**6** are shown in Figure 3.3. The porphyrin **1** and **2** shows that the electron density of HOMO is localized on the porphyrin macrocycle, whereas in LUMO it is mainly populated on porphyrin macrocycle with parts dispersed over the phenylacetylene group. In porphyrin **3** and **4**, the HOMO is populated on the porphyrin macrocycle and the LUMO is mainly concentrated on the naphthalimide unit with parts dispersed over the porphyrin macrocycle. In porphyrins **5** and **6** the electron density of HOMO is concentrated on triphenyl amine donor group whereas the LUMOs are populated on the naphthalimide unit with parts dispersed over the porphyrin macrocycle. The theoretically calculated HOMO levels of the porphyrins **1**, **2**, **3**, **4**, **5** and **6** are –5.25 eV, –5.20 eV, –5.28 eV, –5.22 eV, –5.03 eV and –5.01 eV whereas LUMO levels are –2.75 eV, –2.56 eV, –2.90 eV, –2.84 eV, –2.97 eV and –2.84 eV respectively. The theoretically calculated HOMO and LUMO energy level of porphyrin **5** and **6**, exhibits a low HOMO–LUMO band gap of about 2.06 eV and 2.17 eV compared to porphyrins **1**, **2**, **3** and **4**.
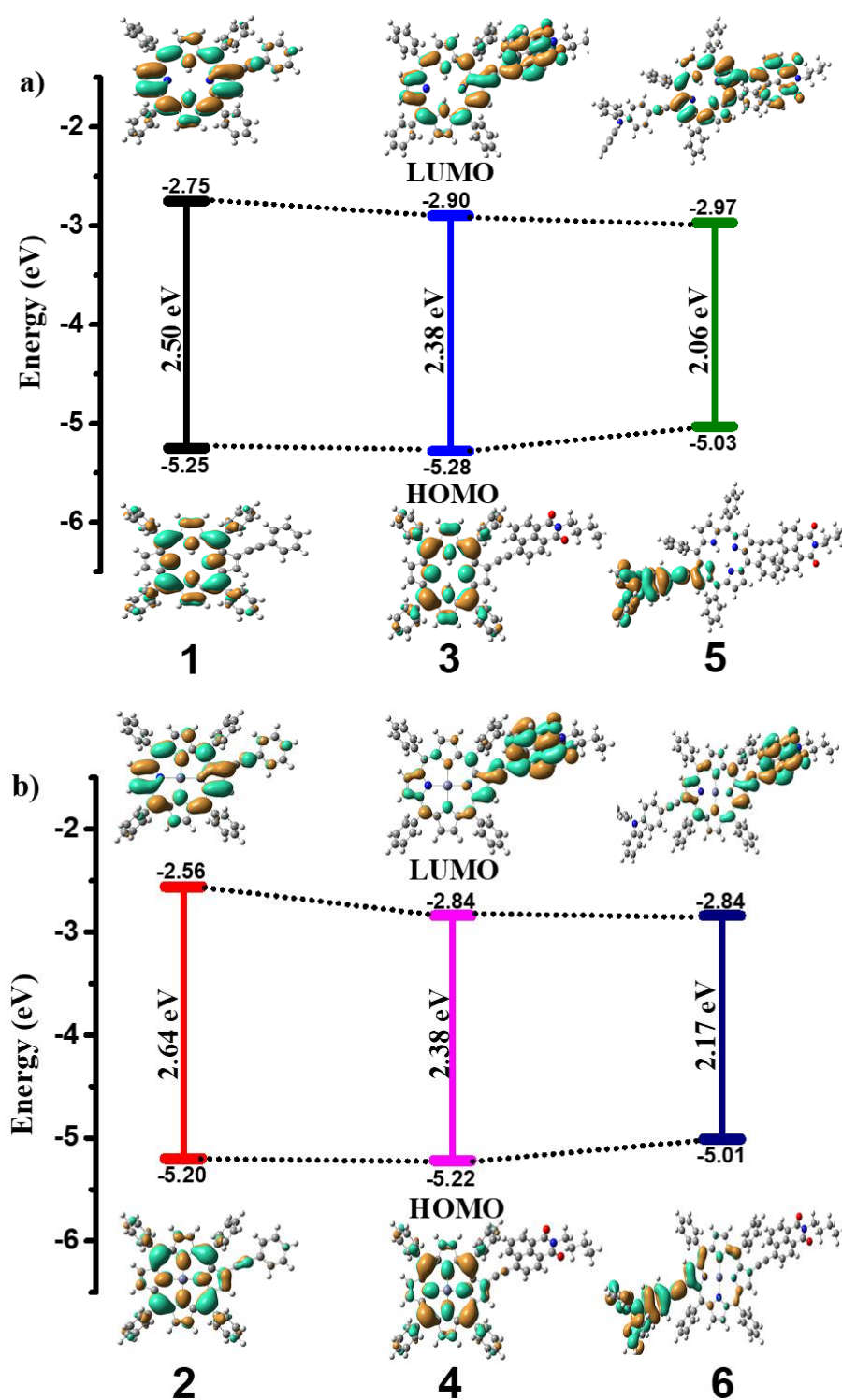
Figure 3.3. Energy level diagram and the frontier HOMO and LUMO on B3LYP/6-31G optimized structures of porphyrins (a) **1**, **3**, **5** and (b) **2**, **4**, **6**.

The time-dependent density functional theory (TD-DFT) calculation was performed to explore the electronic absorption spectra of porphyrin **1**–**6**, using B3LYP/6-31G level and the data are tabulated in Table 3.2. The TD-DFT calculation of porphyrin **1**–**6** shows two absorption bands in the UV-visible region, the Soret band and the Q-band. The porphyrin **1**–**6** shows absorption bands around 378–675 nm in the Soret band and the Q-band region. The porphyrins **1**, **2**, **3**, **4**, **5** and **6** exhibits absorption band around 603, 554, 613, 572, 675 and 628 nm in the low energy Q-band region and are assigned to ICT transitions. The major ICT transitions for porphyrin **1**–**6** arises from HOMO →LUMO.

Table 3.2. Calculated Electronic Transitions of porphyrin **1**–**6**.

Compounds	λ_{max}	Composition & Molecular contribution	f^a	Assignment
1	387	HOMO–2→LUMO (0.39)	1.63	π–π*
	603	HOMO→LUMO (0.59)	0.04	ICT
2	380	HOMO–1→LUMO+1 (0.34)	1.12	π–π*
	554	HOMO→LUMO (0.48)	0.03	ICT
3	380	HOMO→LUMO+1 (0.34)	1.22	π–π*
	613	HOMO →LUMO (0.61)	0.05	ICT
4	378	HOMO–1→LUMO+1 (0.37)	0.84	π–π*
	572	HOMO→LUMO (0.62)	0.08	ICT
5	486	HOMO–3→LUMO (0.39)	1.08	π–π*
	675	HOMO →LUMO (0.67)	0.35	ICT
6	416	HOMO–5→LUMO (0.45)	0.61	π–π*
	628	HOMO →LUMO (0.67)	0.48	ICT

f^a Oscillator strength

The porphyrin **1**, **2**, **3**, **4**, **5** and **6** exhibits absorption band between 387, 380, 380, 378, 486 and 416 nm in the high energy Soret band region and are attributed to π–π* transitions. The π–π* transitions for porphyrin **1**–**6** occurs from HOMO–2→LUMO, HOMO–1→LUMO+1, HOMO→LUMO+1, HOMO–3→LUMO and HOMO–5→LUMO, respectively. The TD-DFT calculated values was in good agreement with the experimental data.

3.5. Experimental Section

General: All chemicals were used as received unless otherwise noted. All moisture sensitive reactions were performed under argon/nitrogen atmosphere. The NMR spectra were recorded at room temperature (298 K). Chemical shifts are given in ppm with respect to tetramethylsilane as internal standard ($CDCl_3$, 7.26 ppm, 77.0 ppm). ^{1}H NMR and ^{13}C NMR spectra were recorded using a 400 MHz and 100 MHz spectrometer. Multiplicities are given as s (singlet), d (doublet), t (triplet) and m (multiplet) are given in Hertz. TLC analysis was carried out using silica gel 60 F_{254} plates. UV-visible absorption spectra were recorded on a Cary-100 Bio UV-visible spectrophotometer. Emission spectra were taken in a The Fluoromax-4C, S/n. 1579D-1417-FM Fluorescence software Ver 3.8.0.60. UV/Vis and emission spectrums of all compounds were recorded in dichloromethane solution. The density functional theory (DFT) calculation were carried out at the B3LYP/6-31G level for C, N, H, O, Zn in the Gaussian 09 program. HRMS was recorded on TOF-Q mass spectrometer.

Synthesis

Synthesis of 5,10,15,20-tetraphenyl-7-(phenylethynyl) porphyrin (1).

7-bromo-5,10,15,20-tetraphenylporphyrin **10** (0.150 g, 0.21 mmol), ethynylbenzene **7** (0.033 g, 0.32 mmol) in THF: TEA (1: 1, v/v), palladium(0)-tetrakis(triphenylphosphine) (0.070 g, 0.06 mmol), and CuI (0.010 g, 0.05 mmol) were added under argon atm at room temperature. The reaction mixture was stirred for 12 h at 70 °C, and then cooled to room temperature. The solvent was then evaporated under reduced pressure and the resultant mixture was diluted with DCM and the organic layer was collected, dried over anhydrous Na_2SO_4 and evaporated under vacuum. The solid was adsorbed on silica gel and purified by column chromatography, using a DCM: hexane (20: 80) mixture to produce (0.080 g, 53%) of compound **1** as purple solid. ^{1}H NMR (400 MHz, $CDCl_3$): δ ppm= -2.66 (s, 2 H) 7.37 (m, 4 H) 7.64 - 7.82 (m, 13 H) 8.23 (s, 8 H) 8.76 - 8.89 (m, 6 H) 9.09 (s, 1 H). ^{13}C NMR

(100 MHz, CDCl$_3$): δ ppm= 85.58, 98.48, 119.58, 119.69, 119.74, 120.04, 123.47, 126.28, 126.37, 127.43, 128.25, 131.64, 134.12, 134.16, 140.80, 141.43, 141.67, 141.72, 141.77. HRMS (ESI-TOF): m/z calculated for C$_{52}$H$_{34}$N$_4$ [M+nH]$^+$ 715.2856, found 715.2834.

Synthesis of 5,10,15,20-tetraphenyl-7-(phenylethynyl)porphyrin, zinc (2).

5,10,15,20-tetraphenyl-7-(phenylethynyl) porphyrin **1** (0.100 g, 0.14 mmol), Zn (OAc)$_2$, (0.289 g, 1.32 mmol) in MeOH: CHCl$_3$ (3 : 1, v/v), were added and the reaction mixture was stirred for 1 h at room temperature. The solvent was then evaporated under reduced pressure and the resultant mixture was diluted with DCM/water and the organic layer was collected, dried over anhydrous Na$_2$SO$_4$ and evaporated under vacuum. The solid was adsorbed on silica gel and purified by column chromatography, using a DCM: hexane (40: 60) mixture to produce (0.095 g, 87%) of compound **2** as red solid. ^{1}H NMR (400 MHz, CDCl$_3$): δ ppm= 7.35-7.40 (m, 4 H), 7.60 - 7.78 (m, 13 H) 8.23 (s, 8 H) 8.89-8.95 (m, 6 H) 9.26 (s, 1 H). ^{13}C NMR (100 MHz, CDCl$_3$): δ ppm= 86.41, 99.28, 121.38, 121.74, 124.22, 126.22, 126.76, 126.85, 128.07, 128.72, 132.30, 134.41, 134.62, 139.17, 142.21, 142.83, 148.49, 150.36, 150.90, 151.01, 151.32. HRMS (ESI-TOF): m/z calculated for C$_{52}$H$_{32}$N$_4$Zn [M+nH]$^+$ 777.1991, found 777.1996.

Synthesis of 2-butyl-6-((5,10,15,20-tetraphenylporphyrin-7-yl) ethynyl)-1H-benzo[de] isoquinoline-1,3(2H)-dione (3).

7-bromo-5,10,15,20-tetraphenylporphyrin **10** (0.200 g, 0.28 mmol), 2-butyl-6-ethynyl-1H-benzo[de]isoquinoline-1,3(2H)-dione **8** (0.104 g, 0.37 mmol) in THF: TEA (1: 1, v/v), palladium(0)-tetrakis(triphenylphosphine) (0.070 g, 0.06 mmol), and CuI (0.010 g, 0.05 mmol) were added under argon atm at room temperature. The reaction mixture was stirred for 12 h at 70 °C, and then cooled to room temperature. The solvent was then evaporated under reduced pressure and the resultant mixture was diluted with DCM and the organic layer was collected, dried over anhydrous Na$_2$SO$_4$ and evaporated under

vacuum. The solid was adsorbed on silica gel and purified by column chromatography, using a DCM: hexane (30: 70) mixture to produce (0.195 g, 78%) of compound **3** as black solid. ^{1}H NMR (400 MHz, CDCl$_3$): δ ppm= -2.66 (s, 2 H), 1.02 (t, J=7.28 Hz, 3 H), 1.46 - 1.54 (m, 2 H), 1.79 (quin, J=7.53 Hz, 2 H), 4.22 (m, 2 H), 7.28 - 7.35 (m, 3 H), 7.52 (t, J=7.65 Hz, 2 H), 7.69 (d, J=7.78 Hz, 1 H), 7.72 - 7.85 (m, 10 H), 8.20 - 8.27 (m, 7 H), 8.53 (d, J=7.53 Hz, 1 H), 8.61 (dd, J=10.79, 7.78 Hz, 2 H), 8.75 - 8.79 (m, 2 H), 8.83 - 8.88 (m, 1 H), 8.92 (s, 2 H), 9.21 (s, 1 H). ^{13}C NMR (100 MHz, CDCl$_3$): δ ppm= 13.90, 20.45, 29.71, 40.33, 95.09, 96.02, 120.06, 120.38, 120.42, 120.58, 121.53, 122.78, 126.77, 126.84, 126.87, 126.95, 127.88, 128.05, 128.55, 128.72, 129.09, 130.07, 130.90, 131.25, 131.41, 133.25, 134.44, 134.55, 134.59, 134.63, 141.23, 141.73, 141.92, 141.97, 163.90, 164.15. HRMS (ESI-TOF): m/z calculated for C$_{62}$H$_{43}$N$_5$O$_2$ [M+nH] $^+$ 890.3490, found 890.3493.

Synthesis of 2-butyl-6-((5,10,15,20-tetraphenylporphyrin-7-yl)ethynyl)-1H-benzo[de] isoquinoline-1,3(2H)-dione, Zinc (4).

2-butyl-6-((5,10,15,20-tetraphenylporphyrin-7-yl) ethynyl)-1H-benzo[de]isoquinoline-1,3(2H)-dione **3** (0.100 g, 0.11 mmol), Zn (OAc)$_2$, (0.270 g, 1.23 mmol) in MeOH: CHCl$_3$ (3 : 1, v/v), were added and the reaction mixture was stirred for 1 h at room temperature. The solvent was then evaporated under reduced pressure and the resultant mixture was diluted with DCM/water and the organic layer was collected, dried over anhydrous Na$_2$SO$_4$ and evaporated under vacuum. The solid was adsorbed on silica gel and purified by column chromatography, using a DCM: hexane (50: 50) mixture to produce (0.090 g, 86%) of compound **4** as black solid. ^{1}H NMR (400 MHz, CDCl$_3$): δ ppm= 0.81 (t, J=7.28 Hz, 3 H) 1.11 - 1.19 (m, 2 H) 1.26 - 1.32 (m, 2 H) 3.30 (t, J=7.40 Hz, 2 H) 7.20 - 7.25 (m, 1 H) 7.46 (t, J=7.65 Hz, 3 H) 7.52 - 7.56 (m, 1 H) 7.64 (dt, J=15.62, 7.62 Hz, 2 H) 7.73 - 7.82 (m, 9 H) 8.09 - 8.14 (m, 3 H) 8.19 - 8.25 (m, 6 H) 8.52 (d, J=8.28 Hz, 1 H) 8.72 (d, J=5.02 Hz, 1 H) 8.86 (d, J=4.77 Hz, 1 H) 8.90 - 8.95 (m, 3 H) 9.28 (s, 1 H). ^{13}C NMR (100 MHz, CDCl$_3$): δ ppm= 13.62, 20.01, 29.70, 39.32, 95.17, 96.48, 120.30, 120.77, 121.22, 121.32, 121.50,

121.92, 124.21, 126.52, 126.65, 126.74, 127.58, 127.74, 128.36, 128.55, 129.80, 130.82, 131.17, 131.98, 132.38, 132.56, 132.89, 133.15, 134.23, 134.47, 138.90, 142.04, 142.57, 142.59, 163.95, 164.10. HRMS (ESI-TOF): m/z calculated for $C_{62}H_{41}N_5O_2Zn$ [M+nH]$^+$ 952.2624, found 952.2644.

Synthesis of 4-((17-bromo-5,10,15,20-tetraphenylporphyrin-7-yl)ethynyl)-N,N-diphenylaniline (12).

4-ethynyl-N, N-diphenyl aniline **9** (0.078 g, 0.28 mmol), TPPBr$_2$ mixture **11** (0.45 g, 0.58 mmol) in THF: TEA (1: 1, v/v), palladium(0)-tetrakis(triphenylphosphine) (0.100 g, 0.08 mmol), and CuI (0.010 g, 0.05 mmol) were added under argon atm at room temperature. The reaction mixture was stirred for 12 h at 70 °C, and then cooled to room temperature. The solvent was then evaporated under reduced pressure and the resultant mixture was diluted with DCM and the organic layer was collected, dried over anhydrous Na$_2$SO$_4$ and evaporated under vacuum. The solid was adsorbed on silica gel and purified by column chromatography, using a DCM: hexane (20: 80) mixture to produce (0.211 g, 79%) compound **12** mixture with slight separation of substituted TPPBr$_2$ mixture on TLC Figure S13. However, compound **12** mixture were separated by silica gel column chromatography. The separation of the porphyrin **12a** isomer was evidenced from the ^{1}H NMR characterization Figure S14. However, it has to be mentioned that we have clear ^{1}H NMR evidence that only one dibrominated product was isolated as black solid. ^{1}H NMR of 12 mixture (400 MHz, CDCl$_3$): δ ppm= -2.79, -2.67 (s,s, 4 H) 6.95 - 7.02 (m, 4 H) 7.05 - 7.12 (m, 4 H) 7.13 - 7.22 (m, 12 H) 7.29 - 7.35 (m, 8 H) 7.69 - 7.80 (m, 23 H) 8.04 - 8.11 (m, 3 H) 8.15 - 8.25 (m, 13 H) 8.67 - 8.78 (m, 4 H) 8.78 - 8.92 (m, 7 H) 8.95 - 8.99 (d, 1 H) 9.03 (s, 1 H). ^{1}H NMR of 12a (400 MHz, CDCl$_3$): δ ppm= -2.65 (s, 2 H) 7.01 (d, J=8.55 Hz, 2 H) 7.10 (t, J=7.32 Hz, 2 H) 7.15-7.25 (m, J=8.54 Hz, 6 H) 7.30 - 7.37 (m, 4 H) 7.55 (d, J=8.55 Hz, 1 H) 7.70 - 7.80 (m, 11 H) 8.19 - 8.24 (m, 7 H) 8.72 (d, J=4.88 Hz, 1 H) 8.78 (s, 2 H) 8.82 (d, J=4.88 Hz, 1 H) 8.87 (s, 2 H) 9.04 (s, 1 H). ^{13}C NMR (100 MHz, CDCl$_3$): δ ppm= 85.5, 99.6, 119.9, 120.1,

120.5, 121.9, 123.5, 125.0, 126.7, 126.8, 127.8, 127.9, 128.6, 129.4, 133.1, 134.6, 141.9, 142.1, 147.3, 147.6. HRMS (ESI-TOF): m/z calculated for $C_{64}H_{42}N_5Br$ [M+2]$^+$ 962.2681, found 962.2686.

Synthesis of 2-butyl-6-((17-((4-(diphenylamino)phenyl)ethynyl)-5,10,15,20-tetraphenyl porphyrin-7-yl)ethynyl)-1H-benzo[de]isoquinoline-1,3(2H)-dione (5).

4-((17-bromo-5,10,15,20-tetraphenylporphyrin-7-yl)ethynyl)-N,N-diphenylaniline **12** (0.100 g, 0.10 mmol), 2-butyl-6-ethynyl-1H-benzo[de]isoquinoline-1,3(2H)-dione **8** (0.034 g, 0.12 mmol) in THF: TEA (1: 1, v/v), palladium(0)-tetrakis(triphenylphosphine) (0.070 g, 0.06 mmol), and CuI (0.010 g, 0.05 mmol) were added under argon atm at room temperature. The reaction mixture was stirred for 12 h at 70 °C, and then cooled to room temperature. The solvent was then evaporated under reduced pressure and the resultant mixture was diluted with DCM and the organic layer was collected, dried over anhydrous Na_2SO_4 and evaporated under vacuum. The solid was adsorbed on silica gel and purified by column chromatography, using a DCM: hexane (25: 75) mixture to produce (0.054 g, 47%) compound **5** as black solid. ^{1}H NMR (400 MHz, CDCl$_3$): δ ppm= -2.66 (s, 2 H) 1.01 (t, J=7.63 Hz, 3 H) 1.48 (dd, J=14.95, 7.63 Hz, 2 H) 1.69 - 1.79 (m, 2 H) 4.19 (t, J=7.63 Hz, 2 H) 6.99 (d, J=7.93 Hz, 2 H) 7.08 (t, 2 H) 7.15 - 7.21 (m, 5 H) 7.26 - 7.35 (m, 5 H) 7.50 (td, J=7.63, 3.66 Hz, 2 H) 7.60 - 7.66 (m, 1 H) 7.69 - 7.80 (m, 11 H) 8.19 - 8.26 (m, 8 H) 8.47 (t, J=7.32 Hz, 1 H) 8.52 - 8.61 (m, 2 H) 8.69 (s, 1 H) 8.74 (s., 1 H) 8.84 (d, J=7.93 Hz, 1 H) 8.91 (s, 1 H) 8.98 (d, J=4.27 Hz, 1 H) 9.16 (d, J=3.05 Hz, 1 H). ^{13}C NMR (100 MHz, CDCl$_3$): δ ppm= 13.9, 20.4, 22.7, 29.70, 40.3, 85.5, 95.2, 96.0, 100.0, 121.8, 123.5, 125.0, 126.8, 126.9, 128.7, 129.4, 130.9, 131.4, 133.1, 134.4, 134.6, 140.9, 141.1, 141.7, 141.9, 147.3, 147.6, 163.9, 164.1. HRMS (ESI-TOF): m/z calculated for $C_{82}H_{56}N_6O_2$ [M+nH] $^+$ 1157.4538, found 1157.4544.

Synthesis of 2-butyl-6-((17-((4-(diphenylamino)phenyl)ethynyl)-5,10,15,20-tetraphenyl porphyrin -7-yl)ethynyl)-1H-benzo[de]isoquinoline-1,3(2H)-dione, Zinc (6).

2-butyl-6-((17-((4-(diphenylamino)phenyl)ethynyl)-5,10,15,20-tetraphenylporphyrin-7-yl)ethynyl)-1H-benzo[de]isoquinoline-1,3(2H)-dione **5** (0.050 g, 0.04 mmol), Zn (OAc)$_2$, (0.104g, 0.47 mmol) in MeOH: CHCl$_3$ (3 : 1, v/v), were added and the reaction mixture was stirred for 1 h at room temperature. The solvent was then evaporated under reduced pressure and the resultant mixture was diluted with DCM/water and the organic layer was collected, dried over anhydrous Na$_2$SO$_4$ and evaporated under vacuum. The solid was adsorbed on silica gel and purified by column chromatography, using a DCM: hexane (40: 60) mixture to produce (0.039 g, 81%) of compound **6** as green solid. ^{1}H NMR (400 MHz, CDCl$_3$): δ 9.28 (s, 1H), 9.15 (s, 1H), 8.91 (s, 1H), 8.84 (dd, J = 4.7, 1.6 Hz, 1H), 8.74 (dd, J = 4.7, 3.2 Hz, 1H), 8.67 (s, 1H), 8.60 (d, J = 8.9 Hz, 1H), 8.48 (d, J = 7.2 Hz, 1H), 8.14 – 8.24 (m, 8H), 7.68 – 7.78 (m, 11H), 7.47 – 7.51 (m, 3H), 7.32 (t, J = 12.9, 4.8 Hz, 5H), 7.21 – 7.24 (dd, 2H), 7.16 (d, J = 8.4 Hz, 4H), 7.09 (t, J = 7.3 Hz, 2H), 7.00 (m, 2H), 3.91 (t, 2H), 2.33 (t, J = 7.5 Hz, 2H), 1.35 – 1.41 (m, 2H), 0.95 (t, 3H). MS (MALDI-TOF) m/z: calculated for C$_{82}$H$_{54}$N$_6$O$_2$Zn [M]$^+$ 1220.75, found 1220.60.

3.6. Conclusion

The *β*-functionalized unsymmetrical push–pull porphyrins **1**–**6** were synthesized by the Sonogashira cross-coupling reaction and their photophysical and computational studies were explored. A comparative investigation was carried out to understand the effect of donor and acceptor units on the push−pull porphyrin and their zinc derivatives. The red shifted absorption in the Soret and the Q-bands of porphyrin **5** and **6** resulted from the enhanced π-conjugation of the electron donor and the acceptor units at the opposite *β*, *β′*-positions. The red shifted emission in porphyrin **5** and **6** confirms the strong electronic communication between the electron donor and the acceptor units. The

computational study of porphyrin **5** and **6** exhibits a stabilized HOMO energy levels with low HOMO–LUMO gap of about 2.06 eV and 2.17 eV compared to other porphyrins. These results implies that the *β, β′*-substituted push-pull porphyrins have wide applications in optoelectronics.

3.7. References

[1] Panda, M. K., Ladomenou, K., Coutsolelos, A. G. (2012), Porphyrins in bio-inspired transformations: Light-harvesting to solar cell. *Coord. Chem. Rev.* 256, 2601-2627. (DOI: 10.1016/j.ccr.2012.04.041).

[2] Wasielewski, M. R. (2009), Self-assembly strategies for integrating light harvesting and charge separation in artificial photosynthetic systems. *Acc. Chem. Res.* 42, 1910-1921. (DOI: 10.1021/ar9001735).

[3] So, M. C., Wiederrecht, G. P., Mondloch, J. E., Hupp, J. T., Farha, O. K. (2015), Metal–organic framework materials for light-harvesting and energy transfer. *Chem. comm.* 51, 3501-3510. (DOI: 10.1039/C4CC09596K).

[4] Zhu, J., Maza, W. A., Morris, A. J. (2017), Light-harvesting and energy transfer in ruthenium (II)-polypyridyl doped zirconium (IV) metal-organic frameworks: A look toward solar cell applications. *J. Photochem. Photobiol. A*. 344, 64-77. (DOI: 10.1016/j.jphotochem.2017.04.025).

[5] Campbell, W. M., Burrell, A. K., Officer, D. L., Jolley, K. W. (2004), Porphyrins as light harvesters in the dye-sensitised TiO_2 solar cell. *Coord. Chem. Rev.* 248, 1363-1379. (DOI: 10.1016/j.ccr.2004.01.007).

[6] Hamblin, M. R. (2018), Fullerenes as photosensitizers in photodynamic therapy: pros and cons. *Photochem. Photobiol. Sci.* 17, 1515-1533. (DOI: 10.1039/C8PP00195B).

[7] Guo, P., Chen, P., Ma, W., Liu, M. (2012), Morphology-dependent supramolecular photocatalytic performance of porphyrin nanoassemblies: from molecule to artificial

supramolecular nanoantenna. *J. Mater. Chem.* 22, 20243-20249. (DOI: 10.1039/C2JM33253A).

[8] Balaban, T. S. (2005), Tailoring porphyrins and chlorins for self-assembly in biomimetic artificial antenna systems. *Acc. Chem. Res.* 38, 612-623. (DOI: 10.1021/ar040211z).

[9] Longevial, J. F., Clément, S., Wytko, J., Ruppert, R., Weiss, J., Richeter, S. (2018), Peripherally metalated porphyrins with applications in catalysis, molecular electronics and biomedicine. *Chem. Eur. J.* 24, 15442-15460. (DOI: 10.1002/chem.201801211).

[10] Drain, C. M., Goldberg, I., Sylvain, I., Falber, A. (2005), Synthesis and applications of supramolecular porphyrinic materials. *Functional Molecular Nanostructures*. 55-88. (DOI: 10.1007/b98166).

[11] Di Carlo, G., Orbelli Biroli, A., Pizzotti, M., Tessore, F. (2019), Efficient sunlight harvesting by A4 β-pyrrolic substituted ZnII porphyrins: a mini-review. *Front. Chem.* 7, 177. (DOI: 10.3389/fchem.2019.00177).

[12] Noirbent, G., Dumur, F. (2018), Recent advances on nitrofluorene derivatives: Versatile electron acceptors to create dyes absorbing from the visible to the near and far infrared region. *Materials.* 11, 2425. (DOI: 10.3390/ma11122425).

[13] Xu, Y. L., Ding, W. L., Sun, Z. Z. (2018), How to design more efficient hole-transporting materials for perovskite solar cells? Rational tailoring of the triphenylamine-based electron donor. *Nanoscale.* 10, 20329-20338. (DOI: 10.1039/C8NR04730H).

[14] Sahu, D., Tsai, C. H., Wei, H. Y., Ho, K. C., Chang, F. C., Chu, C. W. (2012), Synthesis and applications of novel low bandgap star-burst molecules containing a triphenylamine core and dialkylated diketopyrrolopyrrole arms for organic photovoltaics. *J. Mater. Chem.* 22, 7945-7953. (DOI: 10.1039/C2JM16760C).

[15] Gudeika, D. (2020), A review of investigation on 4-substituted 1, 8-naphthalimide derivatives. *Synth. Met.* 262, 116328. (DOI: 10.1016/j.synthmet.2020.116328).

[16] Georgiev, N. I., Bojinov, V. B., Marinova, N. (2010), Novel PAMAM light-harvesting antennae based on 1, 8-naphthalimide: synthesis, energy transfer, photophysical and pH sensing properties. *Sens. Actuators B Chem.* 150, 655-666. (DOI: 10.1016/j.snb.2010.08.023).

[17] Luo, J., Xu, M., Li, R., Huang, K. W., Jiang, C., Qi, Q., Zeng, W., Zhang, J., Chi, C., Wang, P., Wu, J. (2014), N-annulated perylene as an efficient electron donor for porphyrin-based dyes: enhanced light-harvesting ability and high-efficiency Co (II/III)-based dye-sensitized solar cells. *J. Am. Chem. Soc.* 136, 265-272. (DOI: 10.1021/ja409291g).

[18] a) Jinadasa, R. W., Li, B., Schmitz, B., Kumar, S., Hu, Y., Kerr, L., Wang, H. (2016), Monobenzoporphyrins as Sensitizers for Dye-Sensitized Solar Cells: Observation of Significant Spacer-Group Effect. *ChemSusChem.* 9, 2239-2249. (DOI: 10.1002/cssc.201600619). b) Hu, Y., Yellappa, S., Thomas, M. B., Jinadasa, R. W., Matus, A., Shulman, M., D'Souza, F., Wang, H. (2017), β-Functionalized Push–Pull opp-Dibenzoporphyrins as Sensitizers for Dye-Sensitized Solar Cells. *Chem. Asian J.* 12, 2749-2762. (DOI: 10.1002/asia.201701117).

[19] a) Gao, K., Fukui, N., Jung, S. I., Yorimitsu, H., Kim, D., Osuka, A. (2016), Pictet–Spengler Synthesis of Quinoline-Fused Porphyrins and Phenanthroline-Fused Diporphyrins. *Angew. Chem. Int. Ed.* 55, 13038-13042. (DOI: 10.1002/anie.201606293). b) Kim, T., Oh, J., Jiang, H. W., Tanaka, T., Osuka, A., Kim, D. (2016), Exciton coupling dynamics in syn-and anti-type β–β linked Zn (ii) porphyrin linear arrays. *Phys. Chem. Chem. Phys.* 18, 23105-23110. (DOI: 10.1039/C6CP04269D).

[20] a) Callot, H. J. (1974), BROMATION DE LA M-TETRAPHENYLPORPHINE. PREPARATION D'ALKYL-ET DE POLYCYANOPORPHINES (1). *Bull. Soc. Chim. Fr.* 1492. b) Callot, H. J. (1973), Bromuration de la meso-tetraphenylporphine.: Structure et reactivite des produits.

Tetrahedron Lett. 14, 4987-4990. (DOI: 10.1016/S0040-4039(01)87629-2).

[21] Bhyrappa, P., Velkannan, V. (2010), Synthesis of *β*-di and tribromoporphyrins and the crystal structures of antipodal tri-substituted Zn (II)-porphyrins. *Tetrahedron Lett.* 51, 40-42. (DOI: 10.1016/j.tetlet.2009.10.039).

[22] Di Carlo, G., Orbelli Biroli, A., Pizzotti, M., Tessore, F., Trifiletti, V., Ruffo, R., Abbotto, A., Amat, A., Angelis, F. D., Mussini, P. R. (2013), Tetraaryl ZnII Porphyrinates Substituted at β-Pyrrolic Positions as Sensitizers in Dye-Sensitized Solar Cells: A Comparison with meso-Disubstituted Push–Pull ZnII Porphyrinates. *Chem. Eur. J.* 19, 10723-10740. (DOI: 10.1002/chem.201300219).

[23] a) Meunier, A., Lebel, O. (2010), A glass forming module for organic molecules: Making tetraphenylporphyrin lose its crystallinity. *Org. Lett.* 12, 1896-1899. (DOI: 10.1021/ol100139t). b) Kumar, R., Sankar, M. (2014), Synthesis, spectral, and electrochemical studies of electronically tunable β-substituted porphyrins with mixed substituent pattern. *Inorg. Chem.* 53, 12706-12719. (DOI: 10.1021/ic501259g).

[24] a) Tagliatesta, P., Lembo, A., Leoni, A. (2013), Synthesis and characterization of eight new tetraphenylporphyrins bearing one or two ferrocenes on the β-pyrrole positions. *New J. Chem.* 37, 3416-3419. (DOI: 10.1039/C3NJ00896G). b) Tagliatesta, P., Pizzoferrato, R. (2015), Synthesis and characterization of new ferrocene, porphyrin and C60 triads, connected by triple bonds. *J. Organomet. Chem.* 787, 27-32. (DOI: 10.1016/j.jorganchem.2015.04.006).

[25] a) Gao, G. Y., Ruppel, J. V., Allen, D. B., Chen, Y., Zhang, X. P. (2007), Synthesis of β-functionalized Porphyrins via palladium-catalyzed carbon− heteroatom bond formations: expedient entry into β-chiral Porphyrins. *J. Org. Chem.* 72, 9060-9066. (DOI: 10.1021/jo701476m). b) Horn, S., Sergeeva, N. N., Senge, M. O. (2007), Conversion of Ni (II)-

Allylporphyrins to α, β-Unsaturated Formylporphyrins via a Nickel-Promoted Reaction. *J. Org. Chem.* 72, 5414-5417. (DOI: 10.1021/jo070550g).

[26] Frisch, M. J., Trucks, G. W., Schlegel, H. B., Scuseria, G. E., Robb, M. A., Cheeseman, J. R., Scalmani, G., Barone, V., Mennucci, B., Petersson, G. A., Nakatsuji, H., Caricato, M., Li, X., Hratchian, H. P., Izmaylov, A. F., Bloino, J., Zheng, G., Sonnenberg, J. L., Hada, M., Ehara, M.; Toyota, K.; Fukuda, R.; Hasegawa, J.; Ishida, M.; Nakajima, T.; Honda, Y.; Kitao, O., Nakai, H., Vreven, T., Montgomery, J. A., Jr., Peralta, J. E., Ogliaro, F., Bearpark, M., Heyd, J. J., Brothers, E., Kudin, K. N., Staroverov, V. N., Kobayashi, R., Normand, J., Raghavachari, K., Rendell, A., Burant, J. C., Iyengar, S. S., Tomasi, J., Cossi, M., Rega, N., Millam, N. J., Klene, M., Knox, J. E., Cross, J. B., Bakken, V., Adamo, C., Jaramillo, J., Gomperts, R., Stratmann, R. E., Yazyev, O., Austin, A. J., Cammi, R., Pomelli, C., Ochterski, J. W., Martin, R. L., Morokuma, K., Zakrzewski, V. G., Voth, G. A., Salvador, P., Dannenberg, J. J., Dapprich, S., Daniels, A. D., Farkas, O., Foresman, J. B., Ortiz, J. V., Cioslowski, J., Fox, D. J. Gaussian 09, Revision A.02, *Gaussian, Inc.*, Wallingford, CT, 2009.

Chapter 4

β-Substituted TCBD Functionalized Push–Pull Porphyrins

4.1. Introduction

Porphyrinoids are employed in mimicking chlorophyll and heme molecules in natural photosynthetic architecture to perform essential roles in oxygen transport and in the generation of charge separated state. [1-3] Porphyrin macrocycles play a key role in light harvesting and electron transfer processes. [4, 5] Porphyrins are aromatic, 18-π-electron conjugated system with ease of modification in the tetrapyrrole unit *via meso* and *β*-functionalization. [6-8] The light-harvesting ability of porphyrins can be improved *via β*-pyrrole functionalization. Porphyrin under light irradiation shows singlet–triplet splitting, long triplet state lifetime, energy/electron transfer process and high quantum yield for intersystem crossing. [9] The properties of porphyrin-based D-A systems can be tuned, by altering the substitutents at the *β*-position of the porphyrin macrocycle. [10, 11] In recent years, the *β*-functionalized push-pull porphyrins have been explored, due to its excellent photophysical and redox properties which shows potential applications in dye-sensitized solar cells (DSSCs), optoelectronics, photonics, chemosensors, catalysis, nonlinear optics (NLO), sensors and photodynamic therapy (PDT). [12-18]

Phenothiazine is a electron-rich tricyclic heterocycles containing lone pair of electrons on nitrogen and sulphur atom of the six-membered ring. The phenothiazine derivatives show potential applications in biological, pharmacological and organic light-emitting diodes (OLEDs). [19, 20] The electron-donating amino-substituents on the aromatic ring of *N*, *N*-dimethylaniline, enhances the electron donating capability and are used as precursors in the synthesis of dyes and synthetic rubber. [21] The incorporation of electron deficient tetracyanoethene (TCNE) unit results in nonplanar push–pull molecules with strong intramolecular charge-transfer (CT). The TCNE/TCNQ functionalized *β*-donor substituted porphyrin derivatives are largely unexplored. [22]

Recently, Yang *et. al.* have reported a series of *meso*-substituted unsymmetrical porphyrins with different click moieties and explored its optical-limiting behaviour. [23] Hong and co-worker synthesized a series of NIR absorbing porphyrin derivatives with different click moieties and employed in enhancing photoacoustic (PA) imaging and photothermal therapy (PTT) technologies. [24]

In this chapter, we report the design and synthesis of *β*-donor, acceptor functionalized porphyrins **1**–**8**. The effect of TCBD functionalization on *β*-substituted porphyrins were investigated and their photophysical, electrochemical and computational studies were explored. The phenothiazine and *N, N*-dimethylaniline donor unit and TCBD acceptor unit were incorporated through π–linkers in the porphyrin macrocycle (Figure 4.1).

1, M= H
2, M= Zn

5, M= H
6, M= Zn

3, M= H
4, M= Zn

7, M= H
8, M= Zn
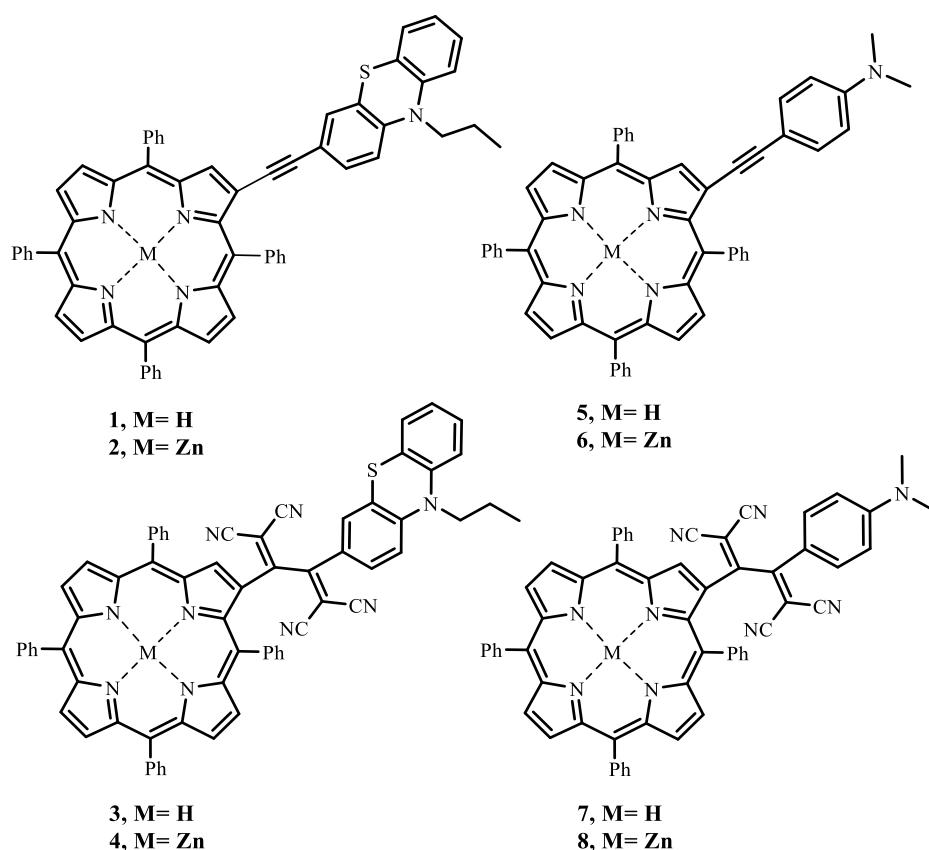
Figure 4.1. Structure of the porphyrins **1**–**8**, and the control compounds **9** and **10**, used in this study.
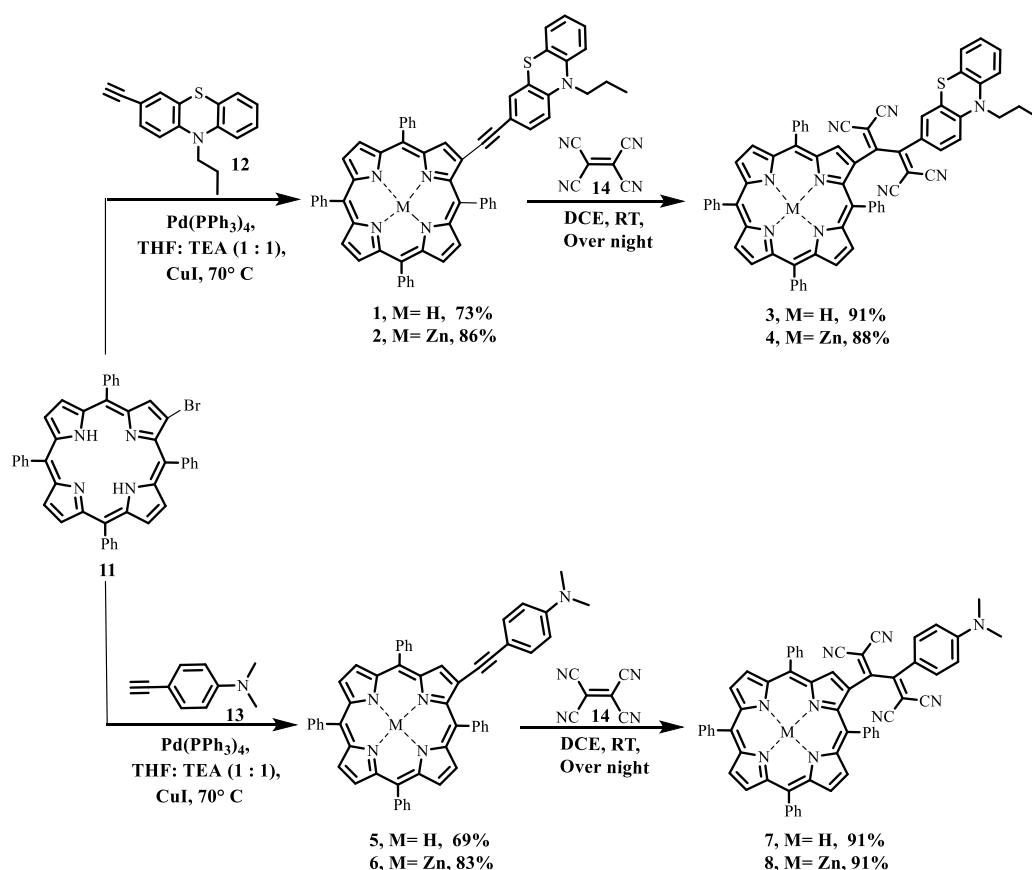
Scheme 4.1. Synthetic routes for porphyrins **1**–**8**.

4.2. Results and Discussion

Synthesis

The synthetic routes of β-donor substituted TCBD functionalized push-pull porphyrins **1**–**8** are shown in Scheme 4.1. The β-monobrominated tetraphenyl porphyrin (TPPBr) **11** were synthesized according to the reported procedures (Scheme 4.1). [25, 26] The Pd-catalyzed Sonogashira cross-coupling reaction of TPPBr **11** using one equiv of 3-ethynyl-10-propyl-10H-phenothiazine **12** and 4-ethynyl-*N*, *N*-dimethylaniline **13** in the presence of Pd(PPh3)4 in THF solvent at 70 °C resulted in porphyrin **1** and **5** in 73 and 69% yields, respectively (Scheme 4.1). The zinc complexation of the porphyrins **1** and **5**, were carried out using Zn(OAc)2 by dissolving in MeOH and CHCl3 (3:1) mixture, which resulted in zinc derivatives **2** and **6** in 86 and 83% yields, respectively. The TCBD functionalized push-pull porphyrins **3**, **4**, **7** and **8** were synthesized *via* [2 + 2] cycloaddition-retroelectrocyclization (CA-RE)

reaction and are shown in Scheme 4.1. The reaction of porphyrin and its zinc derivatives **1**, **2**, **5** and **6** with TCNE **14** in dichloroethane (DCE) resulted in β-substituted TCBD functionalized push-pull porphyrins **3, 4, 7** and **8** in 91, 88, 91 and 91% yields, respectively. The porphyrin derivatives **1**–**8** were characterized by ^{1}H and ^{13}C NMR, HR-MS and MALDI-TOF mass spectra.
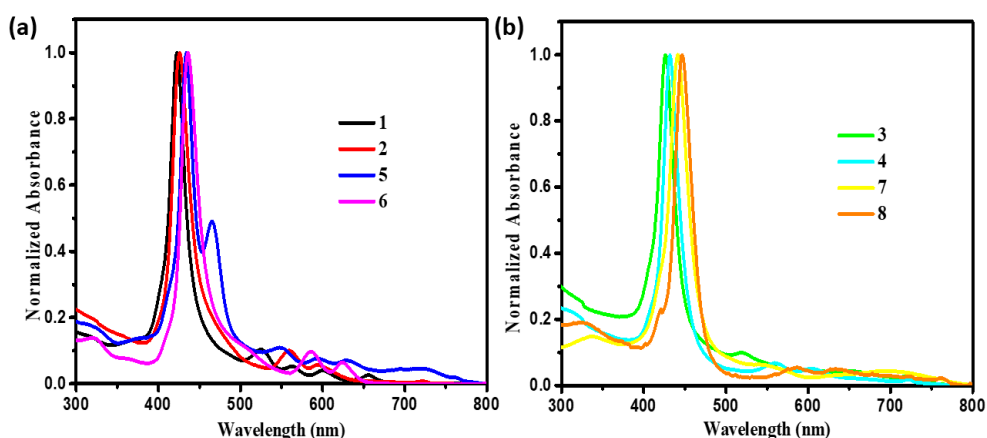
Figure 4.2. Normalized electronic absorption spectra of porphyrins (a) **1**, **2**, **5**, **6** and (b) **3**, **4**, **7**, **8** measured in dichloromethane at 1.0×10^{-5} M concentration.

4.3. Photophysical Properties

The UV-Visible absorption spectra of β-donor substituted TCBD functionalized push-pull porphyrins **1**–**8** were recorded in CH$_2$Cl$_2$ at room temperature, and data are tabulated in Table 4.1. The porphyrin **1**−**8** exhibits a characteristic Soret band around 423–447 nm and Q–bands between 520–722 nm, respectively. The Figure 4.2(**a**) and 4.2(**b**) illustrates the absorption spectra of β-phenothiazine and β-*N*, *N*-dimethylaniline substituted porphyrin and TCBD functionalized porphyrin **1**−**8**. The free base porphyrin **1** and **5** shows a soret band and four Q bands, whereas Zn(II) porphyrin **2** and **6** exhibits a characteristic soret band and two Q bands in the low energy absorption band, respectively. The Zn(II) porphyrin **2**, **4**, **6** and **8** with phenothiazine and *N*, *N*-dimethylaniline at the β-pyrrolic position shows absorption band

in the range of 426–447 nm, which results in a slight red shift by 2–6 nm in soret and Q band region compared to their free base porphyrin analogues **1**, **3**, **5** and **7**. The Zn(II) complexes of *β*-functionalized TCBD porphyrin **4** and **8** shows, the absorption band around 432 and 447 nm, with a slight red shift of 6–11 nm in the soret band region compared to its corresponding *β*-donor substituted porphyrin **2** and **6**. In *β*-donor substituted porphyrin, the *N*, *N*-dimethylaniline substituted porphyrin **5** and **6** exhibits red shifted absorption by 10–11 nm in the soret band region compared to the phenothiazine substituted porphyrin **1** and **2**. The *N*, *N*-dimethylaniline substituted TCBD functionalized porphyrin **7** and **8** shows the absorption band around 441 and 447 nm, with a red shift of 15 nm in the soret band region compared to the phenothiazine substituted TCBD functionalized porphyrin **3** and **4**. These results suggests, the *N*, *N*-dimethylaniline donor unit have better electron donating capability compared to the phenothiazine donor units. The red shifted absorption band of TCBD functionalized porphyrins are attributed to the extended π-conjugation, due to the incorporation of electron deficient TCBD units with a strong intramolecular charge-transfer (CT).
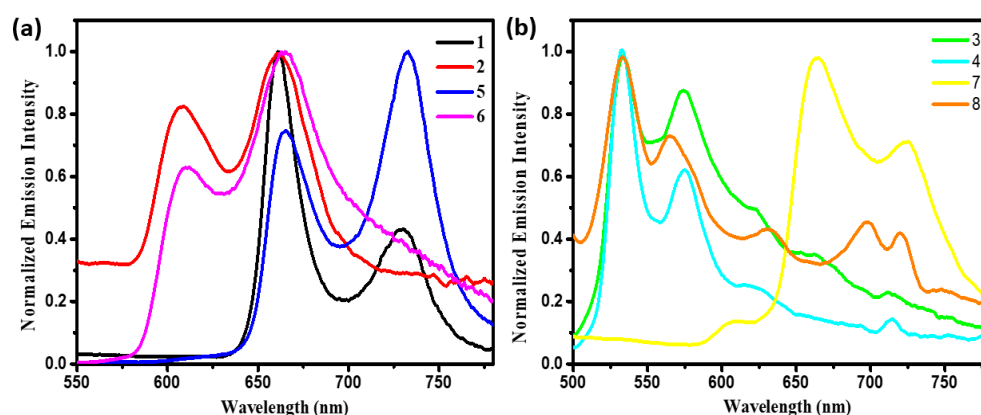
Figure 4.3. Normalized emission spectra of porphyrins (a) **1**, **2**, **5**, **6** and (b) **3**, **4**, **7**, **8** measured in dichloromethane at 1.0×10^{-5} M concentration.

Table 4.1. Photophysical and theoretical data of porphyrin **1**–**8**.

Compound	Soret band (S-band)	λ_{abs} (nm)[a] ε (M^{-1} cm^{-1})	Q-bands	λ_{em} (nm)	Φ_f[b]	H–L gap(eV)[c]
1	423	67680	525, 563, 600, 656	661, 730	0.06	2.31
2	426	41460	559, 596	608, 662	0.02	2.48
3	426	20850	520, 651, 664	533, 575 664	0.01	1.93
4	432	34410	560, 605	532, 573 617	–	1.95
5	434, 465(sh)	40100	551, 594, 629, 722	665, 733	0.21	2.23
6	436	13210	586, 624	611, 665	0.20	2.41
7	441	91030	539, 697	666, 723	–	1.73
8	447	25300	583, 627	533, 562 635, 702 722	–	1.75

[a] Absorbance measured in dichloromethane at 1×10^{-5} M concentration; sh = shoulder; λ_{abs}: absorption wavelength; λ_{em}: emission wavelength; ε: extinction coefficient. [b] The fluorescence quantum yields were recorded using H_2TPP as astandard (Φ_{st} = 0.11). [c] Calculated from computational study.

The emission spectra of porphyrin **1**–**8** were recorded in CH_2Cl_2 at room temperature, and the data are summarized in Table 4.1. Figure 4.3(a) and 4.3(b) shows the emission spectra of porphyrin **1**–**8**. The β-donor substituted porphyrin show a characteristic two emission bands in the low energy region (Figure 4.3a). The free base porphyrin **1** and **5** shows emission band in the range of 661–733 nm and their Zn(II) complexes **2** and **6** emits around 608–665 nm, respectively. The free base porphyrin **1** and **5** shows significant red shift in fluorescence maxima compared to their Zn(II) derivatives **2** and **6** respectively. The β-functionalized TCBD porphyrin **3**, **4**, **7** and **8** shows emission band around 532–723 nm (Figure 4.3b). The TCBD functionalized porphyrins **3**, **4** and **8** shows emission band around 532–722 nm with a blue shift in emission maxima

by 134–161 nm as compared to their *N, N*-dimethylaniline substituted TCBD functionalized porphyrin **7**. The emission bands of porphyrins **3**, **4** and **8** exhibits blue shifted emission around 532–722 nm as compared to their corresponding donor substituted porphyrin **1**, **2** and **6** with emission between 608–730 nm. The TCBD functionalized porphyrins **7** shows almost similar emission maxima compared to its subsequent donor substituted porphyrin **5**. The blue shifted emission of TCBD functionalized porphyrin may be due to the twisted nonplanar conformation of porphyrin molecules with the incorporation of TCBD unit. [27] The fluorescence quantum yields of porphyrin **1**, **2**, **3**, **5** and **6** were observed between 0.01–0.21. The porphyrin **5** and **6** shows highest quantum yield value of 0.21 and 0.20, respectively. Compared to porphyrins **5** and **6**, other porphyrins show significantly reduced fluorescence quantum yields, which may be due to the fast non radiative deactivation of the excited state with intra molecular charge-transfer. [28]
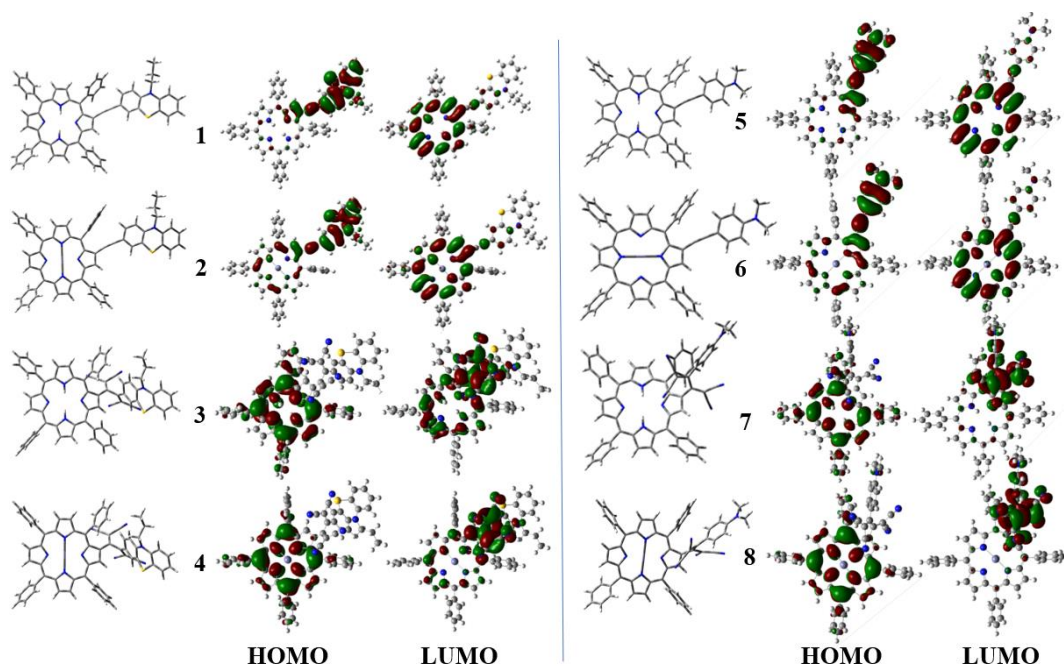
Figure 4.4. Optimized structure, frontier HOMO and LUMO of porphyrins **1**–**8**.

4.4. Theoretical Calculations

To understand the electronic properties of *β*-donor substituted TCBD functionalized porphyrins **1**–**8**, DFT calculations at B3LYP/6-31G level were performed using the Gaussian 09W program. [29] The frontier molecular orbitals (FMOs) of porphyrins are illustrated in Figure 4.4. In case of porphyrin **1** and **5** the electron density of HOMOs are mainly localized on phenothiazine and *N*, *N*- dimethylaniline donor units and the LUMO are concentrated on porphyrin macrocycle. The Zn(II) porphyrin **2** and **6** the HOMOs are mainly populated on phenothiazine and *N*, *N*- dimethylaniline donor units with parts spread over porphyrin macrocycle and the LUMO are concentrated on porphyrin unit. These result exhibits the strong electron donating capability of phenothiazine and *N*, *N*- dimethylaniline donor unit. The phenothiazine substituted TCBD functionalized porphyrin **3** and **4** shows the HOMO are populated on porphyrin macrocycle and the LUMO are populated on TCBD unit with parts on porphyrin macrocycle. The *N*, *N*- dimethylaniline substituted TCBD functionalized porphyrin **7** and **8** shows the HOMO
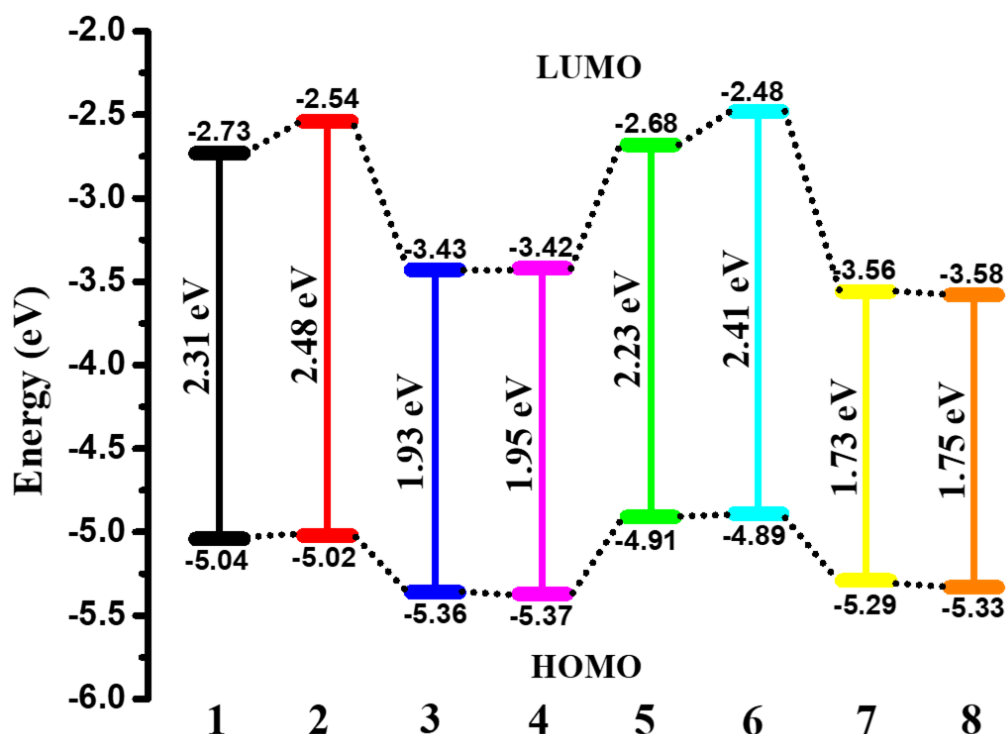
Figure 4.5. Energy level diagram of the frontier orbitals of porphyrin **1**–**8**, estimated by DFT calculations.

are populated on porphyrin macrocycle and the LUMO are populated on TCBD unit which implies the possibility of intramolecular charge transfer from porphyrin macrocycle to TCBD unit. The TCBD functionalized porphyrins **3**, **4**, **7** and **8** shows low HOMO–LUMO band gap compared to their donor substituted porphyrin **1**, **2**, **5** and **6**. The lesser energy gap of TCBD functionalized porphyrins are due to the incorporation of strong electron-accepting TCBD unit. The theoretically calculated HOMO levels of the porphyrins **1**, **2**, **3**, **4**, **5**, **6**, **7** and **8** are –5.04 eV, –5.02 eV, –5.36 eV, –5.37 eV, –4.91 eV, –4.89 eV, –5.29 eV and –5.33 eV whereas LUMO levels are –2.73 eV, –2.54 eV, –3.43 eV, –3.42 eV, –2.68 eV, –2.48 eV, –3.56 eV and –3.58 eV respectively (Figure 4.5).

The electronic transitions, oscillator strength (f) and UV−vis absorption spectra of porphyrin **1**–**8** were calculated using time-dependent density functional theory (TD-DFT) at B3LYP/6-31G level on optimized porphyrins and the data are depicted in Table 4.2. [29] The electronic excitations of porphyrin **1**–**8** shows two absorption bands in UV-visible region. The Soret band with greater oscillator strength arises from the high energy region, where as the Q-bands with lesser oscillator strength occurs in the lower energy region. The electronic absorption in donor substituted porphyrin **1**, **2**, **5** and **6** shows absorption band around 601, 569, 608 and 572 nm in the Q-band region are related to ICT transitions arising from HOMO→LUMO. The S-band in donor substituted porphyrin with greater oscillator strength were assigned to π–π* transitions with compositions arising from HOMO–2→LUMO, HOMO→LUMO+2, and HOMO–3→LUMO. The absorption band in the TCBD functionalized porphyrins **3**, **4**, **7** and **8** shows ICT transition in the low energy Q-band region where as π–π* transition occurs in the high energy soret band region. The absorption band for TCBD functionalized porphyrins **3**, **4**, **7** and

Table 4.2. Calculated Electronic Transitions of porphyrin **1**–**8**.

Compounds	λ_{max}	Composition & Molecular contribution	f^a	Assignment
1	397	HOMO–2→LUMO (0.31)	1.14	π–π*
	601	HOMO→LUMO (0.61)	0.26	ICT
2	386	HOMO→LUMO+2 (0.35)	1.07	π–π*
	569	HOMO→LUMO (0.64)	0.33	ICT
3	379	HOMO–2→LUMO+2 (0.40)	0.61	π–π*
	523	HOMO –1→LUMO +1 (0.68)	0.17	ICT
4	425	HOMO–2→LUMO+1 (0.35)	0.78	π–π*
	519	HOMO–1→LUMO +1 (0.62)	0.15	ICT
5	389	HOMO–3 →LUMO (0.39)	1.43	π–π*
	608	HOMO →LUMO (0.58)	0.25	ICT
6	385	HOMO–2 →LUMO (0.46)	1.44	π–π*
	572	HOMO →LUMO (0.64)	0.33	ICT
7	369	HOMO–4 →LUMO+1 (0.34)	0.53	π–π*
	609	HOMO–2 →LUMO (0.57)	0.16	ICT
8	394	HOMO–1 →LUMO+2 (0.39)	0.50	π–π*
	616	HOMO–2 →LUMO (0.69)	0.12	ICT

f^a Oscillator strength.

8 in the soret band region occurs around 379, 425, 369 and 394 nm and are related to π–π* transitions. The charge-transfer occurs from HOMO–1→LUMO+1 and HOMO–2→LUMO for TCBD functionalized porphyrins whereas the main ICT transitions for Q-band in the donor substituted porphyrin occurs from HOMO→LUMO, respectively. The TD-DFT calculated values was in good agreement with the experimental data.
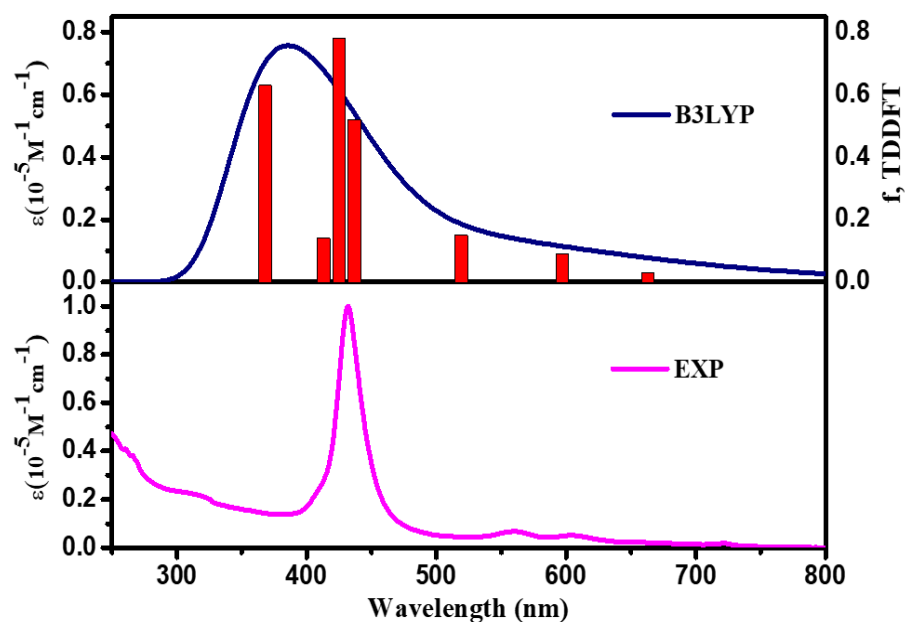
Figure 4.6. Experimental (lower) and TDDFT simulated (upper) UV-vis spectra of porphyrin **4**.

4.5. Experimental Section

General: Experimental data:

All the chemicals were purchased from commercial sources and used without further purification. The NMR spectra were recorded at room temperature (298 K). Chemical shifts are given in ppm with respect to tetramethylsilane as internal standard (CDCl$_3$, 7.26 ppm, 77.0 ppm). ^{1}H NMR and ^{13}C NMR spectra were recorded using a 400 MHz and 100 MHz spectrometer. Multiplicities are given as s (singlet), d (doublet), t (triplet) and m (multiplet) are given in Hertz. TLC analysis was carried out using silica gel 60 F$_{254}$ plates. UV-visible absorption spectra were recorded on a Cary-100 Bio UV-visible spectrophotometer. Emission spectra were taken in a The Fluoromax-4C, S/n. 1579D-1417-FM Fluorescence software Ver 3.8.0.60. UV/Vis and emission spectrums of all compounds were recorded in dichloromethane solution. The density functional theory (DFT) calculation were carried out at the B3LYP/6-31G level for C, N, H, S, Zn in the Gaussian 09 program. HRMS were recorded on a Bruker-Daltonics micrOTOF-Q II mass spectrometer.

Synthesis

Synthesis of compound 1.

7-bromo-5,10,15,20-tetraphenylporphyrin **11** (0.120 g, 0.173 mmol), 3-ethynyl-10-propyl-10H-phenothiazine **12** (0.068 g, 0.260 mmol) in THF: TEA (1: 1, v/v), palladium(0)-tetrakis(triphenylphosphine) (0.070 g, 0.06 mmol), and CuI (0.005 g, 0.025 mmol) were added under argon atm at room temperature. The reaction mixture was stirred for 12 h at 70 °C, and then cooled to room temperature. The solvent was then evaporated under reduced pressure and the resultant mixture was diluted with DCM and the organic layer was collected, dried over anhydrous Na_2SO_4 and evaporated under vacuum. The solid was adsorbed on silica gel and purified by column chromatography, using a DCM: hexane (20: 80) mixture to produce (0.110 g, 73%) of compound **1**. ^{1}H NMR (400 MHz, CDCl3) : δ ppm= 9.03 (s, 1 H), 8.87(s, 2 H) , 8.82(d, 1 H), 8.77(s, 2 H), 8.73(d, 1 H), 8.21(m, 8 H), 7.78–7.74(m, 12 H), 7.19– 7.13(m, 3 H), 7.09(s, 1 H), 6.96(t, 1 H), 6.89(d, 1 H), 6.78(d, 1 H), 3.84(t, 2 H), 1.90–1.85(m, 2 H), 1.06(t, 3 H), -2.67(s, 2 H). ^{13}C NMR (101 MHz, CDCl3): δ ppm= 145.09, 144.80, 142.31, 142.25, 142.01, 141.44, 134.72, 134.69, 131.35, 131.10, 128.87, 128.00, 127.91, 127.64, 127.43, 126.93, 126.88, 126.84, 124.47, 124.19, 122.80, 120.61, 120.20, 120.04, 117.71, 115.65, 114.72, 98.87, 86.13, 49.47, 20.28, 11.48. HRMS (ESI-TOF): m/z calculated for $C_{61}H_{43}N_5S$ [M+nH] $^+$ 878.3312, found 878.3313.

Synthesis of compound 2.

Compound **1** (0.100 g, 0.114 mmol), Zn (OAc)$_2$, (0.249 g, 1.14 mmol) in MeOH: CHCl$_3$ (3 : 1, v/v), were added and the reaction mixture was stirred for 1 h at room temperature. The solvent was then evaporated under reduced pressure and the resultant mixture was diluted with DCM/water and the organic layer was collected, dried over anhydrous Na_2SO_4 and evaporated under vacuum. The solid was adsorbed on silica gel and purified by column chromatography, using a DCM: hexane (35: 65) mixture to produce (0.092 g, 86%) of compound **2**. ^{1}H NMR (400

MHz, CDCl$_3$) : δ ppm= 9.18 (s, 1 H), 8.92(d, 3 H), 8.87(d, 1 H), 8.81(s, 1 H), 8.76(d, 1 H), 8.23–8.19(m, 8 H), 7.77–7.71(m, 12 H), 7.19–7.15(m, 2 H), 7.10(s, 1 H), 6.99–6.93(m, 2 H), 6.89(d, 1 H), 6.78(d, 1 H),, 3.84(t, 2 H), 1.90–1.85(m, 2 H), 1.06(t, 3 H). ^{13}C NMR (101 MHz, CDCl$_3$): δ ppm= 151.25, 150.86, 150.73, 150.26, 148.50, 147.02, 144.92, 144.75, 142.87, 142.32, 138.73, 134.55, 134.45, 132.87, 132.39, 132.32, 132.24, 131.82, 131.35, 131.06, 128.63, 127.72, 127.62, 127.58, 127.40, 126.70, 126.68, 126.32, 124.36, 124.04, 122.73, 121.57, 121.15, 120.88, 117.85, 116.45, 115.59, 114.67, 98.88, 86.40, 49.45, 20.25, 11.47. HRMS (ESI-TOF): m/z calculated for C$_{61}$H$_{41}$N$_5$SZn [M] $^+$ 939.2369, found 939.2368.

Synthesis of compound 3.

Compound **1** (0.050g, 0.057 mmol) and tetracyanoethylene **14** (.018 g, 0.142 mmol) were dissolved in 7 ml 1,2-Dichloroethane. The mixture was stirred overnight at room temperature. The resultant mixture was poured into water and extracted with dichloromethane. After drying over Na$_2$SO$_4$, the remaining liquid was concentrated and purified by column chromatography using (hexane: dichloromethane=40: 60) to produce (.052 g, 91%) of compound **3**. ^{1}H NMR (400 MHz, CDCl$_3$) : δ ppm= 8.97 (d, 1 H), 8.87–8.84(m, 2 H), 8.80(d, 1 H), 8.74(d, 1 H), 8.68–8.64(dd, 2 H), 8.32(m, 4 H), 8.20(m, 4 H), 7.85–7.76(m, 10 H), 7.71–7.67(t, 2 H), 7.17–7.05(m, 3 H), 6.96(t, 1 H), 6.85(d, 1 H), 6.79(d, 1 H), 6.72(s, 1 H), 3.81(t, 2 H), 1.83–1.77(m, 2 H), 1.02–0.98(t, 3 H), -2.29(s, 2 H). ^{13}C NMR (101 MHz, CDCl$_3$): δ ppm= 165.64, 161.70, 141.15, 135.30, 134.63, 134.48, 130.00, 129.28, 127.95, 127.56, 127.41, 127.16, 126.94, 126.81, 126.73, 125.37, 123.68, 120.32, 115.86, 114.77, 110.66, 65.18, 62.46, 49.63, 19.75, 10.94. HRMS (ESI-TOF): m/z calculated for C$_{67}$H$_{43}$N$_9$S [M+nH] $^+$ 1006.3435, found 1006.3445.

Synthesis of compound 4.

Compound **2** (.050 g, 0.053 mmol) and tetracyanoethylene **14** (.017 g, 0.133 mmol) were dissolved in 7 ml 1,2-Dichloroethane. The mixture was stirred overnight at room temperature. The resultant mixture was

poured into water and extracted with dichloromethane. After drying over Na$_2$SO$_4$, the remaining liquid was concentrated and purified by column chromatography using (hexane: dichloromethane=20: 80) to produce (.049 g, 88%) of compound **4**. ^{1}H NMR (400 MHz, CDCl$_3$) : δ ppm= 9.04(s, 1 H), 8.90(d, 1 H), 8.84(s, 2 H), 8.76(d, 1 H), 8.57(d, 2 H), 8.29–8.24(m, 4 H), 8.18(m, 4 H), 7.86–7.73(m, 12 H), 7.18(t, 1 H), 7.12(t, 2 H), 7.00(t, 2 H), 6.90–6.84(m, 2 H), 3.87(t, 2 H), 1.90–1.85(m, 2 H), 1.05(t, 3 H). ^{13}C NMR (101 MHz, CDCl$_3$) : δ ppm= 166.21, 160.59, 152.53, 152.40, 151.69, 150.36, 150.00, 142.83, 142.61, 142.38, 142.15, 141.77, 141.62, 135.06, 134.55, 134.47, 133.63, 133.14, 132.90, 132.53, 130.73, 129.28, 128.04, 127.77, 127.51, 126.79, 126.67, 124.78, 123.96, 123.03, 116.13, 115.04, 112.34, 110.46, 73.16, 71.03, 49.96, 19.99, 11.16. HRMS (ESI-TOF): m/z calculated for C$_{67}$H$_{41}$N$_9$SZn [M+nH] $^+$ 1068.2570, found 1068.2593.

Synthesis of compound 5.

7-bromo-5,10,15,20-tetraphenylporphyrin **11** (0.120 g, 0.173 mmol), 4-ethynyl-N,N-dimethylaniline **13** (0.037 g, 0.260 mmol) in THF: TEA (1: 1, v/v), palladium(0)-tetrakis(triphenylphosphine) (0.070 g, 0.06 mmol), and CuI (0.005 g, 0.025 mmol) were added under argon atm at room temperature. The reaction mixture was stirred for 12 h at 70 °C, and then cooled to room temperature. The solvent was then evaporated under reduced pressure and the resultant mixture was diluted with DCM and the organic layer was collected, dried over anhydrous Na$_2$SO$_4$ and evaporated under vacuum. The solid was adsorbed on silica gel and purified by column chromatography, using a DCM: hexane (20: 80) mixture to produce (0.090 g, 69%) of compound **5**. ^{1}H NMR (400 MHz, CDCl$_3$): δ ppm= 9.01(s, 1 H), 8.85(s, 2 H), 8.80–8.77(m, 3 H), 8.72(d, 1 H), 8.23–8.20(m, 8 H), 7.80–7.72(m, 12 H), 7.25(d, 2 H), 6.67(d, 2 H), 3.03(s, 6 H), -2.66(s, 2 H). ^{13}C NMR (101 MHz, CDCl$_3$): δ ppm= 159.43, 149.86, 142.29, 142.19, 141.93, 141.36, 134.58, 134.53, 133.42, 128.48, 127.73, 126.77, 126.72, 126.68, 120.44, 120.14, 119.94, 119.67, 111.41, 110.74, 100.87, 84.18, 40.25. HRMS (ESI-TOF): m/z calculated for C$_{54}$H$_{39}$N$_5$ [M+nH] $^+$ 758.3278, found 758.3297.

Synthesis of compound 6.

Compound **5** (0.100 g, 0.132 mmol), Zn (OAc)$_2$, (0.289 g, 1.32 mmol) in MeOH: CHCl$_3$ (3 : 1, v/v), were added and the reaction mixture was stirred for 1 h at room temperature. The solvent was then evaporated under reduced pressure and the resultant mixture was diluted with DCM/water and the organic layer was collected, dried over anhydrous Na$_2$SO$_4$ and evaporated under vacuum. The solid was adsorbed on silica gel and purified by column chromatography, using a DCM: hexane (35: 65) mixture to produce (0.090 g, 83%) of compound **6**. ^{1}H NMR (400 MHz, CDCl$_3$) : δ ppm= 9.16(s, 1 H), 8.92(d, 3 H), 8.87(d, 2 H), 8.76(d, 1 H), 8.23–8.20(m, 8 H), 7.78–7.70(m, 12 H), 7.23(d, 2 H), 6.53(d, 2 H), 2.83(s, 6 H). ^{13}C NMR (126 MHz, CDCl$_3$) : δ ppm= 162.33, 149.07, 146.51, 144.64, 142.73, 134.41, 134.30, 133.27, 128.01, 127.73, 126.59, 126.47, 118.54, 111.51, 99.80, 81.52, 40.19 MS (MALDI-TOF) m/z: calculated for C$_{54}$H$_{37}$N$_5$Zn [M]$^+$ 819.23, found 819.53.

Synthesis of compound 7.

Compound **5** (.050 g, 0.066 mmol) and tetracyanoethylene **14** (.021 g, 0.165 mmol) were dissolved in 7 ml 1,2-Dichloroethane. The mixture was stirred overnight at room temperature. The resultant mixture was poured into water and extracted with dichloromethane. After drying over Na$_2$SO$_4$, the remaining liquid was concentrated and purified by column chromatography using (hexane: dichloromethane=40: 60) to produce (.053 g, 91%) of compound **7**. ^{1}H NMR (400 MHz, CDCl$_3$) : δ ppm= 8.96(d, 1 H), 8.86(m, 1 H), 8.79–8.74(dd, 2 H), 8.71(s, 1 H), 8.68–8.64(dd, 2 H), 8.41(d, 2 H), 8.32(d, 2 H), 8.20(m, 2 H), 7.83–7.74(m, 12 H), 7.08(d, 2 H), 6.65(d, 2 H), 3.11(s, 6 H), -2.27(s, 2 H). ^{13}C NMR (101 MHz, CDCl$_3$) : δ ppm= 182.95, 182.34, 175.63, 172.87, 170.16, 166.16, 154.03, 152.68, 147.00, 141.09, 135.61, 135.45, 134.83, 134.66, 133.09, 132.75, 127.70, 127.06, 126.88, 123.48, 115.70, 111.56, 73.34, 67.08, 40.09. MS (MALDI-TOF) m/z: calculated for C$_{60}$H$_{39}$N$_9$ [M]$^+$ 886.03, found 886.65.

Synthesis of compound 8.

Compound **6** (.050 g, 0.061 mmol) and tetracyanoethylene **14** (.019 g, 0.152 mmol) were dissolved in 7 ml 1,2-Dichloroethane. The mixture

was stirred overnight at room temperature. The resultant mixture was poured into water and extracted with dichloromethane. After drying over Na_2SO_4, the remaining liquid was concentrated and purified by column chromatography using (hexane: dichloromethane=20: 80) to produce (.052 g, 91%) of compound **8**. ^{1}H NMR (400 MHz, $CDCl_3$): δ ppm= 9.07(s, 1 H), 8.90(d, 1 H), 8.83(s, 3 H), 8.75(d, 1 H), 8.59(d, 1 H), 8.31–8.29(m, 4 H), 8.19–8.17(d, 4 H), 7.80–7.72(m, 12 H), 7.05(d, 2 H), 6.71(d, 2 H), 3.17(s, 6 H). ^{13}C NMR: After repeated submission peaks were not raised. MS (MALDI-TOF) m/z: calculated for $C_{60}H_{37}N_9Zn$ [M]$^+$ 949.39, found 949.58.

4.6. Conclusion

The β-donor (phenothiazine and *N, N*-dimethylaniline) substituted TCBD functionalized porphyrins **1**–**8** were designed and synthesized by the Sonogashira cross-coupling reaction and [2+2] CA–RE reaction. The effect of TCBD functionalization on the photophysical and computational studies were analysed. The UV–vis absorption spectra of TCBD functionalized porphyrin shows a red shifted absorption due to the incorporation of strong electron accepting TCBD unit. The emission spectra of TCBD functionalized porphyrin exhibits blue shift in the UV-visible region due to the nonplanar conformation of porphyrins due to the incorporation of TCBD units. The computational study reveals, stabilized LUMO levels with low HOMO–LUMO band gap after the incorporation of TCBD acceptor unit. These results provide a new insight for the β-functionalized TCBD porphyrin and their application in energy transfer studies.

4.7. References

[1] Fanelli, A. R., Antonini, E., Caputo, A. (1964), Hemoglobin and Myoglobin, *Adv. Protein Chem.* 19, 73–222. (DOI: 10.1016/S0065-3233(08)60189-8).

[2] Mauzerall, D. (1977), Porphyrins, chlorophyll, and photosynthesis. In Photosynthesis I (pp. 117-124). *Springer*, Berlin, Heidelberg. (DOI: 10.1007/978-3-642-66505-9_5).

[3] Ort, D. R., Merchant, S. S., Alric, J., Barkan, A., Blankenship, R. E., Bock, R., Croce, R., Hanson, M. R., Hibberd, J. M., Long, S. P., Moore, T. A., Moroney, J., Niyogi, K. K., Parry, M. A. J., Peralta-Yahya, P. P., Prince, R. C., Redding, K. E., Spalding, M. H., van Wijk, K. J., Vermaas, W. F. J., von Caemmerer, S., Weber, A. P. M., Yeates, T.O., Yuan, J. S., Zhu, X. G. (2015), Redesigning photosynthesis to sustainably meet global food and bioenergy demand. *Proc. Natl. Acad. Sci. U.S.A.* 112, 8529-8536. (DOI: 10.1073/pnas.1424031112).

[4] Seth, J., Palaniappan, V., Wagner, R. W., Johnson, T. E., Lindsey, J. S., Bocian, D. F. (1996), Soluble synthetic multiporphyrin arrays. 3. Static spectroscopic and electrochemical probes of electronic communication. *J. Am. Chem. Soc.* 118, 11194-11207. (DOI: 10.1021/ja9616138).

[5] (a) Gust, D., Moore, T. A., Moore, A. L. (1993), Molecular mimicry of photosynthetic energy and electron transfer. *Acc. Chem. Res.* 26, 198-205. (DOI:10.1021/ar00028a010). (b) Kadish, K. M., Smith, K. M., Guilard, R. Poalesse, R. (2000). The Porphyrin Handbook, ed. *Academic Press, New York*, vol. 2, Ch. 11, 201-232.

[6] (a) Hiroto, S., Miyake, Y., Shinokubo, H. (2017), Synthesis and functionalization of porphyrins through organometallic methodologies. *Chem. Rev.* 117, 2910-3043. (DOI: 10.1021/acs.chemrev.6b00427). (b) Suslick, K. S., Bhyrappa, P., Chou, J. H., Kosal, M. E., Nakagaki, S., Smithenry, D. W., Wilson, S. R. (2005), Microporous porphyrin solids. *Acc. Chem. Res.* 38, 283-291. (DOI:10.1021/ar040173j).

[7] Higuchi, H., Shimizu, K., Ojima, Z., Sugiura, K., Sakata, Y. (1995), Synthesis and properties of etheno-bridged porphyrin trimers. *Tetrahedron Lett.* 36, 5359-5362. (DOI:10.1016/0040-4039(95)01039-K).

[8] (a) Davis, N. K. S., Thompson, A. L., Anderson, H. L. (2010), Bis-anthracene fused porphyrins: Synthesis, crystal structure, and near-ir absorption. *Org. Lett.* 12, 2124-2127. (DOI:10.1021/ol100619p). (b) Lewtak, J. P., Gryko, D., Bao, D., Sebai, E., Vakuliuk, O., S´cigaj, M., Gryko, D. T. (2011), Naphthalene-fused metallo-porphyrins–synthesis

and spectroscopy. *Org. Biomol. Chem.* 9, 8178-8181. (DOI:10.1039/C1OB06281F). (c) Diev, V. V., Hanson, K., Zimmerman, J. D., Forrest, S. R., Thompson, M. E. (2010), Fused Pyrene–Diporphyrins: Shifting Near-Infrared Absorption to 1.5 µm and Beyond. *Angew. Chem. Int. Ed.* 49, 5523-5526. (DOI:10.1002/anie.201002669).

[9] (a) Whitten, D. G. (1978), Photochemistry of porphyrins and their metal complexes in solution and organized media. *Rev. Chem. Intermed.* 2, 107-138. (b) Fukuzumi, S., Honda, T., Kojima, T. (2012), Structures and photoinduced electron transfer of protonated complexes of porphyrins and metallophthalocyanines. *Coord. Chem. Rev.* 256, 2488-2502. (DOI: 10.1016/j.ccr.2012.01.011).

[10] (a) Ambroise, A., Li, J., Yu, L., Lindsey, J. S. (2000), A self-assembled light-harvesting array of seven porphyrins in a wheel and spoke architecture. *Org. Lett.* 2, 2563-2566. (DOI: 10.1021/ol006036d). (b) Yu, L., Lindsey, J. S. (2001), Rational syntheses of cyclic hexameric porphyrin arrays for studies of self-assembling light-harvesting systems. *J. Org. Chem.* 66, 7402-7419. (DOI: 10.1021/jo010742q).

[11] Gust, D., Moore, T. A., Moore, A. L. (2001), Mimicking photosynthetic solar energy transduction. *Acc. Chem. Res.* 34, 40-48. (DOI: 10.1021/ar9801301).

[12] Song, H. E., Kirmaier, C., Schwartz, J. K., Hindin, E., Yu, L., Bocian, D. F., Lindsey, J. S., Holten, D. (2006), Effects of multiple pathways on excited-state energy flow in self-assembled wheel-and-spoke light-harvesting architectures. *J. Phys. Chem. B.* 110, 19131-19139. (DOI: 10.1021/jp064001a).

[13] Yella, A., Lee, H.-W., Tsao, H. N., Yi, C., Chandiran, A. K., Nazeeruddin, M. K., Diau, E. W.-G., Yeh, C.-Y., Zakeeruddin, S. M., Graetzel, M. (2011), Porphyrin-sensitized solar cells with cobalt (II/III)–based redox electrolyte exceed 12 percent efficiency. *Science.* 334, 629-634. (DOI: 10.1126/science.1209688).

[14] (a) de Visser, S. P., Valentine, J. S., Nam, W. (2010), A biomimetic ferric hydroperoxo porphyrin intermediate. *Angew. Chem. Int. Ed.* 49,

2099-2101. (DOI: 10.1002/anie.200906736). (b) Araghi, M., Mirkhani, V., Moghadam, M., Tangestaninejad, S., Mohammdpoor-Baltork, I. (2012), Synthesis and characterization of a new porphyrin–polyoxometalate hybrid material and investigation of its catalytic activity. *Dalton Trans.* 41, 3087-3094. (DOI: 10.1039/C2DT11865C). (c) Dar, T. A., Uprety, B., Sankar, M., Maurya, M. R. (2019), Robust and electron deficient oxidovanadium (iv) porphyrin catalysts for selective epoxidation and oxidative bromination reactions in aqueous media. *Green Chem.* 21, 1757-1768. (DOI: 10.1039/C8GC03909G).

[15] (a) Vijisha, M. V., Parambath, S., Jagadeesan, R., Arunkumar, C., Chandrasekharan, K. (2019), Nonlinear optical absorption and optical limiting studies of fluorinated pyridyl porphyrins in chlorobenzene: An insight into the photo-induced protonation effects. *Dyes Pigm.* 169, 29-35. (DOI: 10.1016/j.dyepig.2019.05.012). (b) Yella, A., Lee, H.-W., Tsao, H. N., Yi, C., Chandiran, A. K., Nazeeruddin, M. K., Diau, E. W.-G., Yeh, C.-Y., Zakeeruddin, S. M., Graetzel, M. (2011), Porphyrin-sensitized solar cells with cobalt (II/III)–based redox electrolyte exceed 12 percent efficiency. *Science*. 334, 629-634. (DOI: 10.1126/science.1209688).

[16] (a) Yang, W., Zhang, B. (2019), Porphyrin-based nanocomposites for tumor photodynamic therapy. *MRS Bulletin*, 44, 189-194. (DOI: 10.1557/mrs.2019.42). (b) Maeda, C., Ogawa, K., Sadanaga, K., Takaishi, K., Ema, T. (2019), Chiroptical and catalytic properties of doubly binaphthyl-strapped chiral porphyrins. *Chem. Comm.* 55, 1064-1067. (DOI: 10.1039/C8CC09114E). (c) Dar, T. A., Uprety, B., Sankar, M., Maurya, M. R. (2019), Robust and electron deficient oxidovanadium (iv) porphyrin catalysts for selective epoxidation and oxidative bromination reactions in aqueous media. *Green Chem.* 21, 1757-1768. (DOI: 10.1039/C8GC03909G). (d) Kumar, R., Chaudhary, N., Sankar, M., Maurya, M. R. (2015), Electron deficient nonplanar β-octachlorovanadylporphyrin as a highly efficient and selective epoxidation catalyst for olefins. *Dalton Trans.* 44, 17720-17729. (DOI: 10.1039/C5DT02349A). (e) Thompson, S. J., Brennan, M. R., Lee, S. Y., Dong, G. (2018), Synthesis and applications of

rhodium porphyrin complexes. *Chem. Soc. Rev.* 47, 929-981. (DOI: 10.1039/C7CS00582B). (f) Lu, H.-J., Jiang, H.-L., Wojtas, L., Zhang, X. P. (2010), Selective Intramolecular C– H Amination through the Metalloradical Activation of Azides: Synthesis of 1, 3-Diamines under Neutral and Nonoxidative Conditions. *Angew. Chem.* 122, 10390-10394. (DOI: 10.1002/ange.201005552).

[17] (a) Eguchi, D., Sakamoto, M., Teranishi, T. (2018), Ligand effect on the catalytic activity of porphyrin-protected gold clusters in the electrochemical hydrogen evolution reaction. *Chem. Sci.* 9, 261-265. (DOI: 10.1039/C7SC03997B). (b) Barona-Castaño, J. C., Carmona-Vargas, C. C., Brocksom, T. J., de Oliveira, K. T. (2016), Porphyrins as catalysts in scalable organic reactions. *Molecules.* 21, 310. (DOI: 10.3390/molecules21030310).

[18] (a) Reddy, G., Katakam, R., Devulapally, K., Jones, L. A., Della Gaspera, E., Upadhyaya, H. M., Islavath, N., Giribabu, L. (2019), Ambient stable, hydrophobic, electrically conductive porphyrin hole-extracting materials for printable perovskite solar cells. *J. Mater. Chem. C.* 7, 4702-4708. (DOI: 10.1039/C9TC00605B). (b) Cook, L., Brewer, G., Wong-Ng, W. (2017), Structural aspects of porphyrins for functional materials applications. *Crystals*, 7, 223. (DOI: 10.3390/cryst7070223). (c) Smykalla, L., Mende, C., Fronk, M., Siles, P. F., Hietschold, M., Salvan, G., Zahn, D. R. T., Schmidt, O. G., Rüffer, T., Lang, H. (2017), (Metallo) porphyrins for potential materials science applications. *Beilstein J. Nanotechnol.* 8, 1786-1800. (DOI: 10.3762/bjnano.8.180). (d) Rosenthal, I. (1996), in Phthalocyanines − Properties and Applications (Eds.: C. C. Leznoff, A. B. P. Lever), *VCH, New York*, vol. 4, chapter 13. (e) Wohrle, D., Suvorova, O., Gerdes, R., Bartels, O., Lapok, L., Baziakina, N., Makarov, S., Slodek, A. (2004), Efficient oxidations and photooxidations with molecular oxygen using metal phthalocyanines as catalysts and photocatalysts. *J Porphyr Phthalocyanines.* 8, 1020-1041. (DOI: 10.1142/S1088424604000398).

[19] Kim, S. H., Kim, H. W., Sakong, Chun., Namgoong, J., Park, S. W., Ko, M. J., Lee, C. H., Lee, W. I., Kim, J. P. (2011), Effect of five-

members heteroaromatic linkers to the performance of phenothiazine-based dye-sensitized solar cells. *Org. Lett.* 13, 5784-5787. (DOI: 10.1021/ol2023517).

[20] (a) Jucker, E. M. (Ed.). (2002), *Progress in drug research* (Vol. 58). Springer Science & Business Media. (b) Onoabedje, E. A., Egu, S. A., Ezeokonkwo, M. A., & Okoro, U. C. (2019), Highlights of molecular structures and applications of phenothiazine & phenoxazine polycycles. *J. Mol. Struct.* 1175, 956-962. (DOI: 10.1016/j.molstruc.2018.08.064).

[21] (a) Shivarkar, A. B., Gupte, S. P., Chaudhari, R. V. (2005), Selective synthesis of N, N-dimethyl aniline derivatives using dimethyl carbonate as a methylating agent and onium salt as a catalyst. *J. Mol. Catal. A Chem.* 226, 49-56. (DOI: 10.1016/j.molcata.2004.09.025).

[22] Michinobu, T. (2011), Adapting semiconducting polymer doping techniques to create new types of click postfunctionalization. *Chem. Soc. Rev.* 40, 2306-2316. (DOI: 10.1039/C0CS00205D).

[23] Liu, X., Wang, D., Gao, H., Yang, Z., Xing, Y., Cao, H., He, W., Wang, H., Gu, J., Hu, H. (2016), Nonlinear optical properties of symmetrical and asymmetrical porphyrin derivatives with click chemistry modification. *Dyes Pigm.* 134, 155-163. (DOI: 10.1016/j.dyepig.2016.07.010).

[24] Liaoliao Li, L., Wang, D., Wang, L., Ramella, D., Wang, H., Gao, H., Zhang, J., Xing, Y., Li, B., Yang, Z., Cao, H., He, W. (2018), The photoacoustic effect of near-infrared absorbing porphyrin derivatives prepared via click chemistry. *Dyes Pigm.* 148, 501-507. (DOI: 10.1016/j.dyepig.2017.08.003).

[25] (a) Gao, G. Y., Ruppel, J. V., Allen, D. B., Chen, Y., Zhang, X. P. (2007), Synthesis of β-functionalized Porphyrins via palladium-catalyzed carbon− heteroatom bond formations: expedient entry into β-chiral Porphyrins. *J. Org. Chem.* 72, 9060-9066. (DOI: 10.1021/jo701476m). (b) Yeung, M., Ng, A. C., Drew, M. G., Vorpagel, E., Breitung, E. M., McMahon, R. J., Ng, D. K. (1998), Facile Synthesis and Nonlinear Optical Properties of Push− Pull 5, 15-Diphenylporphyrins. *J. Org. Chem.* 63, 7143-7150. (DOI:

10.1021/jo971597c).

[26] Sekaran, B., Jang, Y., Misra, R., D'Souza, F. (2019), Push–Pull Porphyrins via β-Pyrrole Functionalization: Evidence of Excited State Events Leading to High-Potential Charge-Separated States. *Chem. Eur. J.* 25, 12991-13001. (DOI: 10.1002/chem.201902286).

[27] (a) Grover, N., Chaudhri, N., Sankar, M. (2019), β-Functionalized Dibenzoporphyrins with Mixed Substituents Pattern: Facile Synthesis, Structural, Spectral, and Electrochemical Redox Properties. *Inorg. Chem.* 58, 2514-2522. (DOI: 10.1021/acs.inorgchem.8b03106). (b) Roucan, M., Kielmann, M., Connon, S. J., Bernhard, S. S. R., Senge, M. O. (2018), Conformational control of nonplanar free base porphyrins: towards bifunctional catalysts of tunable basicity. *Chem. Commun.* 54, 26-29. (DOI: 10.1039/C7CC08099A). (c) Grover, N., Chaudhri, N., Sankar, M. (2017), Facile Conversion of Ni (II) Cyclopropylchlorins into Novel β-Substituted Porphyrins through Acid-Catalyzed Ring-Opening Reaction. *Inorg. Chem.* 56, 424-437. (DOI: 10.1021/acs.inorgchem.6b02333). (d) Grover, N., Chaudhri, N., Sankar, M. (2019), β-Functionalized Dibenzoporphyrins with Mixed Substituents Pattern: Facile Synthesis, Structural, Spectral, and Electrochemical Redox Properties. *Inorg. Chem.* 58, 2514-2522. (DOI: 10.1021/acs.inorgchem.8b03106).

[28] (a) Fery-Forgues, S., Delavaux-Nicot, B. (2000), Ferrocene and ferrocenyl derivatives in luminescent systems. *J. Photochem. Photobiol. A.* 132, 137-159. (DOI: 10.1016/S1010-6030(00)00213-6). (b) Barlow, S., Marder, S. R. (2000), Electronic and optical properties of conjugated group 8 metallocene derivatives. *Chem. Commun.* 17, 1555-1562. (DOI: 10.1039/B004907G). (c) Kashiwagi, Y., Imahori, H., Araki, Y., Ito, O., Yamada, K., Sakata, Y., Fukuzumi, S. (2003), Strong Inhibition of Singlet Oxygen Sensitization in Pyridylferrocene−Fluorinated Zinc Porphyrin Supramolecular Complexes. *J. Phys. Chem. A.* 107, 5515-5522. (DOI: 10.1021/jp034920q).

[29] Frisch, M. J., Trucks, G. W., Schlegel, H. B., Scuseria, G. E., Robb, M. A., Cheeseman, J. R., Scalmani, G., Barone, V., Mennucci, B.,

Petersson, G. A., Nakatsuji, H., Caricato, M., Li, X., Hratchian, H. P., Izmaylov, A. F., Bloino, J., Zheng, G., Sonnenberg, J. L., Hada, M., Ehara, M.; Toyota, K.; Fukuda, R.; Hasegawa, J.; Ishida, M.; Nakajima, T.; Honda, Y.; Kitao, O., Nakai, H., Vreven, T., Montgomery, J. A., Jr., Peralta, J. E., Ogliaro, F., Bearpark, M., Heyd, J. J., Brothers, E., Kudin, K. N., Staroverov, V. N., Kobayashi, R., Normand, J., Raghavachari, K., Rendell, A., Burant, J. C., Iyengar, S. S., Tomasi, J., Cossi, M., Rega, N., Millam, N. J., Klene, M., Knox, J. E., Cross, J. B., Bakken, V., Adamo, C., Jaramillo, J., Gomperts, R., Stratmann, R. E., Yazyev, O., Austin, A. J., Cammi, R., Pomelli, C., Ochterski, J. W., Martin, R. L., Morokuma, K., Zakrzewski, V. G., Voth, G. A., Salvador, P., Dannenberg, J. J., Dapprich, S., Daniels, A. D., Farkas, O., Foresman, J. B., Ortiz, J. V., Cioslowski, J., Fox, D. J. Gaussian 09, Revision A.02, *Gaussian, Inc*., Wallingford, CT, 2009.

Chapter 5

Donor Substituted Unsymmetrical *β*-Pyrrole Porphyrins

5.1. Introduction

The solar energy usage has substantially increased in recent times compared to conventional energy sources such as coal, gas and fossil fuels in order to meet the rising global demands.[1-3] Porphyrin analogues occur in nature to perform many important roles in photosynthesis such as electron transfer, oxygen transport, *etc*.[4,5] Porphyrin macrocycles are hydrophobic and rigid in nature.[6] Porphyrins mimic the natural photosynthetic architecture to perform the effective conversion of radiant energy into chemical energy.[7, 8] The porphyrin macrocycle comprises of four *meso*- and eight *beta*-positions, which can be further functionalized to enhance the electronic properties of the porphyrin π-system.[9] Porphyrin based donor–acceptor architecture are highly attractive due to their efficient energy transfer and electron transfer processes.[10-12] Porphyrins are widely explored in the fields of dye-sensitized solar cells, nonlinear optics (NLO) and optoelectronics. [13-16] The electron donating triphenylethylene (TPE) are used in organic luminescent materials, which shows aggregation-induced emission (AIE) properties with potential application in electroluminescence devices and chemosensors.[17] The triphenylamine (TPA) donor shows a propeller shape geometry with three phenyl groups connecting the nitrogen atom.[18] The triphenylamine (TPA) incorporated donor–acceptor (D–A) framework improves the hole transporting ability and device performances in organic light emitting diodes (OLEDs).[19] Phenothiazine is a tricyclic heterocycle with nonplanar geometry containing electron-rich sulfur and nitrogen atom, which shows potential application in organic photovoltaics.[20]

The organic dyes incorporating triphenylamine (TPA), *4,4'*-dimethoxy triphenylamine and phenothiazine have been explored as potential sensitizers for DSSC.[21] Our group has reported the push–pull porphyrin containing triphenylamine and naphthalimide substituents at

the opposite *β*, *β*′-positions and explored their charge-separated states in polar solvents. [22] Weihong Zhu and co-workers investigated the effect of electron donors on the efficiency of the DSSCs, by introducing the triphenylamine and dimethoxy triphenylamine unit on the *meso*-position of the porphyrin moiety.[23] Cristea *et al*. have synthesized an array of phenothiazine substituted *meso*-porphyrins and their optical and electrochemical properties were elucidated.[24]

In this chapter, we have designed and synthesized a set of triphenylethylene, triphenylamine, dimethoxy triphenylamine and phenothiazine substituted unsymmetrical *β*-pyrrole functionalized porphyrins and its zinc metal derivatives **1**–**8** and their photophysical, electrochemical and computational studies were explored. The tuning of electronic properties for porphyrins **1**–**8** were investigated by incorporating the donor substituents at the *β*-pyrrolic position of the porphyrin π-system.
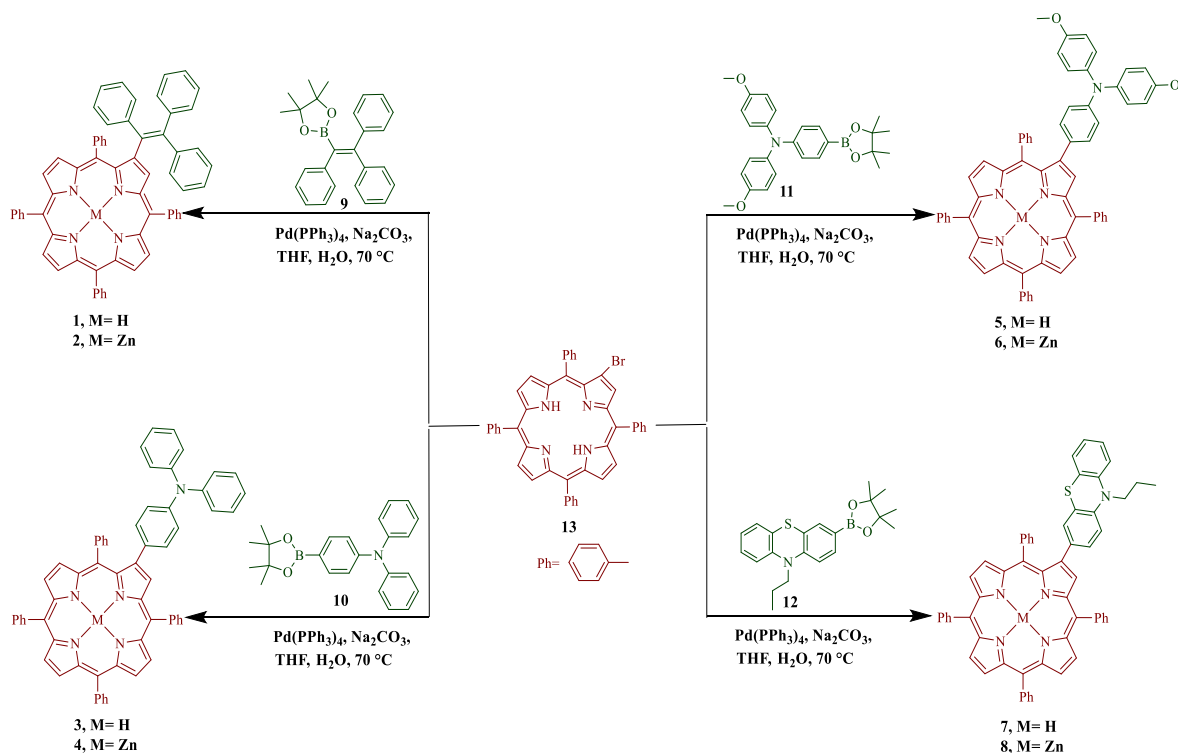
Scheme 5.1. Synthetic routes of the investigated porphyrins **1**–**8**.

5.2. Results and Discussion

The synthesis of porphyrin and its Zn(II) complexes **1**–**8** are shown in Scheme 5.1. The *β*-monobrominated tetraphenyl porphyrin (TPPBr) **13** and the intermediate **9**, **10**, **11** and **12** were synthesized according to the reported procedures (Scheme 5.1). [25-27] The porphyrin **1**, **3**, **5** and **7** were synthesized by the Suzuki cross-coupling reaction. The Pd-catalyzed Suzuki coupling reaction of TPPBr **13** with 1.5 equiv of 4,4,5,5-tetramethyl-2-(1,2,2-triphenylvinyl)-1,3,2-dioxaborolane **9** and *N*, *N*-diphenyl-4-(4,4,5,5-tetramethyl-1,3,2-dioxaborolan-2-yl)aniline **10** in the presence of Pd(PPh$_3$)$_4$ in THF solvent at 70 °C resulted **1** and **3** in 75% and 80% yields, respectively (Scheme 5.1). The porphyrin **5** and **7** were synthesized by Pd-catalyzed Suzuki coupling reaction of TPPBr **13** with 1.5 equiv of 4-methoxy-*N*-(4-methoxyphenyl)-*N*-(4-(4,4,5,5-tetramethyl-1,3,2-dioxaborolan-2 yl)phenyl)aniline **11** and 10-propyl-3-(4,4,5,5-tetramethyl-1,3,2-dioxaborolan-2-yl)-10H-phenothiazine **12** in the presence of Pd(PPh$_3$)$_4$ in THF solvent at 70 °C resulted in 81% and 76% yields, respectively (Scheme 5.1). The zinc metallation on porphyrins **1**, **3**, **5**, and **7** were carried out using Zn(OAc)$_2$ by dissolving in MeOH and CHCl$_3$ (3:1) mixture, which resulted in zinc complexes **2**, **4**, **6**, and **8** with 90, 83, 86 and 83% yields, respectively. The porphyrin derivatives **1**–**8** were characterized by ^{1}H and ^{13}C NMR and HRMS mass spectroscopic techniques.

5.3. Photophysical Properties

The UV-Vis absorption spectra of porphyrins **1**–**8** were recorded in THF at room temperature (Figure 5.1) and the data are tabulated in Table 5.1. The Figure 5.1 illustrates the electronic absorption spectra of *β*-donor substituted porphyrin **1**−**8**, which shows a characteristic Soret band and Q–bands in the UV-Visible region. The zinc complexes **2**, **4**, **6**, and **8** exhibits a characteristic Soret band around 425−428 nm and these were slightly red shifted by 6−8 nm in the high energy region compared to its subsequent free base derivatives **1**, **3**, **5**, and **7**. The porphyrins **1**−**8** shows a characteristic Q–bands around 517−651 nm in

the low energy region. The triphenylethylene substituted porphyrin **1** and **2** shows a small red shifted absorption in the soret band compared to the triphenylamine, dimethoxy triphenylamine and phenothiazine substituted porphyrin **3−8**. The absorption spectra of porphyrin with different donor units **3−8** shows similar absorption band with 1−3 nm red shift in the Soret and Q–band region, for the free base along with Zn(II) complexes. The red shift in the soret and Q band follows the order; for free base **1** > **5** > **3** ≈ **7** and zinc complexes **2** > **4** ≈ **8** > **6**. A similar absorption bands were observed for the free base and zinc complexes, which might be due to the electron donating capability of the donor entities at the *β*-pyrrolic positions.
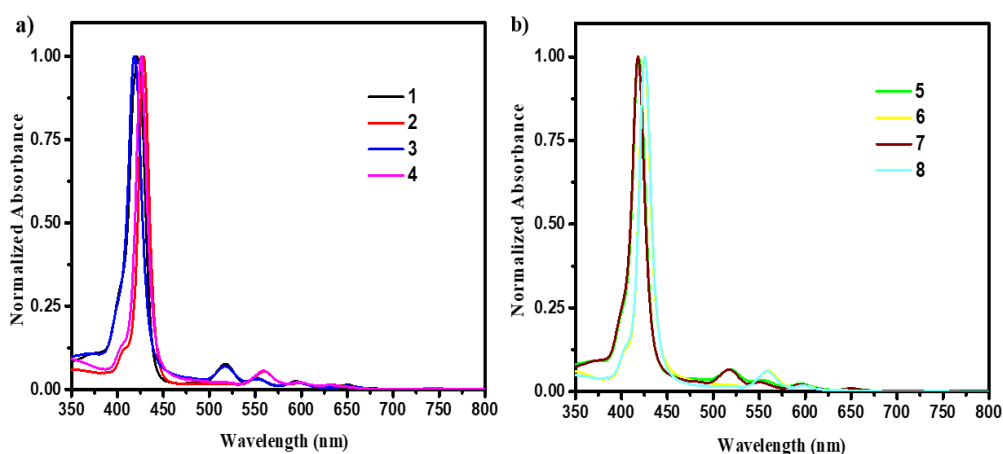
Figure 5.1. Normalized electronic absorption spectra of porphyrin a) **1–4** and b) **5–8** in THF at 1.0×10^{-5} M concentration.

The emission spectra of porphyrin **1**–**8** (Figure 5.2) was recorded in THF at room temperature, and the data are summarized in Table 5.1. The emission spectra of *β*-donor substituted porphyrin **1**–**8** show a characteristic two emission bands in the low energy region around 613–724 nm. The free base porphyrin **1**, **3**, **5** and **7** shows emission band around 655–724 nm and for their Zn(II) complexes **2**, **4, 6, 8** the emission occurs in the range of 613–662 nm, respectively. The triphenylamine substituted porphyrin **3** shows slight red shift of 2–6 nm in the emission maxima compared to other free base porphyrins **1**, **5** and **7**. The triphenylethylene and dimethoxy triphenylamine porphyrin **1** and

5 exhibits small red shift of 3–4 nm in the fluorescence maxima compared to the phenothiazine substituted porphyrin **7**. The triphenylamine and dimethoxy triphenylamine Zn(II) porphyrin **4** and **6** exhibits a red shifted emission maxima of 4–8 nm compared to the triphenylethylene and phenothiazine substituted porphyrin **2** and **8**. The red shifted emission maxima of free base and its Zn(II) porphyrin **1**–**8** may be due to the nonplanarity of β-donor substituted porphyrin which is evidenced from the computational studies. The free base porphyrin **1**, **3**, **5** and **7** shows higher quantum yields compared to its corresponding zinc complexes **2**, **4**, **6, 8**. The fluorescence quantum yield of triphenylamine substituted porphyrin **3** shows high quantum yield value of 0.61.
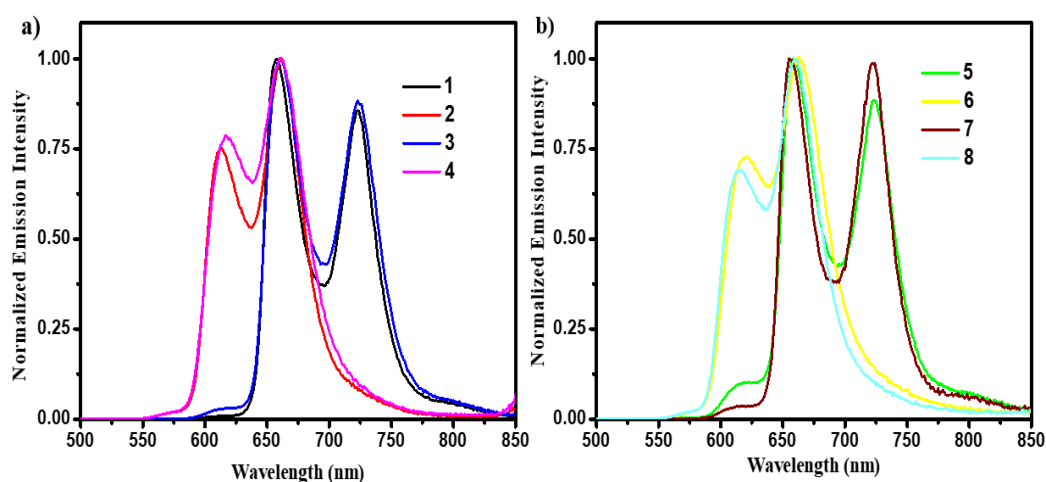
Figure 5.2. Normalized emission spectra of porphyrin a) **1**–**4** and b) **5**–**8** in THF at 1.0×10^{-5} M concentration.

Table 5.1. Photophysical and theoretical data of porphyrin **1–8**.

Compound	λ_{abs} (nm)[a]			λ_{em} (nm)	Φ_f [b]	H–L gap (eV) [c]
	Soret band (S-band)	ε (M^{-1} cm^{-1})	Q-bands			
1	421	23460	517, 552, 594, 650	658, 723	0.55	2.65
2	428	16600	560, 599, 633	613, 662	0.35	2.81
3	418	18270	517, 552, 595, 650	661, 723	0.61	2.47
4	426	99770	559, 598, 632	617, 661	0.41	2.62
5	419	17930	518, 553, 595, 651	659, 724	0.33	2.23
6	425	20940	560, 598	621, 661	0.13	2.38
7	418	14560	517, 551, 594, 650	655, 722	0.24	2.59
8	426	20580	559, 598	613, 660	0.14	2.73

[a] Absorbance measured in THF at 1×10^{-5} M concentration; λ_{abs}: absorption wavelength; λ_{em}: emission wavelength; ε: extinction coefficient. [b] The fluorescence quantum yields were recorded using H_2TPP as a standard ($\Phi_{st} = 0.11$). [c] Calculated from computational study.

5.4. Electrochemical Properties

The electrochemical redox potential of porphyrin **1–8** were investigated by cyclic voltammetry in dichloromethane using 0.1M TBAPF$_6$ as supporting electrolyte.[28-30] The cyclic voltammograms of porphyrin **1–8** and their data are depicted in Figure 5.3 and Table 5.2. The free base porphyrin **1**, **3**, **5** and **7** exhibits, their redox potentials around -1.58 to 1.51 V whereas in zinc porphyrin **2**, **4**, **6** and **8** the redox potentials were observed between -1.80 to 1.41 V. The zinc porphyrin **2**, **4**, **6** and **8** exhibits a cathodic shift in the redox potentials compared to their corresponding free base porphyrin **1**, **3**, **5** and **7**. In general, the porphyrin macrocycle exhibits two oxidation and two reduction waves due to the formation of cations and anions of the porphyrin ring. In *β*-donor

Table 5.2. Electrochemical data of porphyrin **1**–**8**.

Compound	Potential (V vs Ag/Ag$^+$) [d]		E_g (eV) [e]
	E_{red}	E_{ox}	
1	-1.31, -1.58	0.95, 1.18 1.51	2.00
2	-1.46, -1.80	0.80, 1.04, 1.22	2.03
3	-1.29, -1.53	0.89, 1.05, 1.24	2.00
4	-1.43, -1.75	0.81, 0.94, 1.12	2.01
5	-1.30, -1.53	0.65, 1.02, 1.22, 1.41	1.71
6	-1.43, -1.76	0.62, 0.83, 1.10, 1.41	1.85
7	-1.28, -1.52	0.67, 1.02, 1.24	1.70
8	-1.42, -1.75	0.66, 0.85, 1.12	1.90

[d] Electrochemical analysis was estimated by cyclic voltammetry in 0.1 M solution of tetrabutylammonium hexafluorophosphate (TBAPF$_6$) in DCM at 100 mV/s scan rate. [e] Electrochemical band gaps.

substituted porphyrins **1**–**8**, the additional reversible oxidation waves were observed due to the oxidation of the donor units. The triphenylethylene and triphenylamine substituted porphyrin **1**–**4** exhibits two reduction waves corresponding to the porphyrin macrocycle and three reversible oxidation waves representing the porphyrin macrocycle and the donor units. In porphyrin **1**–**4**, the first and second oxidation wave in the region of 0.80 to 1.18 V can be attributed to the porphyrin macrocycle, whereas the third oxidation wave in the region of 1.12 to 1.51 V can be assigned to the triphenylethylene and triphenylamine donor units. The dimethoxy triphenylamine and phenothiazine substituted porphyrin **5**–**8**, exhibits two reduction waves corresponding to the porphyrin macrocycles. The dimethoxy triphenylamine substituted porphyrin **5** and **6** exhibits four reversible oxidation wave corresponding to the porphyrin macrocycle and the dimethoxy
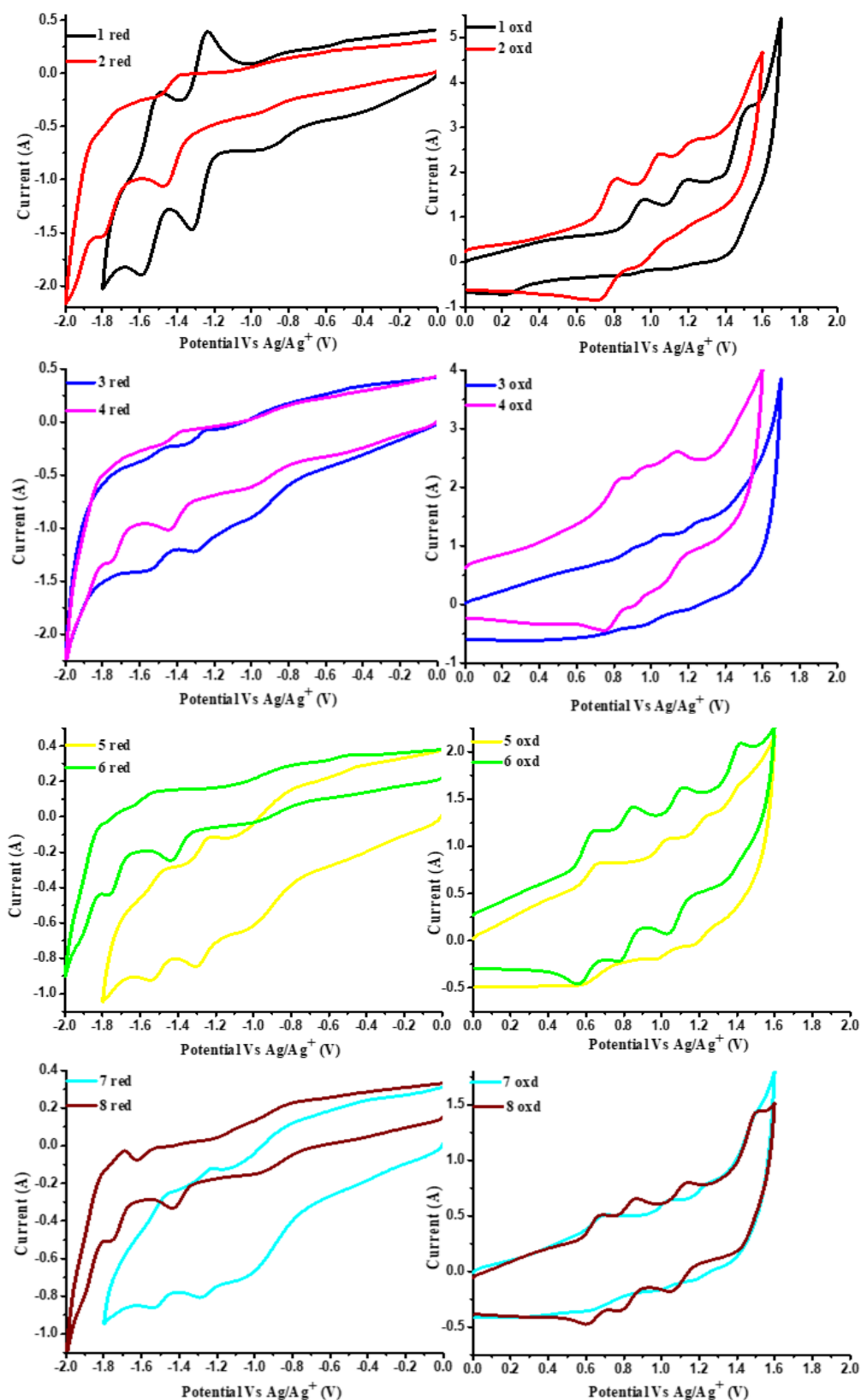
Figure 5.3. Cyclic voltammograms of porphyrin **1**–**8** in dichloromethane containing 0.1 M solution of TBAPF$_6$ with a scan rate of 100 mV/s.

triphenylamine donor unit. In porphyrin **5** and **6**, the first oxidation wave around 0.62 to 0.65 V is attributed to the methoxy unit. The second and third oxidation wave of porphyrin **5** and **6** between 0.83 to 1.22 V, corresponds to the porphyrin macrocycle whereas the fourth oxidation wave can be assigned to the triphenylamine donor unit. In phenothiazine substituted porphyrin **7** and **8**, three reversible oxidation waves were observed which corresponds to the porphyrin macrocycle and the phenothiazine unit. In porphyrin **7** and **8**, the first oxidation wave around 0.66 to 0.67 V is attributed to the phenothiazine unit whereas the second and third oxidation wave between 0.85 to 1.24 V, corresponds to the porphyrin macrocycle. The calculated HOMO energy levels of porphyrin **1**–**8** were -5.24 V, -5.11 V, -5.21 V, -5.11 V, -4.95 V, -4.93 V, -4.96 V and -4.97 V and the LUMO energy levels were -3.24 V, -3.08 V, -3.21 V, -3.10 V, -3.24 V, -3.08 V, -3.26 V and -3.07 V, respectively.

5.5. Theoretical Calculations

The electronic structures of the porphyrin **1**–**8** were deduced by performing DFT calculations at B3LYP/6-31G level using the Gaussian 09W program. [31] The optimized structures of porphyrin **1**–**8** show twisted nonplanar geometry due to the presence of donor substituents at the β-pyrrolic position (Figure 5.4). The energy level diagrams of the porphyrin **1**–**8** are illustrated in Figure 6. In case of porphyrin **1** and **2** the HOMO and LUMO are mainly populated on the porphyrin macrocycle. In porphyrin **3**, **4**, **5** and **6** the HOMO energy levels are localized on triphenylamine and dimethoxy triphenylamine donor units and the LUMO is mainly concentrated on the porphyrin macrocycle. The phenothiazine substituted porphyrins **7** and **8** shows that the majority of the electron density in HOMO were concentrated on the phenothiazine unit with little over the porphyrin ring, whereas the LUMO are localized on the porphyrin macrocycle. The theoretically calculated HOMO levels of the porphyrins **1**, **2**, **3**, **4**, **5**, **6**, **7** and **8** are –4.91 eV, –4.98 eV, –4.78 eV, –4.81 eV, –4.51 eV, –4.55 eV, –4.87 eV and –4.91 eV whereas LUMO levels are –2.26 eV, –2.17 eV, –2.31 eV,

–2.19 eV, –2.28 eV, –2.17 eV, –2.28 eV and –2.18 eV respectively (Figure 5.5). The theoretically calculated HOMO and LUMO energy level reveals that the dimethoxy triphenylamine substituted porphyrin derivatives **5** and **6** exhibits, low HOMO–LUMO band gap of about 2.23 eV and 2.38 eV compared to other donor substituted porphyrins.
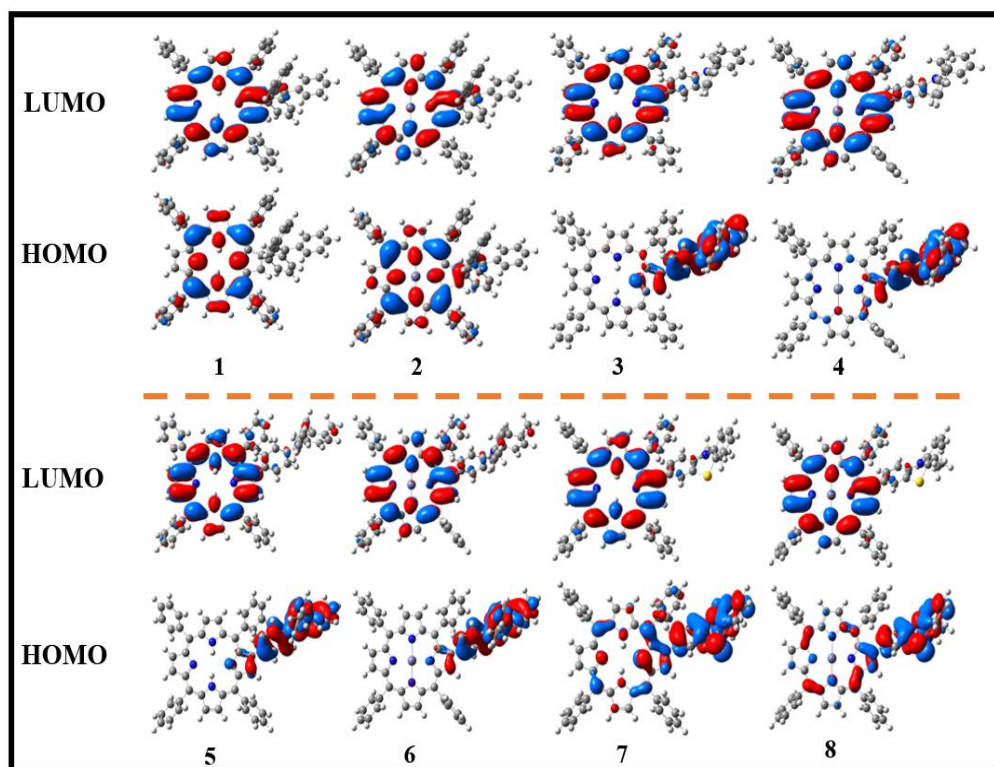
Figure 5.4. Frontier HOMO and LUMO on B3LYP/6-31G optimized structures of porphyrins **1**–**8**.

The electronic absorption spectra, electronic transitions, and oscillator strength (f) were calculated using time-dependent density functional theory (TD-DFT) at B3LYP/6-31G level and the data are depicted in Table 5.3.[31] The TD-DFT calculation of porphyrin **1**–**8** shows two characteristic absorption band, the Soret band with high oscillator strength and the Q-band with lesser oscillator strength. The porphyrin **1**, **2**, **3**, **4**, **5**, **6**, **7** and **8** shows absorption band around 502, 471, 539, 528, 653, 606, 529 and 514 nm in the Q-band region, which is assigned to the ICT transitions. The major ICT transitions for porphyrin **1** and **2** occurs from HOMO–1→LUMO and HOMO–2→LUMO, whereas in

porphyrin **3** and **4** it arises from HOMO–1→LUMO +1. In porphyrin **5**, **6** and **8**, the ICT transition occurs from HOMO →LUMO and in porphyrin **7** it arises from HOMO–1→LUMO +1. In porphyrin **1**, **2**, **3**, **4**, **5**, **6**, **7** and **8** the absorption band observed around 381, 381, 386, 377, 380, 378, 382 and 381 nm in the soret

Table 5.3. Calculated Electronic Transitions of porphyrin **1–8**.

Compounds	λ_{max}	Composition & Molecular contribution	f^a	Assignment
1	381	HOMO–2→LUMO (0.36)	1.11	π–π^*
	502	HOMO–1→LUMO (0.49)	0.13	ICT
2	381	HOMO–1→LUMO+1 (0.32)	1.42	π–π^*
	471	HOMO–2→LUMO (0.55)	0.14	ICT
3	386	HOMO–2→LUMO (0.47)	1.37	π–π^*
	539	HOMO–1→LUMO +1 (0.54)	0.09	ICT
4	377	HOMO–2→LUMO+1 (0.50)	1.34	π–π^*
	528	HOMO–1→LUMO +1 (0.41)	0.06	ICT
5	380	HOMO–3→LUMO+1 (0.53)	0.80	π–π^*
	653	HOMO →LUMO (0.69)	0.07	ICT
6	378	HOMO–2→LUMO+1 (0.47)	1.34	π–π^*
	606	HOMO →LUMO (0.69)	0.09	ICT
7	382	HOMO–2→LUMO (0.43)	1.08	π–π^*
	529	HOMO–1 →LUMO+1 (0.44)	0.09	ICT
8	381	HOMO–2 →LUMO (0.50)	1.40	π–π^*
	514	HOMO →LUMO (0.48)	0.09	ICT

f^a Oscillator strength.

band region, attributes to the π–π^* transitions. In porphyrin **1**, **3**, **7** and **8**, the π–π^* transitions arises from HOMO–2→LUMO whereas in porphyrin **2** and **4**, it occurs from HOMO–1→LUMO+1 and HOMO–2→LUMO+1. In porphyrin **5** and **6**, the π–π^* transitions arises from HOMO–3→LUMO+1 and HOMO–2→LUMO+1. The TD-DFT calculated values of porphyrin **1a–8d** are in good agreement with the experimental values.
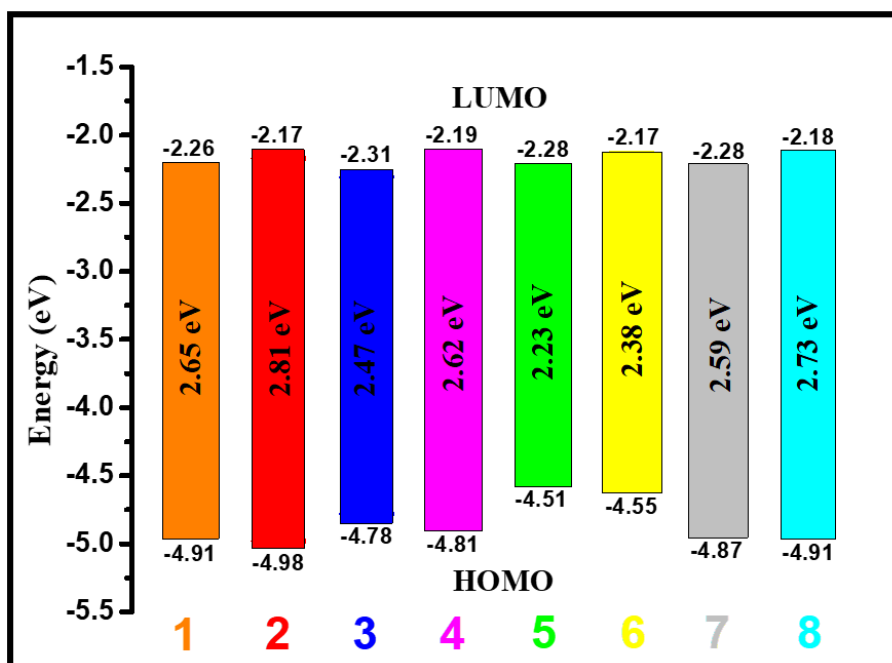
Figure 5.5. Energy level diagram of the frontier orbitals of porphyrin **1**–**8** estimated by DFT calculations.

5.6. Experimental Section

General: All the chemicals were purchased from commercial sources and used without further purification. The NMR spectra were recorded at room temperature (298 K). Chemical shifts are given in ppm with respect to tetramethylsilane as internal standard (CDCl$_3$, 7.26 ppm, 77.0 ppm). ^{1}H NMR spectra were recorded using a 400 MHz and 500 MHz spectrometer. ^{13}C NMR spectra were recorded using a 101 MHz and 126 MHz spectrometer. Multiplicities are given as s (singlet), d (doublet), t (triplet) and m (multiplet) are given in Hertz. TLC analysis was carried out using silica gel 60 F$_{254}$ plates. UV-visible absorption spectra were recorded on a Cary-100 Bio UV-visible spectrophotometer. Emission spectra were recorded in a The Fluoromax-4C, S/n. 1579D-1417-FM Fluorescence software Ver 3.8.0.60. UV/Vis and emission spectrums of all compounds were recorded in THF solution. The density functional theory (DFT) calculation were carried out at the B3LYP/6-31G level for

C, N, H, O, S, Zn in the Gaussian 09 program. HRMS were recorded on a Bruker-Daltonics micrOTOF-Q II mass spectrometer.

Synthesis of compound 1.

7-bromo-5,10,15,20-tetraphenylporphyrin **13** (0.080 g, 0.115 mmol) and 4,4,5,5-tetramethyl-2-(1,2,2-triphenylvinyl)-1,3,2-dioxaborolane **9** (0.066 g, 0.173 mmol) were dissolved in THF (20 mL) and purged by nitrogen for 15 min. Meanwhile, a solution of sodium carbonate (0.750 g, 7.07 mmol) in water (15 mL), was added. After purging, palladium (0) tetrakis(triphenylphosphine) (0.100 g, 0.08 mmol) was added and the reaction mixture was refluxed in an oil bath for 16 h at 70 °C. The solvent was then evaporated under vacuum, the resultant mixture was diluted with DCM and the organic layer was collected, dried over anhydrous Na_2SO_4 and evaporated under vacuum. The solid was adsorbed on silica gel and purified by column chromatography, using a DCM: hexane (20: 80) mixture to yield 0.075 g, 75% of compound **1**. ^{1}H NMR (400 MHz, $CDCl_3$) δ 8.83(d, 2 H), 8.79(d, 1 H), 8.73(d, 1 H), 8.68(d, 1 H), 8.59(s, 1 H), 8.55(d, 1 H), 8.21(s, 5 H), 8.04(s, 2 H), 7.88(s, 1 H), 7.76–7.67(m, 8 H), 7.48(s, 1 H), 7.38(d, 1 H), 7.31(s, 2 H), 7.22–7.18(s, 3 H), 7.09–7.05(m, 1 H), 6.89(s, 3 H), 6.72–6.67(m, 3 H), 6.46(t, 1 H), 6.11–6.09(m, 4 H), -2.72(s, 2 H). ^{13}C NMR (101 MHz, $CDCl_3$) δ 152.11, 149.76, 148.42, 147.66, 143.34, 143.09, 142.53, 142.44, 141.92, 140.54, 140.37, 139.72, 139.20, 136.90, 136.36, 134.63, 134.49, 134.40, 132.99, 132.03, 129.68, 129.01, 128.76, 127.67, 127.62, 127.46, 127.29, 127.22, 126.77, 126.61, 126.51, 126.28, 120.24, 120.17, 120.09, 119.76, 119.63, 106.57. HRMS (ESI-TOF): m/z calculated for $C_{64}H_{44}N_4$ $[M+nH]^+$ 869.3639, found 869.3633.

Synthesis of compound 2.

Compound **1** (0.040 g, 0.046 mmol) and Zn $(OAc)_2$, (0.111 g, 0.506 mmol) in MeOH: $CHCl_3$ (3 : 1, v/v), were added and the reaction mixture was stirred for 1 h at room temperature. The solvent was then evaporated under reduced pressure and the resultant mixture was diluted with DCM/water and the organic layer was collected, dried over anhydrous Na_2SO_4 and evaporated under vacuum. The solid was

adsorbed on silica gel and purified by column chromatography, using a DCM: hexane (35: 65) mixture to yield 0.037 g, 90% of compound **2**.
^{1}H NMR (500 MHz, CDCl$_3$) δ 8.93–8.91(m, 3 H), 8.87(d, 1 H), 8.82(d, 1 H), 8.66(s, 2 H), 8.22–8.18(m, 5 H), 8.08(d, 1 H), 8.01(d, 1 H), 7.86(s, 1 H), 7.77–7.65(m, 8 H), 7.51(t, 1 H), 7.37(d, 1 H), 7.31(m, 2 H), 7.20–7.15(m, 3 H), 7.09(t, 1 H), 6.86(m, 3 H), 6.69–6.66(m, 3 H), 6.35(t, 1 H), 6.04(d, 2 H), 5.97(t, 2 H). ^{13}C NMR (101 MHz, CDCl$_3$) δ 151.36, 150.37, 150.11, 149.99, 147.91, 147.26, 145.29, 144.00, 142.98, 142.91, 142.86, 141.27, 139.84, 137.78, 137.27, 137.02, 136.17, 134.45, 134.04, 132.76, 132.71, 131.94, 131.82, 131.22, 129.56, 128.97, 128.70, 127.57, 127.47, 127.25, 127.17, 127.02, 126.58, 126.54, 126.40, 126.22, 126.14, 125.56, 125.41, 122.25, 121.26, 120.76, 120.41. HRMS (ESI-TOF): m/z calculated for C$_{64}$H$_{42}$N$_4$Zn [M]$^+$ 930.2695, found 930.2662.

Synthesis of compound 3.

7-bromo-5,10,15,20-tetraphenylporphyrin **13** (0.080 g, 0.115 mmol) and N, N-diphenyl-4-(4,4,5,5-tetramethyl-1,3,2-dioxaborolan-2-yl) aniline **10** (0.064 g, 0.173 mmol) were dissolved in THF (20 mL) and purged by nitrogen for 15 min. Meanwhile, a solution of sodium carbonate (0.750 g, 7.07 mmol) in water (15 mL), was added. After purging, palladium (0) tetrakis(triphenylphosphine) (0.100 g, 0.08 mmol) was added and the reaction mixture was refluxed in an oil bath for 16 h at 70 °C. The solvent was then evaporated under vacuum, the resultant mixture was diluted with DCM and the organic layer was collected, dried over anhydrous Na$_2$SO$_4$ and evaporated under vacuum. The solid was adsorbed on silica gel and purified by column chromatography, using a DCM: hexane (20: 80) mixture to yield 0.080 g, 80% of compound **3**. ^{1}H NMR (400 MHz, CDCl$_3$) δ 8.84–8.80(m, 4 H), 8.76(s, 1 H), 8.74(d, 1 H), 8.68(d, 1 H), 8.25–8.21(m, 6 H), 7.98(d, 2 H), 7.75(m, 10 H), 7.55(d, 2 H), 7.40–7.31(m, 5 H), 7.25(t, 3 H), 7.16(d, 3 H), 7.05(t, 2 H), 6.89(d, 1 H), -2.61(s, 2 H). ^{13}C NMR (126 MHz, CDCl$_3$) δ 147.90, 146.28, 145.68, 142.62, 142.33, 141.88, 141.16, 136.84, 136.23, 135.08, 134.65, 134.56, 131.24, 129.51, 129.28, 129.13, 128.86, 127.72, 127.24, 126.80, 126.68, 126.64, 126.17, 124.34, 124.01,

123.66, 122.56, 121.19, 120.52, 120.43, 119.95, 119.72. HRMS (ESI-TOF): m/z calculated for $C_{62}H_{43}N_5$ [M+nH]$^+$ 858.3591, found 858.3562.

Synthesis of compound 4.

Compound **3** (0.040 g, 0.046 mmol) and Zn (OAc)$_2$, (0.112 g, 0.513 mmol) in MeOH: CHCl$_3$ (3 : 1, v/v), were added and the reaction mixture was stirred for 1 h at room temperature. The solvent was then evaporated under reduced pressure and the resultant mixture was diluted with DCM/water and the organic layer was collected, dried over anhydrous Na$_2$SO$_4$ and evaporated under vacuum. The solid was adsorbed on silica gel and purified by column chromatography, using a DCM: hexane (35: 65) mixture to yield 0.035 g, 83% of compound **4**. ^{1}H NMR (400 MHz, CDCl$_3$) δ 8.92(s, 4 H), 8.86(s, 2 H), 8.79(s, 1 H), 8.22(m, 6 H), 7.96(d, 1 H), 7.88(d, 1 H), 7.75(m, 10 H), 7.52–7.50(m, 1 H), 7.46(m, 1 H), 7.39–7.32(m, 5 H), 7.18–7.14(m, 6 H), 7.06(t, 2 H), 6.90(d, 1 H). ^{13}C NMR (126 MHz, CDCl$_3$) δ 147.98, 147.84, 146.05, 142.91, 142.64, 142.37, 140.03, 139.39, 138.15, 138.06, 137.40, 136.90, 136.72, 136.38, 136.00, 135.39, 134.48, 134.33, 133.71, 131.21, 129.10, 127.46, 126.55, 126.52, 126.30, 125.91, 123.95, 122.44, 120.74, 119.63, 118.19. HRMS (ESI-TOF): m/z calculated for $C_{62}H_{41}N_5Zn$ [M]$^+$ 919.2648, found 919.2683.

Synthesis of compound 5.

7-bromo-5,10,15,20-tetraphenylporphyrin **13** (0.080 g, 0.115 mmol) and 4-methoxy-N-(4-methoxyphenyl)-N-(4-(4,4,5,5-tetramethyl-1,3,2-dioxaborolan-2-yl)phenyl)aniline **11** (0.074 g, 0.173 mmol) were dissolved in THF (20 mL) and purged by nitrogen for 15 min. Meanwhile, a solution of sodium carbonate (0.750 g, 7.07 mmol) in water (15 mL), was added. After purging, palladium (0) tetrakis(triphenylphosphine) (0.100 g, 0.08 mmol) was added and the reaction mixture was refluxed in an oil bath for 16 h at 70 °C. The solvent was then evaporated under vacuum, the resultant mixture was diluted with DCM and the organic layer was collected, dried over anhydrous Na$_2$SO$_4$ and evaporated under vacuum. The solid was adsorbed on silica gel and purified by column chromatography, using a

DCM: hexane (20: 80) mixture to yield 0.080 g, 81% of compound **5**.
^{1}H NMR (500 MHz, CDCl$_3$) δ 8.84(s, 2 H), 8.81(dd, 1 H), 8.78(dd, 1 H), 8.75(s, 1 H), 8.72(dd, 1 H), 8.68(dd, 1 H), 8.24–8.21(m, 6 H), 7.97(d, 2 H), 7.77–7.73(m, 9 H), 7.52(t, 1 H), 7.38(t, 2 H), 7.18(d, 2 H), 7.10(d, 4 H), 6.90(d, 4 H), 6.76(d, 2 H), 3.85(s, 6 H), -2.61(s, 2 H). ^{13}C NMR (126 MHz, CDCl$_3$) δ 142.42, 142.36, 141.97, 141.41, 140.95, 139.03, 138.96, 137.38, 136.37, 136.20, 134.63, 134.52, 130.98, 127.71, 127.07, 126.87, 126.83, 126.77, 126.65, 126.59, 126.55, 126.20, 126.17, 126.12, 125.98, 125.79, 123.07, 122.44, 121.20, 121.04, 120.98, 118.12, 114.56, 113.84, 55.57. HRMS (ESI-TOF): m/z calculated for C$_{64}$H$_{47}$N$_5$O$_2$ [M+nH]$^+$ 918.3803, found 918.3788.

Synthesis of compound 6.

Compound **5** (0.040 g, 0.043 mmol) and Zn (OAc)$_2$, (0.105 g, 0.479 mmol) in MeOH: CHCl$_3$ (3 : 1, v/v), were added and the reaction mixture was stirred for 1 h at room temperature. The solvent was then evaporated under reduced pressure and the resultant mixture was diluted with DCM/water and the organic layer was collected, dried over anhydrous Na$_2$SO$_4$ and evaporated under vacuum. The solid was adsorbed on silica gel and purified by column chromatography, using a DCM: hexane (35: 65) mixture to yield 0.036 g, 86% of compound **6**.
^{1}H NMR (500 MHz, CDCl$_3$) δ 8.95–8.91(m, 4 H), 8.87(d, 2 H), 8.80(d, 1 H), 8.24–8.20(m, 6 H), 7.94(d, 2 H), 7.77–7.71(m, 9 H), 7.51(t, 1 H), 7.36(t, 2 H), 7.19(d, 2 H), 7.10(d, 4 H), 6.87(d, 4 H), 6.76(d, 2 H), 3.80(s, 6 H). ^{13}C NMR (126 MHz, CDCl$_3$) δ 155.47, 151.37, 150.45, 150.37, 150.23, 150.14, 150.04, 148.14, 147.48, 146.94, 146.58, 146.32, 143.04, 142.82, 142.78, 142.39, 141.98, 141.55, 139.18, 138.91, 138.80, 135.93, 135.22, 134.45, 134.41, 132.61, 132.31, 132.12, 131.97, 131.93, 131.86, 131.41, 130.95, 127.50, 127.45, 127.11, 126.90, 126.68, 126.58, 126.39, 125.93, 122.39, 121.50, 121.01, 120.92, 120.41, 114.57, 55.58. HRMS (ESI-TOF): m/z calculated for C$_{64}$H$_{45}$N$_5$O$_2$Zn [M]$^+$ 979.2859, found 979.2875.

Synthesis of compound 7.

7-bromo-5,10,15,20-tetraphenylporphyrin **13** (0.080 g, 0.115 mmol) and 10-propyl-3-(4,4,5,5-tetramethyl-1,3,2-dioxaborolan-2-yl)-10H-phenothiazine **12** (0.063 g, 0.173 mmol) were dissolved in THF (20 mL) and purged by nitrogen for 15 min. Meanwhile, a solution of sodium carbonate (0.750 g, 7.07 mmol) in water (15 mL), was added. After purging, palladium (0) tetrakis(triphenylphosphine) (0.100 g, 0.08 mmol) was added and the reaction mixture was refluxed in an oil bath for 16 h at 70 °C. The solvent was then evaporated under vacuum, the resultant mixture was diluted with DCM and the organic layer was collected, dried over anhydrous Na_2SO_4 and evaporated under vacuum. The solid was adsorbed on silica gel and purified by column chromatography, using a DCM: hexane (20: 80) mixture to yield 0.075 g, 76% of compound **7**. ^{1}H NMR (500 MHz, $CDCl_3$) δ 8.84–8.81(m, 3 H), 8.80(d, 1 H), 8.73(s, 2 H), 8.70(d, 1 H), 8.21(m, 6 H), 7.90(d, 2 H), 7.77–7.70(m, 10 H), 7.24–7.22(m, 2 H), 7.18(t, 2 H), 7.11(t, 1 H), 6.97–6.91(m, 3 H), 6.69(d, 1 H), 3.87(t, 2 H), 1.94–1.89(m, 2 H), 1.13(t, 3 H), -2.64(s, 2 H). ^{13}C NMR (126 MHz, $CDCl_3$) δ 142.53, 142.34, 140.45, 135.53, 134.62, 134.59, 134.45, 129.48, 128.88, 127.71, 127.47, 127.33, 127.16, 126.77, 126.65, 126.59, 125.93, 122.24, 121.21, 120.41, 119.95, 119.67, 115.31, 114.53, 49.06, 20.26, 11.50. HRMS (ESI-TOF): m/z calculated for $C_{59}H_{43}N_5S$ [M+nH]$^+$ 854.3312, found 854.3280.

Synthesis of compound 8.

Compound **7** (0.040 g, 0.046 mmol) and Zn (OAc)$_2$, (0.112 g, 0.515 mmol) in MeOH: CHCl$_3$ (3 : 1, v/v), were added and the reaction mixture was stirred for 1 h at room temperature. The solvent was then evaporated under reduced pressure and the resultant mixture was diluted with DCM/water and the organic layer was collected, dried over anhydrous Na_2SO_4 and evaporated under vacuum. The solid was adsorbed on silica gel and purified by column chromatography, using a DCM: hexane (35: 65) mixture to yield 0.035 g, 83% of compound **8**. ^{1}H NMR (500 MHz, $CDCl_3$) δ 8.95–8.91(m, 4 H), 8.86(d, 1 H), 8.83(s, 1 H), 8.81(d, 1 H), 8.23–8.19(m, 6 H), 7.86(d, 2 H), 7.77–7.67(m, 10 H), 7.24–7.21(m, 2 H), 7.19–7.16(m, 2 H), 7.08(t, 1 H), 6.97–6.90(m, 3

H), 6.67(d, 1 H), 3.86(t, 2 H), 1.94–1.90(m, 2 H), 1.13(t, 3 H). ^{13}C NMR (126 MHz, CDCl$_3$) δ 151.26, 150.45, 150.31, 150.25, 150.22, 150.19, 150.13, 147.92, 146.66, 146.30, 145.63, 142.89, 142.79, 142.76, 142.57, 141.23, 134.99, 134.43, 134.33, 133.79, 132.65, 132.13, 132.03, 131.97, 131.91, 131.38, 129.48, 128.78, 127.49, 127.45, 127.13, 126.57, 126.54, 126.50, 125.69, 125.29, 123.93, 122.36, 122.16, 121.49, 120.95, 120.47, 115.26, 114.41, 49.02, 20.25, 11.52. HRMS (ESI-TOF): m/z calculated for C$_{59}$H$_{41}$N$_5$SZn [M]$^+$ 915.2369, found 915.2402.

5.7. Conclusion

The free base **1**, **3**, **5** and **7** and zinc metallated **2**, **4**, **6** and **8** porphyrins were designed and synthesized by the Suzuki cross-coupling reaction and the metallation reaction. The photophysical properties of Zn(II) complexes exhibits a red shifted absorption in the low energy region compared to its corresponding free bases. The *β*-donor substituted porphyrins **3**, **4** and **6** exhibits slight red shift in the fluorescence maxima compared to other porphyrins. The red shifted emission maxima may be due to the nonplanarity of donor units substituted at the *β*-position. The electrochemical properties of zinc porphyrin **2**, **4**, **6** and **8** exhibits a cathodic shift in the redox potentials compared to their corresponding free base porphyrin **1**, **3**, **5** and **7**. The computational study shows that the Q bands in the longer wavelength region corresponds to the ICT transition and the soret band in high energy region relates to π–π* transition. The dimethoxy triphenylamine substituted porphyrin **5** and **6** shows low HOMO–LUMO energy gap compared to other donor substituted porphyrin **1**, **2**, **3**, **4**, **7** and **8**. These results provide a better understanding about the effect of donor substituents on the electronic properties of porphyrin π-system and its application in optoelectronics.

5.8. References

[1] Shahsavari, A., Akbari, M. (2018), Potential of solar energy in developing countries for reducing energy-related emissions. *Renew. Sustain. Energy Rev.* 90, 275-291. (DOI: 10.1016/j.rser.2018.03.065).

[2] Sims, R. E. H. (2004), Renewable energy: a response to climate change. *Sol Energy.* 76, 9-17. (DOI: 10.1016/S0038-092X(03)00101-4).

[3] Muneer, T., Asif, M., Munawwar, S. (2005), Sustainable production of solar electricity with particular reference to the Indian economy. *Renew. Sustain. Energy Rev.* 9, 444-473. (DOI: 10.1016/j.rser.2004.03.004).

[4] Borah, K. D., Bhuyan, J. (2017), Magnesium porphyrins with relevance to chlorophylls. *Dalton Trans.* 46, 6497-6509. (DOI: 10.1039/c7dt00823f).

[5] Rudolf, M., Kirner, S. V., Guldi, D. M. (2016), A multicomponent molecular approach to artificial photosynthesis–the role of fullerenes and endohedral metallofullerenes. *Chem. Soc. Rev.* 45, 612-630. (DOI: 10.1039/c5cs00774g).

[6] Fuhrhop, J. H. (2014), Porphyrin assemblies and their scaffolds. *Langmuir.* 30, 1-12. (DOI: 10.1021/la402228g).

[7] Balaban, T. S. (2005), Tailoring porphyrins and chlorins for self-assembly in biomimetic artificial antenna systems. *Acc. Chem. Res.* 38, 612-623. (DOI: 10.1021/ar040211z).

[8] LaVan, D. A., Cha, J. N. (2006), Approaches for biological and biomimetic energy conversion. *Proc. Natl. Acad. Sci. U.S.A.* 103, 5251-5255. (DOI: 10.1073/pnas.0506694103).

[9] Makhlouf, M. M., Shehata, M. M. (2021), Impact of Zn^{2+} introduced into the central cavity of meso-tetra (4-pyridyl) porphine on its spectroscopic features. *Opt. Mater.* 113, 110893. (DOI: 10.1016/j.optmat.2021.110893).

[10] Kilså, K., Kajanus, J., Macpherson, A. N., Mårtensson, J., Albinsson, B. (2001), Bridge-dependent electron transfer in porphyrin-based donor− bridge− acceptor systems. *J. Am. Chem. Soc.* 123, 3069-3080. (DOI: 10.1021/ja003820k).

[11] Panda, M. K., Ladomenou, K., Coutsolelos, A. G. (2012), Porphyrins in bio-inspired transformations: Light-harvesting to

solar cell. *Coord. Chem. Rev.* 256, 2601-2627. (DOI: 10.1016/j.ccr.2012.04.041).

[12] D'Souza, F., Ito, O. (2009), Supramolecular donor–acceptor hybrids of porphyrins/phthalocyanines with fullerenes/carbon nanotubes: electron transfer, sensing, switching, and catalytic applications. *Chem. Commun.* 33, 4913-4928. (DOI: 10.1039/b905753f).

[13] Xie, M., Bai, F. Q., Zhang, H. X., Zheng, Y. Q. (2016), The influence of an inner electric field on the performance of three types of Zn-porphyrin sensitizers in dye sensitized solar cells: a theoretical study. *J. Mater. Chem. C.* 4, 10130-10145. (DOI: 10.1039/C6TC02457B).

[14] De La Torre, G., Vázquez, P., Agullo-Lopez, F., Torres, T. (2004), Role of structural factors in the nonlinear optical properties of phthalocyanines and related compounds. *Chem. Rev.* 104, 3723-3750. (DOI: 10.1021/cr030206t).

[15] Screen, T. E., Lawton, K. B., Wilson, G. S., Dolney, N., Ispasoiu, R., Goodson III, T., Martin, S. J., Bradley, D. D. C., Anderson, H. L. (2001), Synthesis and third order nonlinear optics of a new soluble conjugated porphyrin polymer. *J. Mater. Chem.* 11, 312-320. (DOI: 10.1039/b007250h).

[16] Qian, W., Hernando Campos, J. (2018), Preparation and processing of molecular materials with optoelectronic properties. (ISBN:9788449080548)

[17] Zhao, Z., Gao, S., Zheng, X., Zhang, P., Wu, W., Kwok, R. T. K., Xiong, Y., Leung, N. L. C., Chen, Y., Gao, X., Lam, J. W. Y., Tang, B. Z. (2018), Rational Design of Perylenediimide-Substituted Triphenylethylene to Electron Transporting Aggregation-Induced Emission Luminogens (AIEgens) with High Mobility and Near-Infrared Emission. *Adv. Funct. Mater.* 28, 1705609. (DOI: 10.1002/adfm.201705609).

[18] Blanchard, P., Malacrida, C., Cabanetos, C., Roncali, J., Ludwigs, S. (2019), Triphenylamine and some of its derivatives

as versatile building blocks for organic electronic applications. *Polym Int.* 68, 589-606. (DOI: 10.1002/pi.5695).

[19] Zhang, Y., Song, J., Qu, J., Qian, C. P., Wong, W. Y. (2020), Recent progress of electronic materials based on 2, 1, 3-benzothiadiazole and its derivatives: synthesis and their application in organic light-emitting diodes. *Sci. China Chem.* 1-17. (DOI: 10.1007/s11426-020-9901-4).

[20] Kim, G., Yeom, H. R., Cho, S., Seo, J. H., Kim, J. Y., Yang, C. (2012), Easily attainable phenothiazine-based polymers for polymer solar cells: advantage of insertion of S, S-dioxides into its polymer for inverted structure solar cells. *Macromolecules*, 45, 1847-1857. (DOI: 10.1021/ma202661b).

[21] Tian, Y., Tao, L., Chen, C., Lu, H., Li, H., Yang, X., Cheng, M. (2021), Facile synthesized fluorine substituted benzothiadiazole based dopant-free hole transport material for high efficiency perovskite solar cell. *Dyes Pigm.* 184, 108786. (DOI: 10.1016/j.dyepig.2020.108786).

[22] Sekaran, B., Jang, Y., Misra, R., D'Souza, F. (2019), Push–Pull Porphyrins via β-Pyrrole Functionalization: Evidence of Excited State Events Leading to High-Potential Charge-Separated States. *Chem. Eur. J.* 25, 12991-13001. (DOI: 10.1002/chem.201902286).

[23] Liu, B., Zhu, W., Wang, Y., Wu, W., Li, X., Chen, B., Long, Y. T., Xie, Y. (2012), Modulation of energy levels by donor groups: an effective approach for optimizing the efficiency of zinc-porphyrin based solar cells. *J. Mater. Chem.* 22, 7434-7444. (DOI: 10.1039/c2jm16804a).

[24] Gal, E., Brem, B., Pereţeanu, I., Găină, L., Lovasz, T., Perde-Schrepler, M., Silaghi-Dumitrescuc, L., Cristea, C., Silaghi-Dumitrescu, L. (2013), Novel meso-phenothiazinylporphyrin dyes: Synthesis, optical, electrochemical properties and PDT assay. *Dyes Pigm.* 99, 144-153. (DOI: 10.1016/j.dyepig.2013.04.034).

[25] Sekaran, B., Jang, Y., Misra, R., D'Souza, F. (2019), Push–Pull Porphyrins via β-Pyrrole Functionalization: Evidence of Excited State Events Leading to High-Potential Charge-Separated States. *Chem. Eur. J.* 25, 12991-13001. (DOI: 10.1002/chem.201902286).

[26] Ekbote, A., Han, S. H., Jadhav, T., Mobin, S. M., Lee, J. Y., Misra, R. (2018), Stimuli responsive AIE active positional isomers of phenanthroimidazole as non-doped emitters in OLEDs. *J. Mater. Chem. C.* 6, 2077-2087. (DOI: 10.1039/c7tc05450e).

[27] Nicolas, M., Fabre, B., Chapuzet, J. M., Lessard, J., Simonet, J. (2000), Boronic ester-substituted triphenylamines as new Lewis base-sensitive redox receptors. *J. Electroanal. Chem.* 482, 211-216. (DOI: 10.1016/S0022-0728(00)00052-8).

[28] Chaudhri, N., Cong, L., Grover, N., Shan, W., Anshul, K., Sankar, M., Kadish, K. M. (2018), Synthesis and electrochemical characterization of acetylacetone (acac) and ethyl acetate (EA) appended β-trisubstituted push–pull porphyrins: Formation of electronically communicating porphyrin dimers. *Inorg. Chem.* 57, 13213-13224. (DOI: 10.1021/acs.inorgchem.8b01690).

[29] Rathi, P., Kumar, S., Banerjee, D., Soma, V. R., Sankar, M. (2020), Unsymmetrical β-functionalized 'push–pull'porphyrins: synthesis and photophysical, electrochemical and nonlinear optical properties. *Dalton Trans.* 49, 3198-3208. (DOI: 10.1039/C9DT04252K).

[30] Ahmad Dar, T., Mandeep, Sankar, M. (2018), Synthesis, spectral and electrochemical redox properties of N-methyl fused nickel (II) porphyrin. *J Porphyr Phthalocyanines.* 22, 1106-1110. (DOI: 10.1142/S1088424618501109).

[31] Frisch, M. J., Trucks, G. W., Schlegel, H. B., Scuseria, G. E., Robb, M. A., Cheeseman, J. R., Scalmani, G., Barone, V., Mennucci, B., Petersson, G. A., Nakatsuji, H., Caricato, M., Li, X., Hratchian, H. P., Izmaylov, A. F., Bloino, J., Zheng, G.,

Sonnenberg, J. L., Hada, M., Ehara, M.; Toyota, K.; Fukuda, R.; Hasegawa, J.; Ishida, M.; Nakajima, T.; Honda, Y.; Kitao, O., Nakai, H., Vreven, T., Montgomery, J. A., Jr., Peralta, J. E., Ogliaro, F., Bearpark, M., Heyd, J. J., Brothers, E., Kudin, K. N., Staroverov, V. N., Kobayashi, R., Normand, J., Raghavachari, K., Rendell, A., Burant, J. C., Iyengar, S. S., Tomasi, J., Cossi, M., Rega, N., Millam, N. J., Klene, M., Knox, J. E., Cross, J. B., Bakken, V., Adamo, C., Jaramillo, J., Gomperts, R., Stratmann, R. E., Yazyev, O., Austin, A. J., Cammi, R., Pomelli, C., Ochterski, J. W., Martin, R. L., Morokuma, K., Zakrzewski, V. G., Voth, G. A., Salvador, P., Dannenberg, J. J., Dapprich, S., Daniels, A. D., Farkas, O., Foresman, J. B., Ortiz, J. V., Cioslowski, J., Fox, D. J. Gaussian 09, Revision A.02, *Gaussian, Inc.*, Wallingford, CT, 2009.

Chapter 6

Acceptor Functionalized Unsymmetrical β-Porphyrins

6.1. Introduction

In the light harvesting process of natural photosynthetic system, the porphyrin analogues have been widely used in energy and electron transfer processes.[1-3] The porphyrin macrocycle are aromatic molecules with square planar geometry consisting of four pyrrole ring connected by four methine carbons.[4] The porphyrin macrocycles are attractive due to their tunable photophysical and electrochemical properties with a wide range of applications in optoelectronics, photonics, nonlinear optics (NLO) and photodynamic therapy (PDT).[5-7] The metallated porphyrins are of interest owing to its biologically important properties, as witnessed for hemes and chlorophylls.[8] Natural and synthetic porphyrin derivatives and its analogues have been explored for their unique electronic properties in the areas of catalysts, therapeutic agents, sensors, molecular recognition, and dye sensitized solar cells (DSSCs).[9-12]

1,8-Naphthalimides (NI) is a fluorescent molecule with planar structure, which exhibits electron-accepting character with remarkable photo, thermal, and chemical stability.[13] Naphthalimide based D–A systems exhibits potential applications in memory devices, bulk heterojunction organic solar cells, perovskite solar cells, OLEDs and also in the pharmaceutical field for anti-cancer treatments.[14-18] Benzothiazoles are a class of sulfur-containing heterocycles made of benzene ring fused to a thiazole ring. The benzothiazoles are stable, aromatic ring system containing reactive sites for further functionalization.[19] The D–A systems containing benzothiazole scaffold show wide applications in diverse pharmacological agents, natural products, and synthetic intermediates. [20,21] Quinoxalines are a class of nitrogen-containing heterocyclic compounds, in which carbon atoms are replaced by N atoms in the naphthalene ring. Quinoxalines are formed by the fusion of benzene ring with pyrazine ring and are identified as benzopyrazine.[22]

The acceptor substituted β-porphyrins are not much explored due to its synthetic difficulties.[23] The acceptor functionalized porphyrins have been employed in a wide range of application such as electron transfer, sensing, switching, and catalysis.[24] Our group has reported ethynyl naphthalimide substituted β-porphyrins and investigated their charge-separated states upon photoexcitation.[25] Nonell *et al*. reported thiazolo[4,5-c]porphycenes and explored its photosensitizing properties.[26] Nath *et al*. have reported the synthesis of 2-(1H-imidazo[4,5-*b*]phenazine-2-yl)-5, 10, 15, 20-tetraphenyl porphyrin in good yields.[27]

In this chapter, we have designed and synthesized the acceptor functionalized unsymmetrical β-porphyrin **1a**–**8d**, with the electron-deficient naphthalimide, *p*- and *m*-benzothiazole and quinoxaline units at the β-pyrrolic position. The photophysical and computational studies of porphyrins **1a**–**8d** were explored and the influence of acceptor units on the electronic properties of the porphyrin π-system were investigated.
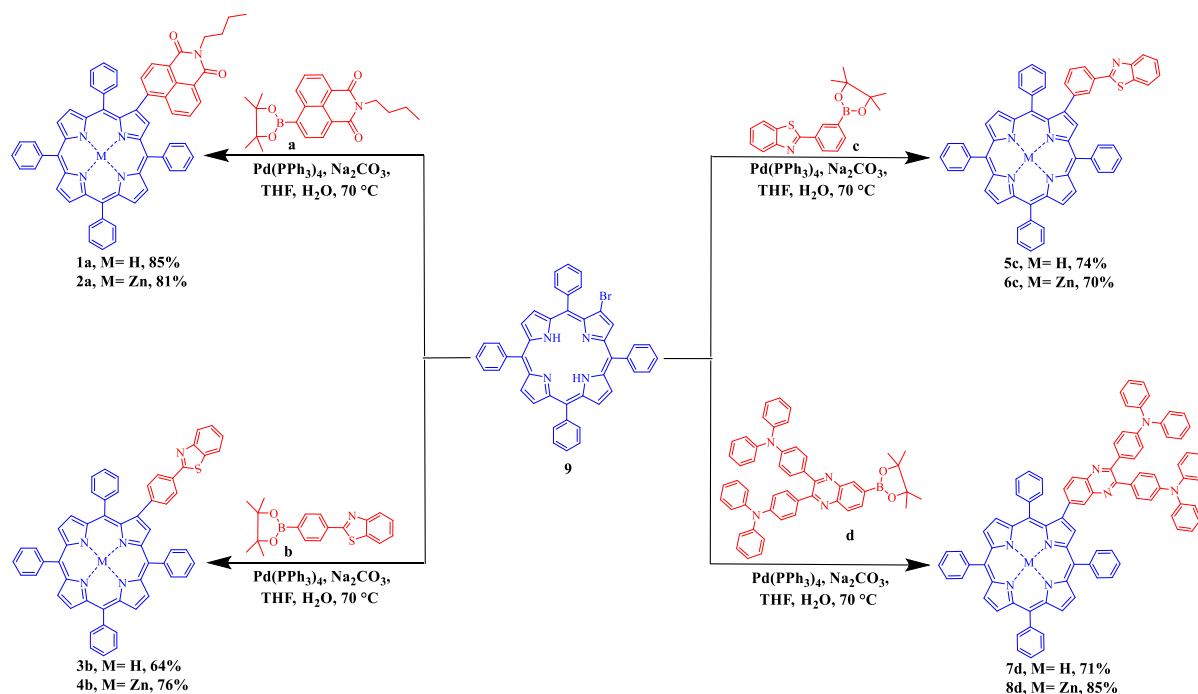
Scheme 6.1. Synthetic routes of investigated porphyrins **1a**–**8d**.

6.2. Results and Discussion

Synthesis

The synthesis of acceptor functionalized β-porphyrin **1a**–**8d** are shown in Scheme 6.1. The β-monobrominated tetraphenyl porphyrin (TPPBr) **9** and the pinacol boronate esters of acceptor **a**, **b**, **c** and **d** were synthesized according to the reported procedure (Scheme 6.1).[25,28–30] The reaction of TPPBr **9** with 1.5 equiv of 2-butyl-6-(4,4,5,5-tetramethyl-1,3,2-dioxaborolan-2-yl)-1H-benzo[de]isoquinoline-1,3(2H)-dione **a** and 2-(4-(4,4,5,5-tetramethyl-1,3,2-dioxaborolan-2-yl)phenyl)benzo[d]thiazole **b** by the Pd-catalyzed Suzuki cross-coupling reaction in presence of Pd(PPh$_3$)$_4$ in THF solvent at 70 °C resulted in porphyrin **1a** and **3b** in 85% and 64% yields, respectively (Scheme 6.1). The porphyrin **5c** and **7d** were synthesized by the Suzuki cross-coupling reaction of TPPBr **9** with 2-(3-(4,4,5,5-tetramethyl-1,3,2-dioxaborolan-2-yl)phenyl)benzo[d]thiazole **c** and 4,4'-(6-(4,4,5,5-tetramethyl-1,3,2-dioxaborolan-2-yl)quinoxaline-2,3-diyl)bis(N,N-diphenylaniline) **d** using Pd(PPh$_3$)$_4$ in THF solvent at 70 °C in 74% and 71% yields, respectively (Scheme 6.1). The Zn(II) metallation of porphyrin **1a**, **3b**, **5c**, and **7d** were carried out using Zn(OAc)$_2$ in MeOH and CHCl$_3$ (3:1) mixture, which resulted **2a**, **4b**, **6c**, and **8d** in 81, 76, 70 and 85% yields, respectively. The unsymmetrical porphyrins **1a**–**8d** were characterized by ^{1}H, ^{13}C NMR and HRMS mass spectroscopic techniques.

6.3. Photophysical Properties

The electronic absorption spectra of the acceptor functionalized β-porphyrin **1a**–**8d** were recorded in THF at room temperature (Figure 6.1) and the data are tabulated in Table 6.1. The UV-Visible absorption spectra of porphyrin **1a**–**8d** shows a characteristic absorption band around 421–652 nm, in the Soret and Q–band region. The free base porphyrin **1a**, **3b**, **5c** and **7d** shows a characteristic absorption band around 421 nm in the Soret band and 516−652 nm in the Q–band region. The acceptor functionalized free base porphyrin **1a**, **3b**, **5c** and **7d**

exhibits a similar absorption spectrum in the soret and Q–bands region. The zinc complexes **2a**, **4b**, **6c** and **8d** exhibits a characteristic Soret band around 427−429 nm and Q–bands in the range of 559−599 nm. The zinc complexes **2a**, **4b**, **6c** and **8d** exhibits a red shifted absorption around 6−8 nm in the high energy region compared to its corresponding free base analogues **1a**, **3b**, **5c**, and **7d**. The porphyrins **3b**, **4b**, **5c** and **6c** with *p*- and *m*-substituted benzothiazoles at the *β*-pyrrolic position of the porphyrin macrocycle exhibits a similar absorption spectrum in the Soret and the Q–band region. The absorption spectra of *p*- and *m*-benzothiazole substituted porphyrin **3b**, **4b**, **5c** and **6c** states that the position of the substituents does not influence the electronic properties of the porphyrin macrocycles. The electron-deficient quinoxaline substituted porphyrin **7d** and **8d** shows similar absorption spectrum as that of naphthalimide substituted porphyrin **1a** and **2a**. These results confirms that the electron-deficient naphthalimide, *p*- and *m*-benzothiazole and quinoxaline units have similar effect in the ground state of the porphyrin π-system.
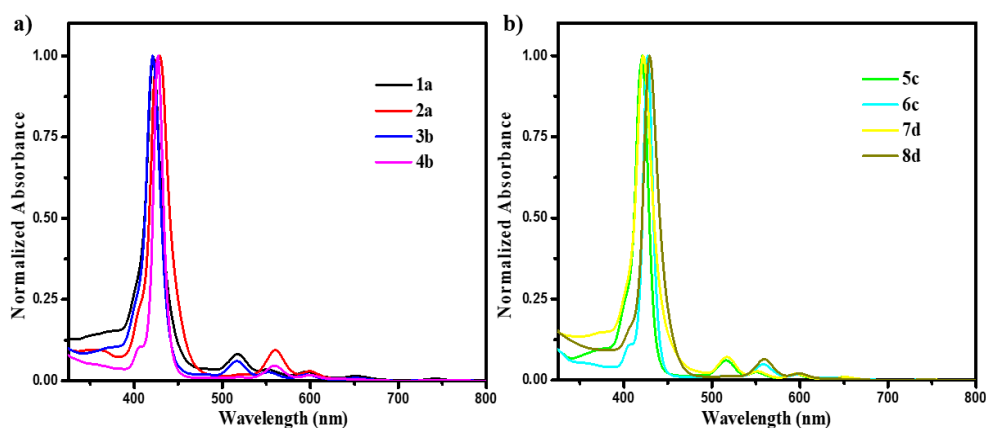
Figure 6.1. Normalized electronic absorption spectra of porphyrin a) **1a–4b** and b) **5c–8d** in THF at 1.0×10^{-5} M concentration.

The emission behaviour of porphyrins **1a**–**8d** (Figure 6.2) were studied in THF solvent at room temperature and the data are shown in Table 6.1. The acceptor functionalized *β*-porphyrin **1a**–**8d** exhibits the emission band around 616–725 nm in the longer wavelength region. The emission

spectra of free base porphyrin **1a**, **3b**, **5c** and **7d** arises between 660–725 nm. The emission maxima of free base porphyrin **1a**, **3b**, **5c** and **7d** exhibits a similar emission bands. The emission spectra for zinc complexes were observed between 616–662 nm in low energy region. The electron-deficient naphthalimide substituted Zn(II) porphyrin **2a** exhibits a red shift in the emission maxima of around 2–5 nm in the longer wavelength region compared to benzothiazole and quinoxaline substituted porphyrins **4b**, **6c** and **8d**. The *p*-benzothiazole substituted Zn(II) porphyrin **4b** shows a red shifted emission around 1–3 nm in the longer wavelength region, compared to porphyrin **6c** and **8d**. The *p*-benzothiazole substituted Zn(II) porphyrin **4b** exhibits a slight red shift in the emission maxima of about 3 nm, compared to its *m*-benzothiazole substituted Zn(II) porphyrin **6c**. The quinoxaline substituted Zn(II) porphyrin **8d** exhibits a blue shifted emission maxima compared to other zinc complexes **2a** and **4b**. The fluorescence quantum yield of porphyrin **1a**–**8d** were observed between 0.01–0.12. The fluorescence quantum yield of quinoxaline substituted porphyrin **7d** shows the highest quantum yield value of 0.12, whereas the low quantum yield value of 0.01 were observed for porphyrin **2a** and **6c**.
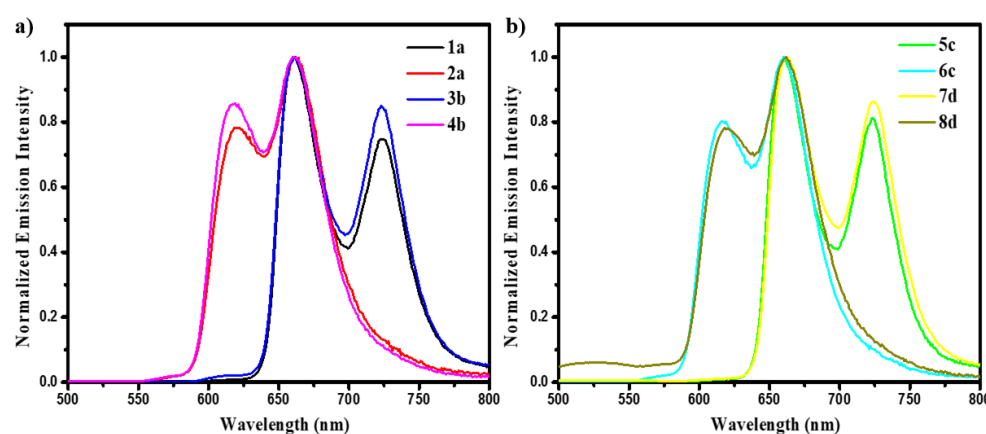
Figure 6.2. Normalized emission spectra of porphyrin a) **1a–4b** and b) **5c–8d** in THF at 1.0×10^{-5} M concentration.

Table 6.1. Photophysical and theoretical data of porphyrin **1a–8d**.

Compound	Soret band (S-band)	λ_{abs} (nm) [a]		λ_{em} (nm)	Φ_f [b]	H–L gap(eV) [c]
		ε (M^{-1} cm^{-1})	Q-bands			
1a	421	57960	517, 551, 596, 652	661, 725	0.04	2.51
2a	429	24770	560, 599,	621, 661	0.01	2.70
3b	421	12950	517, 552, 596, 651	660, 723	0.04	2.60
4b	427	16910	560, 599,	619, 661	0.03	2.77
5c	421	19720	516, 551, 595, 650	660, 723	0.04	2.56
6c	427	18340	559, 598	616, 661	0.01	2.79
7d	422	13160	517, 552, 595, 651	662, 724	0.12	2.51
8d	429	14950	560, 599	618, 662	0.04	2.63

[a] Absorbance measured in THF at 1×10^{-5} M concentration; λ_{abs}: absorption wavelength; λ_{em}: emission wavelength; ε: extinction coefficient. [b] The fluorescence quantum yields were recorded using H$_2$TPP as a standard ($\Phi_{st} = 0.11$). [c] Calculated from computational study.

6.4. Theoretical Calculations

To gain an insight into the electronic distribution of the acceptor functionalized β-porphyrins **1a–8d**, DFT calculations at B3LYP/6-31G level were performed using the Gaussian 09W program.[31] The optimized structure and frontier molecular orbitals of porphyrin **1a–8d** are depicted in Figure 6.3. The frontier molecular orbitals of porphyrin **1a** and **2a** suggests that the HOMO is populated on the porphyrin macrocycle whereas the LUMOs are concentrated on the porphyrin macrocycle and the naphthalimide accepting unit. In case of *p-* and *m-* benzothiazole functionalized porphyrin **3b**, **4b**, **5c** and **6c**, the HOMO is populated on the porphyrin macrocycle and the LUMOs are concentrated on the porphyrin unit with parts dispersed over the phenyl ring of benzothiazole unit. These results of *p-* and *m-*benzothiazole functionalized
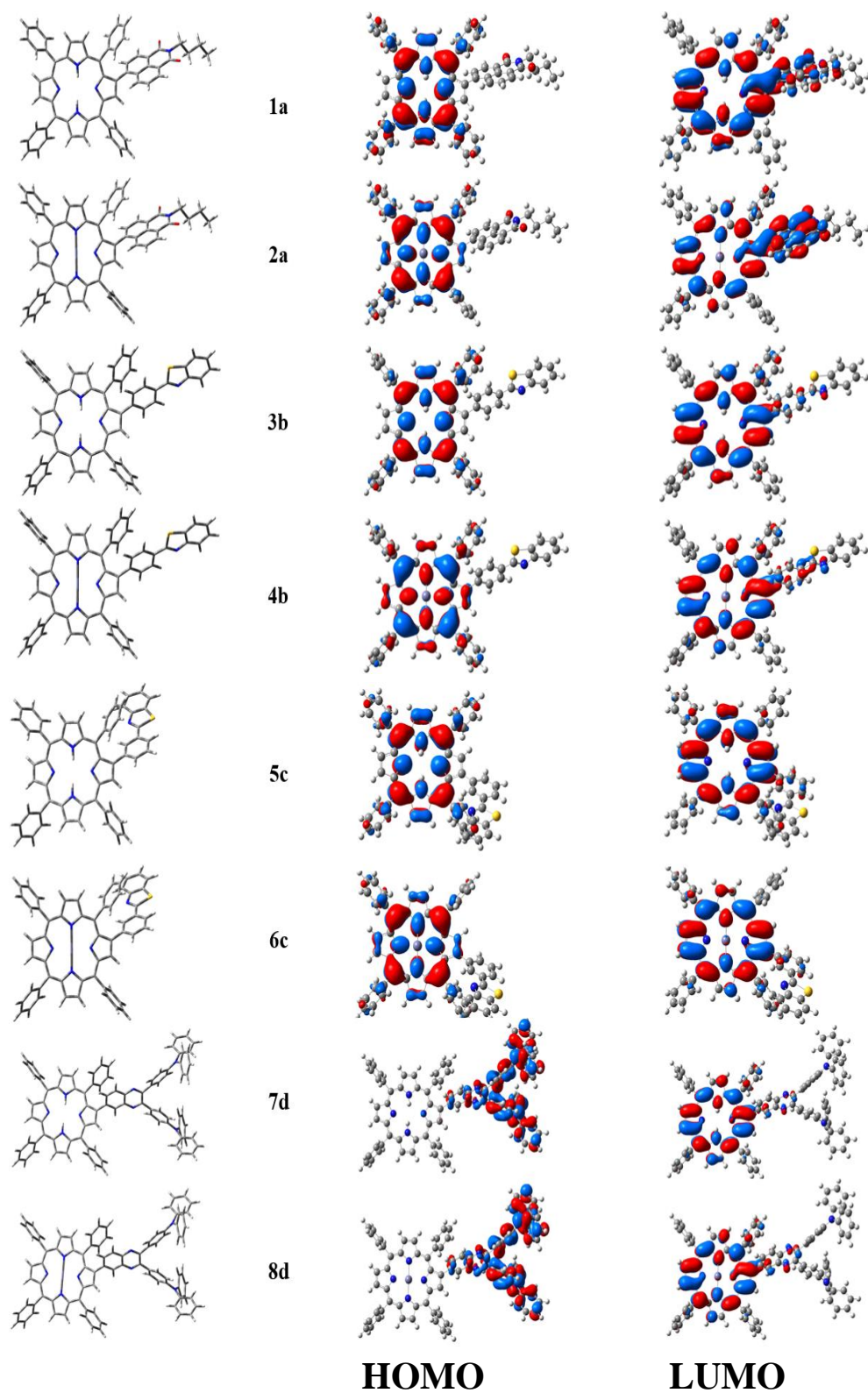
Figure 6.3. Optimized structure, frontier HOMO and LUMO of porphyrins **1a**–**8d**.

porphyrin **3b**–**6c** confirms that the electronic properties of the molecules are not influenced by the position of the substituents. In porphyrin **7d** and **8d**, the HOMO is localized on the triphenylamine donor and quinoxaline acceptor units, whereas the LUMO is concentrated on the porphyrin macrocycle with some parts dispersed on quinoxaline entity. The theoretically calculated HOMO levels of the porphyrins **1a**, **2a**, **3b**, **4b**, **5c**, **6c**, **7d** and **8d** are –5.09 eV, –5.19 eV, –4.98 eV, –5.06 eV, –4.89 eV, –5.00 eV, –4.85 eV and –4.87 eV whereas LUMO levels are –2.58 eV, –2.49 eV, –2.38 eV, –2.29 eV, –2.33 eV, –2.21 eV, –2.34 eV and –2.24 eV, respectively (Figure 6.4). The theoretically calculated HOMO and LUMO energy level reveals that the quinoxaline substituted porphyrin **7d** and **8d** exhibits a stabilized LUMO energy levels compared to other acceptor functionalized porphyrins.

The UV-Visible absorption spectra of the porphyrins **1a**–**8d** were evaluated using time-dependent density functional theory (TD-DFT) at B3LYP/6-31G level and the data are listed in Table 6.2.[31] The transitions with composition, oscillator strengths, and assignments are shown in Table 6.2. The TD-DFT calculation of porphyrin **1a**–**8d** shows a characteristic two absorption band, the Soret band and Q-band around 370–598 nm. The porphyrin **1a**, **2a**, **3b**, **4b**, **5c**, **6c**, **7d** and **8d** shows absorption band around 598, 544, 587, 539, 594, 537, 585 and 517 nm in the low energy Q-band region and are assigned to ICT transitions. The major ICT transition for porphyrin **7d** occurs from HOMO–1→LUMO, whereas for porphyrin **1a**–**6c** and **8d** the ICT transitions arises from HOMO→LUMO. In porphyrin **1a**–**8d**, the π–π^* transition occurs between 370–385 nm in the high energy soret band region. The TD-DFT calculated values of porphyrin **1a**–**8d** are in good agreement with the experimental values.

Table 6.2. Calculated Electronic Transitions of porphyrin **1a**–**8d**.

Compounds	λ_{max}	Composition & Molecular contribution	f^a	Assignment
1a	385	HOMO–2→LUMO+2 (0.41)	1.47	π–π*
	598	HOMO→LUMO (0.60)	0.06	ICT
2a	377	HOMO–1→LUMO+1 (0.40)	0.89	π–π*
	544	HOMO→LUMO (0.58)	0.04	ICT
3b	383	HOMO–2→LUMO+1 (0.29)	1.19	π–π*
	587	HOMO →LUMO (0.43)	0.04	ICT
4b	370	HOMO–1→LUMO+1 (0.50)	1.20	π–π*
	539	HOMO→LUMO (0.55)	0.03	ICT
5c	380	HOMO–2→LUMO+1 (0.46)	0.95	π–π*
	594	HOMO →LUMO (0.60)	0.05	ICT
6c	377	HOMO–1→LUMO+2 (0.42)	0.93	π–π*
	537	HOMO →LUMO (0.54)	0.03	ICT
7d	372	HOMO–3→LUMO+2 (0.44)	0.84	π–π*
	585	HOMO–1 →LUMO (0.58)	0.04	ICT
8d	378	HOMO–3 →LUMO+1 (0.47)	1.41	π–π*
	517	HOMO →LUMO (0.67)	0.10	ICT

f^a Oscillator strength.
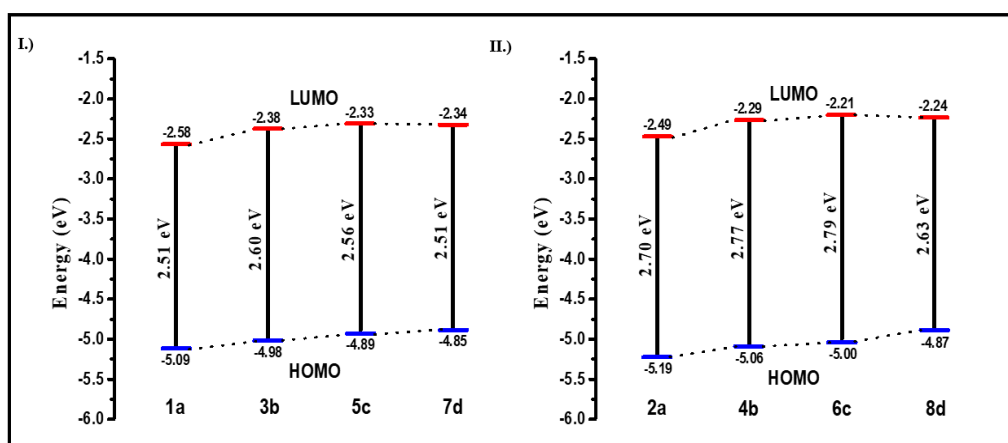
Figure 6.4. Energy level diagram of the frontier orbitals of porphyrin I) **1a**, **3b**, **5c**, **7d** and II) **2a**, **4b**, **6c**, **8d** estimated by DFT calculations.

6.5. Experimental Section

General: All the chemicals were purchased from commercial sources and used without further purification. The NMR spectra were recorded at room temperature (298 K). Chemical shifts are given in ppm with respect to tetramethylsilane as internal standard (CDCl$_3$, 7.26 ppm, 77.0 ppm). ^{1}H NMR spectra were recorded using a 500 MHz spectrometer. ^{13}C NMR spectra were recorded using a 101 MHz and 126 MHz spectrometer. Multiplicities are given as s (singlet), d (doublet), t (triplet) and m (multiplet) are given in Hertz. TLC analysis was carried out using silica gel 60 F$_{254}$ plates. UV-visible absorption spectra were recorded on a Cary-100 Bio UV-visible spectrophotometer. Emission spectra were taken in a The Fluoromax-4C, S/n. 1579D-1417-FM Fluorescence software Ver 3.8.0.60. UV/Vis and emission spectrums of all compounds were recorded in THF solution. The density functional theory (DFT) calculation were carried out at the B3LYP/6-31G level for C, N, H, O, S, Zn in the Gaussian 09 program. HRMS were recorded on a Bruker-Daltonics micrOTOF-Q II mass spectrometer.

Synthesis of compound 1a.

7-bromo-5,10,15,20-tetraphenylporphyrin **9** (0.080 g, 0.115 mmol) and 2-butyl-6-(4,4,5,5-tetramethyl-1,3,2-dioxaborolan-2-yl)-1H-benzo[de]isoquinoline-1,3(2H)-dione **a** (0.065 g, 0.173 mmol) were dissolved in THF (20 mL) and purged by nitrogen for 15 min. Meanwhile, a solution of sodium carbonate (0.750 g, 7.07 mmol) in water (15 mL), was added. After purging, palladium (0) tetrakis(triphenylphosphine) (0.100 g, 0.08 mmol) was added and the reaction mixture was refluxed in an oil bath for 16 h at 70 °C. The solvent was then evaporated under vacuum, the resultant mixture was diluted with DCM and the organic layer was collected, dried over anhydrous Na$_2$SO$_4$ and evaporated under vacuum. The solid was adsorbed on silica gel and purified by column chromatography, using a DCM: hexane (20: 80) mixture to yield (0.085 g, 85 %) of compound **1a**. ^{1}H NMR (500 MHz, CDCl$_3$) δ 8.91–8.89(dd, 2 H), 8.86(s, 1 H), 8.84–8.81(dd, 2 H), 8.76(d, 1 H), 8.56(d, 1 H), 8.50(t, 2 H), 8.26–

8.18(m, 6 H), 7.91(d, 1 H), 7.80–7.72(m, 11 H), 7.30(t, 2 H), 7.01(t, 1 H), 6.87(t, 1 H), 6.47(t, 1 H), 4.27(t, 2 H), 1.84–1.81(m, 2 H), 1.52–1.49(m, 2 H), 1.06(t, 3 H), -2.60(s, 2 H). ^{13}C NMR (101 MHz, CDCl$_3$) δ 165.29, 164.58, 164.25, 142.17, 142.03, 141.74, 140.88, 140.11, 139.67, 139.38, 138.59, 136.66, 136.10, 135.67, 135.52, 135.30, 134.63, 134.56, 133.52, 132.35, 132.05, 131.76, 131.63, 130.78, 130.76, 130.56, 130.21, 130.14, 129.56, 129.53, 127.91, 127.87, 126.95, 126.85, 126.74, 126.05, 125.73, 124.49, 123.57, 122.93, 122.27, 121.17, 120.64, 40.24, 29.70, 20.43, 13.95. HRMS (ESI-TOF): m/z calculated for C$_{60}$H$_{43}$N$_5$O$_2$ [M+nH]$^+$ 866.3490, found 866.3503.

Synthesis of compound 2a.

Compound **1a** (0.040 g, 0.046 mmol) and Zn (OAc)$_2$ (0.111 g, 0.508 mmol) in MeOH: CHCl$_3$ (3 : 1, v/v), were added and the reaction mixture was stirred for 1 h at room temperature. The solvent was then evaporated under reduced pressure and the resultant mixture was diluted with DCM/water and the organic layer was collected, dried over anhydrous Na$_2$SO$_4$ and evaporated under vacuum. The solid was adsorbed on silica gel and purified by column chromatography, using a DCM: hexane (35: 65) mixture to yield (0.035 g, 81%) of compound **2a**. ^{1}H NMR (500 MHz, CDCl$_3$) δ 9.00–8.93(m, 5 H), 8.83(d, 1 H), 8.61(d, 1 H), 8.38–8.34(m, 2 H), 8.27–8.16(m, 6 H), 7.86(d, 1 H), 7.81–7.67(m, 11 H), 7.30–7.25(m, 2 H), 6.96(t, 1 H), 6.81(t, 1 H), 6.40(t, 1 H), 4.11(t, 2 H), 1.77–1.70(m, 2 H), 1.51–1.45(m, 2 H), 1.03(t, 3 H). ^{13}C NMR (126 MHz, CDCl$_3$) δ 164.52, 164.19, 151.13, 150.80, 150.68, 150.66, 150.56, 150.42, 147.58, 147.12, 145.04, 142.64, 142.60, 142.58, 142.25, 135.69, 135.10, 134.55, 134.47, 134.40, 134.28, 133.72, 132.71, 132.43, 132.37, 132.31, 131.79, 131.72, 130.73, 130.15, 129.58, 127.65, 127.62, 126.66, 126.61, 125.95, 125.47, 124.22, 122.11, 121.89, 121.69, 121.41, 121.01, 120.90, 40.09, 29.72, 20.39, 13.94. HRMS (ESI-TOF): m/z calculated for C$_{60}$H$_{41}$N$_5$O$_2$Zn [M]$^+$ 927.2546, found 927.2571.

Synthesis of compound 3b.

7-bromo-5,10,15,20-tetraphenylporphyrin **9** (0.080 g, 0.115 mmol) and 2-(4-(4,4,5,5-tetramethyl-1,3,2-dioxaborolan-2-

yl)phenyl)benzo[d]thiazole **b** (0.058 g, 0.173 mmol) were dissolved in THF (20 mL) and purged by nitrogen for 15 min. Meanwhile, a solution of sodium carbonate (0.750 g, 7.07 mmol) in water (15 mL), was added. After purging, palladium (0) tetrakis(triphenylphosphine) (0.100 g, 0.08 mmol) was added and the reaction mixture was refluxed in an oil bath for 16 h at 70 °C. The solvent was then evaporated under vacuum, the resultant mixture was diluted with DCM and the organic layer was collected, dried over anhydrous Na_2SO_4 and evaporated under vacuum. The solid was adsorbed on silica gel and purified by column chromatography, using a DCM: hexane (20: 80) mixture to yield (0.060 g, 64 %) of compound **3b**. ^{1}H NMR (500 MHz, $CDCl_3$) δ 8.86–8.84(m, 4 H), 8.80(s, 1 H), 8.77(dd, 1 H), 8.74(dd, 1 H), 8.26–8.19(m, 7 H), 8.14(d, 1 H), 7.97–7.92(m, 3 H), 7.87(d, 2 H), 7.79–7.74(m, 11 H), 7.54(t, 1 H), 7.46–7.41(m, 3 H), -2.61(s, 2 H). ^{13}C NMR (101 MHz, $CDCl_3$) δ 168.20, 154.36, 142.42, 142.24, 141.83, 140.56, 135.98, 135.14, 134.62, 134.52, 130.79, 127.76, 127.46, 126.80, 126.68, 126.42, 126.30, 125.10, 123.18, 121.61, 121.18, 120.48, 120.08, 119.96. HRMS (ESI-TOF): m/z calculated for $C_{57}H_{37}N_5S$ [M+nH] $^+$ 824.2842, found 824.2857.

Synthesis of compound 4b.

Compound **3b** (0.040 g, 0.048 mmol) and Zn $(OAc)_2$, (0.117 g, 0.534 mmol) in MeOH: $CHCl_3$ (3 : 1, v/v), were added and the reaction mixture was stirred for 1 h at room temperature. The solvent was then evaporated under reduced pressure and the resultant mixture was diluted with DCM/water and the organic layer was collected, dried over anhydrous Na_2SO_4 and evaporated under vacuum. The solid was adsorbed on silica gel and purified by column chromatography, using a DCM: hexane (35: 65) mixture to yield (0.032 g, 76%) of compound **4b**. ^{1}H NMR (500 MHz, $CDCl_3$) δ 8.97–8.93(m, 5 H), 8.88(d, 1 H), 8.84(d, 1 H), 8.25–8.21(m, 7 H), 8.14(d, 1 H), 7.97(d, 1 H), 7.91(d, 2 H), 7.87(d, 2 H), 7.77–7.73(m, 11 H), 7.54(t, 1 H), 7.47–7.41(m, 3 H). ^{13}C NMR: After repeated submission peaks are not getting raised. HRMS (ESI-TOF): m/z calculated for $C_{57}H_{35}N_5SZn$ [M] $^+$ 885.1899, found 885.1920.

Synthesis of compound 5c.

7-bromo-5,10,15,20-tetraphenylporphyrin **9** (0.080 g, 0.115 mmol) and 2-(3-(4,4,5,5-tetramethyl-1,3,2-dioxaborolan-2-yl)phenyl)benzo[d]thiazole **c** (0.058 g, 0.173 mmol) were dissolved in THF (20 mL) and purged by nitrogen for 15 min. Meanwhile, a solution of sodium carbonate (0.750 g, 7.07 mmol) in water (15 mL), was added. After purging, palladium (0) tetrakis(triphenylphosphine) (0.100 g, 0.08 mmol) was added and the reaction mixture was refluxed in an oil bath for 16 h at 70 °C. The solvent was then evaporated under vacuum, the resultant mixture was diluted with DCM and the organic layer was collected, dried over anhydrous Na_2SO_4 and evaporated under vacuum. The solid was adsorbed on silica gel and purified by column chromatography, using a DCM: hexane (20: 80) mixture to yield (0.070 g, 74 %) of compound **5c**. ^{1}H NMR (500 MHz, CDCl₃) δ 8.86–8.82(m, 5 H), 8.76(d, 1 H), 8.72(d, 1 H), 8.25–8.21(m, 7 H), 8.08(d, 1 H), 7.92–7.89(m, 3 H), 7.77–7.73(m, 10 H), 7.58(d, 1 H), 7.49(t, 1 H), 7.38(t, 1 H), 7.34(t, 1 H), 7.16(m, 3 H), -2.61(s, 2 H). ^{13}C NMR (101 MHz, CDCl₃) δ 168.17, 154.19, 142.44, 142.28, 141.88, 140.40, 139.69, 135.66, 135.11, 134.65, 134.62, 134.54, 132.57, 132.47, 129.99, 128.10, 127.77, 127.53, 126.81, 126.69, 126.28, 126.19, 125.09, 125.00, 123.22, 121.62, 121.16, 120.47, 120.10, 120.00. HRMS (ESI-TOF): m/z calculated for $C_{57}H_{37}N_5S$ [M+nH] $^+$ 824.2842, found 824.2852.

Synthesis of compound 6c.

Compound **5c** (0.040 g, 0.0486 mmol) and Zn (OAc)₂, (0.117 g, 0.534 mmol) in MeOH: CHCl₃ (3 : 1, v/v), were added and the reaction mixture was stirred for 1 h at room temperature. The solvent was then evaporated under reduced pressure and the resultant mixture was diluted with DCM/water and the organic layer was collected, dried over anhydrous Na_2SO_4 and evaporated under vacuum. The solid was adsorbed on silica gel and purified by column chromatography, using a DCM: hexane (35: 65) mixture to yield (0.036 g, 70%) of compound **6c**. ^{1}H NMR (500 MHz, CDCl₃) δ 8.96(d, 1 H), 8.94(s, 4 H), 8.87(d, 1 H), 8.81(d, 1 H), 8.25–8.21(m, 7 H), 8.05(d, 1 H), 7.92–7.86(m, 3 H), 7.80–

7.70(m, 10 H), 7.60(d, 1 H), 7.47(t, 1 H), 7.37–7.31(m, 2 H), 7.14(m, 3 H). ^{13}C NMR (101 MHz, CDCl$_3$) δ 168.29, 154.17, 151.21, 150.56, 150.36, 147.71, 146.46, 146.01, 142.79, 141.22, 140.58, 135.36, 135.08, 134.46, 132.70, 132.56, 132.30, 132.09, 131.54, 130.09, 127.97, 127.54, 127.31, 126.57, 126.22, 125.92, 125.03, 124.75, 123.16, 122.24, 121.58, 121.06, 120.74. HRMS (ESI-TOF): m/z calculated for C$_{57}$H$_{35}$N$_5$SZn [M]$^+$ 885.1899, found 885.1892.

Synthesis of compound 7d.

7-bromo-5,10,15,20-tetraphenylporphyrin **9** (0.080 g, 0.115 mmol) and 4,4'-(6-(4,4,5,5-tetramethyl-1,3,2-dioxaborolan-2-yl)quinoxaline-2,3-diyl)bis(N,N-diphenylaniline) **d** (0.128 g, 0.173 mmol) were dissolved in THF (20 mL) and purged by nitrogen for 15 min. Meanwhile, a solution of sodium carbonate (0.750 g, 7.07 mmol) in water (15 mL), was added. After purging, palladium (0) tetrakis(triphenylphosphine) (0.100 g, 0.08 mmol) was added and the reaction mixture was refluxed in an oil bath for 16 h at 70 °C. The solvent was then evaporated under vacuum, the resultant mixture was diluted with DCM and the organic layer was collected, dried over anhydrous Na$_2$SO$_4$ and evaporated under vacuum. The solid was adsorbed on silica gel and purified by column chromatography, using a DCM: hexane (20: 80) mixture to yield (0.100 g, 71 %) of compound **7d**. ^{1}H NMR (500 MHz, CDCl$_3$) δ 8.87(s, 1 H), 8.85(s, 2 H), 8.84–8.82(m, 2 H), 8.78(d, 1 H), 8.75(d, 1 H), 8.33(s, 1 H), 8.26–8.23(m, 6 H), 7.79–7.71(m, 11 H), 7.54–7.50(m, 6 H), 7.31–7.26(m, 9 H), 7.16(t, 9 H), 7.10–7.05(m, 9 H), -2.57(s, 2 H). ^{13}C NMR (101 MHz, CDCl$_3$) δ 152.99, 152.60, 151.96, 151.47, 148.48, 147.38, 143.63, 142.37, 142.25, 141.83, 140.82, 140.57, 140.27, 139.52, 139.33, 136.29, 134.64, 134.50, 132.87, 132.79, 132.50, 130.91, 130.84, 129.38, 129.36, 128.96, 128.70, 127.82, 127.77, 127.48, 127.35, 126.81, 126.70, 126.24, 124.95, 124.92, 123.43, 123.39, 122.37, 122.32, 121.17, 120.50, 120.10, 120.06. HRMS (ESI-TOF): m/z calculated for C$_{88}$H$_{60}$N$_8$ [M+nH]$^+$ 1229.5014, found 1229.5000.

Synthesis of compound 8d.

Compound **7d** (0.040 g, 0.0325 mmol) and Zn (OAc)$_2$, (0.078 g, 0.358 mmol) in MeOH: CHCl$_3$ (3 : 1, v/v), were added and the reaction mixture was stirred for 1 h at room temperature. The solvent was then evaporated under reduced pressure and the resultant mixture was diluted with DCM/water and the organic layer was collected, dried over anhydrous Na$_2$SO$_4$ and evaporated under vacuum. The solid was adsorbed on silica gel and purified by column chromatography, using a DCM: hexane (35: 65) mixture to yield (0.035 g, 85%) of compound **8d**. ^{1}H NMR (500 MHz, CDCl$_3$) δ 8.99(s, 1 H), 8.96(d, 2 H), 8.94(s, 2 H), 8.89(d, 1 H), 8.85(d, 1 H), 8.31(s, 1 H), 8.25–8.23(m, 6 H), 7.77–7.72(m, 11 H), 7.56–7.52(m, 6 H), 7.31–7.26(m, 9 H), 7.18–7.14(m, 9 H), 7.11–7.05(m, 9 H). ^{13}C NMR (101 MHz, CDCl$_3$) δ 152.93, 152.51, 151.19, 150.63, 150.36, 148.45, 147.74, 147.40, 146.34, 145.95, 142.79, 141.77, 141.39, 140.25, 139.26, 135.91, 134.47, 134.38, 132.89, 132.67, 132.14, 131.60, 130.93, 130.87, 129.39, 129.36, 128.91, 127.56, 127.20, 126.61, 126.03, 124.94, 124.92, 123.42, 123.38, 122.38, 121.58, 121.12, 120.84. HRMS (ESI-TOF): m/z calculated for C$_{88}$H$_{58}$N$_8$Zn [M+nH] $^+$ 1291.4149, found 1291.4153.

6.6. Conclusion

The acceptor functionalized unsymmetrical *β*-porphyrin **1a**–**8d** were synthesized by the Pd-catalysed Suzuki cross-coupling reaction followed by the Zn(II) metallation. The photophysical and computational studies of porphyrin **1a**–**8d** were carried out to understand the influence of acceptor units on the electronic properties of the porphyrin π-system. The electronic absorption spectra confirms that the electron-deficient naphthalimide, *p*- and *m*-benzothiazole and quinoxaline units have similar effect on the electronic properties of the porphyrin macrocycle. The fluorescence quantum yield of quinoxaline substituted porphyrin **7d** shows high quantum yield value of 0.12. The computational study of *p*- and *m*-benzothiazole functionalized porphyrin **3b**–**6c** confirms that the electronic properties of the molecules are not influenced by the position of substituents. The quinoxaline substituted porphyrin **7d** and **8d** exhibits a stabilized LUMO energy levels

compared to other porphyrins. These results provide a new insight for the acceptor functionalized porphyrin and its further applications in optoelectronics.

6.7. References

[1] Wasielewski, M. R. (2009), Self-assembly strategies for integrating light harvesting and charge separation in artificial photosynthetic systems. *Acc. Chem. Res.* 42, 1910-1921. (DOI: 10.1021/ar9001735).

[2] Nikolaou, V., Charisiadis, A., Stangel, C., Charalambidis, G., Coutsolelos, A. G. (2019), Porphyrinoid–Fullerene hybrids as candidates in artificial photosynthetic schemes. *C*, 5, 57. (DOI: 10.3390/c5030057).

[3] Ning, X., Ma, L., Zhang, S., Qin, D., Shan, D., Hu, Y., Lu, X. (2016), Construction of a porphyrin-based nanohybrid as an analogue of chlorophyll protein complexes and its light-harvesting behavior research. *J. Phys. Chem. C.* 120, 919-926. (DOI: 10.1021/acs.jpcc.5b11246).

[4] Saito, S., Osuka, A. (2011), Expanded porphyrins: intriguing structures, electronic properties, and reactivities. *Angew. Chem. Int. Ed.* 50, 4342-4373. (DOI: 10.1002/anie.201003909).

[5] Wang, A., Yu, W., Huang, Z., Zhou, F., Song, J., Song, Y., Long, L., Cifuentes, M. P., Humphrey, M. G., Zhang, L., Shao, J., Zhang, C. (2016), Covalent functionalization of reduced graphene oxide with porphyrin by means of diazonium chemistry for nonlinear optical performance. *Sci. Rep.* 6, 1-12. (DOI: 10.1038/srep23325).

[6] Karam, T. E., Siraj, N., Ranasinghe, J. C., Kolic, P. E., Regmi, B. P., Warner, I. M., Haber, L. H. (2020), Efficient photoinduced energy transfer in porphyrin-based nanomaterials. *J. Phys. Chem. C.* 124, 24533-24541. (DOI: 10.1021/acs.jpcc.0c08985).

[7] Tian, J., Huang, B., Nawaz, M. H., Zhang, W. (2020), Recent advances of multi-dimensional porphyrin-based functional

materials in photodynamic therapy. *Coord. Chem. Rev.* 420, 213410. (DOI: 10.1016/j.ccr.2020.213410).

[8] Gibbons, D., Flanagan, K. J., Pounot, L., Senge, M. O. (2019), Structure and conformation of photosynthetic pigments and related compounds. 15. Conformational analysis of chlorophyll derivatives–implications for hydroporphyrins in vivo. *Photochem. Photobiol. Sci.* 18, 1479-1494. (DOI: 10.1039/c8pp00500a).

[9] Jasinski, S. (2009), Semi-natural and synthetic chiral cycloketo-porphyrin systems-approaching novel photosensitizers (Doctoral dissertation, Friedrich-Alexander-Universität Erlangen-Nürnberg (FAU)).

[10] Lee, J. S., Song, I. H., Shinde, P. B., Nimse, S. B. (2020), Macrocycles and Supramolecules as Antioxidants: Excellent Scaffolds for Development of Potential Therapeutic Agents. *Antioxidants*, 9, 859. (DOI: 10.3390/antiox9090859).

[11] Calogero, G., Bartolotta, A., Di Marco, G., Di Carlo, A., Bonaccorso, F. (2015), Vegetable-based dye-sensitized solar cells. *Chem. Soc. Rev.* 44, 3244-3294. (DOI: 10.1039/c4cs00309h).

[12] Urbani, M., Grätzel, M., Nazeeruddin, M. K., Torres, T. (2014), Meso-substituted porphyrins for dye-sensitized solar cells. *Chem. Rev.* 114, 12330-12396. (DOI: 10.1021/cr5001964).

[13] Poddar, M., Sivakumar, G., Misra, R. (2019), Donor–acceptor substituted 1, 8-naphthalimides: design, synthesis, and structure–property relationship. *J. Mater. Chem. C.* 7, 14798-14815. (DOI: 10.1039/C9TC02634G).

[14] Fu, L., Zhang, Y., Ren, Z., Li, H., Sun, X., Yan, S. (2019), Flexible and Fatigue-Resistant Ternary Electrical Memory Based on Alternative Copolysiloxane with Carbazole Donors and Imidazole-Modified Naphthalimide Acceptors. *Adv. Mater. Technol.* 4, 1900084. (DOI: 10.1002/admt.201900084).

[15] Gautam, P., Sharma, R., Misra, R., Keshtov, M. L., Kuklin, S. A., Sharma, G. D. (2017), Donor–acceptor–acceptor (D–A–A)

type 1, 8-naphthalimides as non-fullerene small molecule acceptors for bulk heterojunction solar cells. *Chem. Sci.* 8. (DOI: 10.1039/c6sc04461a).

[16] Wang, Y., Liao, Q., Chen, J., Huang, W., Zhuang, X., Tang, Y., Bolin Li, B., Yao, X., Feng, X., Zhang, X., Su, M., He, Z., Marks, T. J., Facchetti, A., Guo, X. (2020), Teaching an old anchoring group new tricks: enabling low-cost, eco-friendly hole-transporting materials for efficient and stable perovskite solar cells. *J. Am. Chem. Soc.* 142, 16632-16643. (DOI: 10.1021/jacs.0c06373).

[17] Christopherson, C. J., Mayder, D. M., Poisson, J., Paisley, N. R., Tonge, C. M., Hudson, Z. M. (2020), 1, 8-Naphthalimide-Based Polymers Exhibiting Deep-Red Thermally Activated Delayed Fluorescence and Their Application in Ratiometric Temperature Sensing. *ACS Appl. Mater. Interfaces.* 12, 20000-20011. (DOI: 10.1021/acsami.0c05257).

[18] Banerjee, S., Veale, E. B., Phelan, C. M., Murphy, S. A., Tocci, G. M., Gillespie, L. J., Frimannsson, D. O., Kelly, J. M., Gunnlaugsson, T. (2013), Recent advances in the development of 1, 8-naphthalimide based DNA targeting binders, anticancer and fluorescent cellular imaging agents. *Chem. Soc. Rev.* 42, 1601-1618. (DOI: 10.1039/c2cs35467e).

[19] Gao, X., Liu, J., Zuo, X., Feng, X., Gao, Y. (2020), Recent advances in synthesis of benzothiazole compounds related to green chemistry. *Molecules*, 25, 1675. (DOI: 10.3390/molecules25071675).

[20] Keri, R. S., Patil, M. R., Patil, S. A., Budagumpi, S. (2015), A comprehensive review in current developments of benzothiazole-based molecules in medicinal chemistry. *Eur. J. Med. Chem.* 89, 207-251. (DOI: 10.1016/j.ejmech.2014.10.059).

[21] Gill, R. K., Rawal, R. K., Bariwal, J. (2015), Recent advances in the chemistry and biology of benzothiazoles. *Arch. Pharm. (Weinheim).* 348, 155-178. (DOI: 10.1002/ardp.201400340).

[22] Chugh, A., Kumar, A., Verma, A., Kumar, S., Kumar, P. (2020), A review of antimalarial activity of two or three nitrogen atoms containing heterocyclic compounds. *Med. Chem. Res.* 1-28. (DOI: 10.1007/s00044-020-02604-6).

[23] Di Carlo, G., Orbelli Biroli, A., Pizzotti, M., Tessore, F. (2019), Efficient sunlight harvesting by A4 β-pyrrolic substituted ZnII porphyrins: a mini-review. *Front. Chem.* 7, 177. (DOI: 10.3389/fchem.2019.00177).

[24] D'Souza, F., Ito, O. (2009), Supramolecular donor–acceptor hybrids of porphyrins/phthalocyanines with fullerenes/carbon nanotubes: electron transfer, sensing, switching, and catalytic applications. *Chem. Commun.* 33, 4913-4928. (DOI: 10.1039/b905753f).

[25] Sekaran, B., Jang, Y., Misra, R., D'Souza, F. (2019), Push–Pull Porphyrins via β-Pyrrole Functionalization: Evidence of Excited State Events Leading to High-Potential Charge-Separated States. *Chem. Eur. J.* 25, 12991-13001. (DOI: 10.1002/chem.201902286).

[26] Planas, O., Gallavardin, T., Nonell, S. (2015), A novel fluoro-chromogenic click reaction for the labelling of proteins and nanoparticles with near-IR theranostic agents. *Chem. Commun.* 51, 5586-5589. (DOI: 10.1039/c4cc09070e).

[27] Sharma, S., Nath, M. (2012), An efficient synthetic approach to novel nickel (II) 2-benzazolo-5, 10, 15, 20-tetraphenylporphyrins. *J. Heterocycl. Chem.* 49, 88-92. (DOI: 10.1002/jhet.664).

[28] Ekbote, A., Han, S. H., Jadhav, T., Mobin, S. M., Lee, J. Y., Misra, R. (2018), Stimuli responsive AIE active positional isomers of phenanthroimidazole as non-doped emitters in OLEDs. *J. Mater. Chem. C.* 6, 2077-2087. (DOI: 10.1039/c7tc05450e).

[29] Bijesh, S., Misra, R. (2018). Triphenylamine Functionalized Unsymmetrical Quinoxalines. *Asian J. Org. Chem.*, 7(9), 1882-1892. (DOI: 10.1002/ajoc.201800384).

[30] Nicolas, M., Fabre, B., Chapuzet, J. M., Lessard, J., Simonet, J. (2000), Boronic ester-substituted triphenylamines as new Lewis base-sensitive redox receptors. *J. Electroanal. Chem.* 482, 211-216. (DOI: 10.1016/S0022-0728(00)00052-8).

[31] Frisch, M. J., Trucks, G. W., Schlegel, H. B., Scuseria, G. E., Robb, M. A., Cheeseman, J. R., Scalmani, G., Barone, V., Mennucci, B., Petersson, G. A., Nakatsuji, H., Caricato, M., Li, X., Hratchian, H. P., Izmaylov, A. F., Bloino, J., Zheng, G., Sonnenberg, J. L., Hada, M., Ehara, M.; Toyota, K.; Fukuda, R.; Hasegawa, J.; Ishida, M.; Nakajima, T.; Honda, Y.; Kitao, O., Nakai, H., Vreven, T., Montgomery, J. A., Jr., Peralta, J. E., Ogliaro, F., Bearpark, M., Heyd, J. J., Brothers, E., Kudin, K. N., Staroverov, V. N., Kobayashi, R., Normand, J., Raghavachari, K., Rendell, A., Burant, J. C., Iyengar, S. S., Tomasi, J., Cossi, M., Rega, N., Millam, N. J., Klene, M., Knox, J. E., Cross, J. B., Bakken, V., Adamo, C., Jaramillo, J., Gomperts, R., Stratmann, R. E., Yazyev, O., Austin, A. J., Cammi, R., Pomelli, C., Ochterski, J. W., Martin, R. L., Morokuma, K., Zakrzewski, V. G., Voth, G. A., Salvador, P., Dannenberg, J. J., Dapprich, S., Daniels, A. D., Farkas, O., Foresman, J. B., Ortiz, J. V., Cioslowski, J., Fox, D. J. Gaussian 09, Revision A.02, *Gaussian, Inc.*, Wallingford, CT, 2009.

Chapter 7

Triphenylacrylonitrile (TPAN), 1,1,2,2-tetraphenylethene (TPE) and Carbazole Functionalized β-Porphyrins

7.1. Introduction

In recent years, the renewable solar energy is in high demand due to the depletion of conventional energy sources such as coal, oil and natural gas.[1,2] The porphyrins are used to mimic the natural photosynthetic architectures to perform energy/electron transfer processes.[3] Porphyrin analogues such as heme (iron protoporphyrin) and chlorophyll (a magnesium-containing metalloporphyrin) plays a significant role in sustaining life in living organisms.[4] Porphyrins are π-conjugated aromatic system and shows intense absorption bands in the soret and Q-band in visible region.[5,6] The electronic properties of the porphyrin macrocycles can be tuned by altering the substituents at the meso and β-position of the porphyrin π system.[7] The porphyrin π systems have been investigated for their wide range of applications in therapeutic agents, optoelectronics, molecular recognition, nonlinear optics (NLO), catalysts, photonics, photodynamic therapy (PDT), sensors and dye sensitized solar cells (DSSCs).[8–14]

The 2,3,3-triphenylacrylonitrile (TPAN) and 1,1,2,2-tetraphenylethene (TPE) are propeller-shaped molecular structures with twisted conformations.[15] The Donor–Acceptor (D–A) molecular system with 2,3,3-triphenylacrylonitrile (TPAN) and 1,1,2,2-tetraphenylethene (TPE) moiety are utilized in various fields such as OLEDs, chemical sensing, and detection of stimuli responses, *etc*.[16,17] Carbazole is a tricyclic aromatic heterocyclic compound comprising of two benzene rings fused on both sides of the pyrrole ring.[18] The carbazole-based compounds exhibit high thermal and photochemical stability and are used in a wide range of applications such as fluorescence switches, biological imaging, optical sensors and as charge-transporting materials in organic light-emitting diodes.[19–22]

The substitution of donor and acceptor entities at the β-pyrrolic position of porphyrins are extensively used for the construction of unsymmetrical

porphyrinic architecture. Wagner *et al.* reported a series of *β*-vinyl-substituted porphyrin dyads and used as a light-harvesting sensitizers in DSSC application.[23] Feng *et al.* synthesized a series of vinylated tetraphenyl porphyrins and explored its luminescence properties.[24] Gupta *et al.* have investigated the steady-state and time-resolved fluorescence spectra of carbazole substituted *β*-porphyrins.[25] Our group has reported the *β*-Substituted ferrocenyl porphyrins and investigated their electronic properties.[26]

In this chapter, we wish to report the synthesis of TPAN, TPE and carbazole substituted unsymmetrical *β*-porphyrins **11**–**18** (Figure 1). The photophysical, electrochemical and computational studies of these unsymmetrical porphyrins **11**–**18** were investigated. The effect of electron withdrawing cyano substituted 2,3,3-triphenylacrylonitrile and the electron donating 1,1,2,2-tetraphenylethene and 9-propyl-9H-carbazole units on the photonic and electronic properties of the porphyrin π-systems were explored.
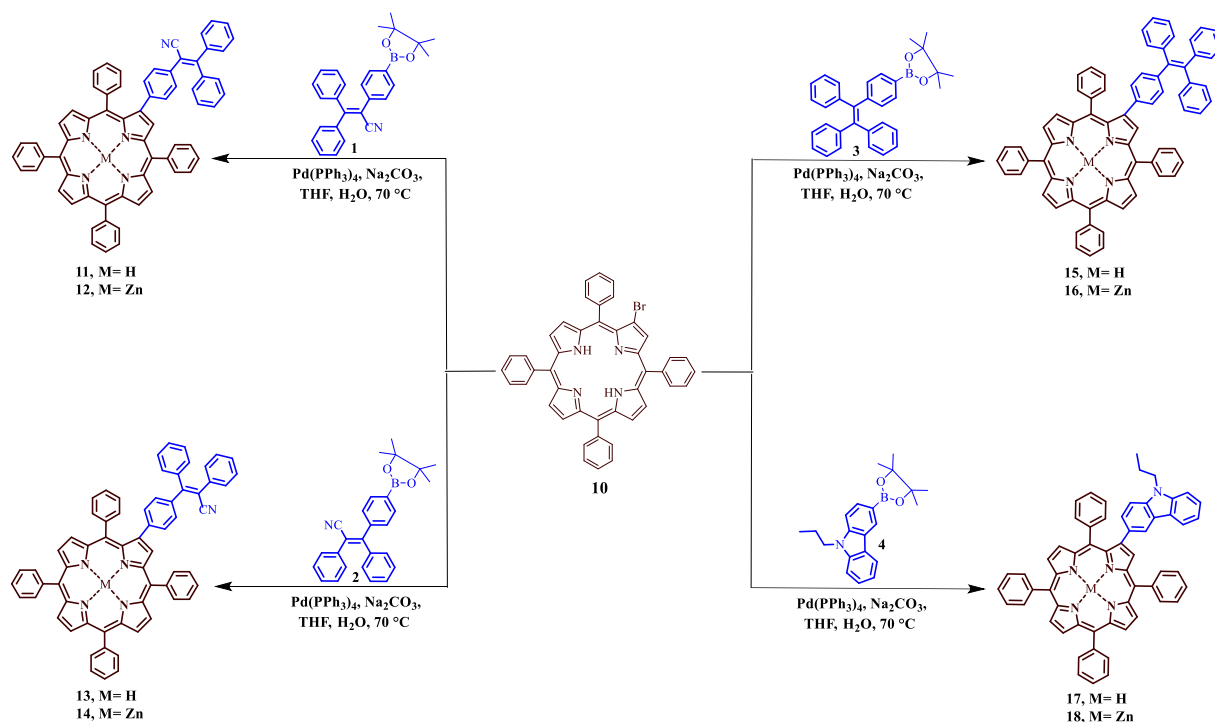
Scheme 7.1. Synthesis of porphyrin derivatives **11**–**18**.

7.2. Results and Discussion

Synthesis

The synthesis of TPAN, TPE and carbazole substituted unsymmetrical *β*-porphyrin and its zinc complexes **11**–**18** are shown in Scheme 7.1. The *β*-monobrominated tetraphenyl porphyrin (TPPBr) **10** and the intermediates, pinacol boronate esters of 2,3,3-triphenylacrylonitrile **1** and **2**, 1,1,2,2-tetraphenylethene **3** and carbazole **4** were synthesized according to the reported procedures (Scheme 7.1).[27–29] The electron accepting cyano substituted 2,3,3-triphenylacrylonitrile functionalized *β*-porphyrins **11** and **13**, and the electron donating 1,1,2,2-tetraphenylethene and carbazole functionalized *β*-porphyrins **15** and **17** were synthesized by the Pd-catalyzed Suzuki cross-coupling reactions. The TPPBr **10** was reacted with 1.5 equiv of 3,3-diphenyl-2-(4-(4,4,5,5-tetramethyl-1,3,2-dioxaborolan-2-yl)phenyl)acrylonitrile **1** and 2,3-diphenyl-3-(4-(4,4,5,5-tetramethyl-1,3,2-dioxaborolan-2-yl)phenyl)acrylonitrile **2** by the Pd-catalyzed Suzuki cross-coupling reaction in presence of Pd(PPh$_3$)$_4$ in THF solvent at 70 °C resulted in porphyrin **11** and **13** in 83% and 78% yields, respectively (Scheme 7.1). The 2,3,3-triphenylacrylonitrile **2** substituted porphyrin **13** is an inseparable mixture of *cis* and *trans* isomers and was reported as 1:1 mixture. [30] The Suzuki cross-coupling reactions of TPPBr **10** with 1.5 equiv of 4,4,5,5-tetramethyl-2-(4-(1,2,2-triphenylvinyl)phenyl)-1,3,2-dioxaborolane **3** and 9-propyl-3-(4,4,5,5-tetramethyl-1,3,2-dioxaborolan-2-yl)-9H-carbazole **4** in the presence of Pd(PPh$_3$)$_4$ in THF solvent at 70 °C, resulted in porphyrin **15** and **17** in 64% and 69% yields, respectively (Scheme 7.1). The zinc metallation of TPAN, TPE and carbazole functionalized *β*-porphyrins **11**, **13**, **15** and **17** were carried out using Zn(OAc)$_2$ in MeOH : CHCl$_3$ mixture (3:1 ratio), resulted in zinc complexes **12**, **14**, **16**, and **18** with 88, 83, 88 and 74% yields, respectively. The TPAN, TPE and carbazole functionalized *β*-porphyrins and its zinc complexes **11**–**18** were characterized by ^{1}H, ^{13}C NMR and HRMS mass spectroscopic techniques.

7.3. Photophysical Properties

The electronic absorption spectra of the *β*-substituted unsymmetrical porphyrin **11**–**18** were recorded in THF at room temperature (Figure 7.1) and the data are shown in Table 7.1. The absorption spectra of electron accepting cyano substituted TPAN functionalized *β*-porphyrins **11**–**14**, and the electron donating TPE and carbazole functionalized *β*-porphyrins **15**–**18** are shown in Figure 7.1. The unsymmetrical porphyrin **11**–**18** shows a characteristic Soret band
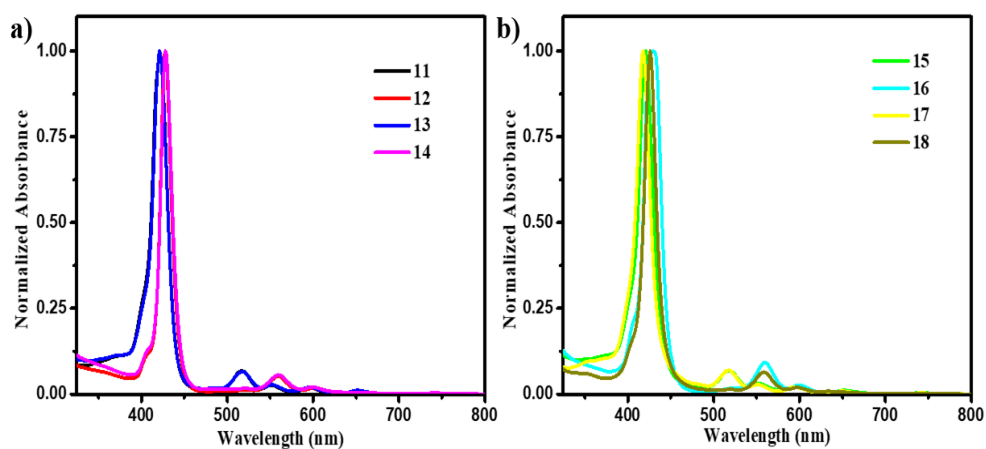
Figure 7.1. Normalized electronic absorption spectra of porphyrin a) **11**–**14** and b) **15**–**18** in THF at 1.0×10^{-5} M concentration.

around 418–430 nm. The absorption spectra of free base porphyrin and its zinc complexes shows four Q–bands and two Q–bands in the low energy region between 517–652 nm. The zinc complexes **12**, **14**, **16**, and **18** exhibits a red shifted absorption of about 7−9 nm in the soret band region compared to its free base analogues **11**, **13**, **15** and **17**. The absorption spectra of 2,3,3-triphenylacrylonitrile substituted porphyrins **11**, **12**, **13** and **14** with different spatial arrangements of cyano moiety at *β*-pyrrolic position exhibits similar absorption band in the Soret and Q–band region. The 1,1,2,2-tetraphenylethene substituted porphyrin **15** and **16** exhibits a slight red shifted absorption spectra compared to other porphyrins. The carbazole functionalized porphyrin **17** and **18** shows a blue shift in the absorption spectra compared to 2,3,3-triphenylacrylonitrile and 1,1,2,2-tetraphenylethene substituted

142

porphyrin **11**–**16**. The red shifted absorption spectra of 1,1,2,2-tetraphenylethene substituted porphyrin may be due to the increase in the phenyl unit present in the tetraphenyl ethene moiety which further enhances π-conjugation of the molecule.

The emission spectra of *β*-substituted unsymmetrical porphyrins **11**–**18** (Figure 7.2) were explored in THF solvent at room temperature, and the data are shown in Table 7.1. The unsymmetrical porphyrins **11**–**18** shows emission band around 616–724 nm in the low
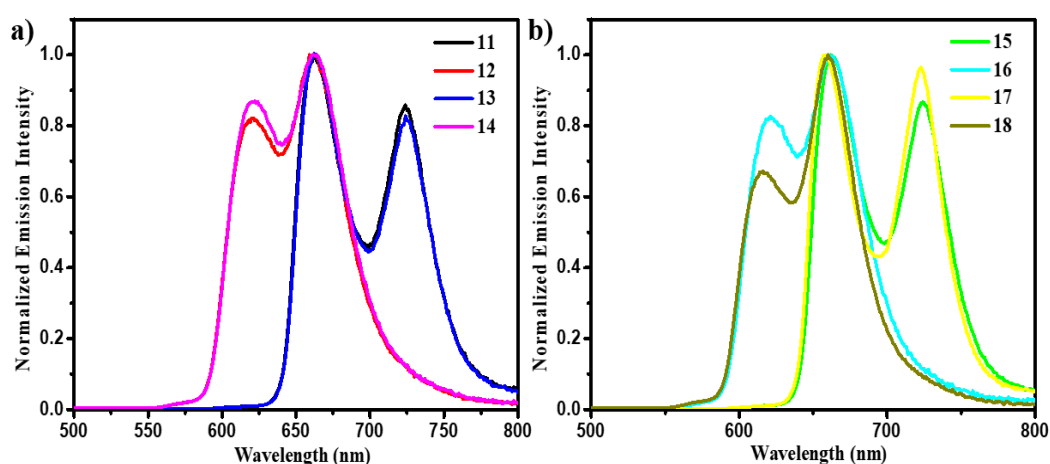
Figure 7.2. Normalized emission spectra of porphyrin a) **11**–**14** and b) **15**–**18** in THF at 1.0×10^{-5} M concentration.

energy region. The 2,3,3-triphenylacrylonitrile and 1,1,2,2-tetraphenylethene substituted porphyrin **11**–**16** exhibits similar emission maxima with a slight red shift of 1–2 nm around 620–724 nm in the low energy region. The free base and zinc complexes of 2,3,3-triphenylacrylonitrile substituted porphyrins **11**–**14** with different spatial arrangements of cyano moiety shows similar emission maxima in the longer wavelength region around 662–724 nm and 620–662 nm, respectively. The 1,1,2,2-tetraphenylethene substituted porphyrins **15** and **16** shows similar emission bands as that of 2,3,3-triphenylacrylonitrile substituted porphyrins. The porphyrins **11**–**16** shows a red shift in the emission maxima of around 4–5 nm in the low energy region compared to 9-propyl-9H-carbazole substituted free base

and Zn(II) porphyrin **17** and **18**. The red shifted emission maxima of porphyrin **11–16** may be due to the enhanced π-conjugation of the phenyl group present in the 2,3,3-triphenylacrylonitrile and 1,1,2,2-tetraphenylethene moiety.

Table 7.1. Photophysical and theoretical data of porphyrin **11–18**.

Compound		λ_{abs} (nm) [a]		λ_{em} (nm)	Φ_f [b]	H–L gap(eV)[c]
	Soret band	ε (M^{-1} cm^{-1})	Q-band			
11	421	21590	517, 552, 595, 651	662, 724	0.10	2.55
12	428	15280	559, 599,	620, 661	0.02	2.77
13	421	19220	517, 552, 596, 652	664, 724	0.06	2.58
14	428	12390	560, 599,	620, 662	0.01	2.76
15	421	10150	518, 552, 595, 652	662, 724	0.05	2.62
16	430	24980	560, 599	621, 661	0.02	2.79
17	418	96230	518, 551, 594, 649	658, 723	0.07	2.63
18	426	16170	559, 598	616, 660	0.04	2.80

[a] Absorbance measured in THF at 1×10^{-5} M concentration; λ_{abs}: absorption wavelength; λ_{em}: emission wavelength; ε: extinction coefficient. [b] The fluorescence quantum yields were recorded using H$_2$TPP as a standard ($\Phi_{st} = 0.11$). [c] Calculated from computational study.

7.4. DFT Calculation

The electronic structures of unsymmetrical porphyrins **11–18** were determined by performing density functional theory (DFT) calculations at B3LYP/6-31G level using the Gaussian 09W program.[31] The optimized structures of 2,3,3-triphenylacrylonitrile and 1,1,2,2-tetraphenylethene substituted porphyrin **11–16** exhibits a propeller shaped nonplanar geometry with TPAN and TPE entity at the *β*-pyrrolic positions (Figure 7.3). In 2,3,3-triphenylacrylonitrile substituted porphyrin **11–14**, the electron density is localized on the porphyrin macrocycle in HOMO whereas in LUMO it is mainly concentrated on porphyrin macrocycle with little over the phenyl ring of the 2,3,3-triphenylacrylonitrile entity. In 1,1,2,2-tetraphenylethene substituted

porphyrin **15** and **16**, the electron density in HOMO is concentrated on the porphyrin macrocycle whereas the LUMOs are populated on the porphyrin macrocycle with some parts dispersed on the phenyl unit of the 1,1,2,2-tetraphenylethene moiety. The carbazole substituted porphyrin **17** and **18** shows that the majority of the electron density in HOMO were concentrated on the porphyrin macrocycle, whereas
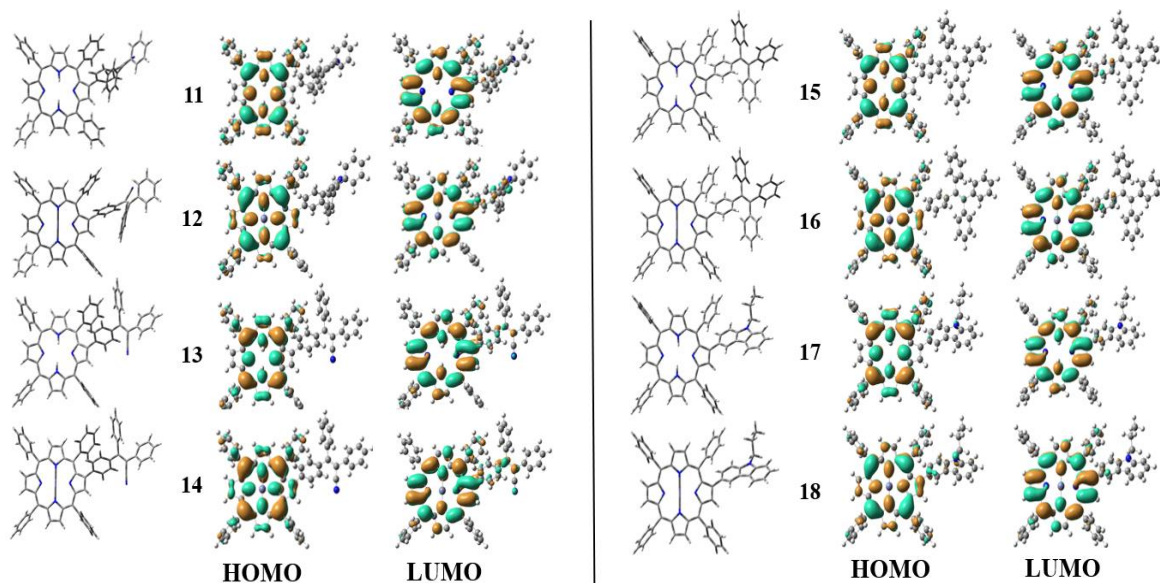
Figure 7.3. Optimized structure, frontier HOMO and LUMO of porphyrins **11**–**18**.

LUMO is populated on the porphyrin macrocycle with little over the phenyl unit of the carbazole moiety. The energy level diagrams of porphyrin **11–18** are shown in Figure 7.4. The theoretically calculated HOMO levels of the porphyrins **11–18** are –4.92 eV, –5.03 eV, –4.96 eV, –5.04 eV, –4.92 eV, –4.99 eV, –4.86 eV and –4.93 eV whereas LUMO levels are –2.37 eV, –2.26 eV, –2.38 eV, –2.28 eV, –2.30 eV, –2.20 eV, –2.23 eV and –2.13 eV respectively. The theoretically calculated HOMO and LUMO energy level states that, a stabilized LUMO energy level with low HOMO–LUMO band gap of about 2.55 eV and 2.58 eV was observed for 2,3,3-triphenylacrylonitrile substituted free base porphyrin **11** and **13** compared to other porphyrins.

Table 7.2. Calculated Electronic Transitions of porphyrin **11**–**18**.

Compounds	λ_{max}	Composition & Molecular contribution	f^a	Assignment
11	398	HOMO–1→LUMO+2 (0.46)	0.94	π–π*
	596	HOMO→LUMO (0.59)	0.05	ICT
12	375	HOMO–1→LUMO+1 (0.44)	1.39	π–π*
	540	HOMO→LUMO (0.55)	0.03	ICT
13	396	HOMO–1→LUMO+2 (0.45)	0.79	π–π*
	589	HOMO →LUMO (0.58)	0.04	ICT
14	376	HOMO–1→LUMO+1 (0.46)	1.36	π–π*
	542	HOMO→LUMO (0.56)	0.04	ICT
15	385	HOMO–2→LUMO (0.43)	1.39	π–π*
	587	HOMO →LUMO (0.58)	0.03	ICT
16	384	HOMO–2→LUMO (0.46)	1.68	π–π*
	538	HOMO →LUMO (0.52)	0.02	ICT
17	377	HOMO–2→LUMO (0.44)	1.31	π–π*
	585	HOMO→LUMO (0.57)	0.03	ICT
18	378	HOMO–2→LUMO (0.44)	1.68	π–π*
	538	HOMO →LUMO (0.45)	0.02	ICT

f^a Oscillator strength.

The UV-visible absorption spectra, electronic transitions, assignments, and oscillator strength (f) were calculated using time-dependent density functional theory (TD-DFT) using B3LYP/6-31G basis set, and the data are depicted in Table 7.2. The UV-Visible absorption spectra of porphyrin **11**–**18** shows two absorption band, the Soret band and the Q-band. The porphyrin **11**, **12**, **13**, **14**, **15**, **16**, **17** and **18** exhibits absorption band around 596, 540, 589, 542, 587, 538, 585 and 538 nm in the low energy Q-band region and are assigned to ICT transition. The major ICT transitions for porphyrin **11**–**18** occurs from HOMO→LUMO. In porphyrin **11**–**18** the absorption band around 398, 375, 396, 376, 385, 384, 377 and 378 nm in the soret band region corresponds to π–π* transition. In porphyrin **11** and **13**, the π–π* transition arises from HOMO–1→LUMO+2, whereas in porphyrin **12** and **14**, it occurs from

HOMO–1→LUMO+1, respectively. The major π–π* transitions for porphyrin **15–18** occurs from HOMO–2→LUMO. The TD-DFT calculated values are in good agreement with the experimental data.
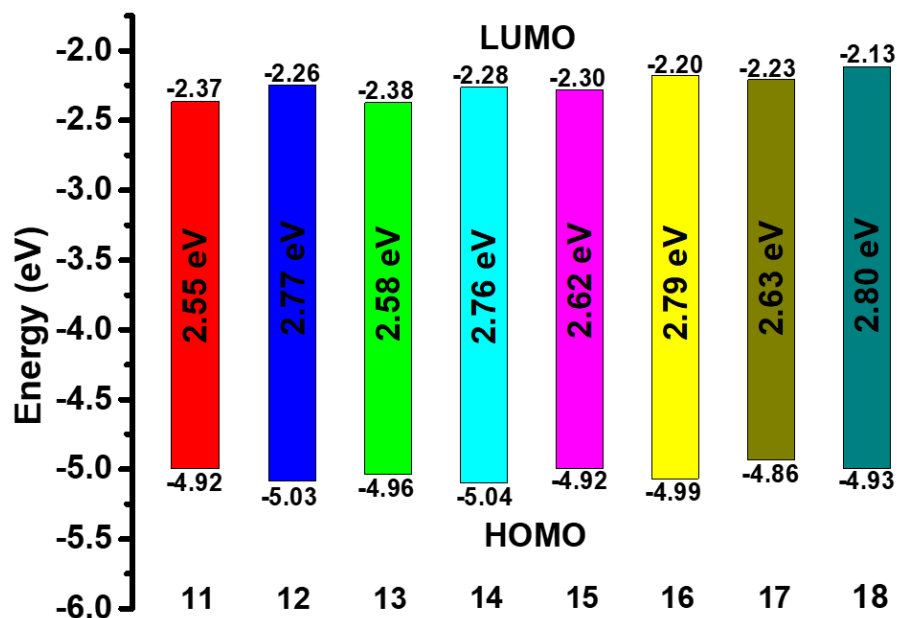
Figure 7.4. Energy level diagram of the frontier orbitals of porphyrin **11–18** estimated by DFT calculations.

7.5. Electrochemical Properties

The electrochemistry of *β*-substituted unsymmetrical porphyrins **11–18** were investigated by the cyclic voltammetry using 0.1M TBAPF$_6$ as supporting electrolyte in dichloromethane, (Figure 7.5) and the data are depicted in Table 7.3.[32–34] In general, porphyrin macrocycle exhibits two oxidation and two reduction waves. The 2,3,3-triphenylacrylonitrile substituted free base porphyrin **11** and **13**, exhibits two reduction waves in the region -1.25 to -1.47 V and three oxidation waves between 0.64 to 1.51 V. In 2,3,3-triphenylacrylonitrile substituted zinc porphyrin **12** and **14**, two reduction waves and two oxidation waves were observed around -1.22 to -1.55 V and 0.55 to 1.10 V, respectively.
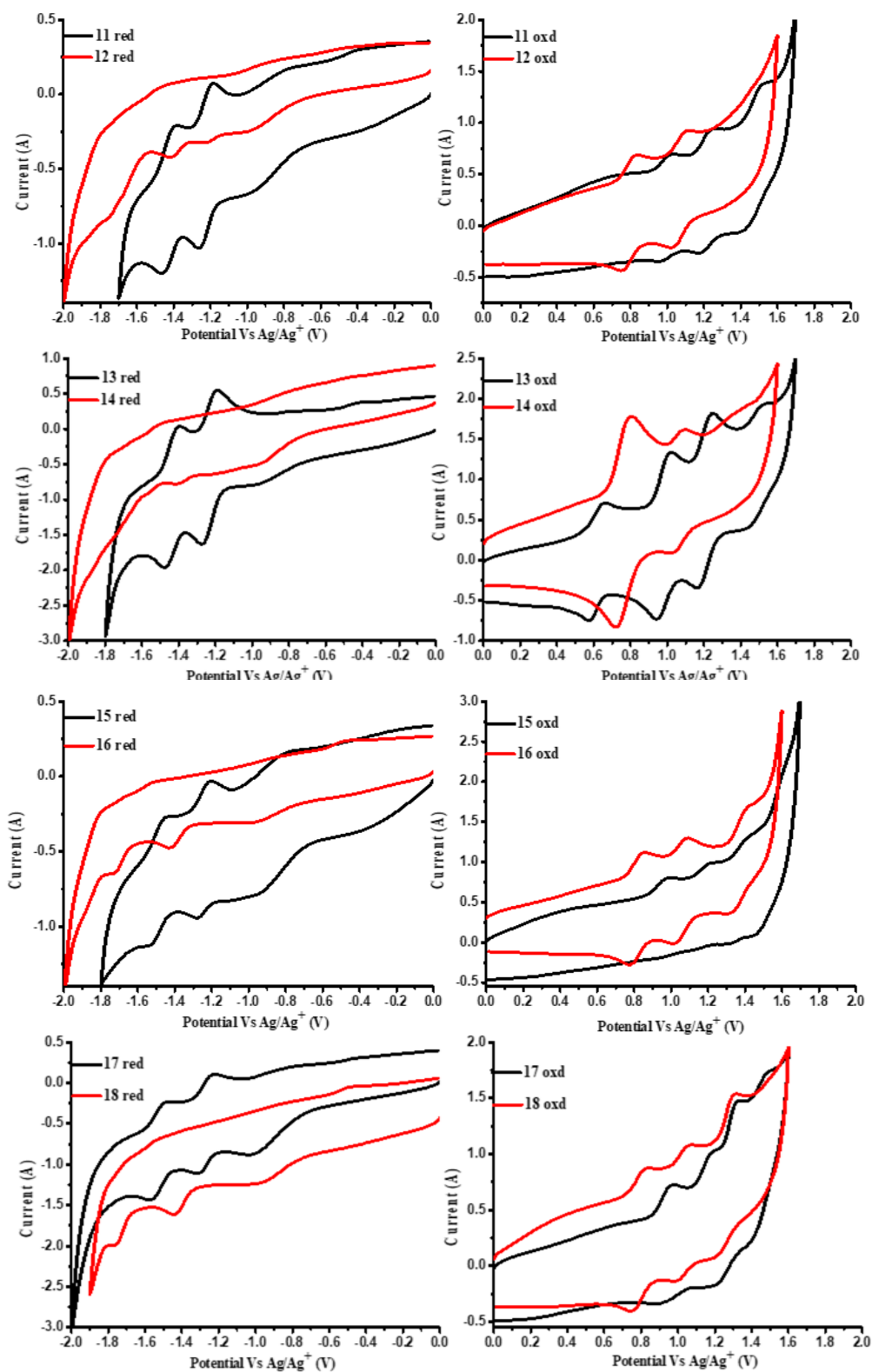
Figure 7.5. Cyclic voltammograms of porphyrin **11**–**18** in dichloromethane containing 0.1 M solution of TBAPF$_6$ with a scan rate of 100 mV/s.

Table 7.3. Electrochemical data of porphyrin **11–18**.

Compound	Potential (V vs Ag/Ag$^+$) [d]		
	E$_{red}$	E$_{ox}$	E$_g$ (eV) [e]
11	-1.25, -1.46	1.00, 1.24 1.51	2.07
12	-1.22, -1.41	0.82, 1.10	1.84
13	-1.27, -1.47	0.64, 1.01, 1.23	1.70
14	-1.40, -1.55	0.55, 1.08	1.96
15	-1.27, -1.52	0.95, 1.20, 1.40	2.03
16	-1.41, -1.72	0.83, 1.08, 1.41	2.04
17	-1.30, -1.56	0.96, 1.17, 1.32	2.04
18	-1.43, -1.75	0.81, 1.05, 1.30	2.03

[d] Electrochemical analysis was estimated by cyclic voltammetry in 0.1 M solution of tetrabutylammonium hexafluorophosphate (TBAPF$_6$) in DCM at 100 mV/s scan rate. [e] Electrochemical band gaps.

The 1,1,2,2-tetraphenylethene and 9-propyl-9H-carbazole substituted porphyrin **15**, **16**, **17** and **18** shows two reduction waves around -1.27 to -1.75 V and are assigned to porphyrin macrocycle, whereas three oxidation waves in the range of 0.81 to 1.41 V, attributed to the porphyrin macrocycle and the tetraphenylethene and carbazole donor units. In 1,1,2,2-tetraphenylethene substituted porphyrin **15** and **16**, three reversible oxidation waves were observed, in which the first and second oxidation wave in the region of 0.83 to 1.20 V is attributed to the porphyrin macrocycle, and the third oxidation wave around 1.40 V corresponds to the tetraphenylethene donor unit. In 9-propyl-9H-carbazole substituted porphyrin **17** and **18**, the first and second oxidation wave, observed in the region of 0.81 to 1.17 V, corresponds to the porphyrin macrocycle whereas the third oxidation wave in the region of 1.30 to 1.32 V is attributed to the carbazole donor unit. The zinc porphyrin **12** exhibit a anodic shift in their reduction potentials, whereas

in the oxidation potentials a cathodic shift was observed, compared to their corresponding free base analogue **11**. The zinc porphyrin **14**, **16** and **18** exhibits a cathodic shift in the oxidation and reduction potentials compared to their corresponding free base analogues **13**, **15** and **17**. The onset oxidation and reduction potentials were utilized to evaluate the HOMO/ LUMO energy levels for porphyrin **11**–**18**, which are -5.32/-3.25 V, -5.12/-3.28 V, -4.95/-3.25 V, -5.05/-3.09 V, -5.27/-3.24 V, -5.13/-3.09 V, -5.25/-3.21 V and -5.11/-3.08 V, respectively. The 2,3,3-triphenylacrylonitrile substituted porphyrin **13** exhibits a stabilized HOMO energy levels with low electrochemical band gap of about 1.70 V.

7.6. Experimental Section

General: All the chemicals were purchased from commercial sources and used without further purification. The NMR spectra were recorded at room temperature (298 K). Chemical shifts are given in ppm with respect to tetramethylsilane as internal standard ($CDCl_3$, 7.26 ppm, 77.0 ppm). ^{1}H NMR spectra were recorded using a 500 MHz spectrometer. ^{13}C NMR spectra were recorded using a 101 MHz and 126 MHz spectrometer. Multiplicities are given as s (singlet), d (doublet), t (triplet) and m (multiplet) are given in Hertz. TLC analysis was carried out using silica gel 60 F_{254} plates. UV-visible absorption spectra were recorded on a Cary-100 Bio UV-visible spectrophotometer. Emission spectra were taken in a The Fluoromax-4C, S/n. 1579D-1417-FM Fluorescence software Ver 3.8.0.60. UV/Vis and emission spectrums of all compounds were recorded in THF solution. The density functional theory (DFT) calculation were carried out at the B3LYP/6-31G level for C, N, H, Zn in the Gaussian 09 program. HRMS were recorded on a Bruker-Daltonics micrOTOF-Q II mass spectrometer.

Synthesis of compound 11.

7-bromo-5,10,15,20-tetraphenylporphyrin **10** (0.080 g, 0.115 mmol) and 3,3-diphenyl-2-(4-(4,4,5,5-tetramethyl-1,3,2-dioxaborolan-2-yl)phenyl)acrylonitrile **1** (0.070 g, 0.173 mmol) were dissolved in THF (20 mL) and purged by nitrogen for 15 min. Meanwhile, a solution

of sodium carbonate (0.750 g, 7.07 mmol) in water (15 mL), was added. After purging, palladium (0) tetrakis(triphenylphosphine) (0.100 g, 0.08 mmol) was added and the reaction mixture was refluxed in an oil bath for 16 h at 70 °C. The solvent was then evaporated under vacuum, the resultant mixture was diluted with DCM and the organic layer was collected, dried over anhydrous Na_2SO_4 and evaporated under vacuum. The solid was adsorbed on silica gel and purified by column chromatography, using a DCM: hexane (20: 80) mixture to yield 0.085 g, 83% of compound **11**. ^{1}H NMR (500 MHz, $CDCl_3$) δ 8.82(s, 3H), 8.80(d, 1H), 8.75(d, 1H), 8.73(d, 1H), 8.70(s, 1H), 8.23–8.21(m, 6H), 7.90(d, 2H), 7.77–7.73(m, 9H), 7.52–7.50(m, 3H), 7.47(m, 3H), 7.35–7.32(m, 5H), 7.21(d, 2H), 7.15–7.13(m, 2H), 7.05(d, 2H), -2.63(s, 2H). ^{13}C NMR (126 MHz, $CDCl_3$) δ 156.93, 142.53, 142.25, 141.83, 140.80, 140.67, 139.34, 136.05, 134.64, 134.57, 131.77, 130.80, 130.39, 130.01, 129.82, 129.07, 128.67, 128.49, 128.41, 127.76, 127.47, 126.81, 126.70, 126.66, 126.31, 121.19, 120.49, 120.05, 119.82, 111.78. HRMS (ESI-TOF): m/z calculated for $C_{65}H_{43}N_5$ [M+nH] $^+$ 871.3795, found 871.3742.

Synthesis of compound 12.

Compound **11** (0.040 g, 0.044 mmol) and Zn (OAc)$_2$, (0.107 g, 0.492 mmol) in MeOH: CHCl$_3$ (3 : 1, v/v), were added and the reaction mixture was stirred for 1 h at room temperature. The solvent was then evaporated under reduced pressure and the resultant mixture was diluted with DCM/water and the organic layer was collected, dried over anhydrous Na_2SO_4 and evaporated under vacuum. The solid was adsorbed on silica gel and purified by column chromatography, using a DCM: hexane (35: 65) mixture to yield 0.037 g, 88% of compound 1**2**. ^{1}H NMR (500 MHz, $CDCl_3$) δ 8.95–8.90(m, 4H), 8.88(d, 1H), 8.83(d, 2H), 8.24–8.20(m, 6H), 7.87(d, 2H), 7.78–7.72(m, 9H), 7.53–7.50(m, 3H), 7.47–7.46(m, 3H), 7.34–7.30(m, 5H), 7.22(d, 2H), 7.17–7.15(m, 2H), 7.06(d, 2H). ^{13}C NMR (126 MHz, $CDCl_3$) δ 156.79, 151.22, 150.57, 150.34, 147.71, 146.87, 146.52, 146.37, 142.92, 142.69, 141.46, 140.86, 139.71, 139.38, 135.80, 135.12, 134.44, 132.79, 132.20, 132.15,

132.04, 131.57, 131.47, 130.81, 130.41, 130.02, 129.79, 129.05, 128.54, 128.48, 128.41, 127.56, 127.27, 126.60, 126.09, 122.83, 122.33, 121.58, 121.07, 120.59, 120.10, 111.88. HRMS (ESI-TOF): m/z calculated for $C_{65}H_{41}N_5Zn$ [M]$^+$ 939.2369, found 939.2368.

Synthesis of compound 13.

7-bromo-5,10,15,20-tetraphenylporphyrin **10** (0.080 g, 0.115 mmol) and (Z)-2,3-diphenyl-3-(4-(4,4,5,5-tetramethyl-1,3,2-dioxaborolan-2-yl) phenyl) acrylonitrile **2** (0.070 g, 0.173 mmol) were dissolved in THF (20 mL) and purged by nitrogen for 15 min. Meanwhile, a solution of sodium carbonate (0.750 g, 7.07 mmol) in water (15 mL), was added. After purging, palladium (0) tetrakis(triphenylphosphine) (0.100 g, 0.08 mmol) was added and the reaction mixture was refluxed in an oil bath for 16 h at 70 °C. The solvent was then evaporated under vacuum, the resultant mixture was diluted with DCM and the organic layer was collected, dried over anhydrous Na_2SO_4 and evaporated under vacuum. The solid was adsorbed on silica gel and purified by column chromatography, using a DCM: hexane (20: 80) mixture to yield 0.080 g, 78% of compound **13**. ^{1}H NMR (500 MHz, CDCl$_3$) δ 8.84–8.82(m, 3H), 8.80(s, 1H), 8.76–8.72(m, 2H), 8.69–8.67(m, 1H), 8.26–8.20(m, 6H), 7.97–7.92(m, 2H), 7.79–7.72(m, 10H), 7.54(d, 2H), 7.40–7.28(m, 10H), 7.24(d, 1H), 7.20(d, 1H), 7.09(d, 1H), 6.79(d, 1H), -2.61(d, 2H). ^{13}C NMR (126 MHz, CDCl$_3$) δ 157.67, 157.55, 153.23, 142.47, 142.38, 142.26, 142.17, 142.06, 141.84, 141.75, 141.11, 140.93, 140.72, 139.51, 139.30, 137.54, 136.30, 136.14, 135.14, 134.97, 134.73, 134.62, 134.51, 131.11, 130.23, 130.07, 129.83, 129.71, 128.99, 128.64, 128.46, 128.34, 128.10, 127.73, 126.79, 126.67, 126.36, 126.19, 121.17, 120.41, 120.00, 111.28, 110.91. HRMS (ESI-TOF): m/z calculated for $C_{65}H_{43}N_5$ [M+nH]$^+$ 871.3795, found 871.3742.

Synthesis of compound 14.

Compound **13** (0.040 g, 0.044 mmol) and Zn (OAc)$_2$, (0.107 g, 0.492 mmol) in MeOH: CHCl$_3$ (3 : 1, v/v), were added and the reaction mixture was stirred for 1 h at room temperature. The solvent was then

evaporated under reduced pressure and the resultant mixture was diluted with DCM/water and the organic layer was collected, dried over anhydrous Na_2SO_4 and evaporated under vacuum. The solid was adsorbed on silica gel and purified by column chromatography, using a DCM: hexane (35: 65) mixture to yield 0.036 g, 83% of compound **14**. ^{1}H NMR (500 MHz, CDCl$_3$) δ 8.95–8.91(m, 4H), 8.89–8.86(m, 1H), 8.83(d, 1H), 8.78(d, 1H), 8.24–8.20(m, 6H), 7.94–7.89(m, 2H), 7.76(m, 10H), 7.56(s, 2H), 7.41(d, 2H), 7.32–7.31(m, 6H), 7.23–7.21(m, 3H), 7.11(d, 1H), 7.03(d, 1H), 6.80(d, 1H). ^{13}C NMR (101 MHz, CDCl$_3$) δ 151.17, 150.61, 150.37, 150.33, 150.25, 150.11, 148.15, 147.78, 147.64, 146.43, 146.25, 142.94, 142.85, 142.70, 141.97, 141.56, 140.53, 136.06, 135.89, 135.44, 135.04, 134.47, 132.70, 132.17, 132.07, 131.99, 131.62, 131.54, 131.13, 130.31, 130.25, 130.09, 129.96, 129.85, 129.75, 129.43, 129.07, 128.84, 128.65, 128.46, 128.35, 128.11, 127.56, 127.05, 126.59, 126.12, 125.96, 122.89, 122.06, 121.86, 121.10, 120.60, 116.23, 111.20, 110.21. HRMS (ESI-TOF): m/z calculated for $C_{66}H_{45}N_5Zn$ [M]$^+$ 939.2369, found 939.2368.

Synthesis of compound 15.

7-bromo-5,10,15,20-tetraphenylporphyrin **10** (0.080 g, 0.115 mmol) and 4,4,5,5-tetramethyl-2-(4-(1,2,2-triphenylvinyl)phenyl)-1,3,2-dioxaborolane **3** (0.079 g, 0.173 mmol) were dissolved in THF (20 mL) and purged by nitrogen for 15 min. Meanwhile, a solution of sodium carbonate (0.750 g, 7.07 mmol) in water (15 mL), was added. After purging, palladium (0) tetrakis(triphenylphosphine) (0.100 g, 0.08 mmol) was added and the reaction mixture was refluxed in an oil bath for 16 h at 70 °C. The solvent was then evaporated under vacuum, the resultant mixture was diluted with DCM and the organic layer was collected, dried over anhydrous Na_2SO_4 and evaporated under vacuum. The solid was adsorbed on silica gel and purified by column chromatography, using a DCM: hexane (20: 80) mixture to yield 0.070 g, 64% of compound **15**. ^{1}H NMR (500 MHz, CDCl$_3$) δ 8.84–8.80(m, 3H), 8.77(d, 1H), 8.72–8.70(m, 2H), 8.67(d, 1H), 8.25–8.21(m, 6H), 7.93(d, 2H), 7.79–7.73(m, 11H), 7.50(t, 1H), 7.33(t, 2H), 7.23(d, 2H),

7.20(d, 2H) 7.12–7.10(m, 9H), 7.06–7.04(m, 2H), 6.82(d, 2H), -2.63(s, 2H). ^{13}C NMR (126 MHz, CDCl$_3$) δ 144.18, 143.86, 142.61, 142.32, 141.88, 141.04, 140.88, 140.72, 136.22, 134.66, 131.74, 131.42, 131.33, 130.46, 129.65, 127.84, 127.72, 127.62, 127.51, 127.24, 126.80, 126.68, 126.65, 126.50, 126.46, 126.31, 126.19, 121.26, 120.38, 119.92, 119.75. HRMS (ESI-TOF): m/z calculated for C$_{70}$H$_{48}$N$_4$ [M+nH] $^+$ 871.3795, found 871.3742.

Synthesis of compound 16.

Compound 1**5** (0.040 g, 0.042 mmol) and Zn (OAc)$_2$, (0.102 g, 0.466 mmol) in MeOH: CHCl$_3$ (3 : 1, v/v), were added and the reaction mixture was stirred for 1 h at room temperature. The solvent was then evaporated under reduced pressure and the resultant mixture was diluted with DCM/water and the organic layer was collected, dried over anhydrous Na$_2$SO$_4$ and evaporated under vacuum. The solid was adsorbed on silica gel and purified by column chromatography, using a DCM: hexane (35: 65) mixture to yield 0.037 g, 88% of compound **16**. ^{1}H NMR (500 MHz, CDCl$_3$) δ 8.95–8.90(m, 4H), 8.86(d, 1H), 8.81–8.79(m, 2H), 8.25–8.20(m, 6H), 7.90(d, 2H), 7.75–7.73(m, 11H), 7.49(t, 1H), 7.31(t, 2H), 7.23(d, 2H), 7.20(d, 2H), 7.15–7.11(m, 9H), 7.06(d, 2H), 6.82(d, 2H). ^{13}C NMR (101 MHz, CDCl$_3$) δ 151.28, 150.49, 150.25, 150.20, 150.14, 150.07, 149.21, 147.94, 147.38, 146.71, 144.26, 143.91, 143.00, 142.77, 141.84, 140.87, 140.51, 137.48, 135.95, 135.47, 134.44, 132.70, 132.12, 132.04, 131.91, 131.76, 131.42, 131.34, 130.31, 129.62, 127.82, 127.60, 127.49, 127.05, 126.56, 126.43, 126.27, 125.96, 122.43, 120.49. HRMS (ESI-TOF): m/z calculated for C$_{70}$H$_{46}$N$_4$Zn [M] $^+$ 939.2369, found 939.2368.

Synthesis of compound 17.

7-bromo-5,10,15,20-tetraphenylporphyrin **10** (0.080 g, 0.115 mmol) and 9-propyl-3-(4,4,5,5-tetramethyl-1,3,2-dioxaborolan-2-yl)-9H-carbazole **4** (0.058 g, 0.173 mmol) were dissolved in THF (20 mL) and purged by nitrogen for 15 min. Meanwhile, a solution of sodium carbonate (0.750 g, 7.07 mmol) in water (15 mL), was added. After purging, palladium (0) tetrakis(triphenylphosphine) (0.100 g, 0.08

mmol) was added and the reaction mixture was refluxed in an oil bath for 16 h at 70 °C. The solvent was then evaporated under vacuum, the resultant mixture was diluted with DCM and the organic layer was collected, dried over anhydrous Na_2SO_4 and evaporated under vacuum. The solid was adsorbed on silica gel and purified by column chromatography, using a DCM: hexane (20: 80) mixture to yield 0.065 g, 69% of compound **17**. ^{1}H NMR (500 MHz, CDCl$_3$) δ 8.88–8.84(m, 3H), 8.83–8.80(dd, 2H), 8.72(d, 1H), 8.67(d, 1H), 8.27–8.21(m, 6H), 8.05(s, 1H), 8.02(d, 1H), 7.90(d, 2H), 7.77–7.71(m, 9H), 7.50–7.44(m, 3H), 7.23(d, 1H), 7.15(d, 1H), 6.98(t, 2H), 6.81(t, 1H), 4.31(t, 2H), 2.00–1.96(m, 2H), 1.03(t, 3H), -2.57(s, 2H). ^{13}C NMR (101 MHz, CDCl$_3$) δ 142.71, 142.43, 141.97, 140.84, 140.65, 139.02, 135.55, 134.66, 134.62, 134.54, 128.93, 128.30, 127.71, 126.79, 126.66, 126.62, 125.66, 125.34, 122.95, 122.41, 122.21, 121.50, 120.49, 119.88, 119.64, 118.62, 108.67, 107.72, 44.54, 22.39, 11.86. HRMS (ESI-TOF): m/z calculated for $C_{59}H_{43}N_5$ [M+nH]$^+$ 871.3795, found 871.3742.

Synthesis of compound 18.

Compound **17** (0.040 g, 0.048 mmol) and Zn (OAc)$_2$, (0.117 g, 0.535 mmol) in MeOH: CHCl$_3$ (3 : 1, v/v), were added and the reaction mixture was stirred for 1 h at room temperature. The solvent was then evaporated under reduced pressure and the resultant mixture was diluted with DCM/water and the organic layer was collected, dried over anhydrous Na_2SO_4 and evaporated under vacuum. The solid was adsorbed on silica gel and purified by column chromatography, using a DCM: hexane (35: 65) mixture to yield 0.032 g, 74% of compound **18**. ^{1}H NMR (500 MHz, CDCl$_3$) δ 8.97(d, 2H), 8.94(s, 3H), 8.86(d, 1H), 8.79(d, 1H), 8.27–8.22(m, 6H), 8.04(s, 1H), 8.01(d, 1H), 7.89(d, 2H), 7.79–7.71(m, 9H), 7.50–7.45(m, 3H), 7.22(t, 1H), 7.17(d, 1H), 6.97(s, 2H), 6.79(t, 1H), 4.34(t, 2H), 2.02–1.98(m, 2H), 1.06(t, 3H). ^{13}C NMR (126 MHz, CDCl$_3$) δ 151.40, 150.41, 150.17, 150.10, 150.03, 148.42, 148.20, 147.22, 143.02, 142.83, 141.43, 140.82, 138.84, 135.41, 134.44, 134.39, 132.62, 131.97, 131.83, 131.31, 129.96, 128.20, 127.49, 126.58, 126.54, 125.23, 122.97, 122.66, 122.31, 122.09, 121.48, 120.89, 120.45,

118.50, 108.61, 107.56, 44.53, 22.40, 11.86. HRMS (ESI-TOF): m/z calculated for $C_{60}H_{45}N_5Zn$ [M]$^+$ 939.2369, found 939.2368.

7.7. Conclusion

The TPAN, TPE and carbazole substituted unsymmetrical β-porphyrins **11–18** were designed and synthesized. The photophysical, electrochemical and computational studies of these porphyrin **11–18** were explored. The effect of TPAN, TPE and carbazole units on the photonic and electronic properties of the porphyrin π-systems were investigated. The absorption spectra of porphyrin **11–14** suggests that the 2,3,3-triphenylacrylonitrile with different spatial arrangements of cyano unit exhibits similar effect on the porphyrin macrocycle. The red shifted emission maxima of porphyrin **11–16** may be due to the enhanced π-conjugation of the phenyl group present in the 2,3,3-triphenylacrylonitrile and 1,1,2,2-tetraphenylethene moiety. The electrochemical properties of zinc porphyrin **14**, **16** and **18** exhibits a cathodic shift in the oxidation and reduction potentials compared to their corresponding free base analogues **13**, **15** and **17**. The computational studies of porphyrin **11–18** suggests, that the 2,3,3-triphenylacrylonitrile substituted porphyrin **11** and **13** exhibits a stabilized LUMO energy levels with low HOMO–LUMO band gap of about 2.55 eV and 2.58 eV compared to other porphyrins.

7.8. References

[1] Saxena, R. C., Adhikari, D. K., Goyal, H. B. (2009), Biomass-based energy fuel through biochemical routes: A review. *Renew. Sustain. Energy Rev.* 13, 167-178. (DOI: 10.1016/j.rser.2007.07.011).

[2] Dincer, I. (2000), Renewable energy and sustainable development: a crucial review. *Renew. Sustain. Energy Rev.* 4, 157-175. (DOI:10.1016/S1364-0321(99)00011-8).

[3] Das, S. K., Song, B., Mahler, A., Nesterov, V. N., Wilson, A. K., Ito, O., D'Souza, F. (2014), Electron transfer studies of high

potential zinc porphyrin–fullerene supramolecular dyads. *J. Phys. Chem. C.* 118, 3994-4006. (DOI: 10.1021/jp4118166).

[4] Labbé, R. F., Vreman, H. J., Stevenson, D. K. (1999), Zinc protoporphyrin: a metabolite with a mission. *Clin. Chem.* 45, 2060-2072. (DOI: 10.1093/clinchem/45.12.2060).

[5] Lewtak, J. P., Gryko, D. T. (2012), Synthesis of π-extended porphyrins via intramolecular oxidative coupling. *Chem. Commun.* 48, 10069-10086. (DOI: 10.1039/C2CC31279D).

[6] Kurotobi, K., Kim, K. S., Noh, S. B., Kim, D., Osuka, A. (2006), A Quadruply Azulene-Fused Porphyrin with Intense Near-IR Absorption and a Large Two-Photon Absorption Cross Section. *Angew. Chem. Int. Ed.* 45, 3944-3947. (DOI: 10.1002/anie.200600892).

[7] Chaudhri, N., Grover, N., & Sankar, M. (2017), Versatile synthetic route for β-functionalized chlorins and porphyrins by varying the size of Michael donors: Syntheses, photophysical, and electrochemical redox properties. *Inorg. Chem.* 56, 11532-11545. (DOI: 10.1021/acs.inorgchem.7b01158).

[8] O'Connor, A. E., Gallagher, W. M., Byrne, A. T. (2009), Porphyrin and nonporphyrin photosensitizers in oncology: preclinical and clinical advances in photodynamic therapy. *Photochem. Photobiol.* 85, 1053-1074. (DOI: 10.1111/j.1751-1097.2009.00585.x).

[9] Xu, S., Liu, H. W., Huan, S. Y., Yuan, L., Zhang, X. B. (2021), Recent progress in utilizing near-infrared J-aggregates for imaging and cancer therapy. *Mater. Chem. Front.* 5, 1076-1089. (DOI: 10.1039/D0QM00557F).

[10] Chou, J. H., Kosal, M. E., Nalwa, H. S., Rakow, N. A., Suslick, K. S. (2000), Applications of porphyrins and metalloporphyrins to materials chemistry. *The porphyrin handbook*, 6, 43-131.

[11] Elouarzaki, K., Le Goff, A., Holzinger, M., Thery, J., Cosnier, S. (2012), Electrocatalytic oxidation of glucose by rhodium porphyrin-functionalized MWCNT electrodes: application to a fully molecular catalyst-based glucose/O2 fuel cell. *J.   Am. Chem. Soc.* 134, 14078-14085. (DOI: 10.1021/ja304589m).

[12] Özbek, O., Isildak, Ö., Berkel, C. (2020), The use of porphyrins in potentiometric sensors as ionophores. *J. Incl. Phenom. Macrocycl. Chem.* 1-9. (DOI: 10.1007/s10847-020-01004-y).

[13] Mathew, S., Astani, N. A., Curchod, B. F., Delcamp, J. H., Marszalek, M., Frey, J., Rothlisberger, U., Nazeeruddin, M. K., Grätzel, M. (2016), Synthesis, characterization and ab initio investigation of a panchromatic ullazine–porphyrin photosensitizer for dye-sensitized solar cells. *J. Mater. Chem. A.* 4, 2332-2339. (DOI: 10.1039/C5TA08728G).

[14] Wu, S. L., Lu, H. P., Yu, H. T., Chuang, S. H., Chiu, C. L., Lee, C. W., Diau, E. W. G., Yeh, C. Y. (2010), Design and characterization of porphyrin sensitizers with a push-pull framework for highly efficient dye-sensitized solar cells. *Energy Environ. Sci.* 3, 949-955. (DOI: 10.1039/C003872P).

[15] Jadhav, T., Dhokale, B., Mobin, S. M., Misra, R. (2015), Aggregation induced emission and mechanochromism in pyrenoimidazoles. *J. Mater. Chem. C.* 3, 9981-9988. (DOI: 10.1039/C5TC02181B).

[16] Cekaviciute, M., Petrauskaite, A., Nasiri, S., Simokaitiene, J., Volyniuk, D., Sych, G., Budreckiene, R., Grazulevicius, J. V. (2020), Towards blue AIE/AIEE: synthesis and applications in OLEDs of tetra-/triphenylethenyl substituted 9, 9-Dimethylacridine derivatives. *Molecules*, 25, 445. (DOI: 10.3390/molecules25030445).

[17] Mei, J., Leung, N. L. C., Kwok, R. T. k., Lam, J. W. Y., Tang, B. Z. (2015), Aggregation-induced emission: together we shine,

united we soar!. *Chem. Rev.* 115, 11718-11940. (DOI: 10.1021/acs.chemrev.5b00263).

[18] Woon, K. L., Ariffin, A., Ho, K. W., Chen, S. A. (2018), Effect of conjugation and aromaticity of 3, 6 di-substituted carbazoles on triplet energy and the implication of triplet energy in multiple-cyclic aromatic compounds. *RSC Adv.* 8, 9850-9857. (DOI: 10.1039/C8RA00674A).

[19] Dumur, F. (2020), Recent advances on carbazole-based photoinitiators of polymerization. *Eur. Polym. J.* 125, 109503. (DOI: 10.1016/j.eurpolymj.2020.109503).

[20] Naik, P., Su, R., Elmorsy, M. R., El-Shafei, A., Adhikari, A. V. (2018), Investigation of new carbazole based metal-free dyes as active photo-sensitizers/co-sensitizers for DSSCs. *Dyes Pigm.* 149, 177-187. (DOI: 10.1016/j.dyepig.2017.09.068).

[21] Wex, B., Kaafarani, B. R. (2017), Perspective on carbazole-based organic compounds as emitters and hosts in TADF applications. *J. Mater. Chem. C.* 5, 8622-8653. (DOI: 10.1039/C7TC02156A).

[22] Dumur, F. (2015), Carbazole-based polymers as hosts for solution-processed organic light-emitting diodes: Simplicity, efficacy. *Org. Electron.* 25, 345-361. (DOI: 10.1016/j.orgel.2015.07.007).

[23] Mitchell, R., Wagner, K., Barnsley, J. E., van der Salm, H., Gordon, K. C., Officer, D. L., Wagner, P. (2017), Synthesis and Light-Harvesting Potential of Cyanovinyl β-Substituted Porphyrins and Dyads. *Eur. J. Org. Chem.* 2017, 5750-5762. (DOI: 10.1002/ejoc.201701003).

[24] Xue, J. Q., Feng, Y. Q., Wang, L., Wu, L. H. (2007), The synthesis and spectroscopic investigation of vinylated meso-tetraphenylporphyrin. *Chin. Chem. Lett.* 18, 1319-1322. (DOI: 10.1016/j.cclet.2007.09.032).

[25] Kesavan, P. E., Pandey, V., Ishida, M., Furuta, H., Mori, S., Gupta, I. (2020), Synthesis, Photophysical Properties and Computational Studies of beta-Substituted Porphyrin Dyads. *Chem. Asian J.* 15, 2015-2028. (DOI: 10.1002/asia.202000463).

[26] Sharma, R., Gautam, P., Mobin, S. M., Misra, R. (2013), β-Substituted ferrocenyl porphyrins: synthesis, structure, and properties. *Dalton Trans.* 42, 5539-5545. (DOI: 10.1039/C3DT00003F).

[27] Sekaran, B., Jang, Y., Misra, R., D'Souza, F. (2019), Push–Pull Porphyrins via β-Pyrrole Functionalization: Evidence of Excited State Events Leading to High-Potential Charge-Separated States. *Chem. Eur. J.* 25, 12991-13001. (DOI: 10.1002/chem.201902286).

[28] Ekbote, A., Han, S. H., Jadhav, T., Mobin, S. M., Lee, J. Y., Misra, R. (2018), Stimuli responsive AIE active positional isomers of phenanthroimidazole as non-doped emitters in OLEDs. *J. Mater. Chem. C.* 6, 2077-2087. (DOI: 10.1039/C7TC05450E).

[29] Nicolas, M., Fabre, B., Chapuzet, J. M., Lessard, J., Simonet, J. (2000), Boronic ester-substituted triphenylamines as new Lewis base-sensitive redox receptors. *J. Electroanal. Chem.* 482, 211-216. (DOI: 10.1016/S0022-0728(00)00052-8).

[30] Dhokale, B., Jadhav, T., Mobin, S. M., Misra, R. (2015), Meso alkynylated tetraphenylethylene (TPE) and 2, 3, 3-triphenylacrylonitrile (TPAN) substituted BODIPYs. *J. Org. Chem.* 80, 8018-8025. (DOI: 10.1021/acs.joc.5b01117).

[31] Frisch, M. J., Trucks, G. W., Schlegel, H. B., Scuseria, G. E., Robb, M. A., Cheeseman, J. R., Scalmani, G., Barone, V., Mennucci, B., Petersson, G. A., Nakatsuji, H., Caricato, M., Li, X., Hratchian, H. P., Izmaylov, A. F., Bloino, J., Zheng, G., Sonnenberg, J. L., Hada, M., Ehara, M.; Toyota, K.; Fukuda, R.;

Hasegawa, J.; Ishida, M.; Nakajima, T.; Honda, Y.; Kitao, O., Nakai, H., Vreven, T., Montgomery, J. A., Jr., Peralta, J. E., Ogliaro, F., Bearpark, M., Heyd, J. J., Brothers, E., Kudin, K. N., Staroverov, V. N., Kobayashi, R., Normand, J., Raghavachari, K., Rendell, A., Burant, J. C., Iyengar, S. S., Tomasi, J., Cossi, M., Rega, N., Millam, N. J., Klene, M., Knox, J. E., Cross, J. B., Bakken, V., Adamo, C., Jaramillo, J., Gomperts, R., Stratmann, R. E., Yazyev, O., Austin, A. J., Cammi, R., Pomelli, C., Ochterski, J. W., Martin, R. L., Morokuma, K., Zakrzewski, V. G., Voth, G. A., Salvador, P., Dannenberg, J. J., Dapprich, S., Daniels, A. D., Farkas, O., Foresman, J. B., Ortiz, J. V., Cioslowski, J., Fox, D. J. Gaussian 09, Revision A.02, *Gaussian, Inc.*, Wallingford, CT, 2009.

[32] Chaudhri, N., Cong, L., Grover, N., Shan, W., Anshul, K., Sankar, M., Kadish, K. M. (2018), Synthesis and electrochemical characterization of acetylacetone (acac) and ethyl acetate (EA) appended β-trisubstituted push–pull porphyrins: Formation of electronically communicating porphyrin dimers. *Inorg. Chem.* 57, 13213-13224. (DOI: 10.1021/acs.inorgchem.8b01690).

[33] Rathi, P., Kumar, S., Banerjee, D., Soma, V. R., Sankar, M. (2020), Unsymmetrical β-functionalized 'push–pull' porphyrins: synthesis and photophysical, electrochemical and nonlinear optical properties. *Dalton Trans.* 49, 3198-3208. (DOI: 10.1039/C9DT04252K).

[34] Ahmad Dar, T., Mandeep, Sankar, M. (2018), Synthesis, spectral and electrochemical redox properties of N-methyl fused nickel (II) porphyrin. *J Porphyr Phthalocyanines.* 22, 1106-1110. (DOI: 10.1142/S1088424618501109).

Chapter 8

Conclusions and Future Scope

8.1. Conclusions

The porphyrins are promising scaffolds, which are essential to perform a key role in electron and energy transfer processes such as storage and transport of oxygen, photosynthesis and many more.[1–3] The photonic and electronic properties of the porphyrins can be fine-tuned by diverse electron donor or acceptor entities at the β-pyrrolic positions.[4,5] Tuning of optical and electronic properties of the porphyrin macrocycle have been investigated to improve the efficiency of a wide range of applications including organic light emitting diodes, photodynamic therapy, nonlinear optics, dye sensitized solar cells and single molecule switches.

In this regard, we have synthesized various donor and acceptor substituted unsymmetrical β-functionalized porphyrins and investigated their photophysical, electrochemical and computational studies.

In chapter 3, β-functionalized unsymmetrical push–pull porphyrins **1**–**6** were designed and synthesized *via* β-mono and dibrominated TPP by the Sonogashira cross-coupling reaction and their photophysical and computational studies were explored. A comparative investigation was carried out to understand the effect of donor and acceptor units on the push−pull porphyrin and their zinc derivatives. The red shifted absorption in the Soret and the Q-bands of porphyrin **5** and **6** resulted from the enhanced π-conjugation of the electron donor and the acceptor units at the opposite β, β'-positions. The red shifted emission in porphyrin **5** and **6** confirms the strong electronic communication between the electron donor and the acceptor units. The computational study of porphyrin **5** and **6** exhibits a stabilized HOMO energy levels with low HOMO–LUMO gap of about 2.06 eV and 2.17 eV compared to other porphyrins. These results implies that the β, β'-substituted push-pull porphyrins have wide applications in optoelectronics.[6]

163

In chapter 4, *β*-donor substituted TCBD functionalized porphyrins **1**–**8** were designed and synthesized by the Sonogashira cross-coupling reaction and [2+2] cycloaddition–retro electrocyclization (CA–RE) reaction. The effect of TCBD functionalization on the photophysical and computational studies were investigated. The UV–vis absorption spectra of TCBD functionalized porphyrin shows a red shifted absorption due to the incorporation of strong electron accepting TCBD unit with strong intramolecular charge-transfer (CT). The emission spectra of TCBD functionalized porphyrin exhibits blue shift in the UV-visible region due to the twisted nonplanar conformation between the porphyrin and TCBD units. The computational study reveals, stabilized LUMO levels with low HOMO–LUMO band gap after the incorporation of TCBD acceptor unit. These results provide a new insight for the *β*-functionalized TCBD porphyrin and their application in energy transfer studies.[7]

In chapter 5, the donor substituted unsymmetrical free base *β*-pyrrole porphyrins **1**, **3**, **5** and **7** were designed and synthesized by the Suzuki cross-coupling reaction and their metallation was carried out using Zn(OAc)$_2$, which resulted in metal derivatives of porphyrin **2**, **4**, **6**, and **8**. The photophysical properties of Zn(II) complexes exhibits a red shifted absorption in the low energy region compared to its corresponding free bases. The *β*-donor substituted porphyrins **3**, **4** and **6** exhibits slight red shift in the fluorescence maxima compared to other porphyrins. The red shifted emission maxima may be due to the nonplanarity of donor units substituted at the *β*-position. The porphyrin **5** and **7** exhibits a low electrochemical band gap of 0.71 and 0.70 V compared to rest of the porphyrins. The computational study shows that the dimethoxy triphenylamine substituted porphyrin **5** and **6** shows low HOMO–LUMO energy gap compared to other donor substituted porphyrin **1**, **2**, **3**, **4**, **7** and **8**. These results provide a better understanding about the effect of donor substituents on the electronic properties of porphyrin π-system and its application in optoelectronics.

In chapter 6, the acceptor functionalized unsymmetrical *β*-porphyrin **1a**–**8d** were designed and synthesized by the Pd-catalysed

Suzuki cross-coupling reaction followed by the Zn(II) metallation. The photophysical and computational studies of porphyrin **1a**–**8d** were carried out to understand the influence of acceptor units on the electronic properties of the porphyrin π-system. The electronic absorption spectra confirms that the electron-deficient naphthalimide, *p*- and *m*-benzothiazole and quinoxaline units have similar effect on the electronic properties of the porphyrin macrocycle. The fluorescence quantum yield of quinoxaline substituted porphyrin **7d** shows high quantum yield value of 0.12. The computational study of porphyrin **1a**–**8d** reveals that the porphyrin **1a** and **7d** exhibits a low HOMO–LUMO band gap compared to other free base and Zn(II) porphyrins. The *p*- and *m*-benzothiazole functionalized porphyrin **3b**–**6c** confirms that the electronic properties of the molecules are not influenced by the position of substituents. These results provide a new insight for the acceptor functionalized porphyrin and its further applications in optoelectronics.

In chapter 7, The TPAN, TPE and carbazole substituted unsymmetrical *β*-porphyrins **11**–**18** were designed and synthesized *via* Pd-catalyzed Suzuki cross-coupling reaction and zinc metallation reaction. The effect of TPAN, TPE and carbazole units on the photonic and electronic properties of the porphyrin π-systems were investigated. The absorption spectra of porphyrin **11**–**14** suggests that the 2,3,3-triphenylacrylonitrile with different spatial arrangements of cyano unit exhibits similar effect on the porphyrin macrocycle. The red shifted emission maxima of porphyrin **11**–**16** may be due to the enhanced π-conjugation of the phenyl group present in the 2,3,3-triphenylacrylonitrile and 1,1,2,2-tetraphenylethene moiety. The electrochemical properties of zinc porphyrin **14**, **16** and **18** exhibits a cathodic shift in the oxidation and reduction potentials compared to their corresponding free base analogues **13**, **15** and **17**. The computational studies of porphyrin **11**–**18** suggests, that the 2,3,3-triphenylacrylonitrile substituted porphyrin **11** and **13** exhibits a stabilized LUMO energy levels with low HOMO–LUMO band gap of about 2.55 eV and 2.58 eV compared to other porphyrins.

8.2. Future Scope

The thesis highlights an important strategy for designing the *β*-functionalized porphyrin based D–A systems, to fine tune the photonic and electronic properties of the porphyrin macrocycle. The HOMO–LUMO gap of the *β*-functionalized porphyrins can be perturbed by varying the π-linkers, donors and acceptor units at the *β*-pyrrolic positions. The incorporation of TCBD acceptor units at the *β*-pyrrolic position of the porphyrin macrocycle resulted in the significant tuning of the HOMO–LUMO gap. The incorporation of strong electron accepting TCBD unit resulted in a red shifted absorption with strong intramolecular charge-transfer (CT). The *β*-substituted porphyrins with broad absorption spectra in the visible region could be promising candidate for various applications such as organic light emitting diodes, photodynamic therapy, organic field-effect transistor and perovskite solar cell.

8.3. References

[1] Kadish, K. M., Smith, K. M., Guilard, R. (2010). The porphyrin handbook. *World scientific*, 2011, 1-20.

[2] Chatterjee, T., Shetti, V. S., Sharma, R., Ravikanth, M. (2017). Heteroatom-containing porphyrin analogues. *Chem. Rev.* 117(4), 3254-3328. (DOI: 10.1021/acs.chemrev.6b00496).

[3] Singhal, A. (2017). Meso-linked multiporphyrins as model for light harvesting systems: Review. *Nat Prod Chem Res*, 5, 259. (DOI: 10.4172/2329-6836.1000259).

[4] Rio, Y., Rodriguez-Morgade, M. S., Torres, T. (2008). Modulating the electronic properties of porphyrinoids: a voyage from the violet to the infrared regions of the electromagnetic spectrum. *Org. Biomol. Chem.*, 6(11), 1877-1894. (DOI: 10.1039/b800617b).

[5] Bromby, A. D., Jansonius, R. P., Sutherland, T. C. (2013). Synthesis and optical and electronic properties of core-modified

21, 23-dithiaporphyrins. *J. Org. Chem.* 78(4), 1612-1620. (DOI: 10.1021/jo302707f).

[6] Sekaran, B., Jang, Y., Misra, R., D'Souza, F. (2019). Push–Pull Porphyrins via β-Pyrrole Functionalization: Evidence of Excited State Events Leading to High-Potential Charge-Separated States. *Chem. Eur. J.*, 25(56), 12991-13001. (DOI: 10.1002/chem.201902286). †

[7] Sekaran, B., Dawson, A., Jang, Y., MohanSingh, K. V., Misra, R., D'Souza, F, (2021) Charge-Transfer in Panchromatic Porphyrin-Tetracyanobuta-1,3-diene-Donor Conjugates: Switching the Role of Porphyrin in the Charge Separation Process. *Chem. Eur. J. Accepted Author Manuscript.* (DOI: 10.1002/chem.202102865) †